AUTOMATED SHIRT COLLAR MANUFACTURING

DLA 900-87-0017 Task 0014

FINAL REPORT

VOLUME III:

Sewing Head Control for High Speed Stitch Contour Tracking

Frank W. Paul
Principal Investigator

and

Alan W. Bennett
Research Assistant

Center for Advanced Manufacturing
and
Clemson Apparel Research

Clemson University
Clemson, SC

June 1992

DISCLAIMER NOTICE

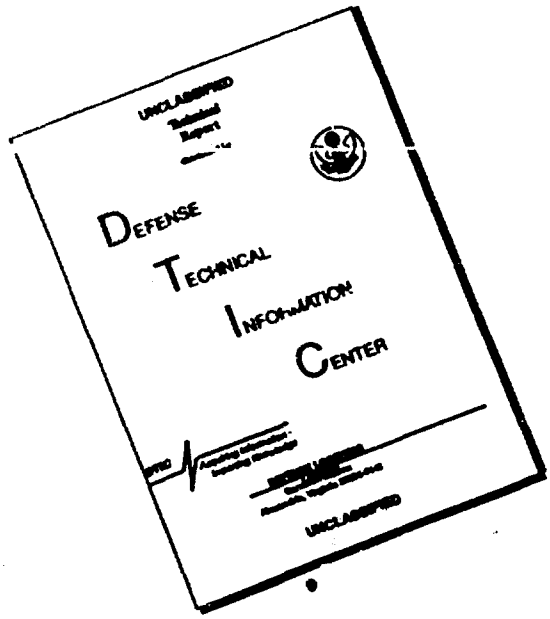

THIS DOCUMENT IS BEST QUALITY AVAILABLE. THE COPY FURNISHED TO DTIC CONTAINED A SIGNIFICANT NUMBER OF PAGES WHICH DO NOT REPRODUCE LEGIBLY.

P00011 to DLA900-87-D-0017

SECURITY CLASSIFICATION OF THIS PAGE

REPORT DOCUMENTATION PAGE

1a. REPORT SECURITY CLASSIFICATION Unclassified	1b. RESTRICTIVE MARKINGS
2a. SECURITY CLASSIFICATION AUTHORITY	3. DISTRIBUTION / AVAILABILITY OF REPORT Unclassified Distribution Unlimited
2b. DECLASSIFICATION / DOWNGRADING SCHEDULE	
4. PERFORMING ORGANIZATION REPORT NUMBER(S)	5. MONITORING ORGANIZATION REPORT NUMBER(S)
6a. NAME OF PERFORMING ORGANIZATION Clemson University Clemson Apparel Research 6b. OFFICE SYMBOL (If applicable)	7a. NAME OF MONITORING ORGANIZATION Defense Personnel Support Center
6c. ADDRESS (City, State, and ZIP Code) 500 Lebanon Road Pendleton, SC 29670	7b. ADDRESS (City, State, and ZIP Code) 2800 South 20th Street P.O. Box 8419 Philadelphia, PA 19101-8419
8a. NAME OF FUNDING / SPONSORING ORGANIZATION Defense Logistics Agency 8b. OFFICE SYMBOL (If applicable)	9. PROCUREMENT INSTRUMENT IDENTIFICATION NUMBER DLA 900-87-D-0017 Delivery Order 0014
8c. ADDRESS (City, State, and ZIP Code) Room 4B195 Cameron Station Alexandria, VA 22304-6100	10. SOURCE OF FUNDING NUMBERS PROGRAM ELEMENT NO. 78011S; PROJECT NO.; TASK NO.; WORK UNIT ACCESSION NO.

11. TITLE (Include Security Classification)
Automated Shirt Collar Manufacturing
Vol. III: Sewing Head Control for High Speed Stitch Contour Tracking - unclassified

12. PERSONAL AUTHOR(S)
F. W. Paul, Principal Investigator; Alan W. Bennett, Research Assistant

13a. TYPE OF REPORT	13b. TIME COVERED	14. DATE OF REPORT (Year, Month, Day)	15. PAGE COUNT
Final	FROM n/a TO _____	1992 June 23	

16. SUPPLEMENTARY NOTATION

17. COSATI CODES			18. SUBJECT TERMS (Continue on reverse if necessary and identify by block number)
FIELD	GROUP	SUB-GROUP	

19. ABSTRACT (Continue on reverse if necessary and identify by block number)

A prototype of a two axis belt driven CNC stitching machine has been designed and built for use in the apparel industry. The objectives of this research are: (1) determine the performance requirements of the stitcher; (2) develop a mathematical model of the stitcher; and (3) recommend the design changes necessary for the stitcher to meet the specifications based on the simulation of the stitcher model.

20. DISTRIBUTION / AVAILABILITY OF ABSTRACT ☒ UNCLASSIFIED/UNLIMITED ☐ SAME AS RPT. ☐ OTIC USERS	21. ABSTRACT SECURITY CLASSIFICATION Unclassified
22a. NAME OF RESPONSIBLE INDIVIDUAL Frank W. Paul	22b. TELEPHONE (Include Area Code) 803-656-3291 22c. OFFICE SYMBOL

DD FORM 1473, 84 MAR 83 APR edition may be used until exhausted. All other editions are obsolete.

SECURITY CLASSIFICATION OF THIS PAGE

ACKNOWLEDGMENTS

The authors would like to thank all those who were involved with support of this project. Especially, it is appropriate to thank the Defense Logistics Agency, Department of Defense, for support of this work under contract number DLA 900-87-0017 Task 0014. This work was conducted through Clemson Apparel Research, a facility whose purpose is the advancement of apparel manufacturing technology, by the Center for Advanced Manufacturing, Clemson University and Jet Sew, Barneveld, N.Y.

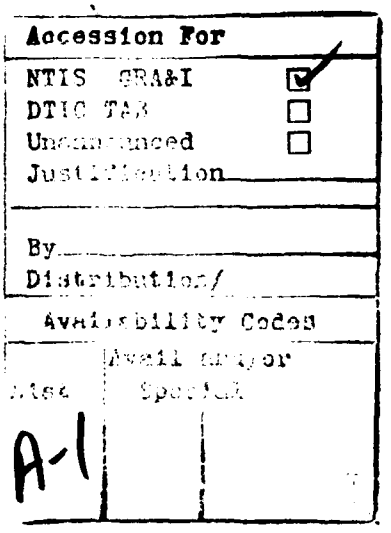

ABSTRACT

A prototype of a two axis belt driven CNC stitching machine has been designed and built for use in the apparel manufacturing industry. The stitcher is designed such that the sewing head translation in the horizontal X and Y axes is actuated by brushless servomotors through timing belts attached to the X and Y carriages. The X axis stroke length can be increased to accommodate various sizes of garment parts such as shirt collars, shirt pockets, shirt sleeves, etc. The objectives of this thesis are to: (1) determine the performance requirements of the stitcher, (2) develop a mathematical model of the stitcher and (3) recommend the design changes necessary for the stitcher to meet the specifications based on the simulation of the stitcher model.

The stitcher must be capable of operating at a maximum translating velocity of 7.5 in./sec since the maximum stitch length sewn by the stitcher is 0.1 in. and the maximum needle speed is 75 stitches/sec. It must also maintain the velocity within ±5% of the commanded velocity and be capable of accelerating and decelerating at a rate of 281 in./sec^2 to maintain consistent stitch length. The positioning accuracy of the stitcher must be within ±0.02 in. (0.5 mm) of the commanded position.

Three principle design changes are recommended to achieve these specifications: (1) the stitcher frame must be

made stiffer, (2) the drive train must be made stiffer and (3) the mass translated by the servo systems should be reduced. Experimental analysis of the stitcher showed that the mode of vibration of the stitcher frame in the Y axis occurs at a relatively low frequency. Therefore, it must be redesigned with the use of larger structural members or a single unit frame rather than two subframes. The timing belts in the drive train are also too flexible; the spring constants of the timing belts were found to be 6.24E5 N/m in the X axis and 1E6 N/m in the Y axis. Therefore, the belts must be replaced with transmission devices, such as ball screw drives, that are approximately two orders of magnitudes stiffer. The mass of the load in each axis must also be reduced by approximately 50%. This can be accomplished by designing the stitcher so that the fabric assembly is held by a fixture and translated rather than moving the sewing head. The simulation of the stitcher model shows that the performance requirements can be met if the recommended design changes are implemented.

ACKNOWLEDGEMENTS

I must take this opportunity to thank Dr. Frank W. Paul for his insightful guidance and suggestions, without which this research would not have been completed. I would also like to thank Dr. E. Harry Law and Dr. Marvin W. Dixon for their suggestions and assistance as committee members. Also appreciated are the efforts of Ernst Schrameyer, Tad Olewicz and Jet Sew Inc. in designing and manufacturing the CNC stitcher used in this research and the technical assistance of Tony Aspland at Clemson Apparel Research.

I must also acknowledge the friendship and assistance of my colleagues in the Robotics Lab and those who preceded me in graduation; they helped make my tenure as a graduate student more educational and enjoyable.

I am also grateful to my Aunt and Uncle, Marlene and David Nicholas for accommodating me in Clemson during the final stages of the thesis preparation. Most important is the appreciation I wish to express to my brother, Brian, for his support and friendship, and, above all, my parents, Dan and Charlene, to whom I am forever grateful for their love and encouragement in all of my endeavors.

TABLE OF CONTENTS

Table of Contents (Continued)

LIST OF FIGURES

List of Figures (Continued)

List of Figures (Continued)

List of Figures (Continued)

List of Figures (Continued)

CHAPTER I

INTRODUCTION

The apparel industry must use flexible manufacturing techniques because of numerous stylistic changes and the variety of sizes demanded by the market. A high degree of flexibility has been provided in the past by skilled labor. However, this is no longer feasible in the presence of foreign competition with low cost labor; therefore, the competitiveness of the apparel industry in the United States has declined [1]. Thus, the apparel industry must compete through the use of automated production methods [2]. Three basic processes involved in apparel production are:

cutting: This consists of the processes involved in reducing bulk fabrics and bolts of fabric into smaller components for the apparel garment product.

joining: This is the process of assembling the cut components using any necessary means such as sewing, fusing, adhesion, etc..

pressing: This refers to shaping material with pressure with or without the addition of heat and/or steam [3].

The joining process, consisting primarily of sewing due to its superior visual qualities and structural properties, typically limits the production rate of an apparel manufacturing process [2]. Therefore, as the apparel industry is automated, attention must be focused on the sewing operation.

Background

An example of an apparel manufacturing process is shirt collar assembly. One step in the assembly of a dress shirt collar is attaching the collar to the collar band. The collar band is the component that attaches the collar to the shirt body, as shown in Figure 1.1. A workstation to assemble shirt collars which uses a rotating indexer to move the collar assembly through the various operations has been proposed by Jet Sew Inc. of Barneveld, New York. The workstation performs the following assembly sequence as defined in Figure 1.2.

1. One component of the collar band is placed on the rotating indexer.
2. The turned and pressed collar is placed on the collar band component.
3. The top piece of the collar band is then placed on the assembly.
4. The shirt collar assembly is joined together by sewing.
5. The completed collar assembly is removed from the workstation.

This research will address the machinery used in the sewing process in the proposed workstation.

Sewing Equipment

Sewing machinery can be classified according to the degree of operator involvement in the sewing process. The operator is involved in all phases of the sewing process in a manually controlled machine. These processes include obtaining the fabric, positioning the fabric prior to and during

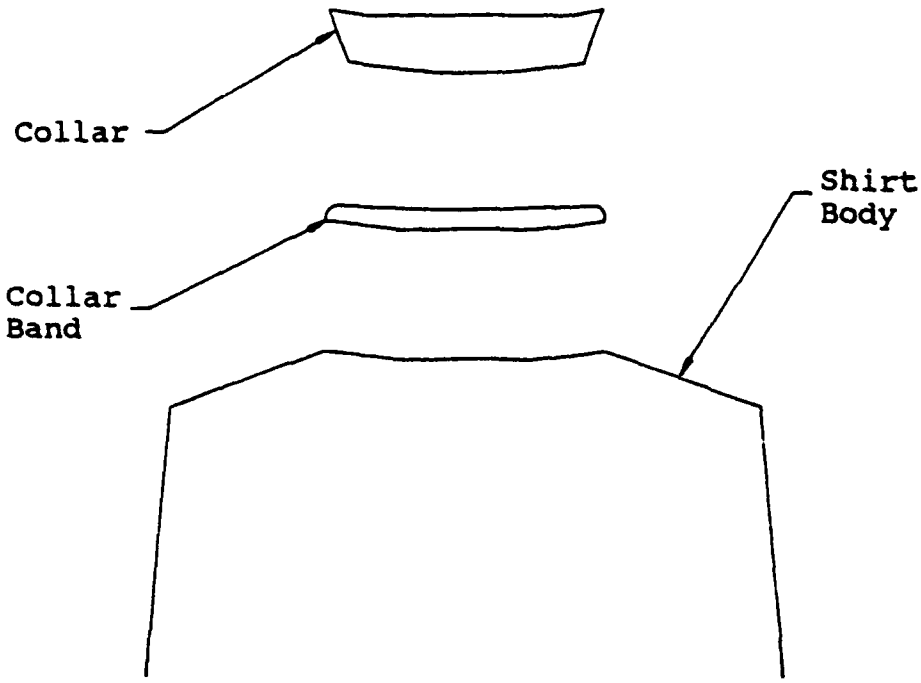

(a) The shirt body and shirt collar components.

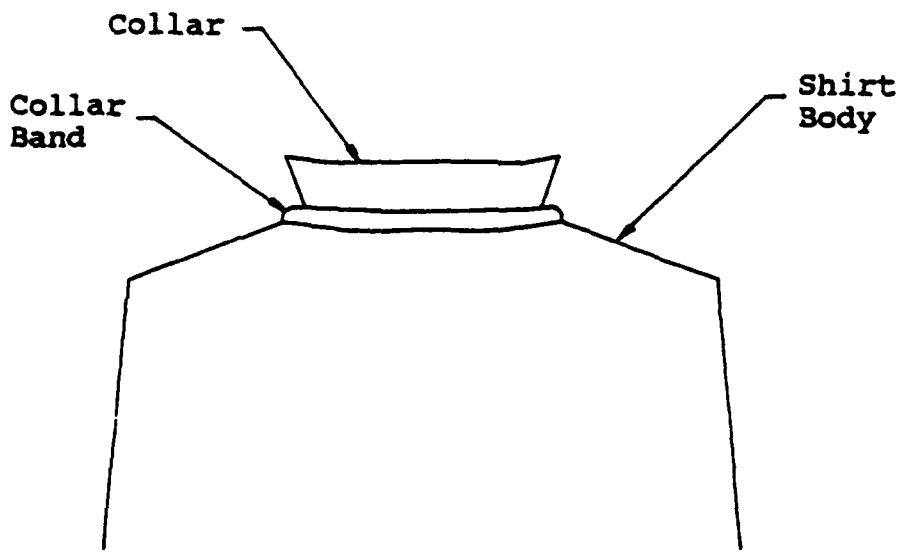

(b) The assembled shirt collar.

Figure 1.1. A collar, collar band and shirt body.

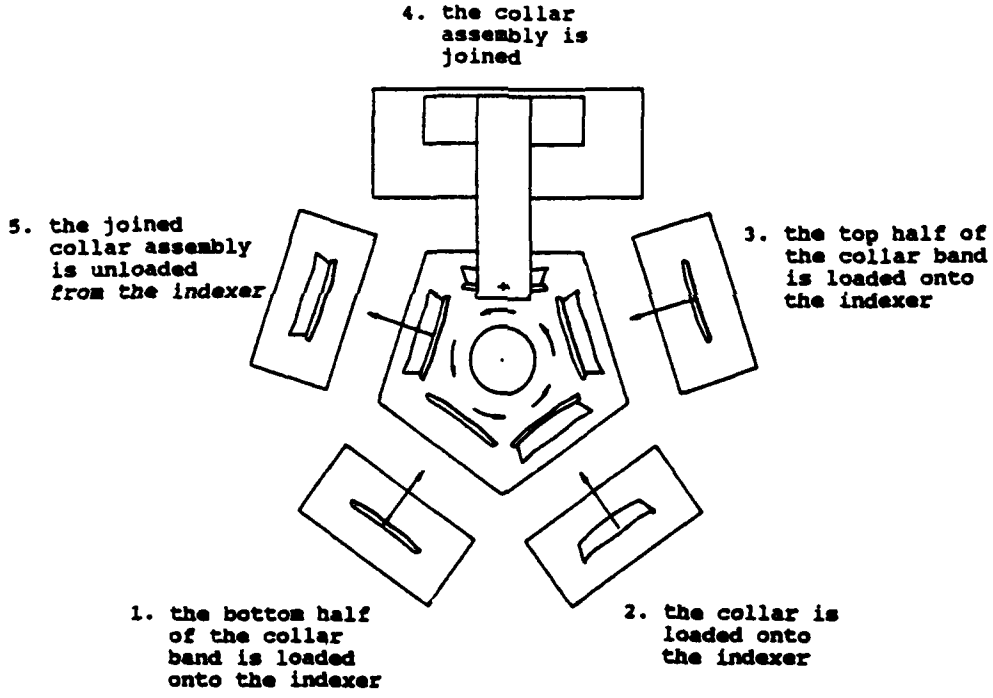

Figure 1.2. The proposed shirt collar assembly workstation.

the sewing operation and removing the fabric from the sewing machine. The operator obtains and positions the fabric using semi-automatic sewing machines, while the machine automatically controls the sewing operation. The removal of the fabric workpiece may or may not be accomplished automatically. An automatic sewing machine controls all of the functions during the sewing process, with the operator simply presenting the machine a set of fabric assemblies to be joined.

A profile stitcher, also referred to as an X-Y stitcher, is a type of automatic sewing machine that is capable of sewing sharp corners and variable radius curves. Programmable profile stitchers are software controlled with the stitching program residing on media such as an EPROM chip or a floppy disk [3]. The sewing machine used in this research study is a programmable profile stitcher.

Profile Stitcher Design Philosophies

There are three design philosophies which can be used to create relative motion between the fabric assembly and the sewing head in profile stitchers. One design moves the fabric assembly and its holding fixture under a fixed sewing head, while another moves the sewing head with the fabric assembly and the holding fixture remaining fixed. These two designs are frequently combined in a third design that moves the sewing head in one direction and the fabric assembly in the other.

The physical differences in these design philosophies are the amount of structural mass that must be moved and the complexity of the material handling system required. A typical cast iron sewing head weighs approximately 75 pounds, while the fabric assembly and holding fixture weigh at least an order of magnitude less. Therefore, there is a significant dynamic advantage in moving the fabric assembly and holding fixture rather than the sewing head. However, this type of arrangement may require a more complex material handling system capable of moving the fabric assembly along a given path. Each of these problems may be encountered in the case of a design which moves the sewing head in one direction and the fabric and holding fixture in the other.

In each of these designs, relative motion between the sewing head and the fabric occurs in the X and Y directions, as shown in Figure 1.3a. This relative motion is restricted in the Y direction by the depth of the sewing head throat, shown in Figure 1.3b. The stroke limit in the X direction depends upon the structural design of the supporting frame and servo drive system.

Stitching Machinery Industry Overview

The Pfaff 3557 collar topstitching machine shown in Figure 1.4 moves the fabric assembly with the feed-dog mechanism on the stationary sewing head. The collar is loaded with its edge aligned flush against a stationary vertical guiding surface with the distance between the sewing needle and the vertical surface determining the width of the seam.

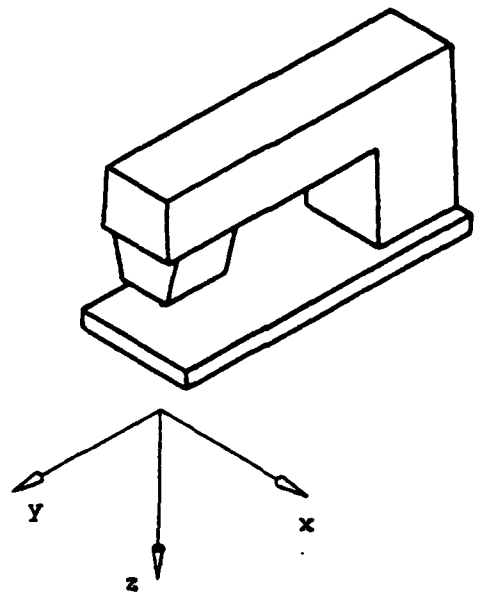

(a) The sewing head reference frame.

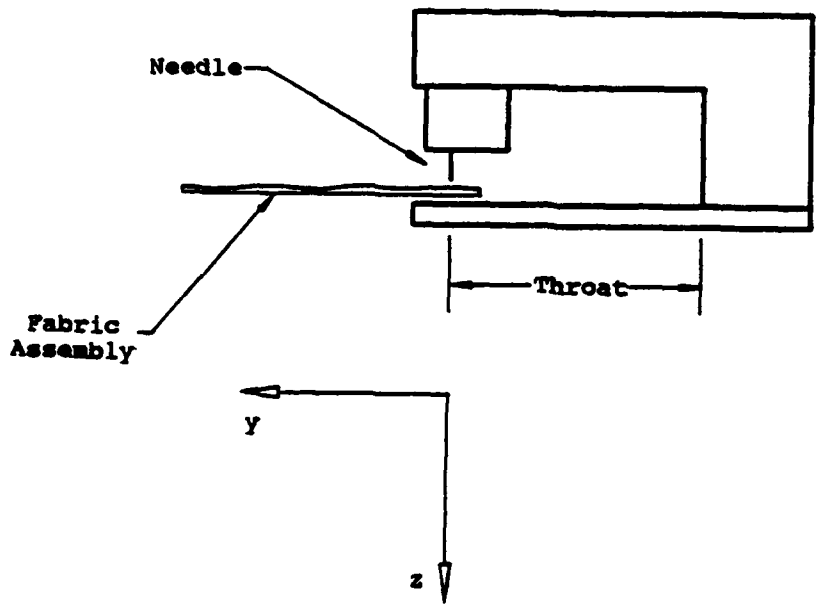

(b) The sewing head stitching a fabric assembly.

Figure 1.3 A typical sewing head for use on a CNC stitching machine.

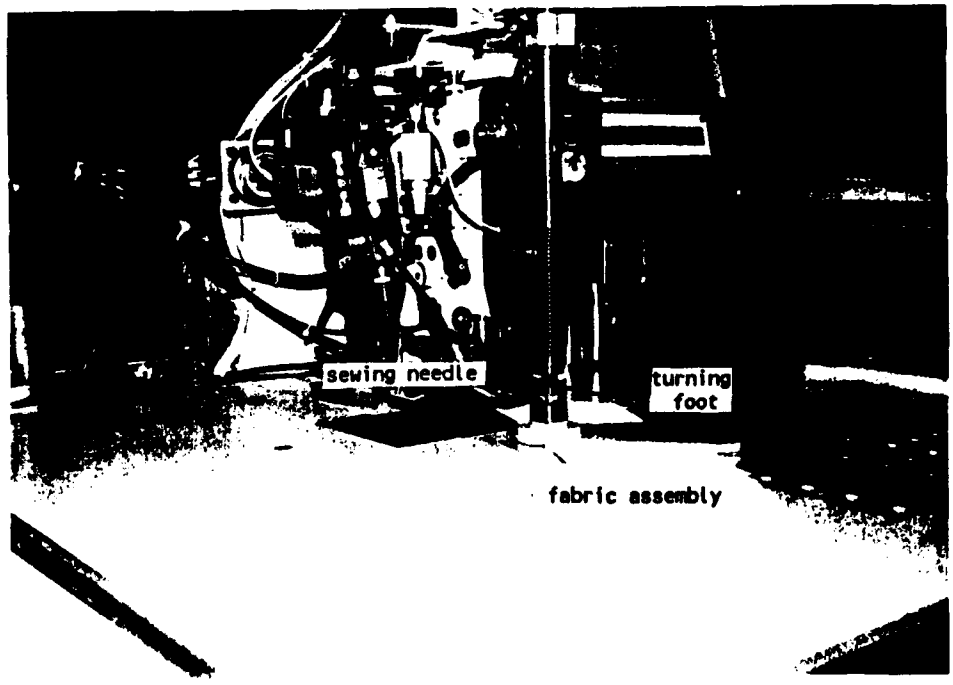

Figure 1.4 The Pfaff 3557 collar topstitching unit.

The feed-dog then moves the fabric assembly using the vertical surface as a guide. The sewing needle pauses in the down position when it encounters a corner along the edge of the fabric assembly, allowing the turning foot to rotate the assembly about the needle. This method of following an edge profile requires a relatively stiff fabric assembly such as a shirt collar or sleeve cuff, which is comprised of several layers of fabric. It is primarily useful in topstitching fabric assemblies that have finished, or hemmed, edges. Unhemmed edges, such as those in an unturned collar assembly, do not necessarily describe the shape of the desired stitch path and can therefore result in undesired stitch lines. When working on the proper type of fabric assembly this type of stitching machine is extremely flexible.

A v-top pocket hemmer, made by Jet Sew, moves the template holding the fabric assembly rather than the sewing head. This machine is not flexible; it is limited to sewing a v-top pocket within a given set of dimensions.

The Adler 973-S-204-3 automatic collar runstitching machine shown in Figure 1.5a moves the sewing head while the fabric remains fixed. The sewing head is supported by a hinged cantilever with two joints, allowing motion in two orthogonal directions. The collar assembly is held by an expandable template while the sewing head stitches the fabric profile, which is stored as position points in an EPROM chip.

The Necchi UAN 2684 in Figure 1.5b also moves the sewing head rather than the fabric assembly. This stitcher is

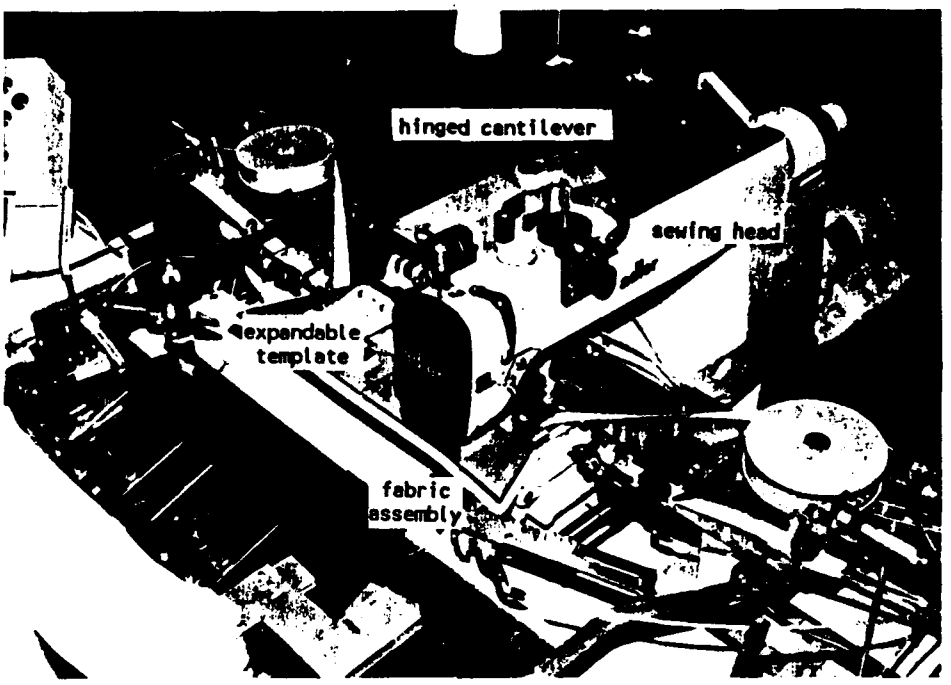

(a) The Adler 973-S-204-3 automatic collar runstitching machine.

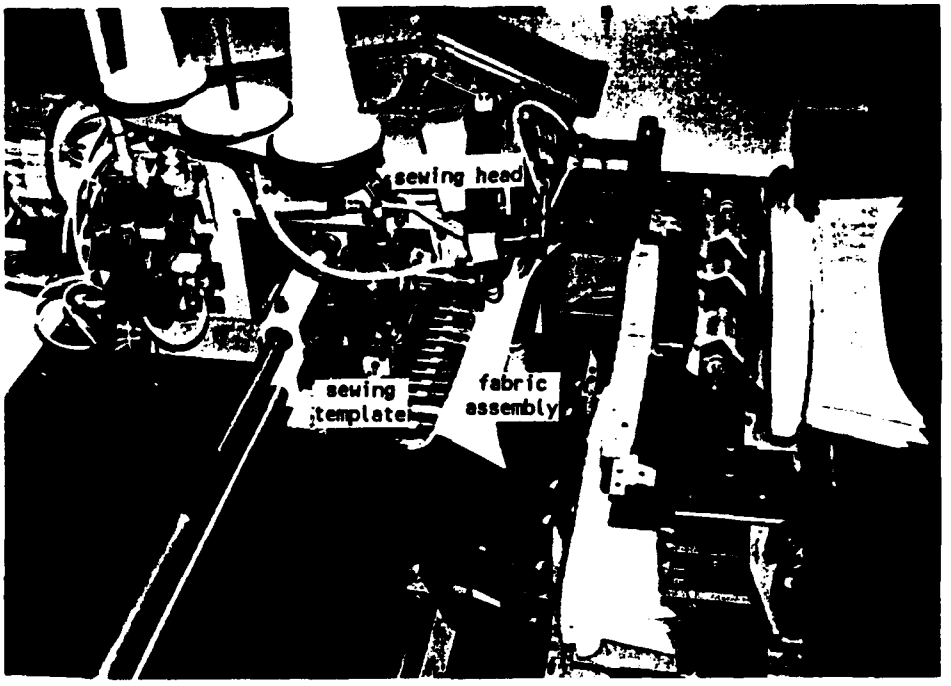

(b) The Necchi UAN 2684 stitching machine.

Figure 1.5 Stitching machines that move the sewing head rather than the fabric assembly.

equipped with a template to hold the shirt collar and collar band in a fixed position while the sewing head moves on linear bearings during sewing.

Another Necchi machine, the UAN 2531/A automatic pocket setting stitcher, shown in Figure 1.6, moves the fabric in one direction and the sewing head in the other. This type of machine is practical only for small garment components, such as a shirt pocket or collar. While one axis may exhibit a dynamic advantage by moving the fabric assembly, the other does not. Therefore, the dynamic advantage gained by moving the fabric in one axis is lost by moving the sewing head in the other.

The flexibility of each these machines is limited because they are designed for a specific garment part. Retooling is required in each case to stitch different garment parts. The existing designs also do not permit the expansion of the X stroke length shown in Figure 1.3a.

Literature Survey

Most documented research in automated sewing systems, such as an ongoing Japanese project undertaken by MITI, address robotic sewing and/or material handling [8,9]. No significant research material has been found for apparel sewing systems which address appropriate controller design concepts. However, considerable research has been conducted on two axis CNC contouring control applied to machine tools, welding systems and robotics.

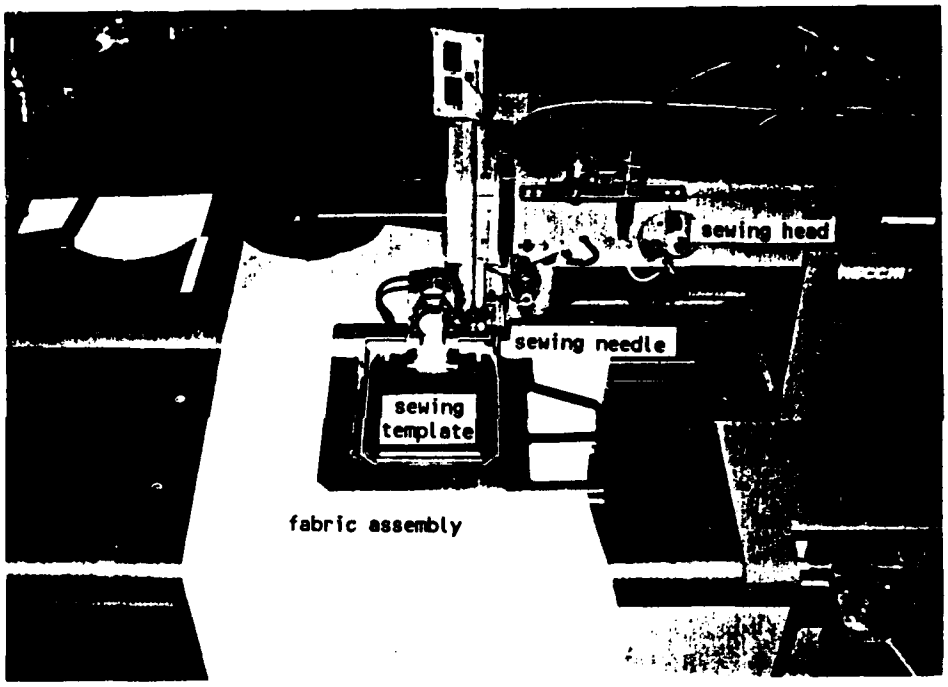

Figure 1.6 The Necchi UAN 2531/A stitching machine.

Contour trajectory control of a two axis CNC tool may be achieved using independent axis controllers or coupled controllers. Independent axis control has individual closed loop control drives. Each command signal is independent of the other axis. The command signal of each axis in a coupled controller depends upon the behavior of the other axis.

Poo et al. [10] investigated independent control for a two axis orthogonal system, with each axis modeled as a second order type I system. Three reference contours were considered: (1) constant acceleration along a line parallel to one axis, (2) constant velocity along a line inclined at an angle to one axis, and (3) constant angular velocity around a circle. These reference paths result in parabolic, ramp and sinusoidal reference signals respectively for each axis. The authors show that the contour error depends heavily on gain of each axis. If the axes have equal loop gains, there is no contour error; if the axes have unequal gains, a contour error exists.

Doriswami and Gulliver [11] present the formulation of a somewhat more sophisticated control system for independent axis control. The controller on each axis is a linear, time invariant controller using full state feedback and a digital filter. In the study, each axis consists of a ball screw driven feed drive actuated by a DC servomotor. The system is evaluated with reference signals consisting of analytical and combinations of analytical functions. The controller was found to be more robust than a conventional PID controller in

the presence of parameter variations, disturbances, nonlinearities and noise. The digital filter design depends on the nature of the input function(s). Therefore, the results are not applicable to the general case of a nonanalytical input reference, as may be the case in an industrial situation.

An independent axis preview control scheme based on information about the future reference was applied to a welding system by Tomizuka et al. [12]. A set of reference points is generated on line while a sensor is used to track the weld path. Reference points from a given number of sample instants in the future (called the preview step) are used in a optimal control formulation. A conventional optimal control scheme sums the cost function for all data points from time zero to infinity; however, the preview case sums only through the preview step and assumes the remaining points comprise a straight line. The control law resulting from this formulation consists of a proportional, derivative, integral and preview term. The preview controller was simulated assuming the open loop dynamics of the torch positioning system consist of a first order lag term and an integrator. The preview control was found to reduce position and velocity errors more effectively than conventional PID control. Preview distances of 3 to 5 time steps were found to be sufficient.

The formulation and experimental evaluation of a coupled compensator has been presented by Kulkarni and Srinivasan

[13]. The experimental system consists of an orthogonal two axis ball screw system driven by DC servomotors. Two controllers were designed using an optimal control formulation and tested on the two axis system with three reference contours: (1) a line inclined 45° to the X axis, (2) a right angle corner, with one line segment inclined 53° to the X axis and the other -37° to the Y axis, and (3) a circle with constant angular velocity. The controllers were designed for a first order system and then tested on a more accurate third order model. The first controller, with integral action, results in zero contour error and less overshoot than the uncoupled case. However, when the controller was applied to a more accurate third order model, its sensitivity to the unmodeled higher order dynamics was apparent as a more oscillatory response. Furthermore, the oscillation could not be damped by reformulating the controller using different weighing factors in the performance index.

Experimental results by Kulkarni and Srinivasan confirmed the sensitivity of the system to nonlinearities and higher order dynamics that were neglected in the simulation. This controller reduces to a conventional PID controller when reformulated based on a system model with dynamically identical axes. The second controller investigated contains no integral action; it reduces to a conventional PD controller when the axes are perfectly matched. This controller results in somewhat less oscillation than the previously described controller when it is applied to the third order model.

Experimentation confirmed the sensitivity of the controller to nonlinearities and higher order dynamics but showed that the system is less oscillatory with this controller than with the one described previously. When planned acceleration and deceleration is employed, less contour error results at the corners of the trajectory. The authors note that preview control can also be extended to these controllers. However, it may not be necessary if planned acceleration and deceleration is used.

Research Objectives and Problem Statement

The objective of this research is to develop an analytical model of a two axis CNC stitcher used in the apparel industry and to use the model to evaluate and improve the design of the stitcher. The development of the stitcher may include control issues such as the use of preview control, coupled control or optimal control design and hardware design considerations. The problem can be formally stated as follows:

> Analyze the dynamics and develop a mathematical model of each axis of a two axis belt driven CNC stitcher and determine the performance requirements that the stitcher must meet. Investigate the hardware design modifications and/or control system changes that can improve the performance of the stitcher and determine which design and control modifications should be made to meet the performance requirements.

The first objective to be achieved in addressing the problem is to develop a dynamic mathematical model of each axis of the stitcher. The model will be developed based on the experimentally determined behavior of the stitcher and

analyzed to determine possible methods of improving the stitcher performance. Finally, design changes will be proposed that will allow the stitcher to meet the performance requirements. These may include applying another design philosophy such as moving the fabric assembly rather than the sewing head, using different or additional feedback variables or a different type of controller.

Thesis Organization

Chapter II presents the design and operation of the stitching equipment used in this thesis research and the determination of its performance requirements. The development of the linear and nonlinear models of the stitcher based on its experimentally determined dynamic behavior is presented in Chapter III. The models are also validated by simulating the response of the stitcher to a test reference signal and comparing the simulation to the tracking performance of the actual stitcher. The linear model of the stitcher is analyzed in Chapter IV and possible methods of improving the performance of the stitcher are considered. Design changes that allow the stitcher to meet the performance requirements determined in Chapter II are also proposed and simulated on the nonlinear model. Chapter V presents conclusions drawn from the work and recommendations for further research.

CHAPTER II

DESIGN, OPERATION AND PERFORMANCE REQUIREMENTS OF THE CNC STITCHER

Stitcher Design and Operation

The stitcher used in this research is configured in such a way that the sewing head moves and the fabric remains fixed during sewing. This design limits the material handling to transferring and holding the fabric instead of moving it along a prescribed path for stitching. Because of this design, the stitcher may also be used in other workstations, assembling garment parts other than shirt collars.

Stitcher Configuration

The configuration of the stitcher is shown in Figure 2.1. The CNC stitcher consists of a sewing head and its sewing motor mounted on a two axis orthogonal X-Y table. The X-Y table consists of a X carriage and a Y carriage, each actuated by a brushless DC servomotor powered by a linear amplifier. The X and Y carriages are driven by timing belts, which are driven by the servomotors through a 6:1 speed reduction ratio. Each gear set consists of a polymer gear driven by a metallic motor shaft pinion to reduce mechanical backlash and deadband.

The actual stitcher used in this research is shown in Figures 2.2a and 2.2b. Two belts on each end of the X-carriage are used to drive the X-axis, while the Y-axis belt is

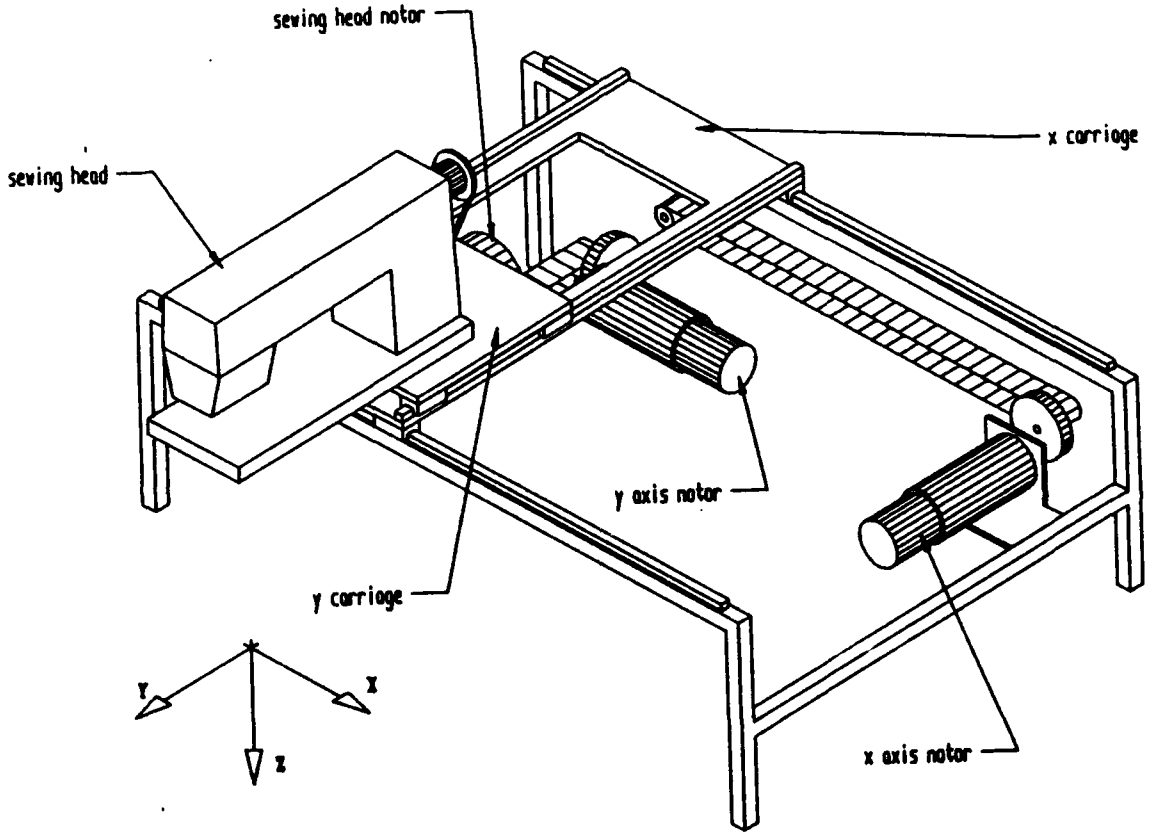

Figure 2.1. CNC stitcher configuration.

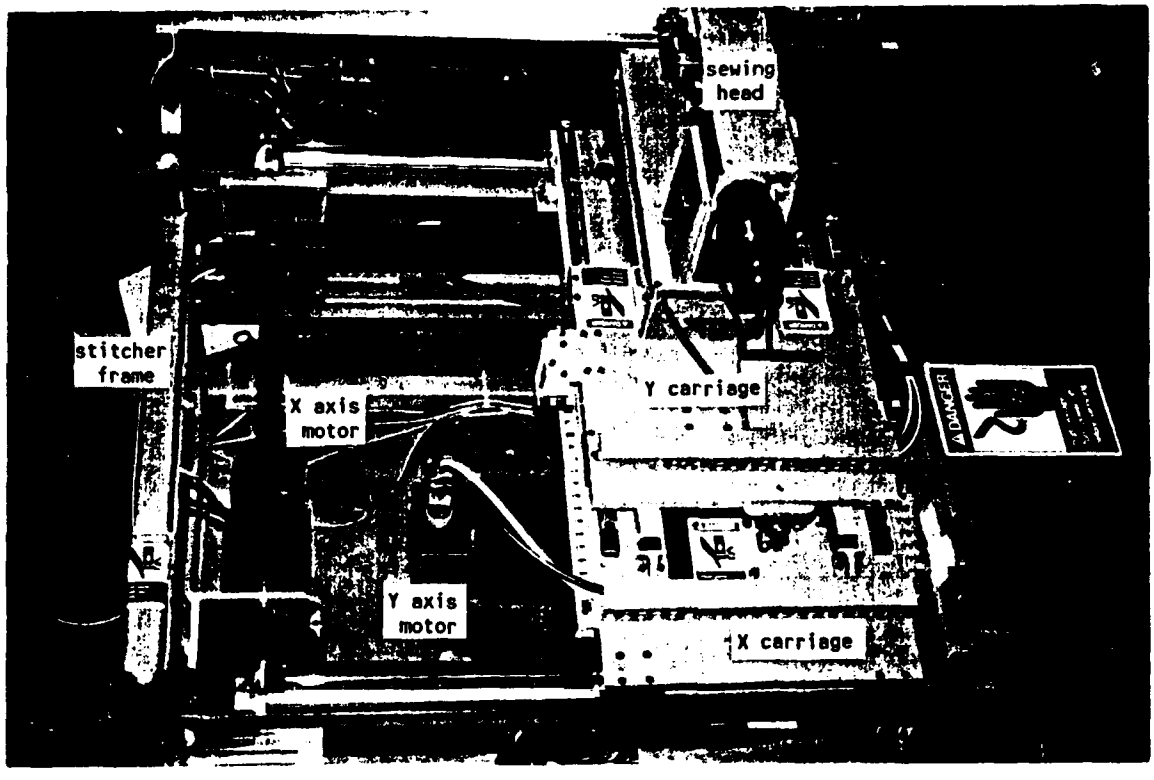

(a) The X and Y axes of the CNC stitcher.

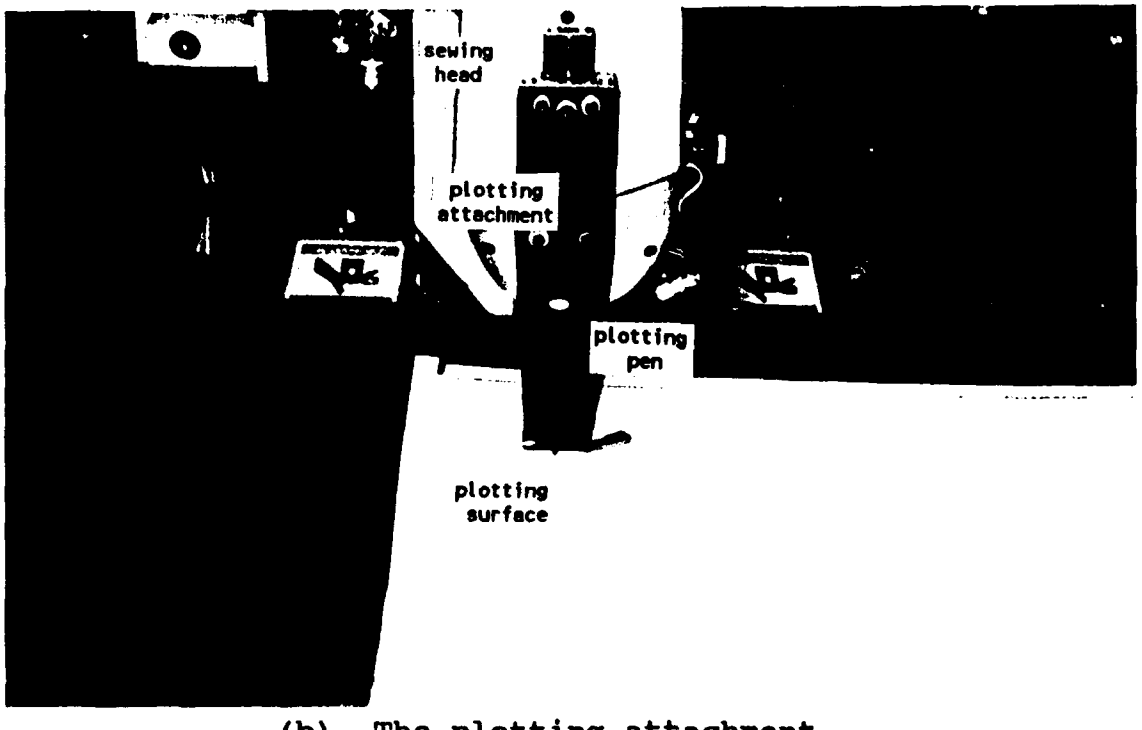

(b) The plotting attachment.

Figure 2.2. The CNC stitcher.

centered on Y-carriage. A plotting pen can be attached to the sewing head to track the X-Y carriage position during operation, as shown in Figure 2.2b.

Drive System

Each brushless DC servomotor has an integrally mounted incremental optical encoder. The motors have a 60 in-lb stall torque and a maximum speed of 4000 rpm. The encoders are TTL compatible with 2000 line counts and three channels: A, B and Index.

The various functions of the drivers are set or monitored by the user via an RS-232 serial port. The functions include: amplifier tuning, changing the operating mode, setting limit values, monitoring certain variables and obtaining diagnostic information. All of the settings are stored in nonvolatile static RAM.

The amplifier can operate in one of four modes: velocity control mode, torque control mode, manual amplifier tuning mode or automatic amplifier tuning mode. The normal operating mode of the amplifiers is the velocity control mode. They must be tuned using the manual tuning mode due to the flexibility of the timing belts. In the automatic tuning mode, the motors are stepped forward and backward at a user defined frequency and motor speed while an internal algorithm is used to set the gains for proper operation. This mode cannot be used with flexible transmissions such as the timing belts due to the phase difference between the motor shaft and the load caused by the flexibility. Therefore, the automatic

tuning mode is only applicable with relatively stiff transmission systems.

One port on each driver can be programmed through the RS-232 interface to output a voltage proportional to one of the following system variables: the current drawn by the motor, the motor speed, the motor position, the command signal, or the current limit. The signal can be observed using an oscilloscope or other readout instrument. The equipment list for the drive system is shown in Appendix A.

Servo Controller

The stitcher is controlled by a two axis PC mounted motion control board. The host microprocessor is used for memory, I/O functions and, in some operations, velocity profile generation. Closed loop control is achieved by a separate motion control integrated circuit (IC) on the board.

Controller Design

The motion control IC is designed for single input single output systems. The internal block diagram of the IC in Figure 2.3 shows that the reference signal and feedback signal are summed and compensated through a digital filter defined as a discrete transfer function D(z). The resulting command can be used to drive a linear amplifier through the motor command port or a pulse width modulated (PWM) amplifier through the PWM port. The sample timer sets the sampling time, T_s.

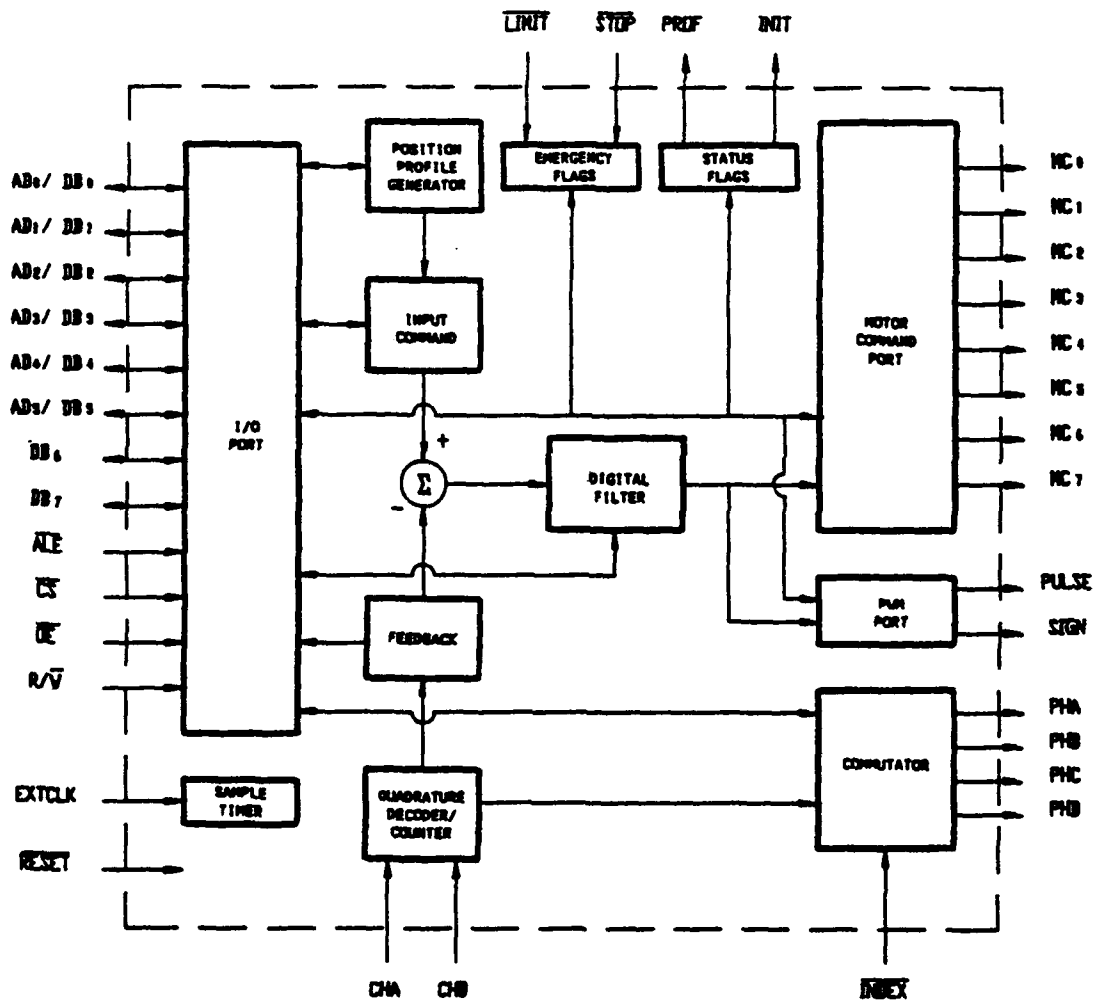

Figure 2.3. The internal block diagram of the motion control integrated circuit.

The digital filter is designed with the form

$$D(z) = K\left(\frac{z-A}{z+B}\right). \qquad (2.1)$$

The locations of the pole and zero in the digital filter are programmable by the user. It is implemented in the time domain as:

$$u(n) = K[e(n) - Ae(n-1)] - Bu(n-1), \qquad (2.2)$$

where n is the sampling instant, u is the command signal and e is the error signal.

Controller Operation

The motion control IC can operate in the following four control modes:

1. position control - controls point to point positioning without using the velocity profile generator;
2. proportional velocity control - controls the motor speed using only the proportional gain of the filter;
3. integral velocity control - performs continuous velocity profiling using velocity and acceleration limits specified by the user; and
4. trapezoidal profile control - controls point to point positioning using the velocity profile generator.

The motion control IC is set in the position control mode during the sewing operation of the stitcher.

Control system tuning is accomplished using the tuning program MC provided with the control card. The MC program performs three basic functions: (1) it allows the user to set various registers in the motion control chip, including the

THIS PAGE IS MISSING IN ORIGINAL DOCUMENT

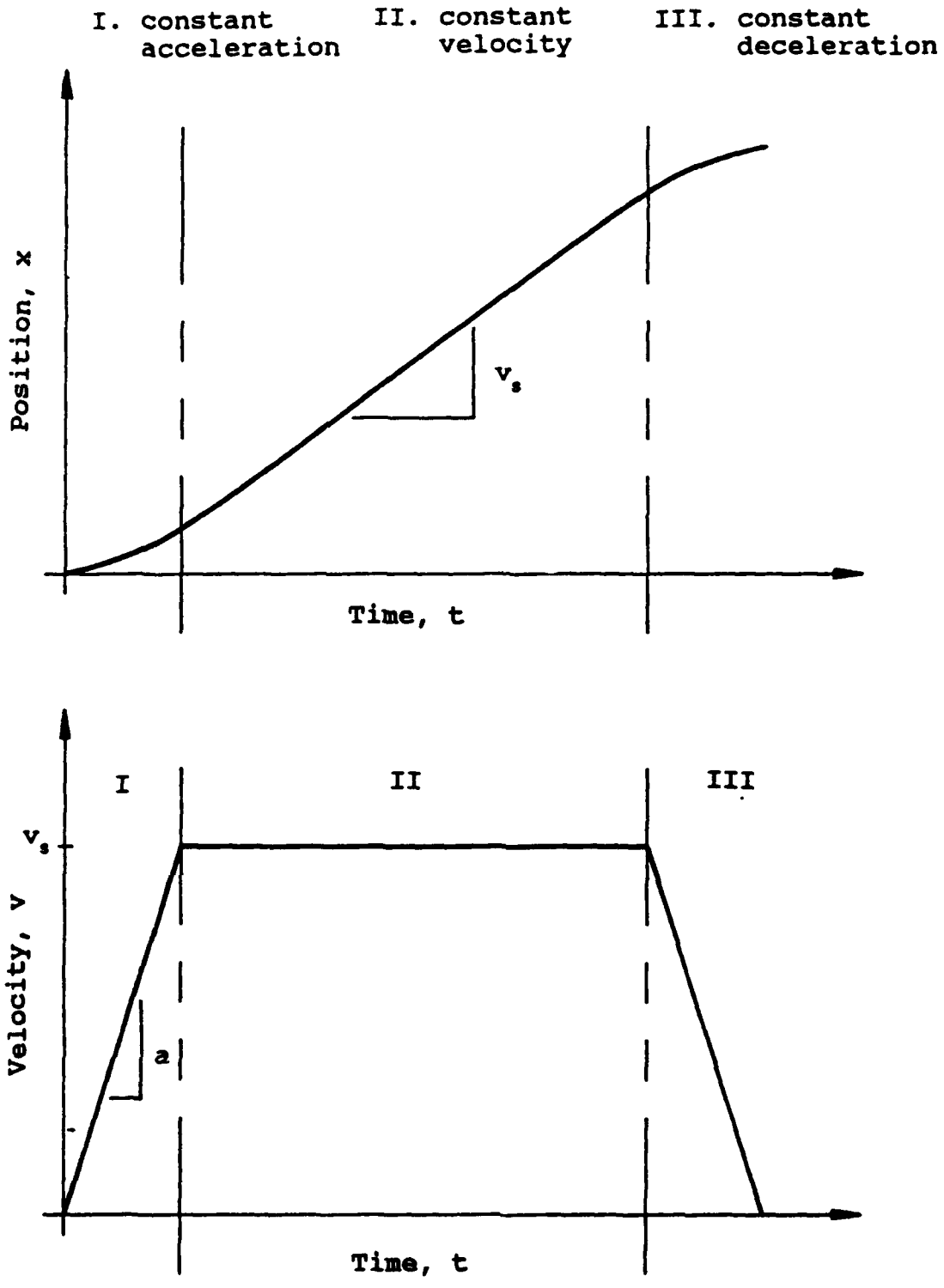

Figure 2.4. General motion profiles of the reference signal.

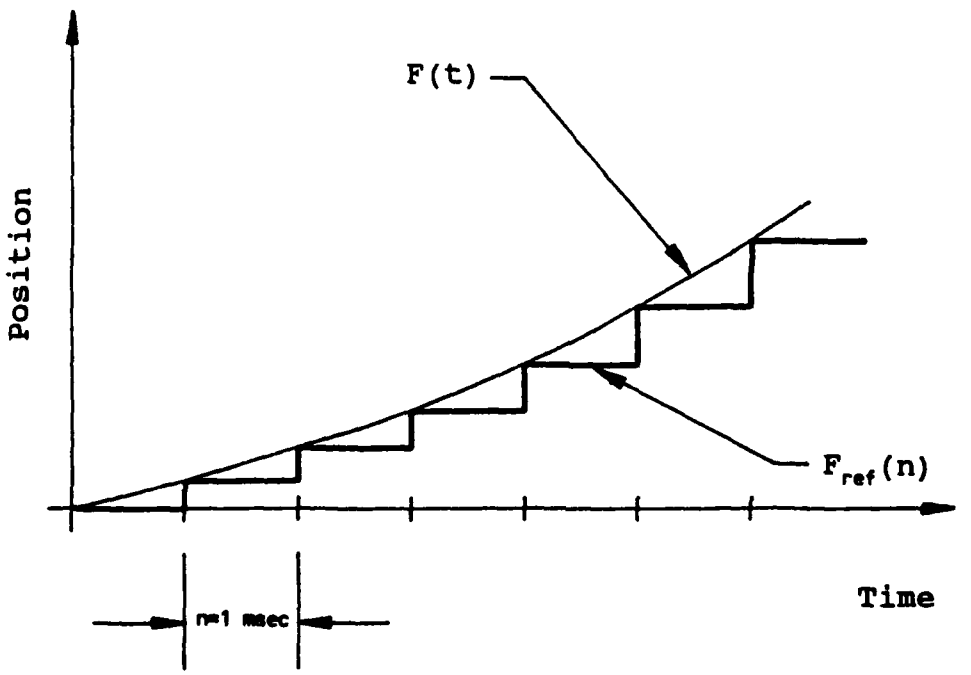

Figure 2.5. The digital approximation of the position function of the reference signal.

Therefore, the distance between each point in time is 1 millisecond and the spacial distance between each discrete command depends on the slew velocity and the acceleration specified by the user. The motion profile is generated by QuickScript using a host microprocessor rather than the profile generator in the motion control IC.

Two types of two axis coordinated motion are possible in following a stitch path consisting of several segments: discrete coordinated motion and interpolated motion. In discrete coordinated motion, each movement of the axes begins when the previous movement has ended. For instance, the stitcher begins stitching line segment B in the stitch path in Figure 2.6a when it has completed line segment A. The reference path for this case, shown in Figure 2.6b, is the same as the stitch path from which it was generated. In interpolated motion, the stitcher begins following line segment B in the stitch path in Figure 2.6a when deceleration begins in line segment A. The resulting reference path has "rounded" corners as shown in Figure 2.6c. Typical position reference signals for the X and Y axes for these two types of motion are shown in Figure 2.7.

Performance Requirements

The performance requirements of the stitcher are based on the quality requirements of the sewn product. The quality of a garment is greatly influenced by two sewing attributes: uniformity of stitch length and stitch location.

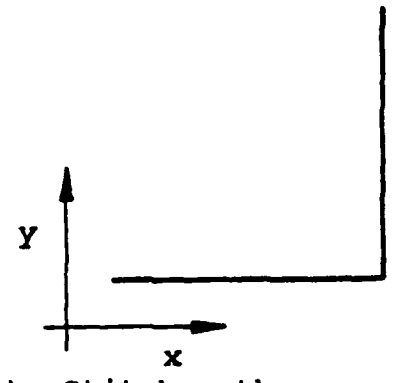

(a) Stitch path.

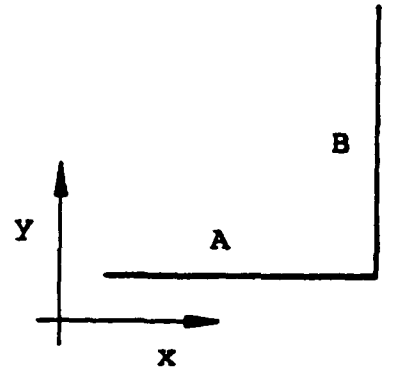

(b) Reference path using discrete coordinated motion.

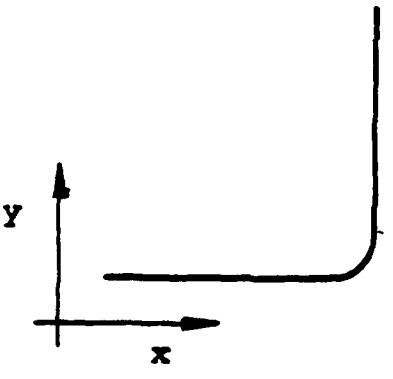

(c) Reference path using interpolated motion.

Figure 2.6. The stitch path and reference signals.

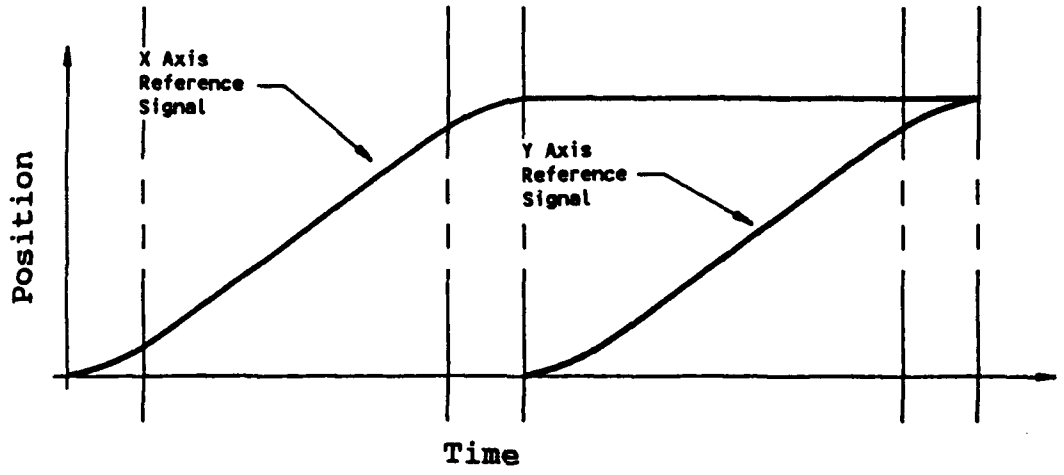

(a) Reference signal generated using discrete coordinated motion.

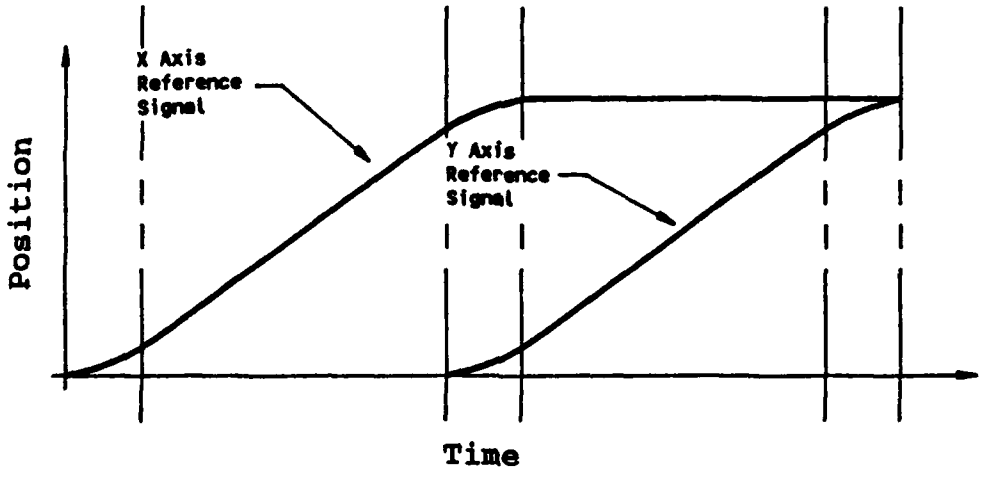

(b) Reference signal generated using interpolated motion.

Figure 2.7. Reference signals for each axis.

The operating velocity of the sewing head is determined by the speed of the sewing motor, N_s, which sews one stitch per revolution, and the desired stitch length using the following relation:

$$V_h = N_s L_s, \tag{2.3}$$

where N_s is the sewing motor speed in (stitch/sec), L_s is the stitch length in (in/stitch) and V_h is the sewing head velocity in (in/sec). The maximum speed of the sewing motor on the CNC stitcher is 75 stitches per second, and the maximum stitch length used in the apparel industry is approximately 0.1 inches. Therefore, the maximum operating velocity of the sewing head is 7.5 (in/sec) for the stitcher.

The stitch length must be maintained within ±5% of the desired stitch length during constant velocity commands. Therefore, the operating velocity must be maintained within ±5% of the setpoint, which is difficult when sewing around sharp corners. For instance, if the reference path consists of a right angle, with one segment parallel to the X-axis and one parallel to the Y-axis, the sewing head must decelerate from the operating velocity to rest in one axis and accelerate from rest to the operating velocity in the other. The sewing motor also must be decelerated and accelerated to keep the stitch length constant in this process. However, the quality specifications in the apparel industry allow the two stitches sewn immediately before the corner and the two stitches sewn immediately after the corner to be of different lengths. Since the sewing motor in the CNC stitcher is run

at a constant speed, the sewing head must accelerate and decelerate within two stitches, or at a rate of approximately 281 (in/sec^2) when the motor speed is 75 stitches/sec and the stitch length is 0.1 inches.

The accuracy required in the stitch placement was determined by measuring the accuracy of a commercial stitcher made by Adler (model 973-S-204-3). The stitch path for collars sewn by the Adler machine were compared to the commanded path used to generate the desired stitch path. Figure 2.8 shows the maximum error orthogonal to the stitch path to be 0.5 mm (0.02 in). This accuracy was adopted as a performance requirement for the CNC stitcher being developed in this project.

In the normal operation of the stitcher, interpolated motion will be used. Therefore, the acceleration will affect the stitch placement in the corners as well as the stitch length. The stitch path and reference path generated using interpolated motion are shown in Figure 2.9 for a right angle corner. The stitcher begins decelerating in the X axis and simultaneously begins accelerating in the Y axis at the initial time $t_i=0$ and $x=x_0$. The acceleration and deceleration ends at $t=t_f$ and $y=y_f$. The position of a point on the reference path at any given time is

$$x(t)=v_{x0}t-\frac{1}{2}at^2 \qquad (2.4a)$$

in the X axis and

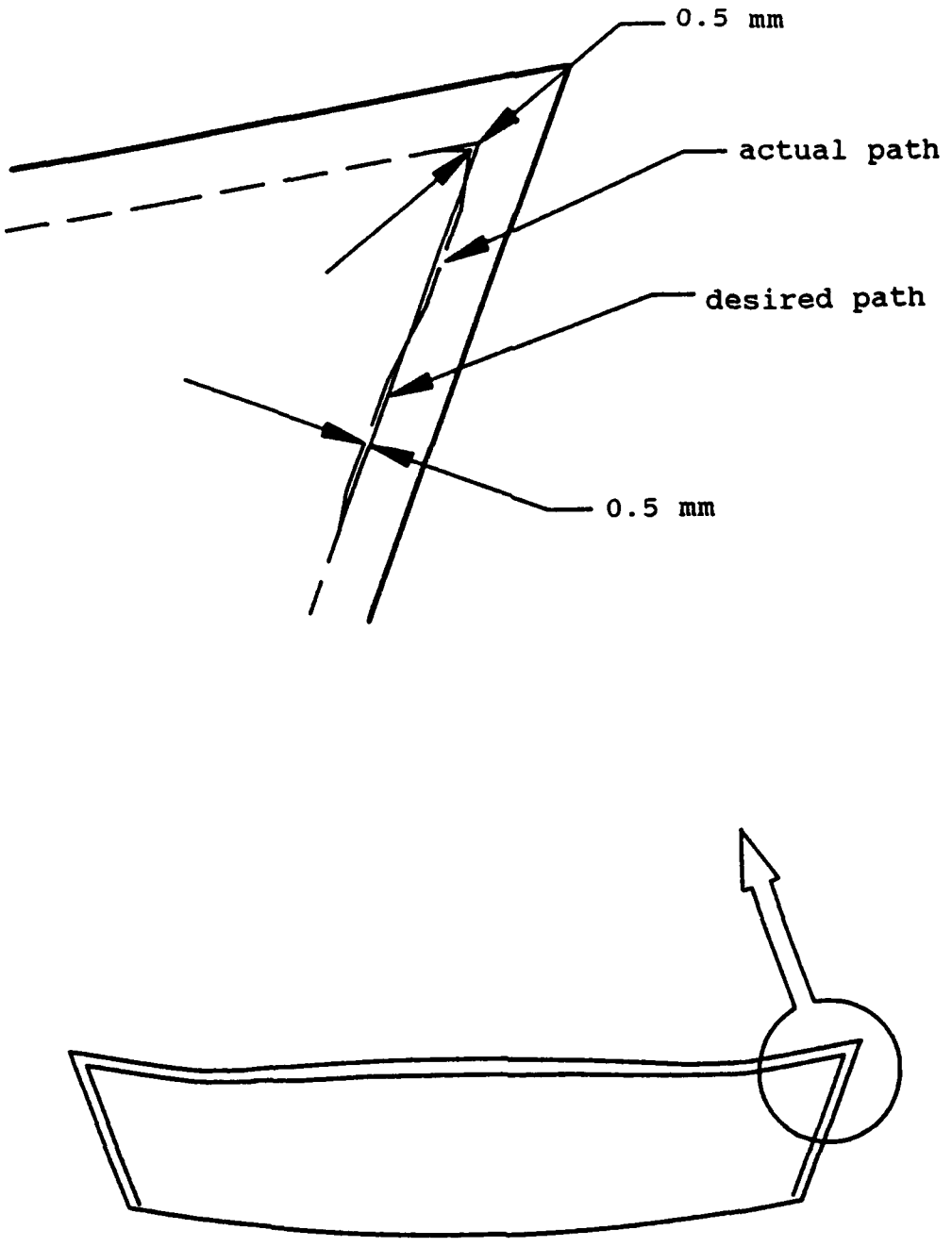

Figure 2.8. The position accuracy requirement of the stitcher for collar point sewing.

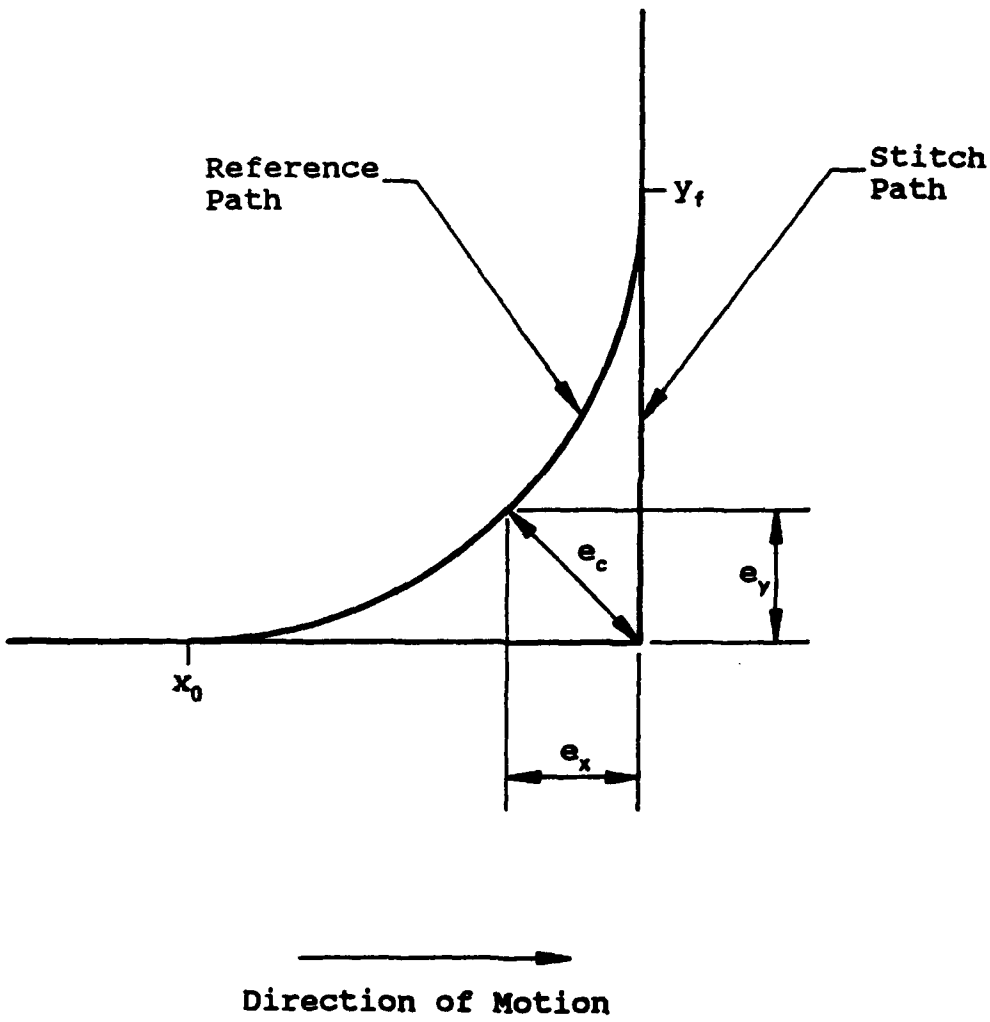

Figure 2.9. Errors associated with reference path generation using interpolated motion.

$$y(t)=\frac{1}{2}at^2 \tag{2.4b}$$

in the Y axis, where v_{x0} is the velocity in the X axis at x=0 and the acceleration set point, a, is constant. The error in each axis is

$$e_x(t)=\frac{v_x^2}{2a}-v_{x0}t+\frac{1}{2}at^2 \tag{2.5a}$$

and

$$e_y(t)=-\frac{1}{2}at^2. \tag{2.5b}$$

The maximum error between the stitch path and the reference path is in the radial direction of the reference path at the corner of the stitch path. It is defined as

$$e_c=\sqrt{e_x(t_m)^2+e_y(t_m)^2}, \tag{2.6}$$

where

$$\begin{aligned} t_m&=\frac{1}{2}(t_f-t_i) \\ &=\frac{v_s}{a} \end{aligned} \tag{2.7}$$

and v_s is the velocity setpoint. Substituting Equation (2.7) into Equation (2.6) and noting that the maximum error permissible is 0.02 inches, the required acceleration setpoint was found to be 546 (in/sec^2) when interpolated motion is used in a right angle corner. The error between the stitch path and the reference path increases as the angle of the corner decreases. However, most stitch lines sewn in the apparel

industry contain right angle corners rather than acute angle corners; therefore, a stitch path with a right angle corner was considered.

The performance requirements of the stitcher can be summarized as follows.

(1) The stitcher must be capable of operating with the sewing head moving at 7.5 (in/sec) and maintaining the velocity within ±5% of the velocity setpoint.

(2) The sewing head must accelerate to the operating velocity within two stitches, or at a rate of 281 (in/sec^2).

(3) The positioning accuracy of the stitcher must be within 0.02 inches (0.5 mm) of the commanded path.

CHAPTER III

SYSTEM MODELING

A linear model of the stitcher was developed based on the experimentally determined dynamic behavior of the stitcher. System nonlinearities were then introduced into a nonlinear model of the stitcher that was used for simulation of the stitcher to evaluate its tracking performance. Finally, the linear model was analyzed to determine the changes that may be made in the stitcher to improve its tracking performance. The experimental procedures used to determine the behavior of the stitcher and the results are described in detail in Appendix B.

Linear Model Development

Each axis of the CNC stitcher was conceptually divided into three subsystems, shown in Figure 3.1, to model the CNC stitcher: (1) the controller, (2) the actuating system, and (3) the load. The controller subsystem consists of the PC mounted motion control card. The actuating system consists of the amplifier, the motor and the rigid portion of the drive train, which includes the gear set and, in the case of the X axis, the drive shaft. The load subsystem consists of the sewing head, the timing belts and the stitcher frame. There is assumed to be no dynamic coupling between the two axes because of their orthogonal structural design; therefore, they were each modeled and analyzed independently.

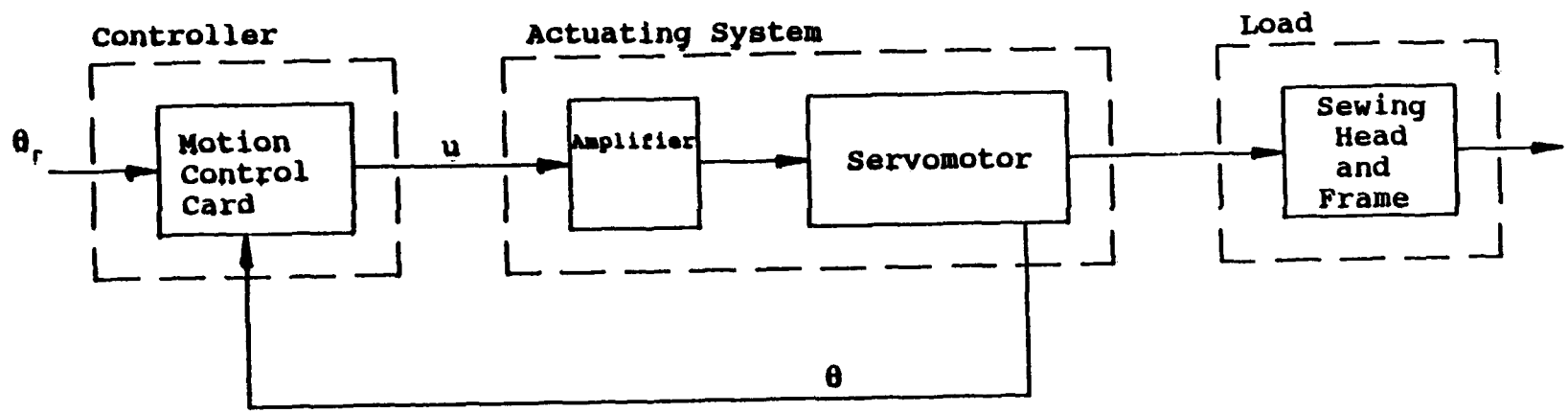

Figure 3.1. Subsystems of each axis of the CNC stitcher.

Actuating System Model

The actuating systems were mechanically separated from the stitcher by disconnecting the timing belts and removing the controller leads from the amplifier terminals. The frequency response of each open loop actuating system was then experimentally determined so that a mathematical model could be developed to match the experimentally determined frequency response of the system. Two simplifying assumptions were made in developing the model: (1) the brushless servomotors can be modeled as DC permanent magnet brush type motors and (2) there is no backlash or deadband in the gear sets.

Experimental Results

A two channel FFT analyzer was used to generate a swept sine input signal for the actuating systems, monitor the resulting motor shaft speed and generate the Bode plot of each system relating the amplifier input terminal voltage, u, and the motor speed, ω. The resulting Bode plots, normalized to the zero frequency gains, are shown in Figures 3.2a and 3.2b.

The actuating system steady-state gains were also determined for the open loop system by applying a constant voltage to the amplifier input terminals and measuring the resulting motor shaft speed. The gains were found to be 40 (rad/s/volt) for the entire operating range in each axis.

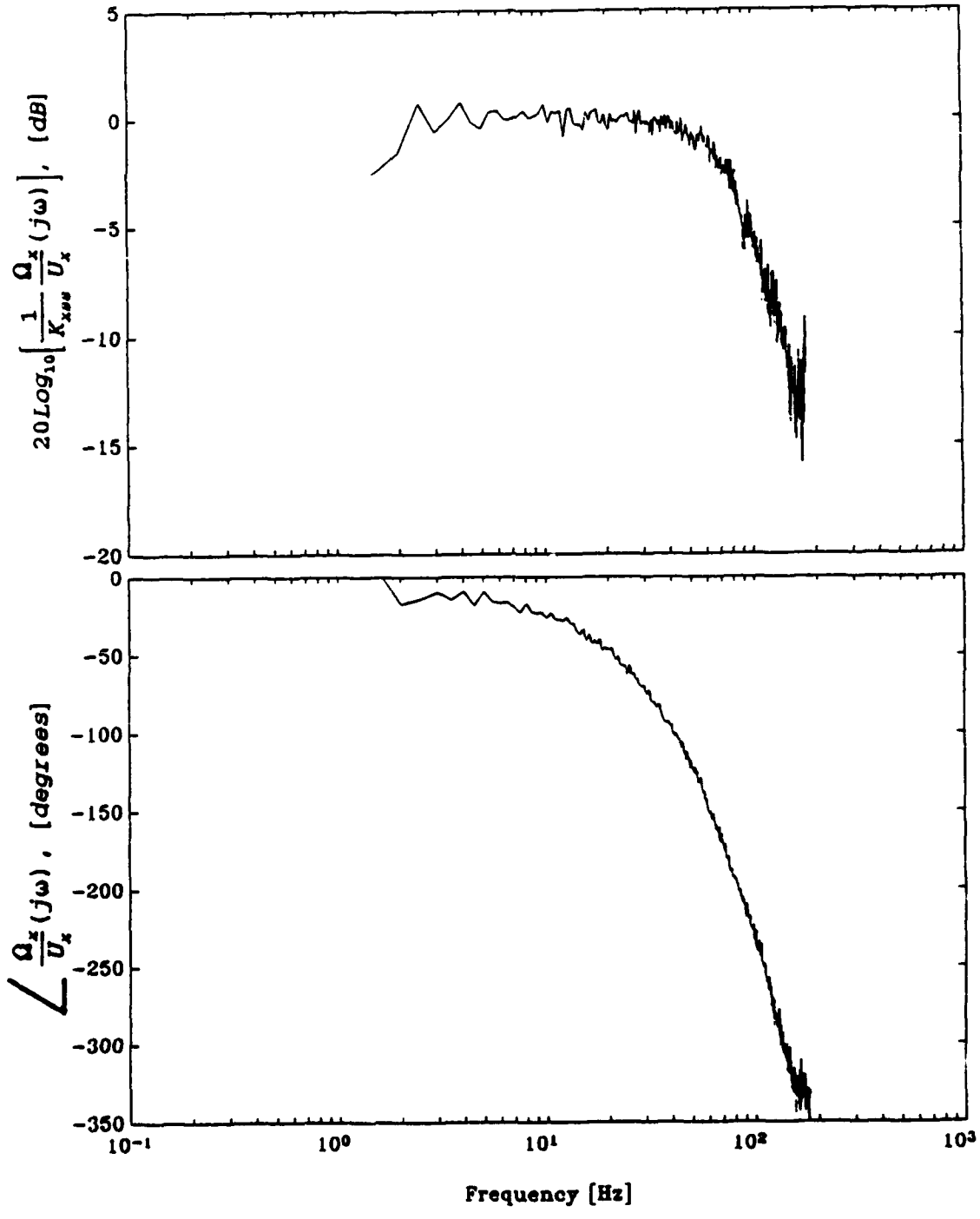

(a) X axis actuating system, $G_x(s)$

Figure 3.2. Open loop actuating system Bode plots.

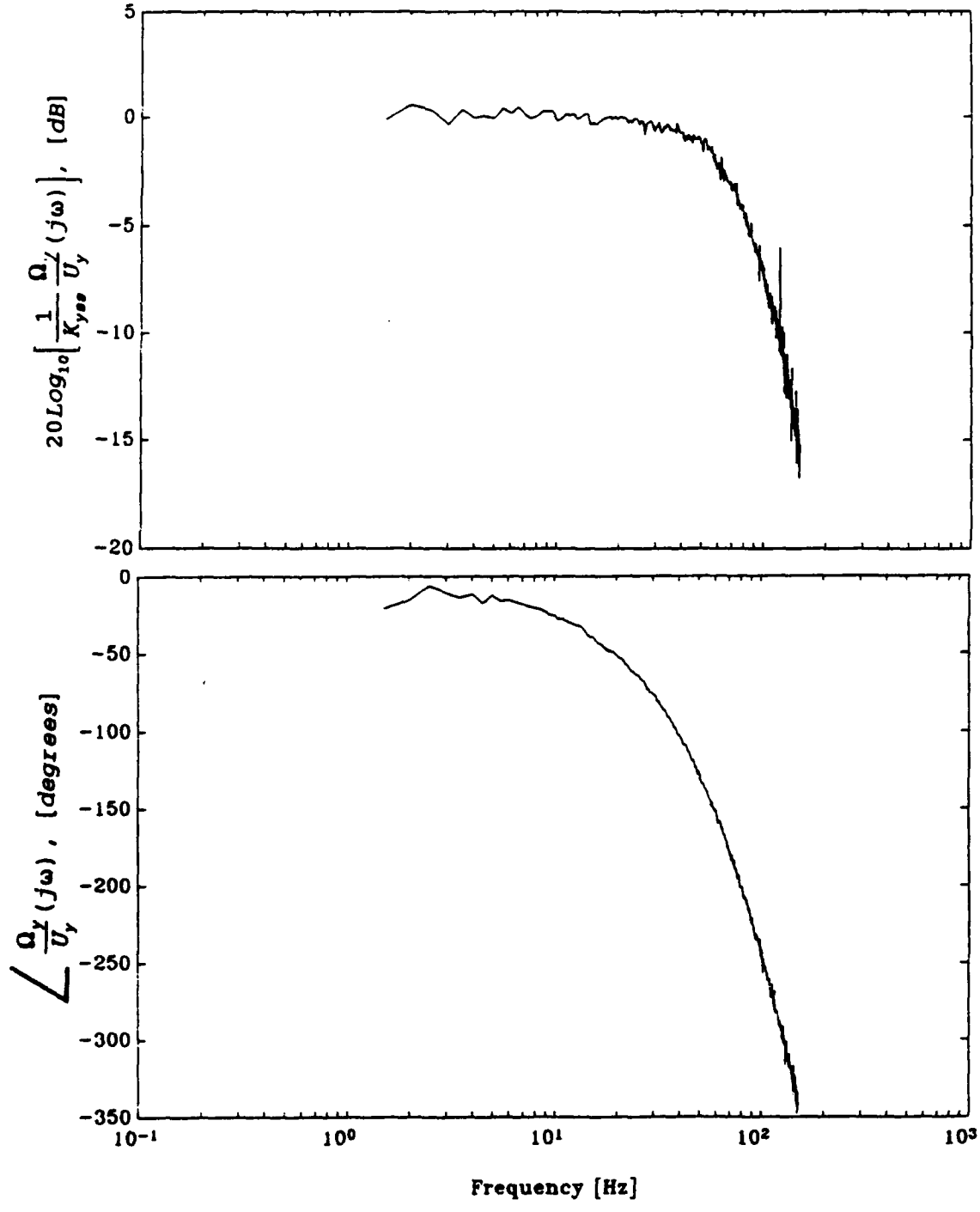

(b) Y axis actuating system, $G_y(s)$

Figure 3.2 (Continued).

Model Development

The magnitude portions of the Bode plots of the actuating systems indicate that each system is second order. However, the phase angle of each system approaches negative infinity at high frequencies instead of asymptotically approaching ϕ=-180° like a typical second order system. This indicates that a time delay is present in the amplifier. Therefore, each system was modeled as a second order system with a time delay. The time delay function, $e^{-\tau s}$, was approximated with a first order Padé approximation given by

$$e^{-\tau s} \approx \frac{2-\tau s}{2+\tau s} \tag{3.1}$$

where the delay time, τ, is 3 milliseconds. The determination of the time delay is discussed in Appendix C. The linear block diagram of the linear model of the actuating system used for each axis is shown in Figure 3.3. In the figure, J_m is the inertia of the motor rotor and the rotating elements of the system, B_m is the equivalent viscous friction coefficient and Ka is the amplifier gain. The electrical parameters, Kt, Kv, R and L, were obtained from the manufacturer's data as found in Appendix A, and the pulley radius, r, is 1.16 inches (29 mm).

The transfer functions of the X axis actuating system, $G_{ax}(s)$, and the Y axis actuating system, $G_{ay}(s)$, were found to be

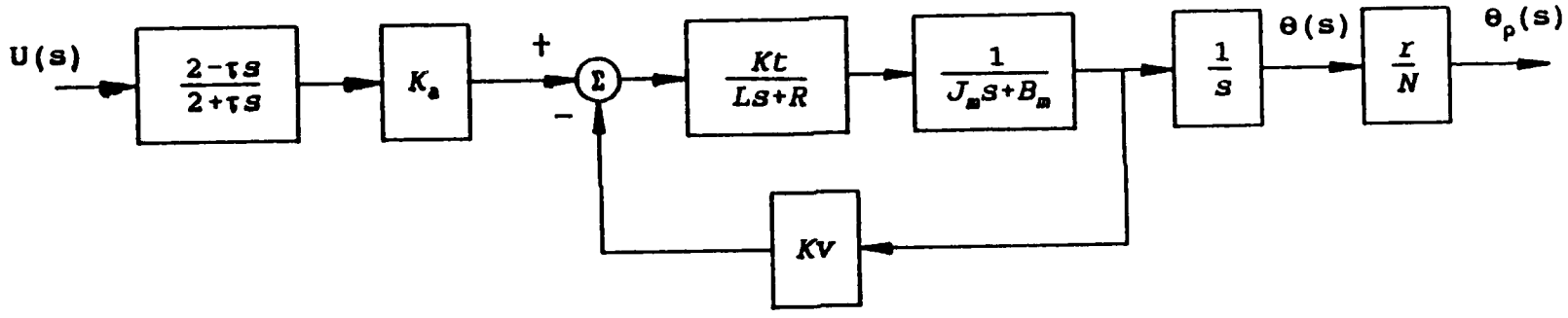

Figure 3.3. General block diagram of each actuating system.

$$G_{ax}(s) = \frac{\Omega_x}{U_x}(s) = \frac{1.1E7(667-s)}{(s+667)(s+353+356j)(s+353-356j)} \qquad (3.2a)$$

and

$$G_{ay}(s) = \frac{\Omega_y}{U_y}(s) = \frac{6.5E6(667-s)}{(s+667)(s+279+286j)(s+279-286j)} \qquad (3.2b)$$

using the methodology described in Appendix C. The frequency response magnitude of each transfer function was normalized by dividing it by the zero frequency gain as shown in the Bode plots in Figures 3.4 and 3.5. The natural frequency and bandwidth of the X axis actuating system is approximately 80 Hz (500 rad/sec) and the damping ratio is 0.7. The natural frequency and bandwidth of the Y axis actuating system is approximately 64 Hz (400 rad/sec) with a damping ratio of 0.7. The accuracy of the phase angle of the model deteriorates at high frequencies because a first order approximation of the time delay is used rather than the exact time delay function.

Load Model

The load was connected to the actuating systems with the timing belts in both axes of the stitcher. The frequency response of the actuating system/load combination of each axis was experimentally determined, and the parameters of the load model were adjusted so that the Bode plot of the actuating system/load model compared favorably with that of the actual system.

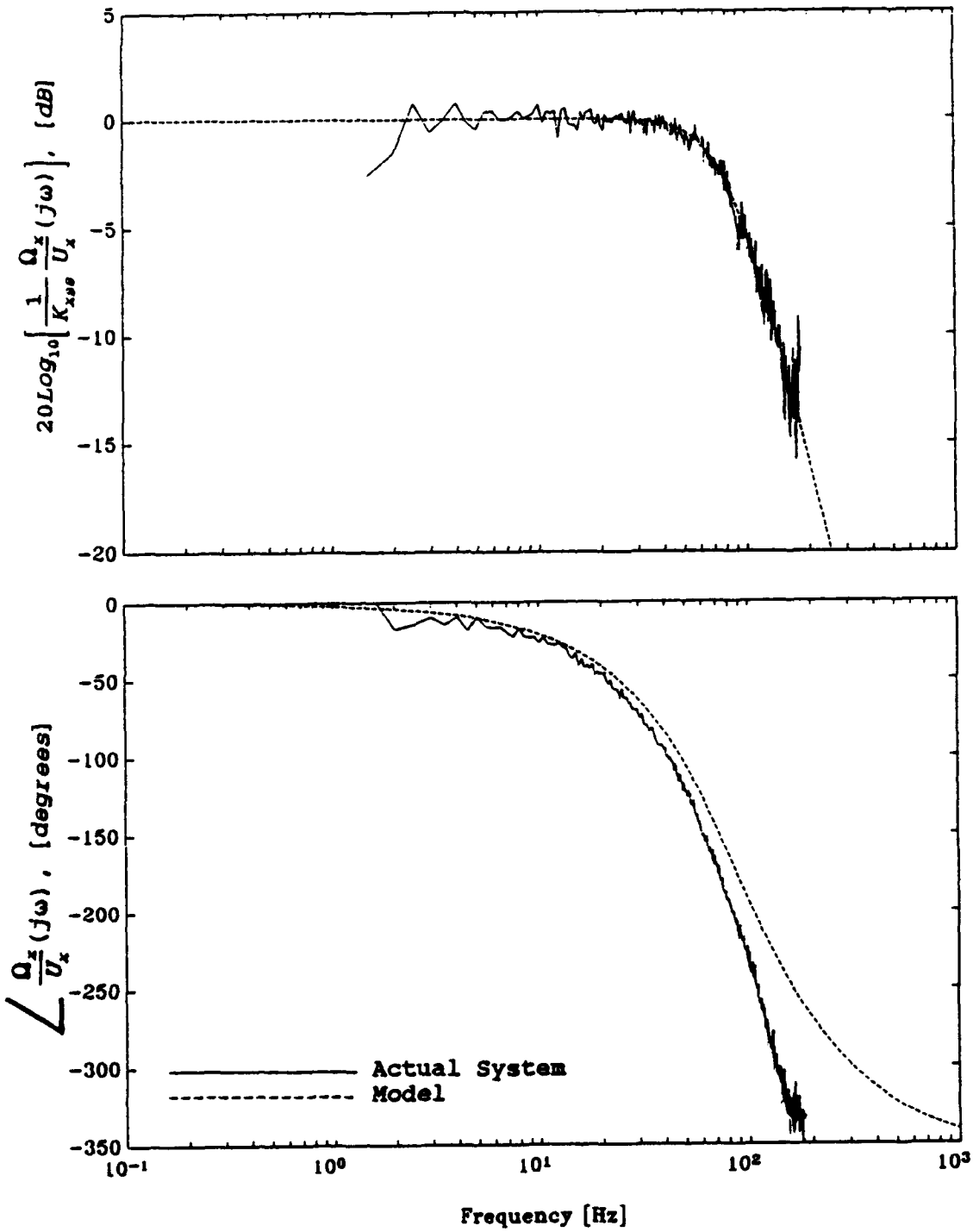

Figure 3.4. X axis actuating system Bode plots, actual system and model.

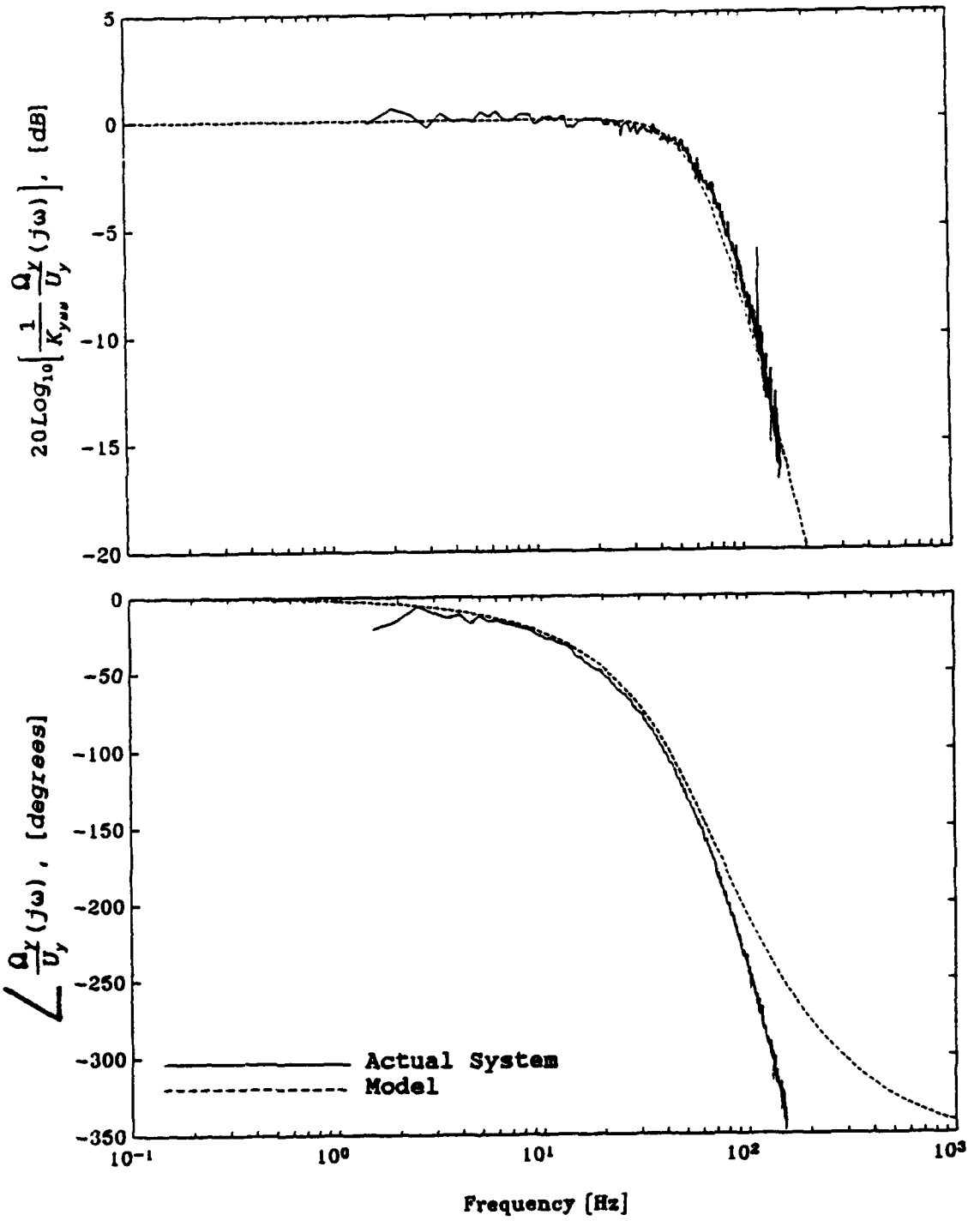

Figure 3.5. Y axis actuating system Bode plots, actual system and model.

Experimental Results

The FFT analyzer was used to determine the open loop frequency response of the actuating system/load combinations. The resulting Bode plots shown in Figures 3.6 and 3.7 were normalized to the steady state gains by dividing the magnitude plots by the zero frequency gains. The experimental procedure used to determine the frequency response and the results are presented in Appendix B.

X Axis Load Model Development

The simplified representation of the X axis used in modeling is shown in Figure 3.8a. This representation consists of a mass attached to a timing belt driven by a servomotor through a speed reducing gear set. The experiment performed on the X axis indicated that the load dynamics can be represented by a second order lumped parameter model as shown in Figure 3.8b. This lumped parameter model consists of a mass attached to an actuating pulley through a series of springs that are used to model the timing belt elasticity.

The experiment described in Appendix B that was performed to determine the nonlinear effects of the timing belt showed that the belt may be represented by a linear spring that acts in tension and compression. Therefore, the lumped parameter model of the X axis may be simplified as shown in Figure 3.9a. The analytical development of this simplification is presented in Appendix C. The free body diagram of the mass in Figure 3.9b shows θ_{px} as the pulley position and θ_x, with $\theta_x = N\theta_{px}$, as the motor shaft angular position. The

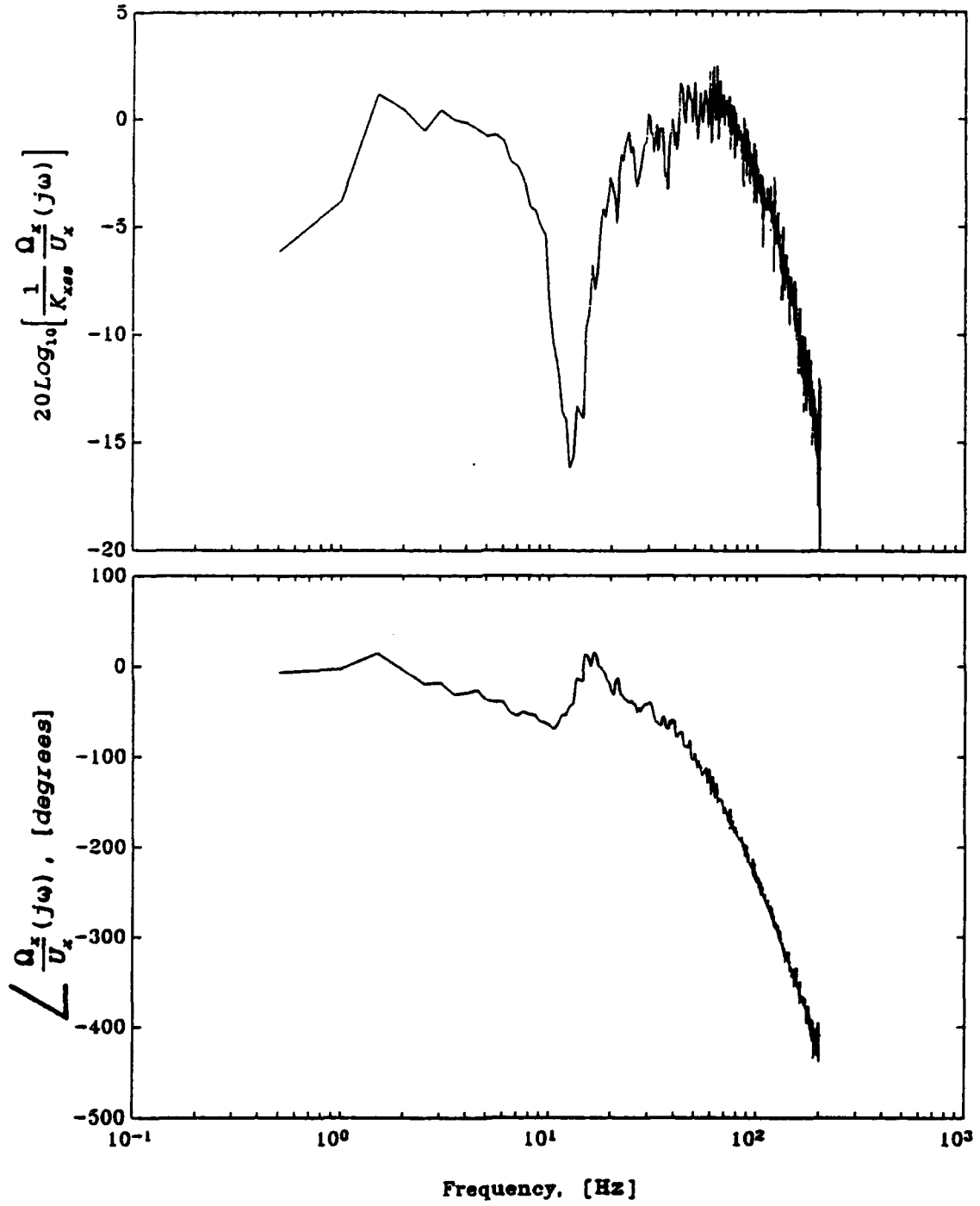

Figure 3.6. X axis actuating system/load Bode plot.

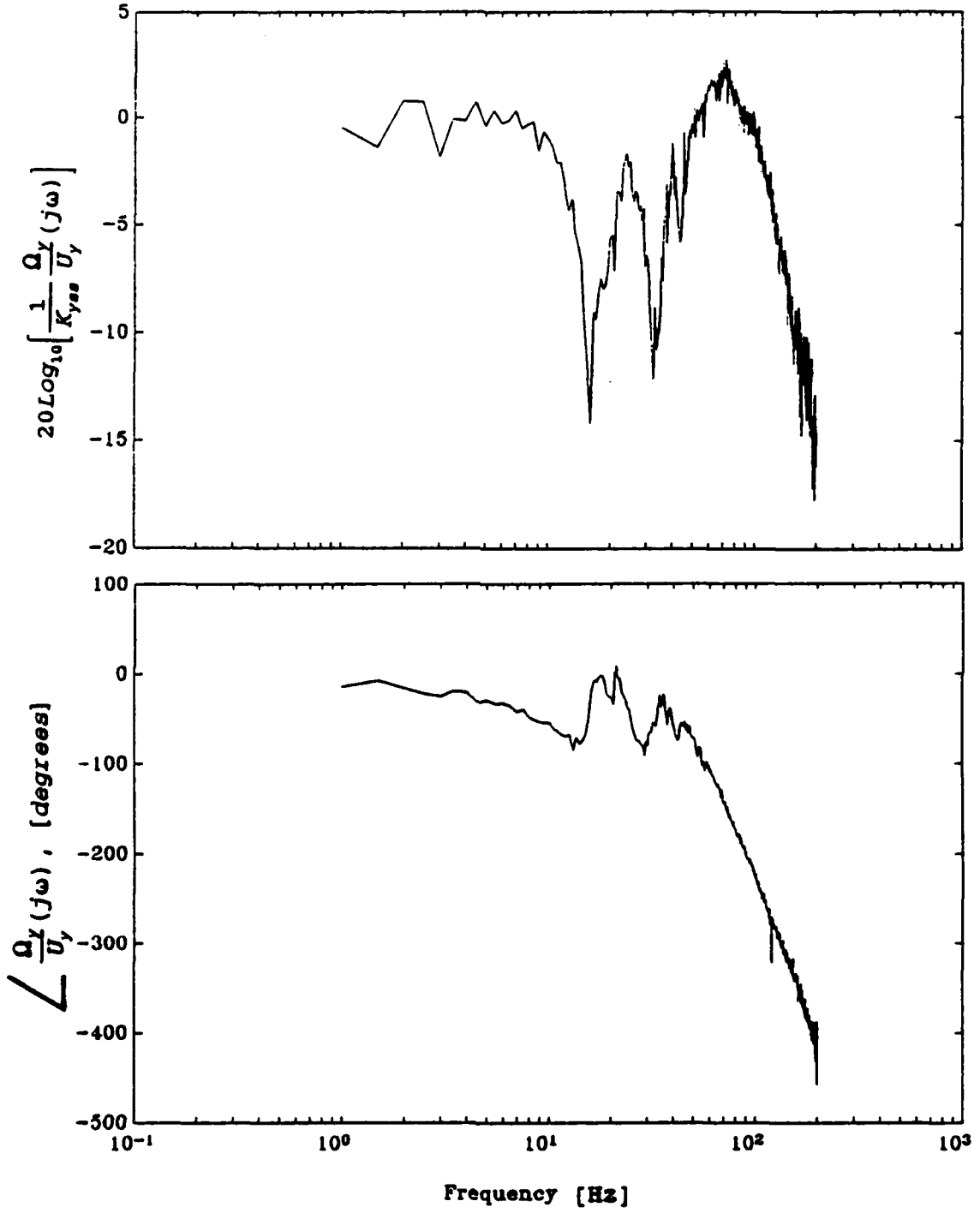

Figure 3.7. Y axis actuating system/load Bode plot.

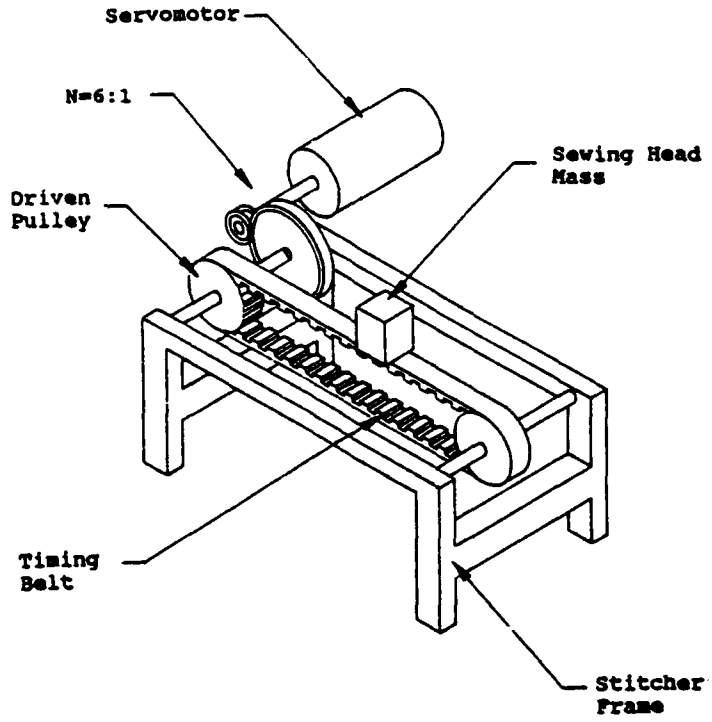

(a) The simplified representation of the axis.

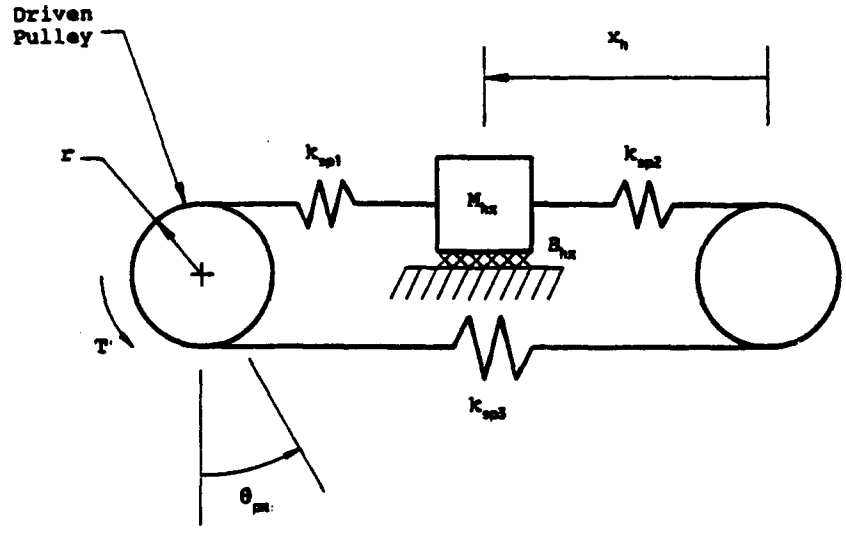

(b) The lumped parameter model of the axis.

Figure 3.8. The X axis model.

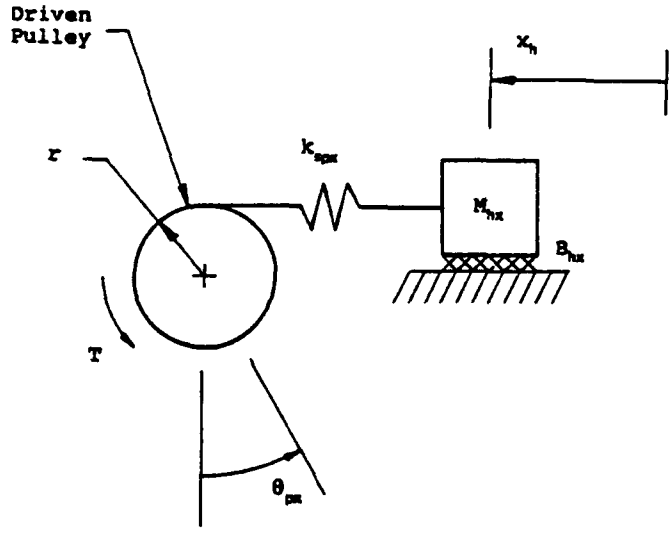

(a) The lumped parameter model with a linear spring.

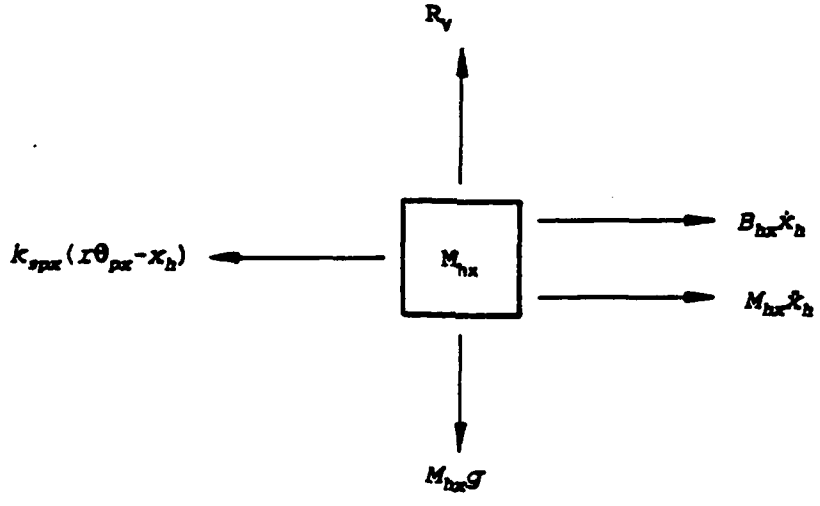

(b) The mass free body diagram.

Figure 3.9. The X axis load lumped parameter model and free body diagram.

equation of motion describing the motion of the mass is given by

$$M_{hx}\ddot{x}_h = k_{spx}\left(\frac{r}{N}\theta_x - x_h\right) - B_{hx}\dot{x}_h \qquad (3.3)$$

where k_{spx} is the spring rate, M_{hx} is the mass, B_{hx} is the equivalent viscous friction coefficient and x_h is the sewing head (mass) position.

The load and actuating system models were combined as shown in Figure 3.10a to form the X axis model. The block diagram is rearranged in Figure 3.10b to illustrate the transfer function $G_x(s)$ relating the motor shaft angle, θ_x, and the amplifier input terminal voltage, U_x. The mass of the load was measured directly; therefore, the spring constant of the timing belt could be determined directly from the resonant frequency of the load seen in the Bode plot. The value of the viscous damping coefficient was then adjusted such that the Bode plot of $sG_x(s)$ approximates the actual system Bode plot. The mass, damping and stiffness were estimated to be:

M_{hx} = 111 kg,

k_{spx} = 6.24E5 N/m and

B_{hx} = 3330 kg/sec.

The methodology used to determine the values is described in Appendix C.

The experimentally determined Bode plot of the X axis and the Bode plot of the model using the above parameters of the model are shown in Figure 3.11. The frequency response

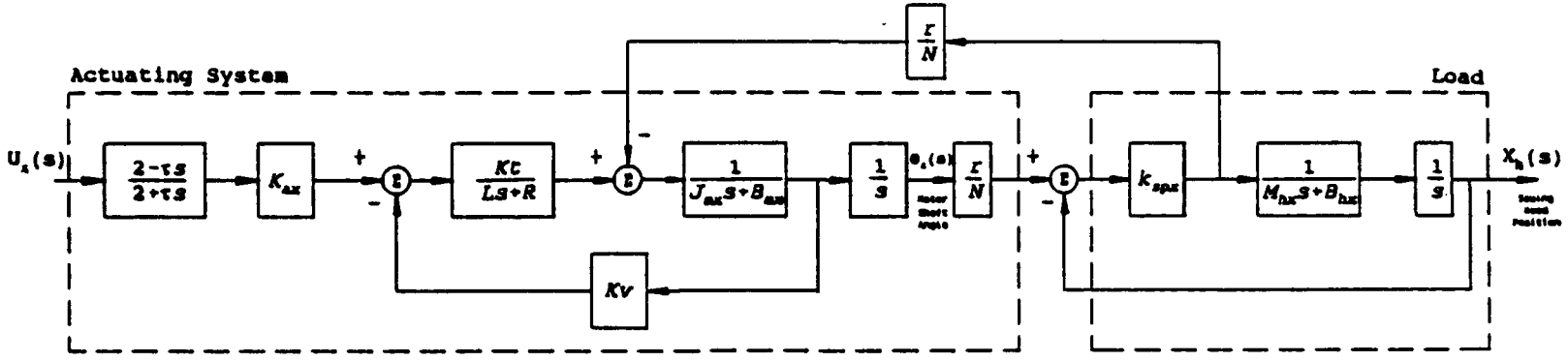

(a) Block diagram illustrating X_h/U_x.

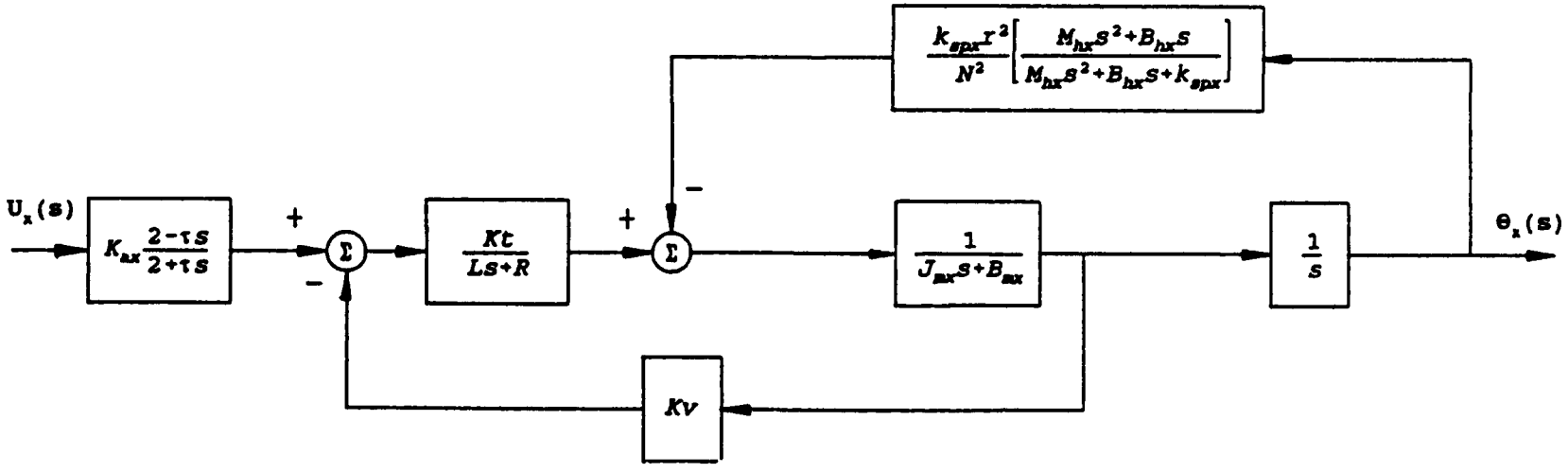

(b) Block diagram illustrating θ_x/U_x.

Figure 3.10. X axis actuating system/load block diagrams.

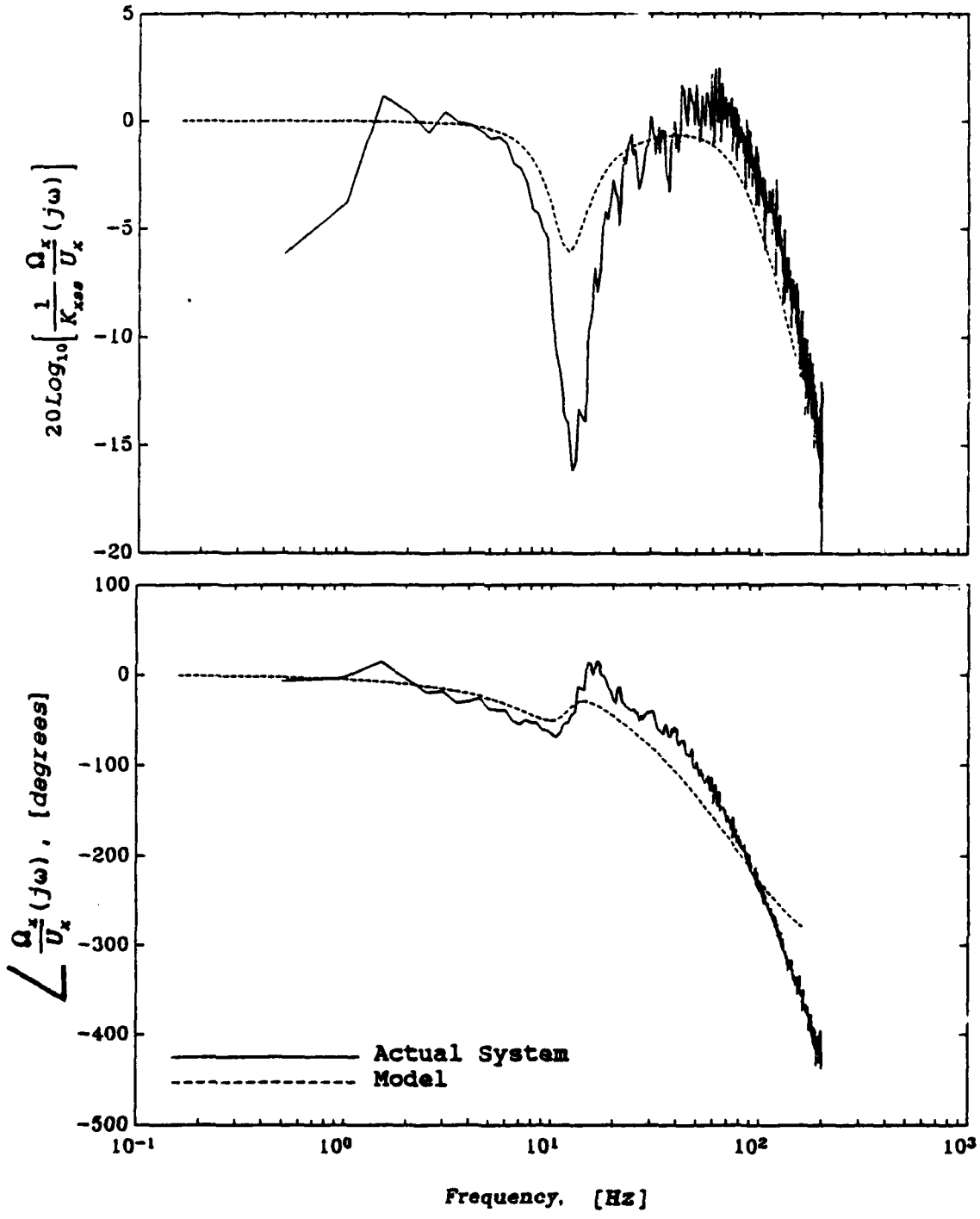

Figure 3.11. X axis actuating system/load Bode plots, actual system and model.

magnitude of the model was normalized to the zero frequency gain to match the actual frequency response. The resonant peaks in the experimental data and in the model occur at the same frequencies. However, slight differences are present between the Bode plots due to nonlinearities and unmodeled higher order dynamics in the system.

Y Axis Load Model Development

Experimentation performed on the Y axis showed that the dynamics of the load are described by two resonant frequencies. Therefore, the Y axis load must be modeled by two masses. One resonance is due to the mass attached to the timing belt, as in the case of the X axis, while the other is due to the vibration of the stitcher support frame in the Y direction. The lumped parameter model of the Y axis load is shown in Figure 3.12. The mass of the sewing head and its supporting structure is represented by M_{hy} and the timing belt elasticity is represented by the spring k_{spy}. The timing belt in the Y axis was modeled as a linear spring, as in the case of the X axis. The development of the approximation is presented in Appendix C. The mass of the stitcher frame is represented by the mass M_{fy} while the frame flexibility is modeled as the spring k_{fy}. The free body diagrams of the masses in the lumped parameter model are shown in Figure 3.13. The following differential equations describing the sewing head displacement, y_h, the stitcher frame displacement, y_f, and the motor shaft angle, θ_y, were determined from the free body diagrams:

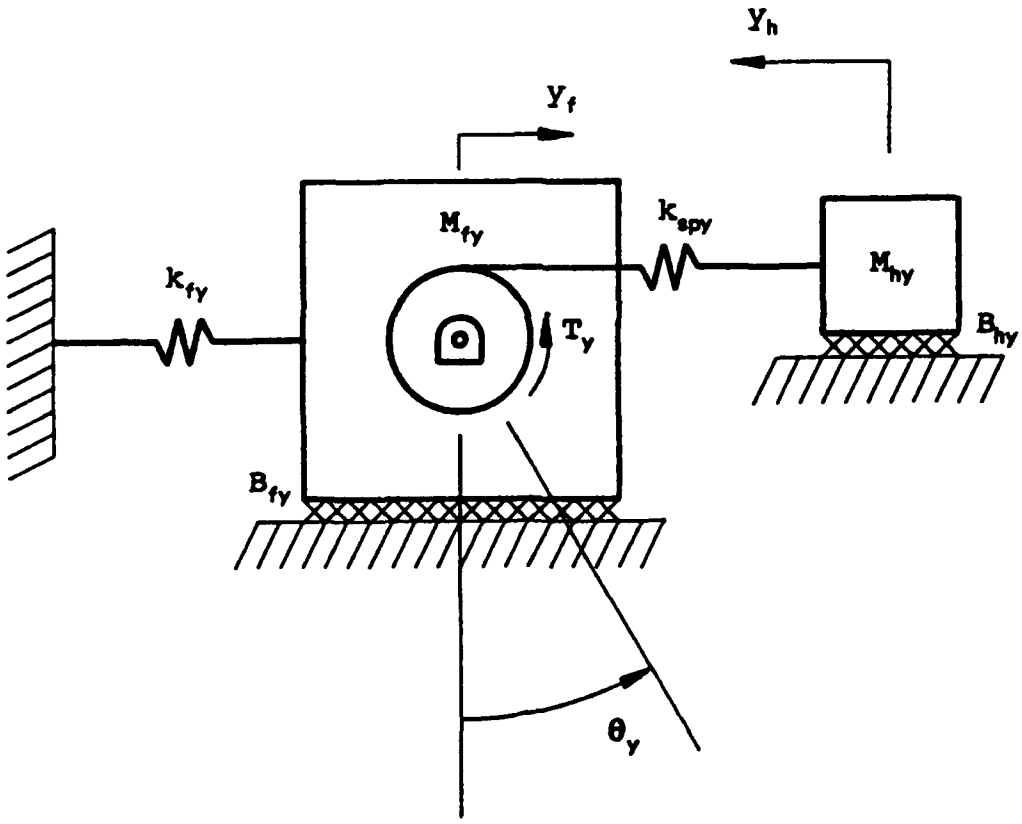

Figure 3.12. Y axis lumped parameter model.

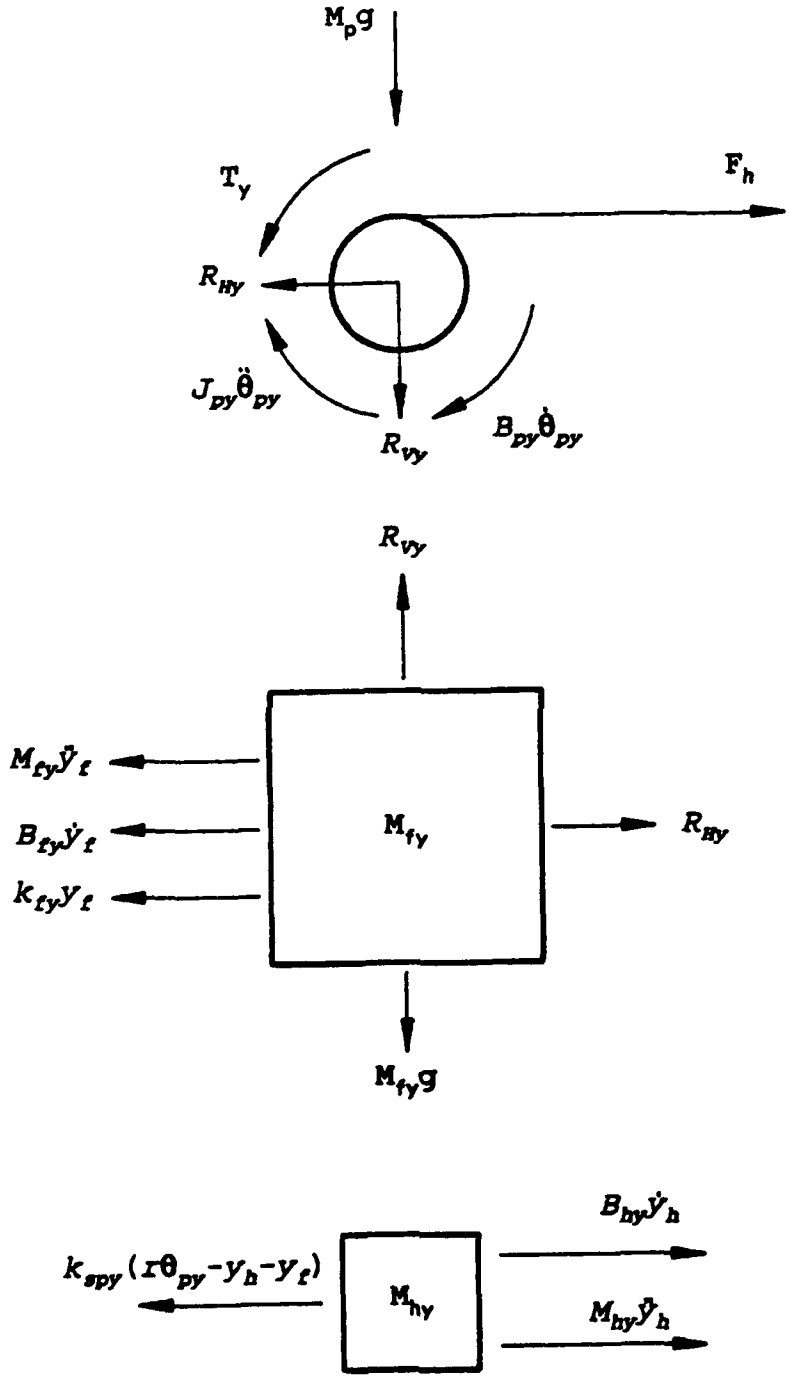

Figure 3.13. Y axis load free body diagrams.

$$M_{hy}\ddot{y}_h = k_{spy}\left(\frac{r}{N}\theta_y - y_h - y_f\right) - B_{hy}\dot{y}_h \qquad (3.4a)$$

and

$$M_{fy}\ddot{y}_f = k_{spy}\left(\frac{r}{N}\theta_y - y_h - y_f\right) - B_{fy}\dot{y}_f - k_{fy}y_f \ . \qquad (3.4b)$$

The block diagram formed by the combination of the actuating system and load models is shown in Figure 3.14a and rearranged in Figure 3.14b to illustrate the transfer function $G_y(s)$ that relates the motor shaft position, θ_y, to the amplifier input terminal voltage, U_y. The mass of the load, M_{hy}, was measured directly as in the case of the X axis and the value of M_{fy} was determined based on the known mass of the X and Y axis loads and the shipping weight of the entire stitcher. The values of the spring constants and viscous damping coefficients were then adjusted on a trial and error basis such that the Bode plot of $sG_y(s)$ approximates the actual system Bode plot. The mass, damping and stiffness values were estimated to be:

M_{hy} = 70 kg,

B_{hy} = 2080 kg/sec,

k_{spy} = 1E6 N/m,

M_{fy} = 175 kg,

B_{fy} = 1000 kg/sec and

k_{fy} = 5E6 N/m,

using the methodology described in Appendix C.

The frequency response of the model, $sG_y(s)$, compared favorably to that of the actual system with these values, as

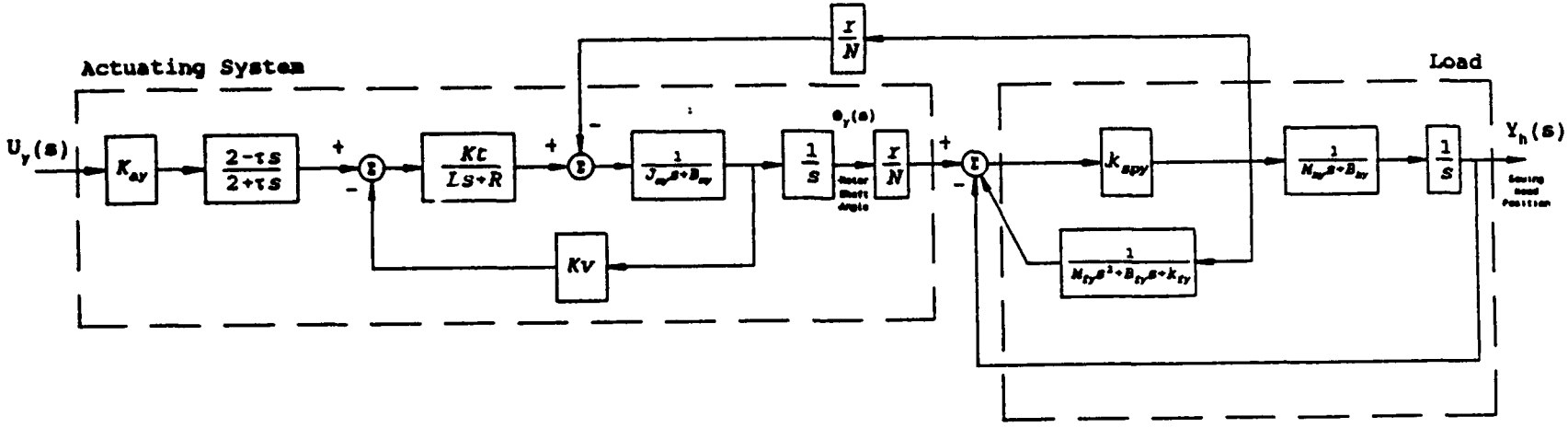

(a) Block diagram illustrating Y_h/U_y.

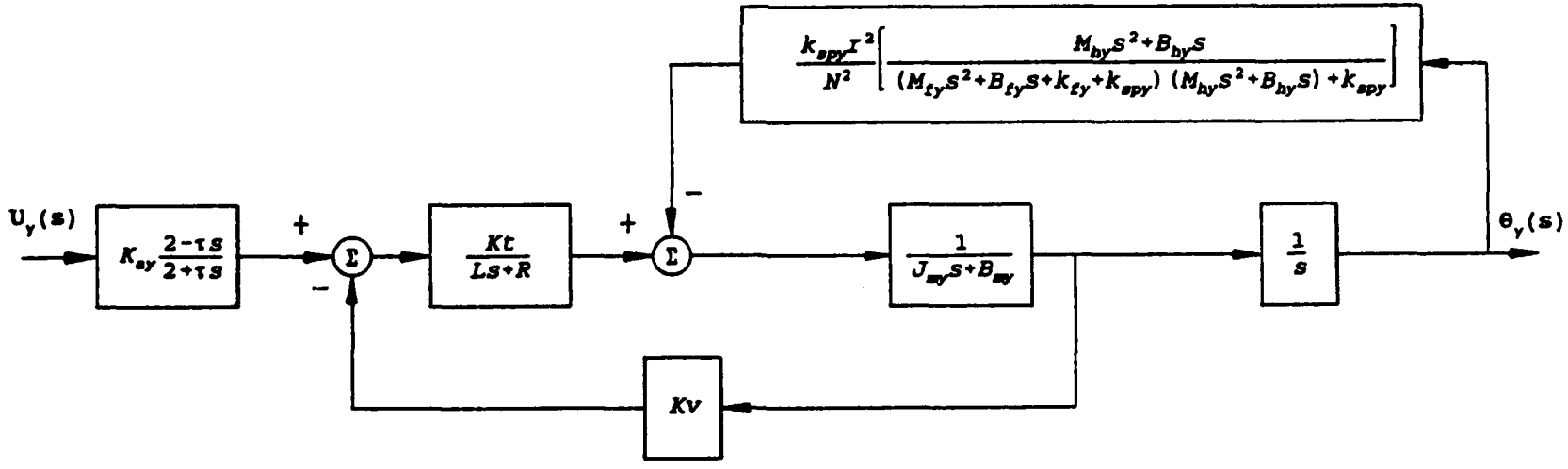

(b) Block diagram illustrating θ_y/U_y.

Figure 3.14. Y axis actuating system and load block diagrams.

shown in the Bode plots in Figure 3.15. The differences in the plots are assumed to be due to unmodeled higher order dynamics and nonlinearities in the system.

Controller Model Development

The PC mounted controller performs two functions in the operation of the stitcher that must be modeled; it provides closed loop operation of the system with dynamic compensation, and it generates the trajectory reference signal. The closed loop compensation is provided in the controller by a digital filter acting on the error signal between the reference trajectory and the actual trajectory of the servomotors. The reference signal is generated from the stitch path specified by the user.

Dynamic Compensation

The discrete time model of the controller is shown in Figure 3.16a with compensation provided by a digital filter, D(z), of the form

$$D(z) = K_d \cdot \frac{z-A}{z+B} \quad . \tag{3.5}$$

The sampling time, T_s, of the system is 136 μsec (ω_s=7.4 kHz). Also included in the model is the digital-to-analog converter (DAC) gain, K_{DAC}, and the encoder gain, K_e. The DAC gain is defined as

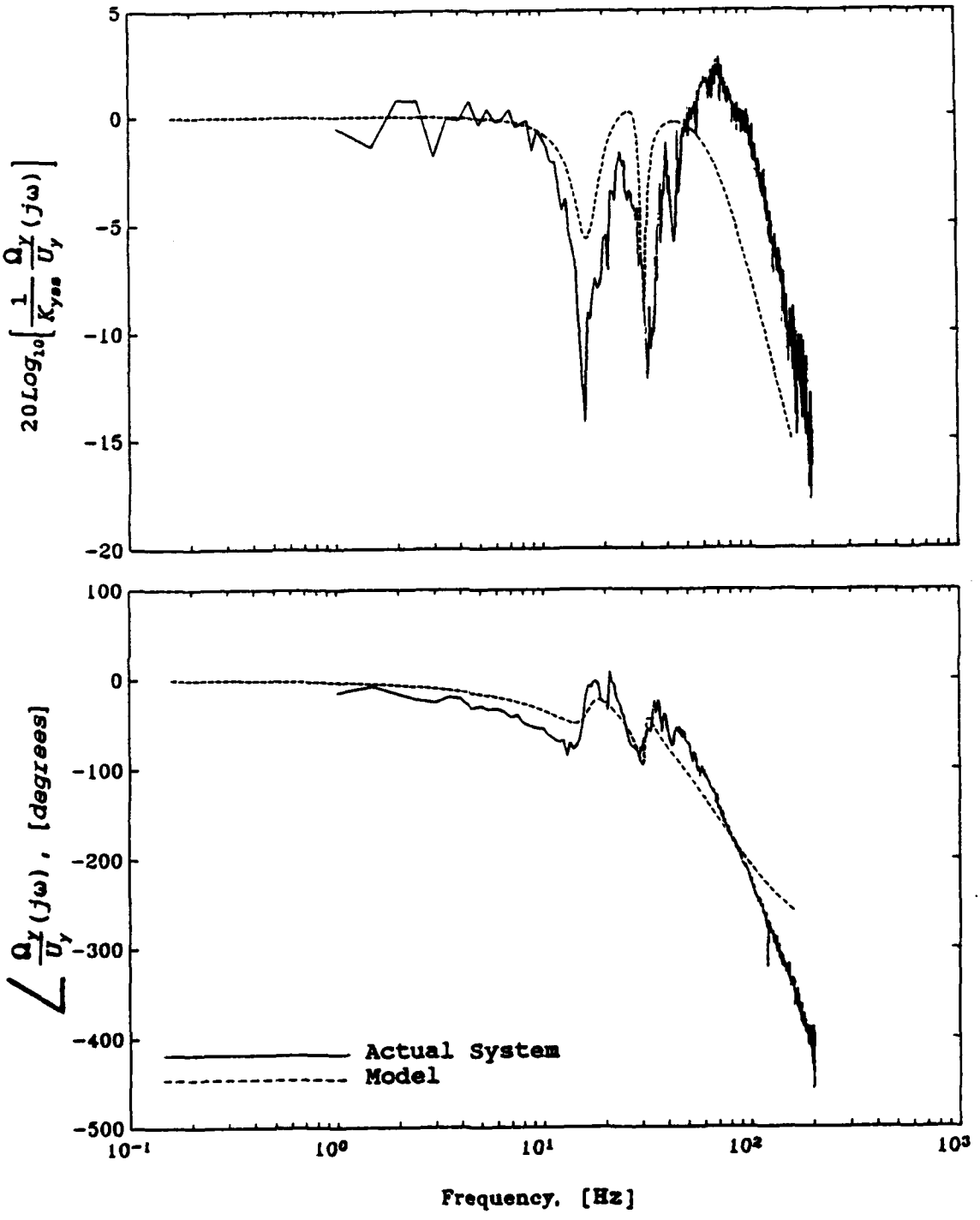

Figure 3.15. Y axis actuating system/load Bode plots, actual system and model.

$$K_{DAC}=\frac{V_{max}-V_{min}}{2^N} \quad , \tag{3.6}$$

where V_{max} and V_{min} are the maximum and minimum values of the command signal generated from a N bit digital command. With a command signal voltage range of -10V to +10V and an eight bit command word, K_{DAC} = 0.07825 (volts/count). The encoder gain is expressed as

$$K_e=\frac{4LC}{2\pi} \quad , \tag{3.7}$$

where LC is the line count of an encoder with quadrature output. Since the encoders used on the stitcher are 2000 line count with quadrature output, K_e = 1273 (counts/rad).

The stitcher model could be analyzed using one of two methods. If the continuous time model of the actuating system and load is represented by an analogous digital model and combined with the digital model of the controller, a direct digital analysis can be performed entirely in the z-plane. The system can also be analyzed entirely in the s-plane using the digitization (DIG) method with a pseudo-continuous-time (PCT) model of the control system. The PCT model is valid if $\omega_s \geq 10\omega_{BW}$, where ω_s is the sampling frequency and ω_{BW} is the system bandwidth. This method requires continuous time approximation of the digital filter and the zero order hold (see Houpis and Lamont [14]). The DIG method was used since ω_s=7.4 kHz, ω_{BWx}=10 Hz and ω_{BWy}=10 Hz.

The linear, continuous time model of the compensator is shown in Figure 3.16b. An analog filter, D(s), and a ZOH

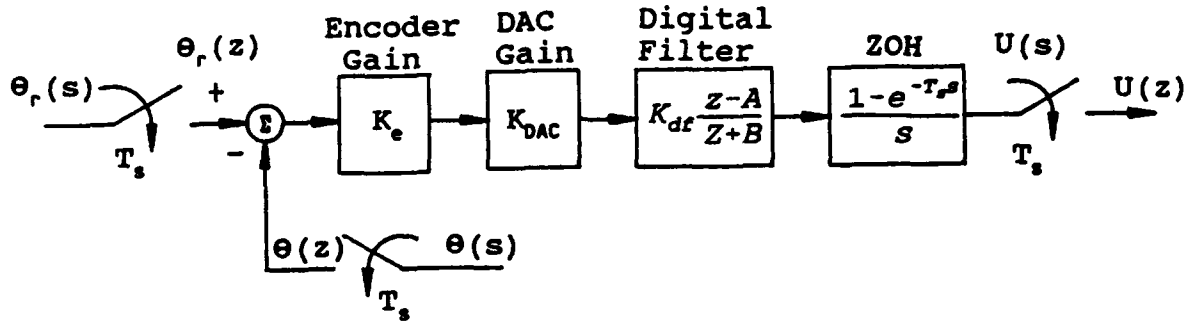

(a) The digital model.

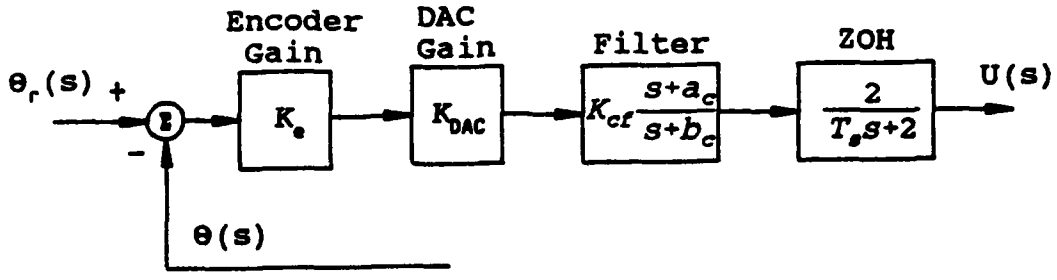

(b) The equivalent continuous model.

Figure 3.16. The controller block diagram.

element, $G_{ZOH}(s)$, were used in the model to represent the digital filter and sample holding action of the compensator. A ZOH function is expressed as

$$G_{ZOH}(s) = \frac{1-e^{-T_s s}}{s} \quad . \tag{3.8}$$

A first order Padé approximation of $G_{ZOH}(s)$ was used to approximate the ZOH dynamics in the model as

$$G_{ZOH}(s) \approx \frac{2}{2+T_s s} \tag{3.9}$$

for linear analysis. Using a first order Tustin approximation, the digital filter was written in continuous time as

$$D(s) = K_{cf}\frac{s+a_c}{s+b_c} \quad , \tag{3.10a}$$

where

$$a_c = \frac{2}{T_s}\left(\frac{1-A}{1+A}\right) \tag{3.10b}$$

$$b_c = \frac{2}{T_s}\left(\frac{1+B}{1-B}\right) \tag{3.10c}$$

and

$$K_{cf} = K_{df}\left(\frac{1+A}{1-B}\right) \quad . \tag{3.10d}$$

The parameters of the digital filter in Equation (3.5) are numerically constrained to values of $1/256 \leq A \leq 255/256$ and $1/256 \leq B \leq 255/256$. Therefore, the parameters of the analog filter defined in Equations (3.10) are bounded by $29 \leq a_c \leq 14591$ and $14821 \leq b_c \leq 7514706$. The filter always acts as a lead compensator because the pole of the continuous filter

cannot be placed closer to the imaginary axis than the zero. Thus, this filter design approximates classical proportional plus derivative (PD) control action.

Reference Signal Generation

The reference signal, represented by θ_{rx} and θ_{ry}, is generated by the motion control software, QS2E, from the user defined stitch path, generating the three region generic motion profiles shown in Figure 3.17. The sewing head accelerates to the operating velocity in Region I, where the reference position and velocity of the sewing head are given by

$$x(k) = \frac{1}{2} a T_c^2 + v(k-1)\, T_c + x(k-1) \qquad (3.11a)$$

and

$$v(k) = a T_c + v(k-1) \ , \qquad (3.11b)$$

where k is the sample number, a is the user specified rate of acceleration, v is the sewing head velocity, x is the sewing head position and T_c is the reference signal update time (T_c = 1 msec). The sewing head then moves at a constant velocity, referred to as the "slewing" velocity, v_s, in Region II. The reference position and velocity are given in this region by

$$x(k) = v_s(k-1)\, T_c + x(k-1) \qquad (3.12a)$$

and

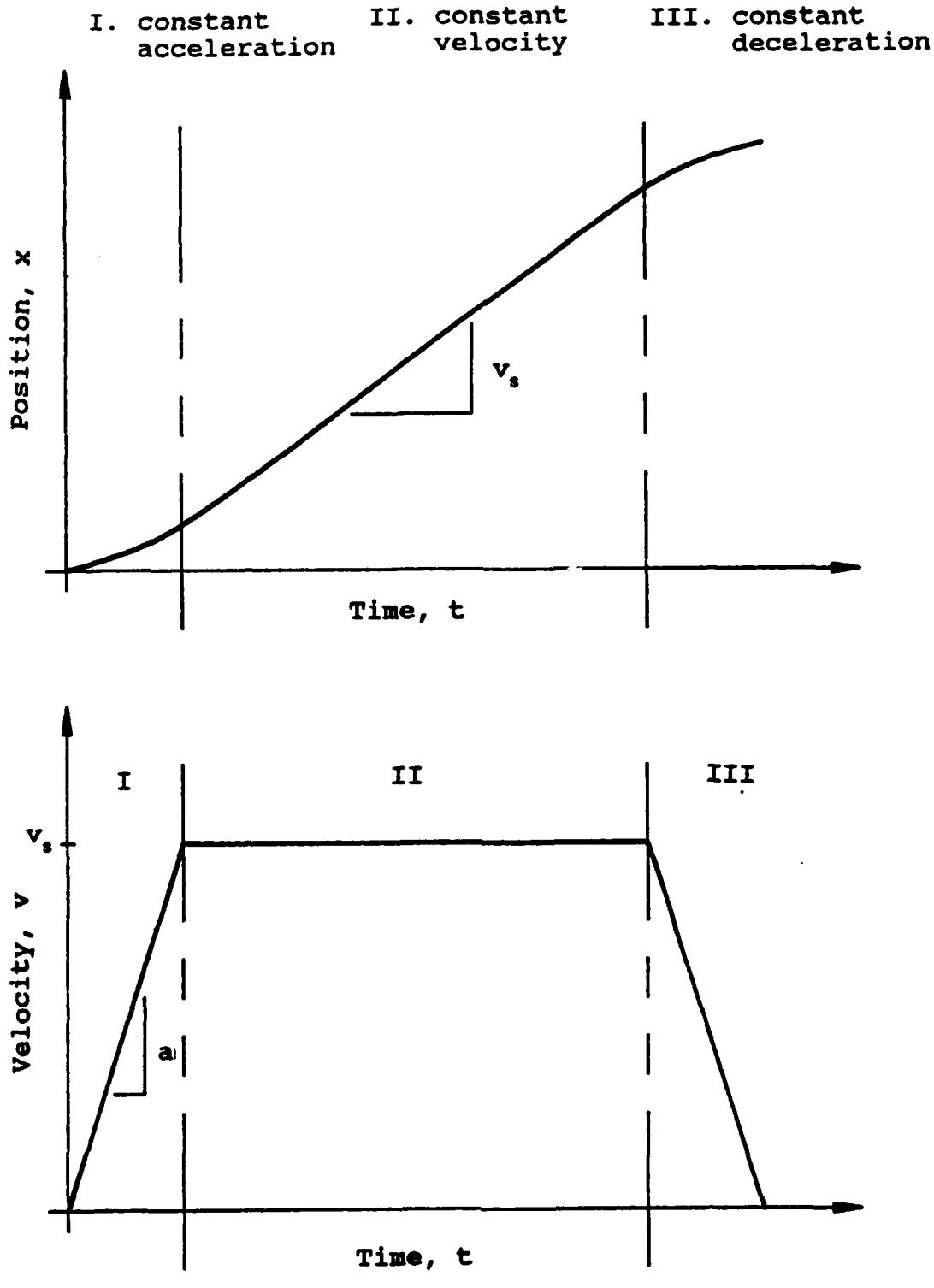

Figure 3.17. Reference signal motion profiles.

$$v(k) = v_s \ . \qquad (3.12b)$$

The sewing head decelerates to zero velocity in Region III with the reference position and velocity given by

$$x(k) = -\tfrac{1}{2} a T_c^2 + v(k-1)\, T_c + x(k-1) \qquad (3.13a)$$

and

$$v(k) = -aT_c + v(k-1) \ . \qquad (3.13b)$$

Computer software was written to simulate the reference signal generation process of the controller using the equations for Regions I, II and III. A two dimensional reference path, generated from the stitch path shown in Figure 3.18a, was used to test the actual CNC stitcher and simulated to drive the model of the stitcher. The stitch path consists of two right angle corners whose segments are parallel to the X and Y axes. Line segments A and C are parallel to the X axis and line segment B is parallel to the Y axis, with each being 2.5 inches long. The slewing velocity and acceleration rate for the reference signal were set the performance specifications; v_s = 7.5 (in/sec) and a = 546 (in/sec^2). Interpolated motion was used to generate the reference signal used in the simulation and actual machine testing. Therefore, the reference signal has "rounded" corners as shown in Figure 3.18b. The points comprising the position coordinates of the simulated reference signal were written to a data file and used to drive the stitcher model.

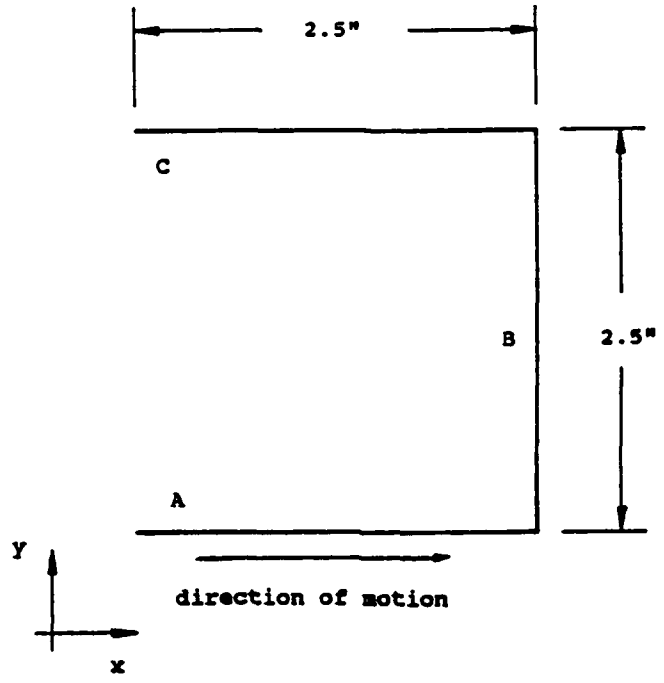

(a) The stitch path.

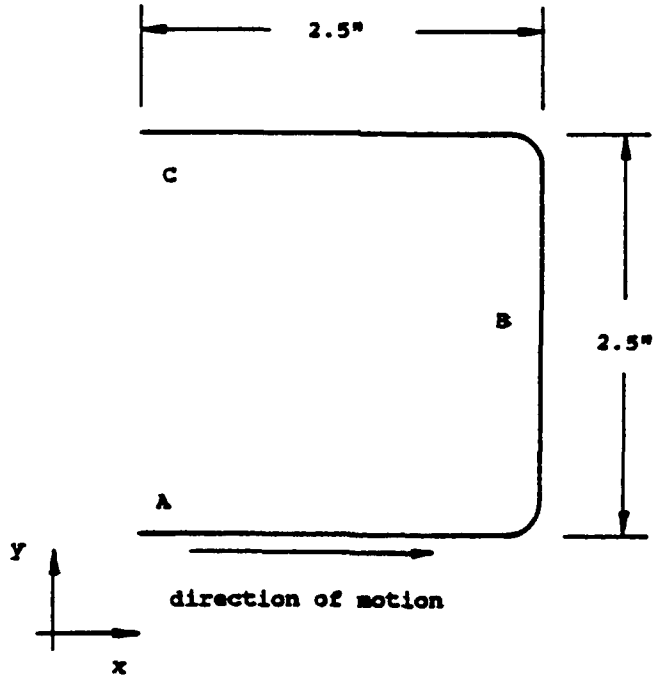

(b) The reference path.

Figure 3.18. Experimental stitch path and reference path.

Nonlinear Model Development

The experimentally determined closed loop step response of the axes indicated the presence of a saturated element in the system for relatively high step sizes. Therefore, the linear model was extended to include this characteristic in a nonlinear model. The nonlinear model includes a current saturation element in the amplifier, the digital form of the controller, the sampler and ZOH and the exact form of the time delay function. This model was used to verify the values of the unknown system parameters in the model and determine the effect that design changes made in the stitcher have on its dynamic tracking performance. The model step response was compared to that of the actual system to verify the model parameters. The response of the model to the simulated reference signal was used to determine the effects of the design changes made in the model.

Experimental Results

The saturation limit of the servo amplifiers was determined from the closed loop position step response of the X axis actuating system. The experiment performed on the X axis was not repeated on the Y axis because the motors and electronics are identical in each axis; similar results can be expected for the Y axis actuating system. The experimental procedure and the step response of the X axis actuating system are presented in Appendix B. The results of the experiment indicate that the amplifier current begins to saturate at a commanded step size of $\pi/2$ radians. This

results in a torque limit since the amplifier current is proportional to the motor torque.

The closed loop step response of the motor shaft and sewing head of each axis was determined for commanded motor shaft step sizes of $3\pi/8$, $\pi/2$, $5\pi/8$ and $3\pi/4$ radians, corresponding to sewing head displacement steps of 0.23, 0.30, 0.38 and 0.45 inches respectively. The motor shaft and sewing head step responses to a $3\pi/8$ radians input for each axis are shown in Figure 3.19. The experimental procedure and results are presented in detail in Appendix B.

X Axis Nonlinear Model

The controller and actuating system/load combination models were combined as shown in Figure 3.20 to form the closed loop model of the X axis. SIMNON was used to solve the nonlinear differential and difference equations which describe the system model. The model, developed in its state form, is given by

$$\dot{x}_h = -\left(\frac{B_{hx}}{M_{hx}}\right)\dot{x}_h - \left(\frac{k_{spx}}{M_{hx}}\right)x_h + \left(\frac{rk_{spx}}{NM_{hx}}\right)\theta_x \qquad (3.14a)$$

$$\ddot{\theta}_x = -\left(\frac{B_{mx}}{J_{mx}}\right)\dot{\theta}_x - \left(\frac{r^2k_{spx}}{N^2J_{mx}}\right)\theta_x + \left(\frac{rk_{spx}}{NJ_{mx}}\right)x_h + \left(\frac{k_t}{J_{mx}}\right)I_x \qquad (3.14b)$$

and

$$\dot{I}_x = \left(\frac{Ka_x}{L}\right)u_x(t-\tau) - \left(\frac{k_v}{L}\right)\dot{\theta}_x - \left(\frac{R}{L}\right)I_x \; . \qquad (3.14c)$$

The current saturation is given by

$$D(z) = 0.25\left(\frac{z-0.918}{z+0.25}\right)$$

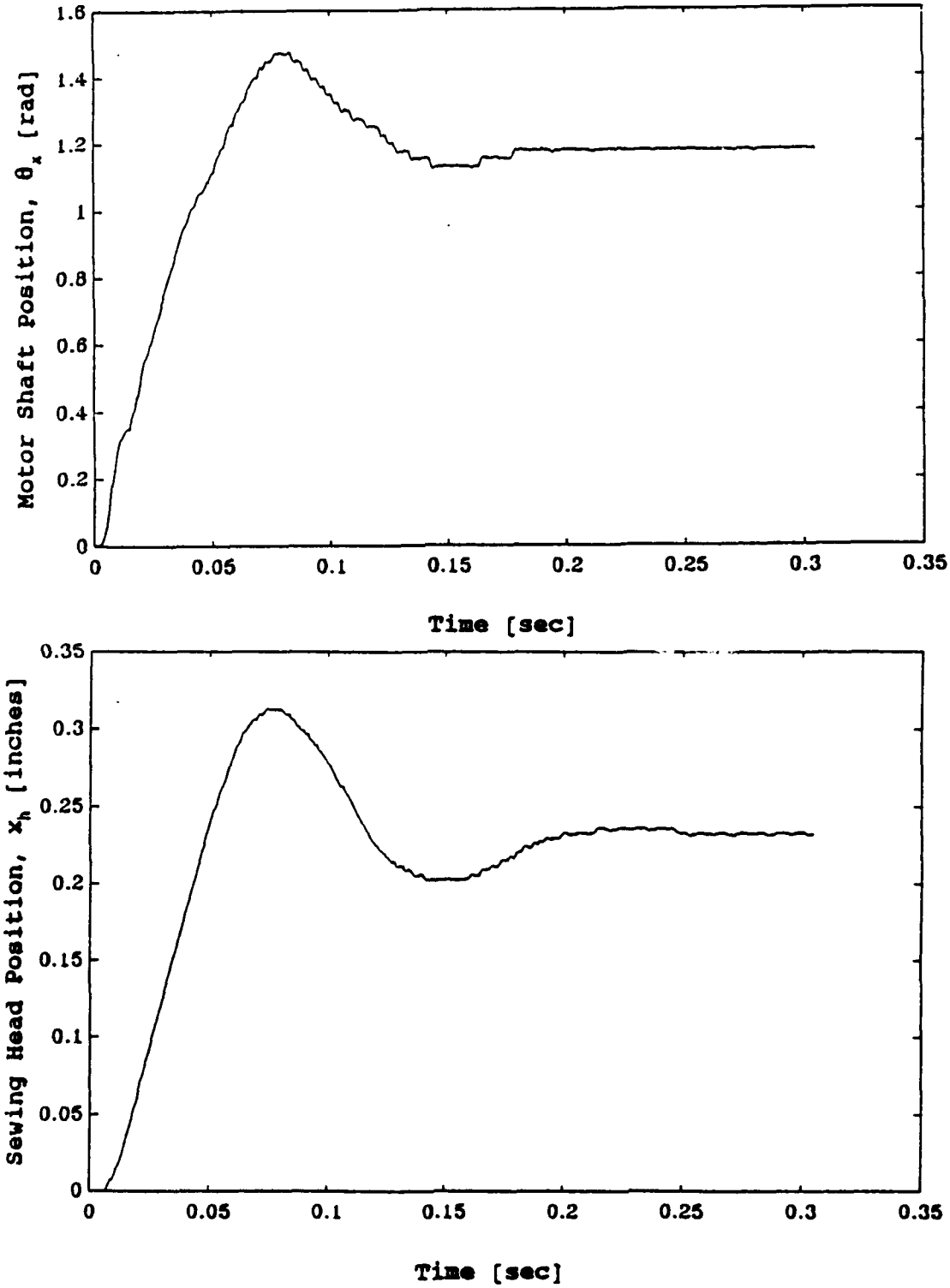

(a) X axis step response.

Figure 3.19. X and Y axis motor shaft and sewing head position step response.

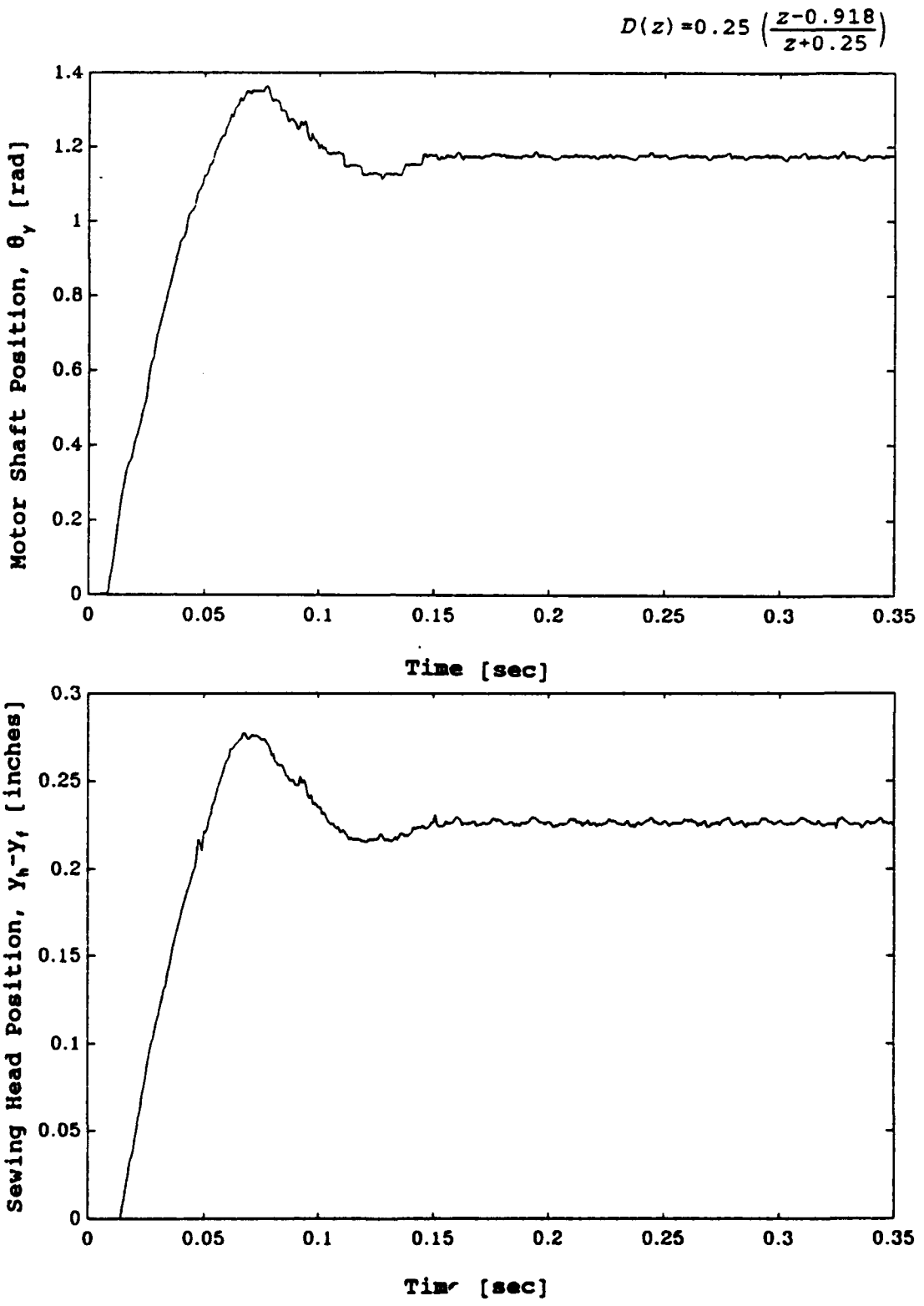

(b) Y axis step response.

Figure 3.19. (Continued).

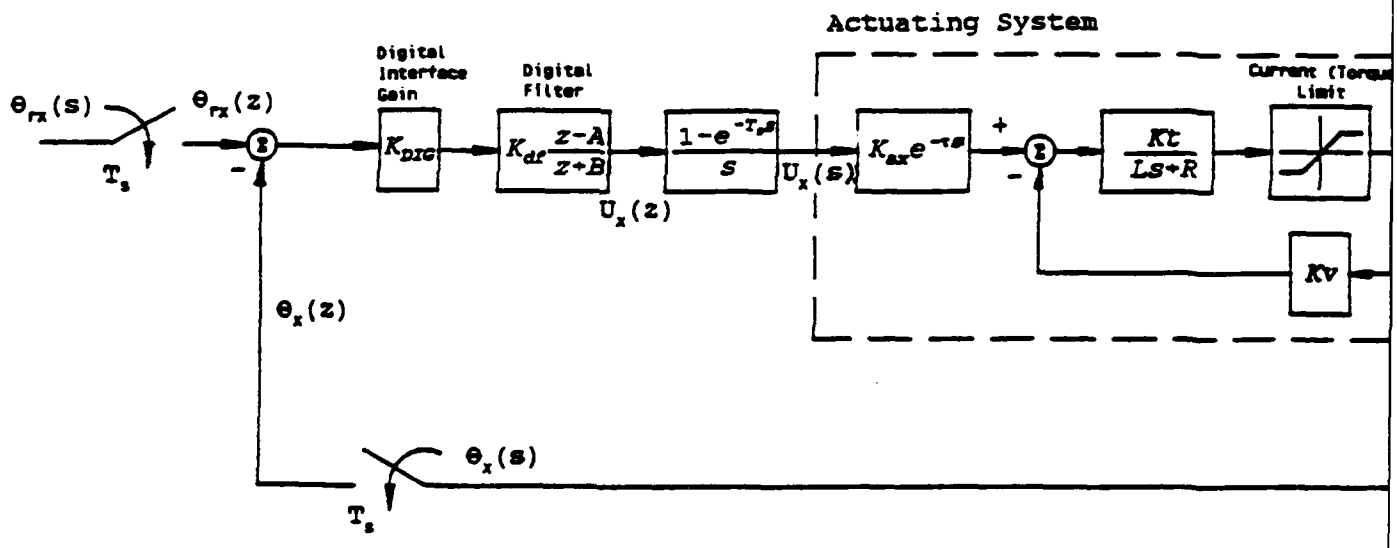

Figure 3.20. X axis nonlinear model block diagram.

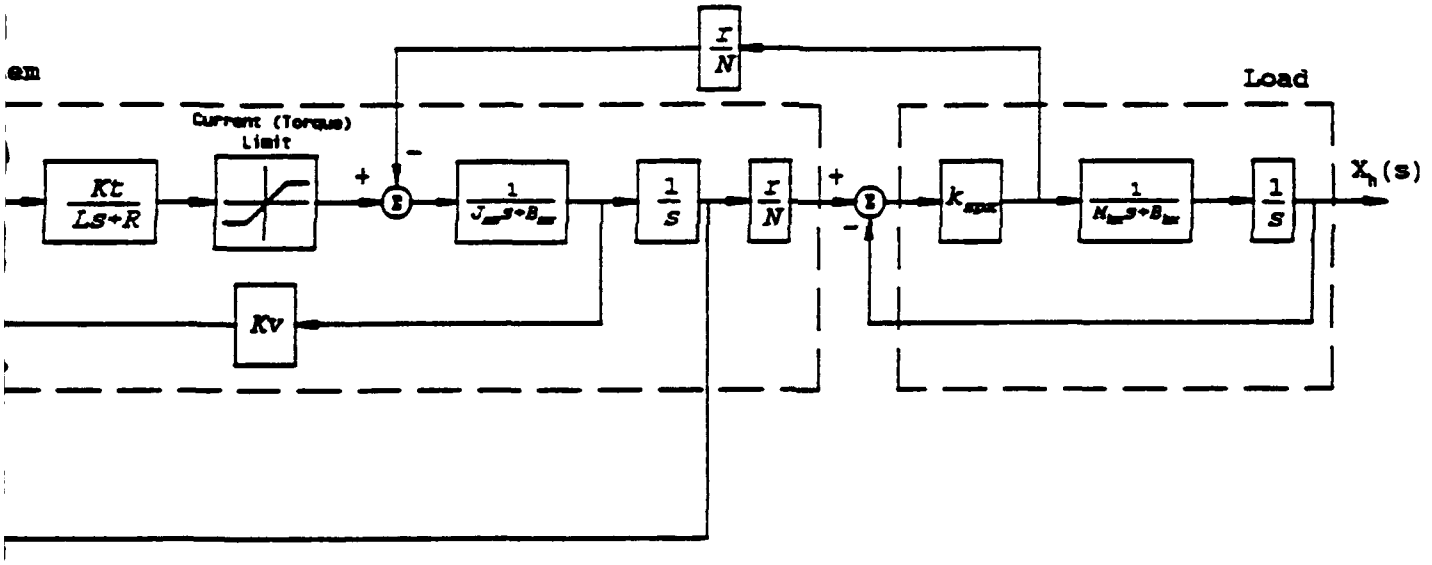
em
Load
Current (Torque) Limit
$\frac{Kt}{Ls+R}$
+
−
$\frac{1}{J_m s+B_m}$
$\frac{1}{s}$
$\frac{r}{N}$
$\frac{r}{N}$
+
−
k_{epic}
$\frac{1}{M_{bar} s+B_{bar}}$
$\frac{1}{s}$
$X_h(s)$
Kv

$$I_x = \begin{cases} I_{xLIMIT} & for \ \int \dot{I}_x dt \geq I_{xLIMIT} \\ \int \dot{I}_x dt & for \ -I_{xLIMIT} < \int \dot{I}_x dt < I_{xLIMIT} \\ -I_{xLIMIT} & for \ \int \dot{I}_x dt \leq -I_{xLIMIT} \end{cases} . \qquad (3.14d)$$

The difference equations implemented by the controller are

$$u_x(n) = K_x e_x(n) - K_x A_x e_x(n-1) + B_x u_x(n-1) \qquad (3.14e)$$

and

$$e_x(n) = \theta_{rx}(n) - \theta_x(n) , \qquad (3.14f)$$

where $K_x = K_{DAC} K_e K_{df}$. The current limit in the model, I_{xLIMIT}, was adjusted to 27 amperes, corresponding to a torque limit of 13.5 Nm, so that the model step response compared favorably to that of the actual system for a step size of $3\pi/8$ radians as shown in Figure 3.21.

Y Axis Nonlinear Model

The subsystems of the Y axis model were combined to form the model shown in Figure 3.22. A nonlinear model was developed for the Y axis containing the amplifier saturation, the digital filter, sampler and ZOH and the time delay function. The following differential equations were used to describe the Y axis dynamics.

$$\ddot{y}_h = -\left(\frac{B_{hy}}{M_{hy}}\right) \dot{y}_h - \left(\frac{k_{spy}}{M_{hy}}\right) y_h - \left(\frac{k_{spy}}{M_{hy}}\right) y_f + \left(\frac{r k_{spy}}{N M_{hy}}\right) \theta_y \qquad (3.15a)$$

$$\ddot{y}_f = -\left(\frac{B_{fy}}{M_{fy}}\right) \dot{y}_f - \left(\frac{k_{spy}+k_f}{M_{fy}}\right) y_f - \left(\frac{k_{spy}}{M_{fy}}\right) y_h + \left(\frac{r k_{spy}}{N M_{hy}}\right) \theta_y \qquad (3.15b)$$

$$D(z) = 0.25\left(\frac{z-0.918}{z+0.25}\right)$$

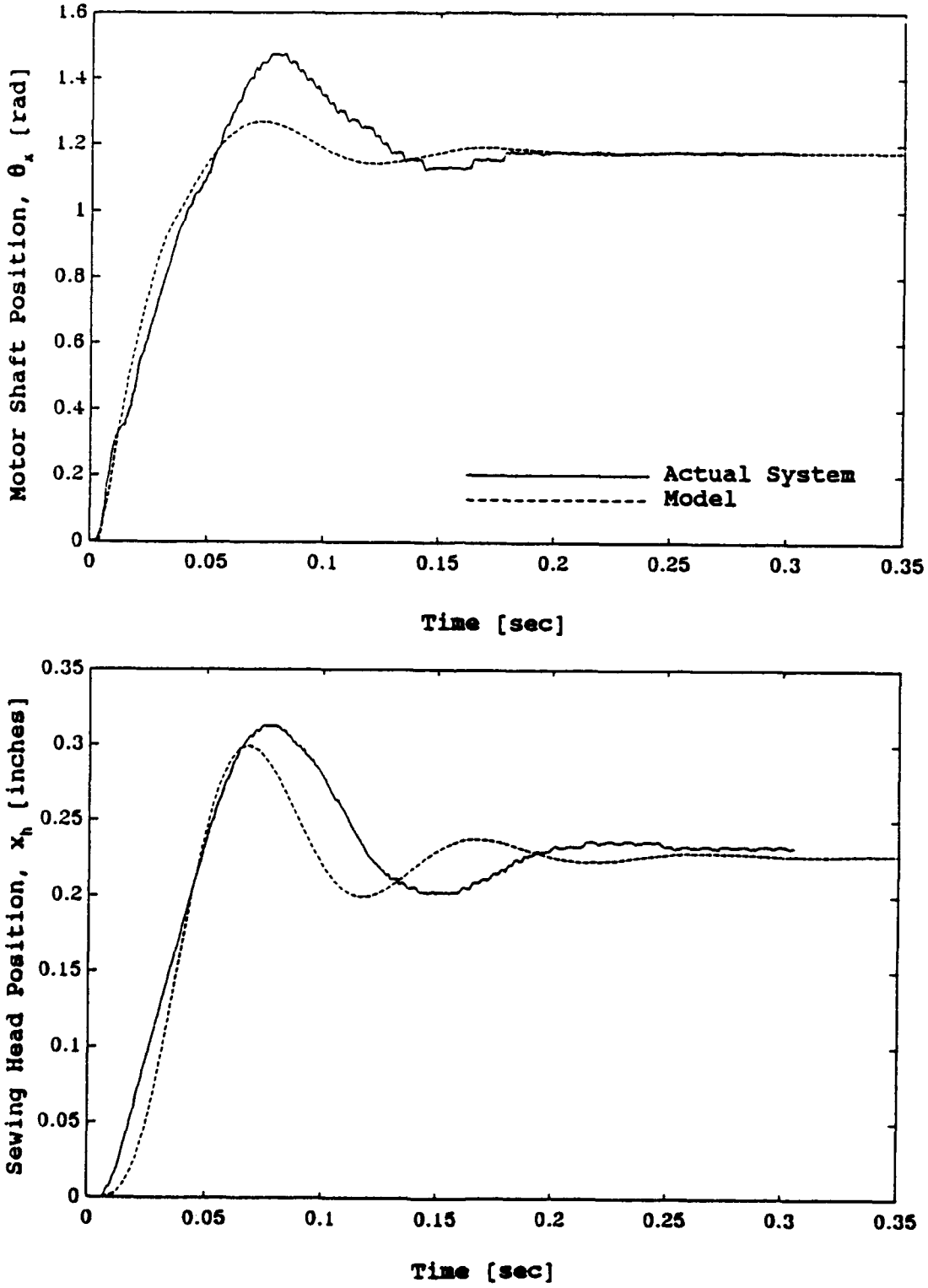

Figure 3.21. X axis motor shaft and sewing head position step response, actual system and model.

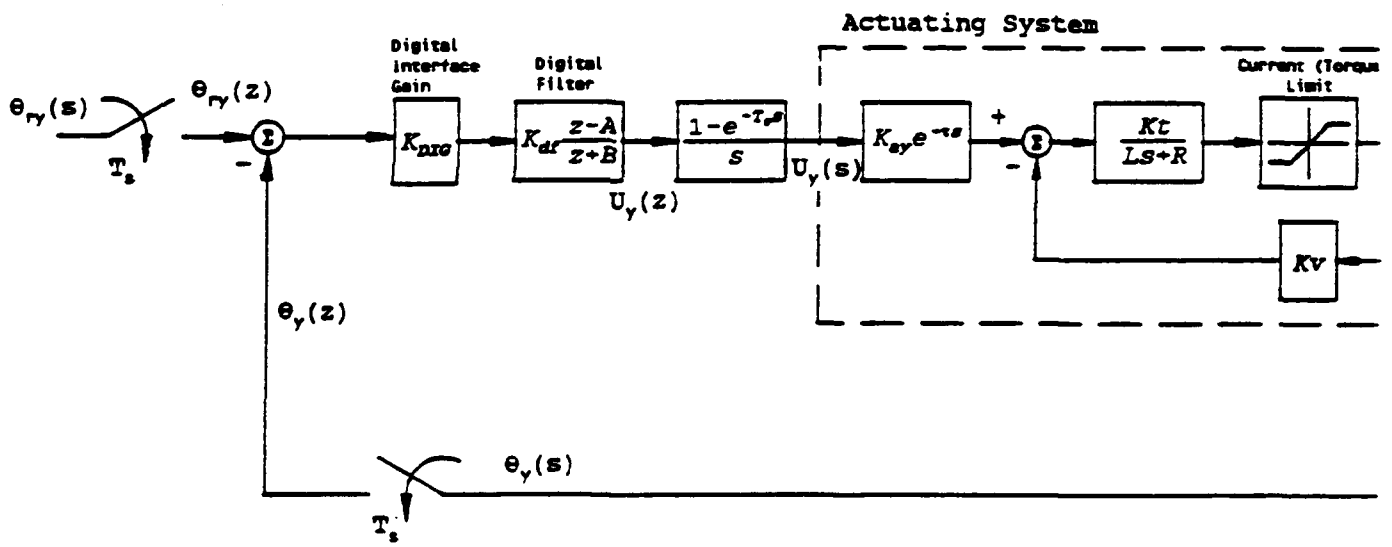

Figure 3.22. Y axis nonlinear model block diagram.

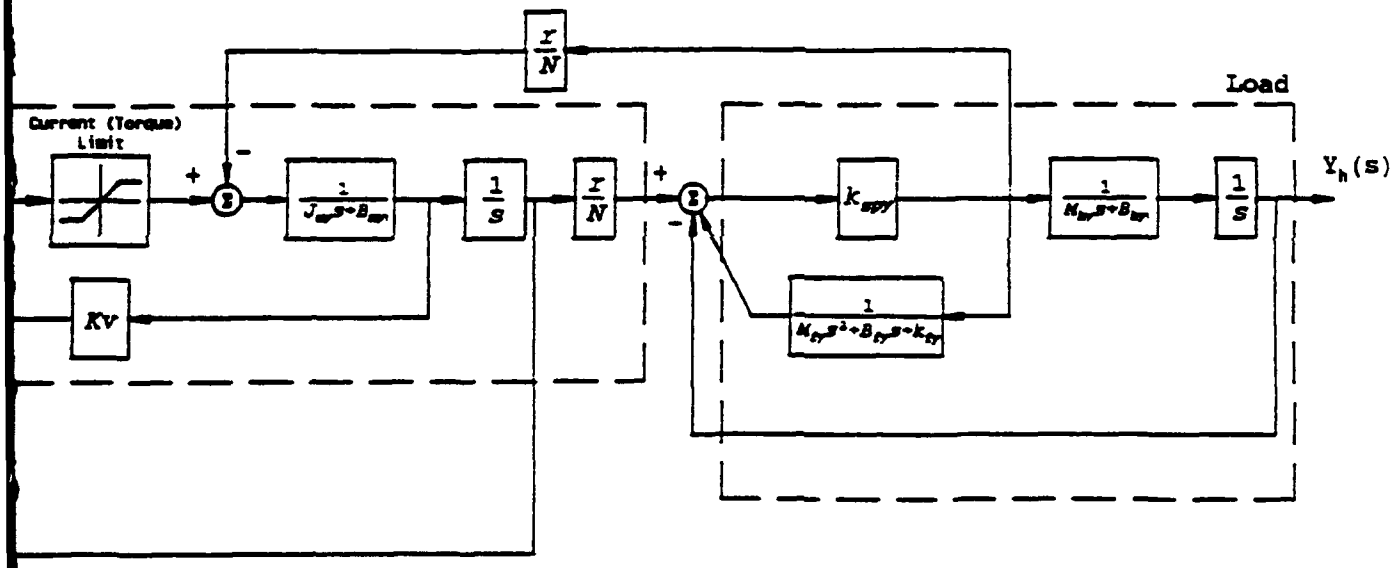
Load
Current (Torque) Limit
+
-
+
-
+
Kv
$Y_h(s)$

$$\ddot{\theta}_y = -\left(\frac{B_{my}}{J_{my}}\right)\dot{\theta}_y - \left(\frac{r^2 k_{spy}}{N^2 J_{my}}\right)\theta_y + \left(\frac{r k_{spy}}{N J_{my}}\right) y_f + \left(\frac{r k_{spy}}{N J_{my}}\right) y_h + \left(\frac{k_t}{J_{my}}\right) I_y \qquad (3.15c)$$

and

$$\dot{I}_y = \left(\frac{K a_y}{L}\right) u_y(t-\tau) - \left(\frac{k_v}{L}\right)\dot{\theta}_y - \left(\frac{R}{L}\right) I_y \ . \qquad (3.15d)$$

The amplifier current saturation is given by

$$I_y = \begin{cases} I_{yLIMIT} & for \ \int \dot{I}_y dt \geq I_{yLIMIT} \\ \int \dot{I}_y dt & for \ -I_{yLIMIT} < \int \dot{I}_y dt < I_{yLIMIT} \\ -I_{yLIMIT} & for \ \int \dot{I}_y dt \leq -I_{yLIMIT} \end{cases} . \qquad (3.15e)$$

The difference equations implemented by the controller are

$$u_y(n) = K_y e_y(n) - K_y A_y e_y(n-1) + B_y u_y(n-1) \qquad (3.15f)$$

and

$$e_y(n) = \theta_{ry}(n) - \theta_y(n) , \qquad (3.15g)$$

where $K_y = K_{DAC} K_e K_{df}$. The step response of the model approximates that of the actual system for a step size of $3\pi/8$ radians, as shown in Figure 3.23, with the current limit, I_{yLIMIT}, adjusted to 27 amperes, corresponding to a torque limit of 13.5 Nm.

Nonlinear Model Validation

The response of the two axis model driven by the simulated reference signal was compared to the tracking of the actual system to determine the validity of the model. The

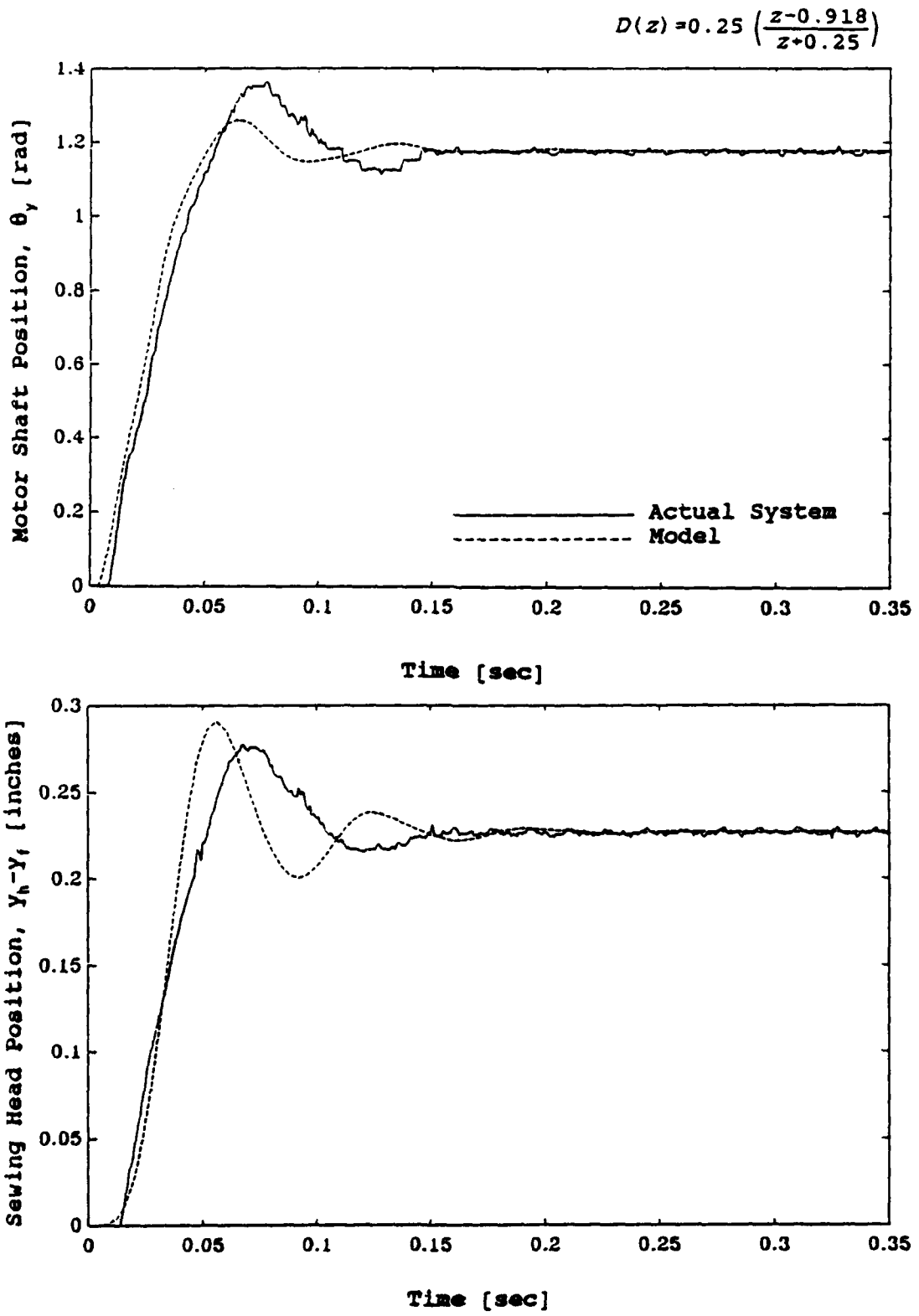

Figure 3.23. Y axis motor shaft and sewing head position step response, actual system and model.

reference signal used to drive the actual stitcher and the model has a trapezoidal velocity profile, with the acceleration/deceleration set to 281 in./sec^2 and the slew velocity set to 7.5 in./sec. The actual and simulated paths of the stitcher are shown in Figure 3.24. This figure shows that a maximum error of 0.08 inches (2.0 mm) occurs in the stitch path in the X axis, and an error of 0.06 inches (1.5 mm) occurs in the Y axis. The maximum errors are a result of the excessive dynamic overshoot of the sewing head as it changes directions at the stitch path corners. The errors in the simulated stitch path corners are 0.067 inches (1.78 mm) in the X axis and 0.05 inches (1.3 mm) in the Y axis. The model correctly predicts that the maximum error occurs in the X axis; however, the magnitude of the error is slightly less in the simulation than in the actual operation of the stitcher. This is assumed to be due to the unmodeled dynamics associated with the gear sets such as backlash and deadband.

Summary of the Modeling Process

Each axis of the CNC stitcher was conceptually divided into three subsystems for modeling: (1) the controller, (2) the actuating system and (3) the load. A linear continuous approximation of the filter, which is implemented digitally as a lead filter in each axis, was developed for linear analysis of the model. Each actuating system model, a second order system with a time delay, was based on the experimentally determined actuating system frequency response. The parameters of the load in each axis were determined based on

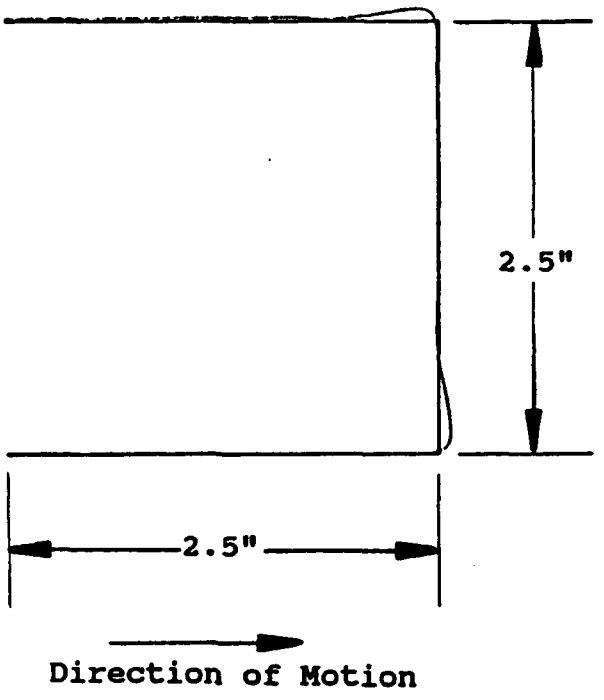

(a) The actual stitcher path.

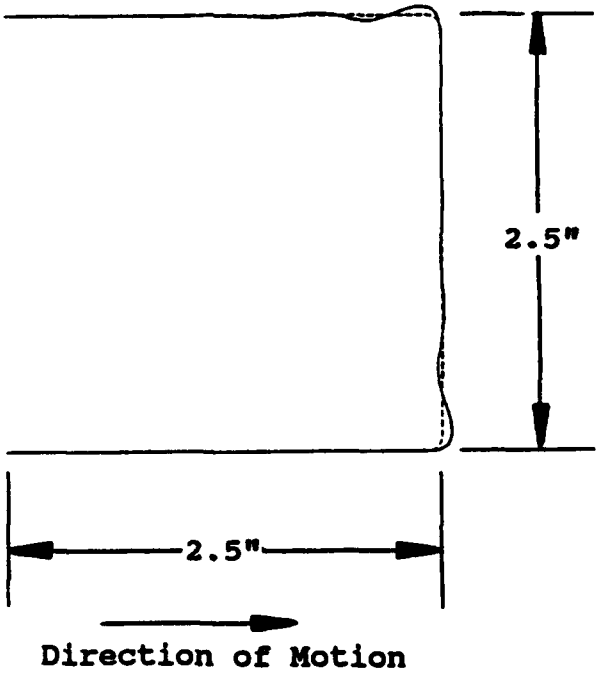

(b) The simulated stitcher path.

Figure 3.24. The actual and simulated stitcher paths.

the experimentally determined frequency response of the actuating system/load combination. The X axis load was modeled as a second order system due to the dynamics of the sewing head/timing belt combination. The dynamics of the Y axis load were found to consist of the sewing head/timing belt combination and the flexibility of the stitcher frame; therefore, the Y axis load was modeled as a fourth order system. The actuating system and load models were then combined to form the axis models, $G_x(s)$ and $G_y(s)$.

The experimentally determined closed loop position step response of each axis indicated that the amplifier current, and therefore the motor torque, becomes saturated at relatively large commanded step sizes. Therefore, a nonlinear model of the stitcher was developed with a current saturation element in the amplifier model of each axis. The digital form of the controller and the exact form of the time delay in the actuating system was also included in the nonlinear model.

The performance of the stitcher was evaluated as it tracked a test stitch path after the linear and nonlinear models were developed. A simulation of the reference signal that was used to test the actual stitcher performance was used to drive the model. The accuracy of the model was determined by comparing the tracking simulation to that of the actual stitcher.

CHAPTER IV

STITCHER MODEL ANALYSIS AND PERFORMANCE IMPROVEMENT

The linear continuous model of the X axis, $G_x(s)$, and the Y axis, $G_y(s)$, were analyzed to determine the dynamic characteristics of the stitcher. The X and Y axis models were then considered with the addition of the linear continuous models of the controller, $D_x(s)$ and $D_y(s)$, to identify the effects the parameters of the controllers have on the stitcher dynamics. Finally, a method of improving the tracking performance of the stitcher was developed.

Stitcher Model Analysis

The block diagrams of the X and Y axis models, shown in Figures 3.20 and 3.22 (pages 73 and 76), show that the timing belt flexibility is outside of the servo loop since the motor shaft position is the feedback variable. This type of system configuration, a positioning system with a flexible link or transmission, is commonly found in robotics and machine tool systems. The root locus of this type of system consists of a pair of complex poles and zeros in the left half plane (LHP) near the imaginary axis of the s-plane. This is shown in Figure 4.1a. If the mechanical flexibility is included within the feedback loop, a critical gain exists for which the poles go unstable, as seen in Figure 4.1b. This situation corresponds to using the sewing head position

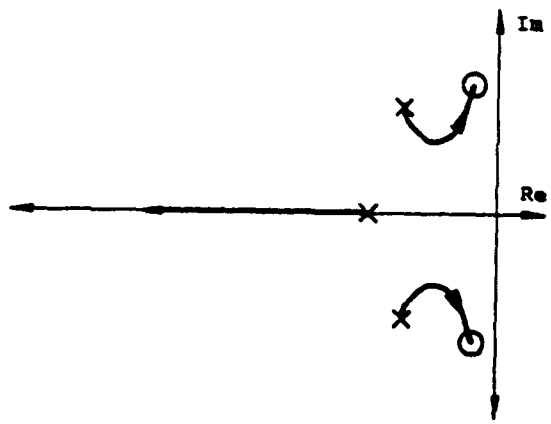

(a) Root locus of a system with a flexible element outside of the feedback loop.

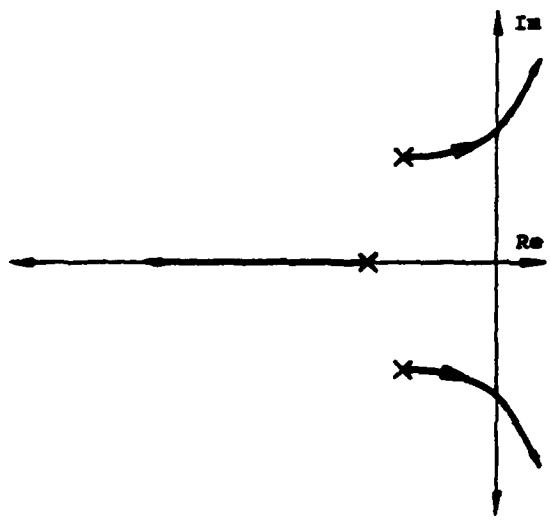

(b) Root locus of a system with a flexible element inside the feedback loop.

Figure 4.1. Characteristic root loci of mechanical systems.

rather than the motor shaft position as the feedback variable.

X Axis Analysis

The block diagram of the X axis model, $G_x(s)$, used in the analysis is shown in Figure 4.2. The Padé approximation of the time delay function results in a negative system gain. Therefore, the 0° root locus of the system in Figure 4.3 was generated rather than a 180° root locus (see D'Azzo and Houpis [15]). This root locus is characteristic of a system with a flexible mechanical element outside of the feedback loop; a pair of poles and zeros lie near the imaginary axis in the LHP. The system also has a zero in the RHP due to the positive zero in the time delay approximation. The poles of the system must be placed at a location with a higher damping ratio since experimentation showed excessive overshoot in each axis. The root locus shows that this is not possible with proportional gain; the dominant poles remain close to the imaginary axis while another pair of poles break away from the real axis and move toward the zero in the RHP.

The X axis model with the controller included is shown in Figure 4.4. This model was analyzed to determine the effectiveness of the controller in controlling the tracking of the stitcher. The root locus of the characteristic equation $1+KD_x(s)G_x(s)$ was computed for several different locations of the filter pole and zero. An example of these is shown in Figure 4.5. This root locus shows that for these values of the filter pole and zero, the dominant poles of the

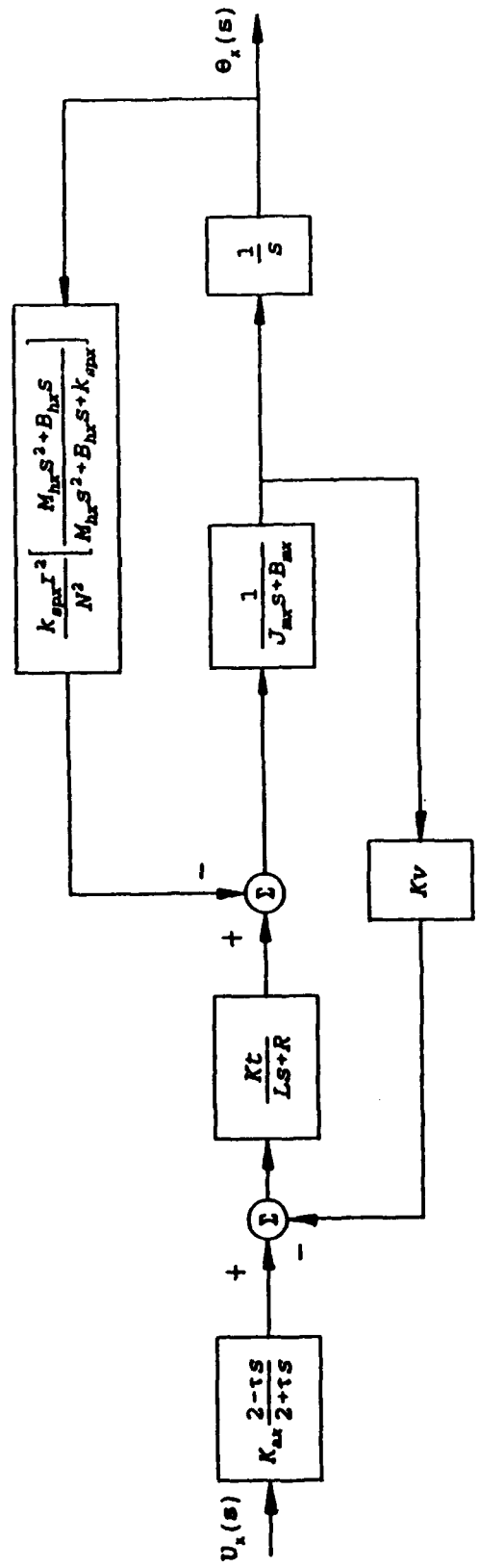

Figure 4.2. The linear continuous model of the X axis, $G_x(s)$.

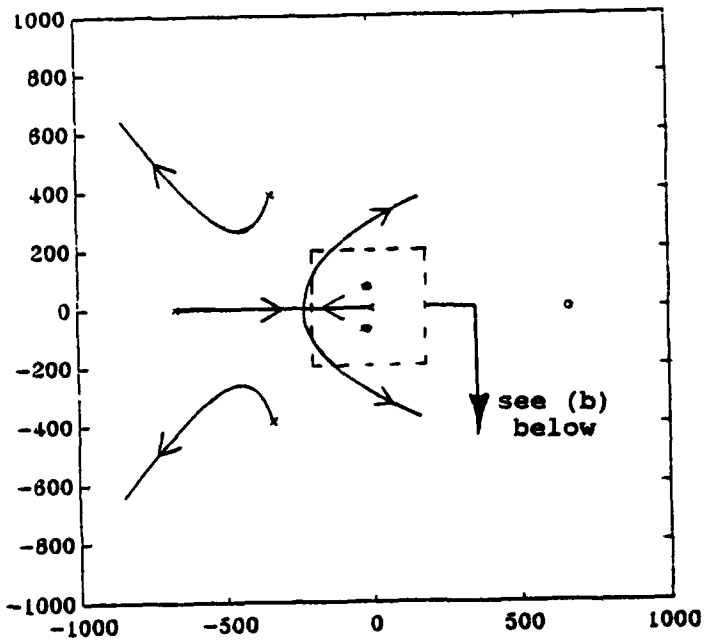

(a) The entire root locus.

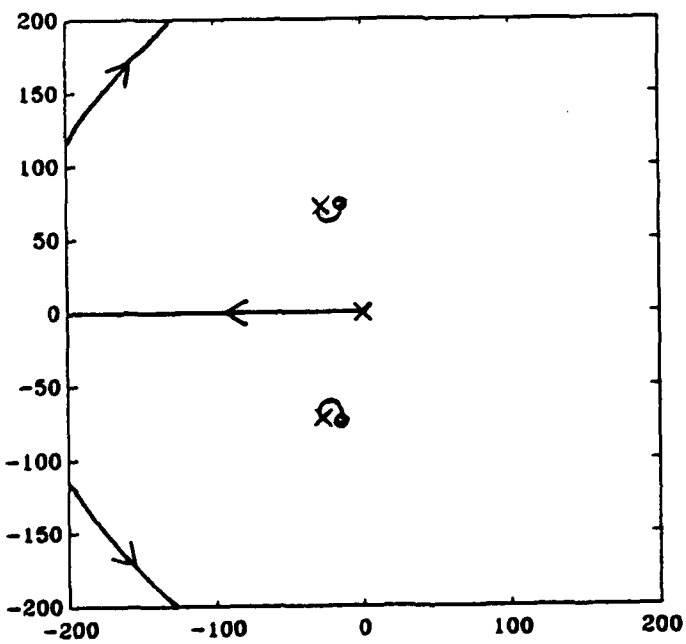

(b) The dominant roots.

Figure 4.3. Root locus of $1+KG_x(s)$.

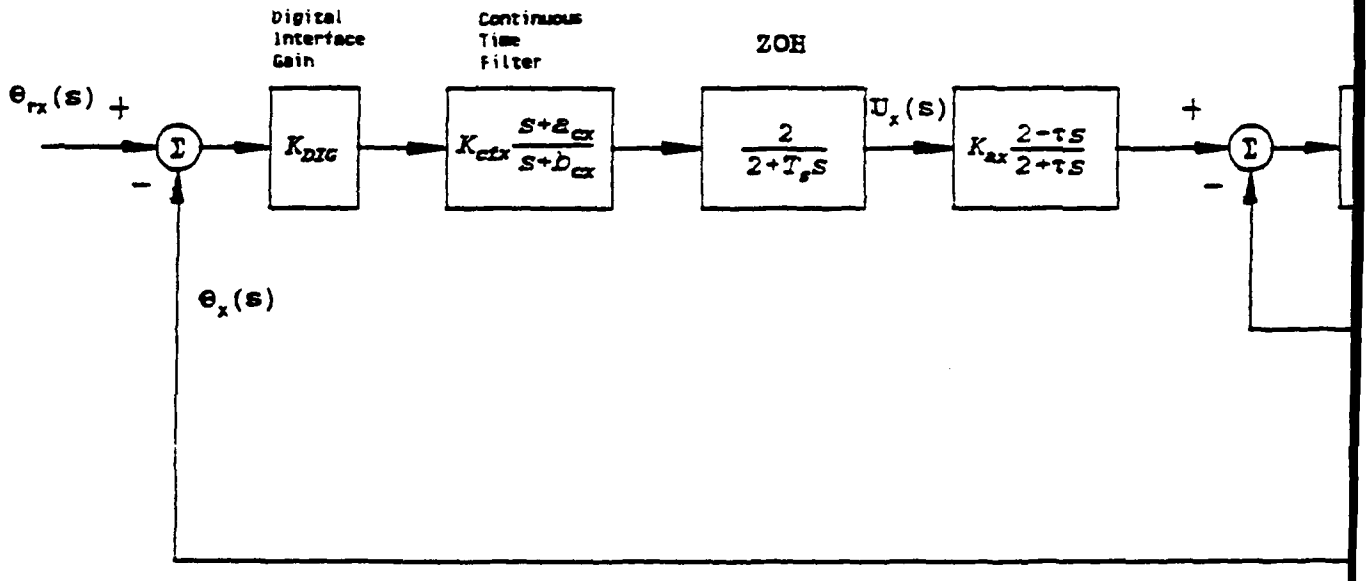

Figure 4.4. The linear continuous model of the X axis and the control $D_x(s)G_x(s)$.

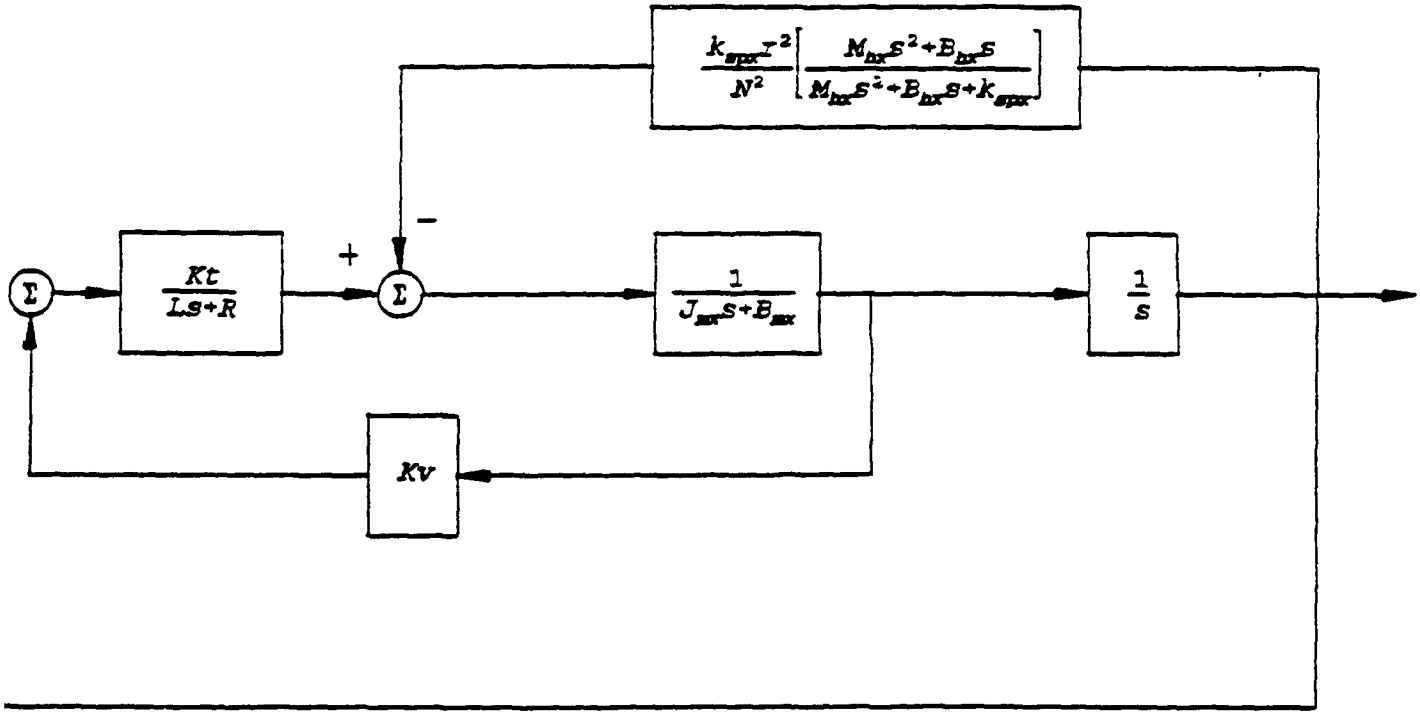
$\frac{k_{apx}r^2}{N^2}\left[\frac{M_{bx}s^2+B_{bx}s}{M_{bx}s^2+B_{bx}s+k_{apx}}\right]$
Σ
$\frac{Kt}{Ls+R}$
+
−
Σ
$\frac{1}{J_{mx}s+B_{mx}}$
$\frac{1}{s}$
Kv

controller,

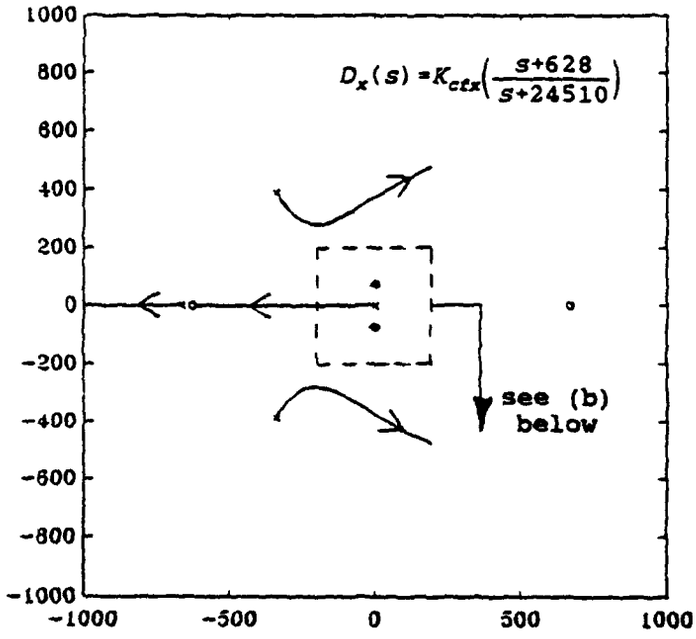

(a) The entire root locus.

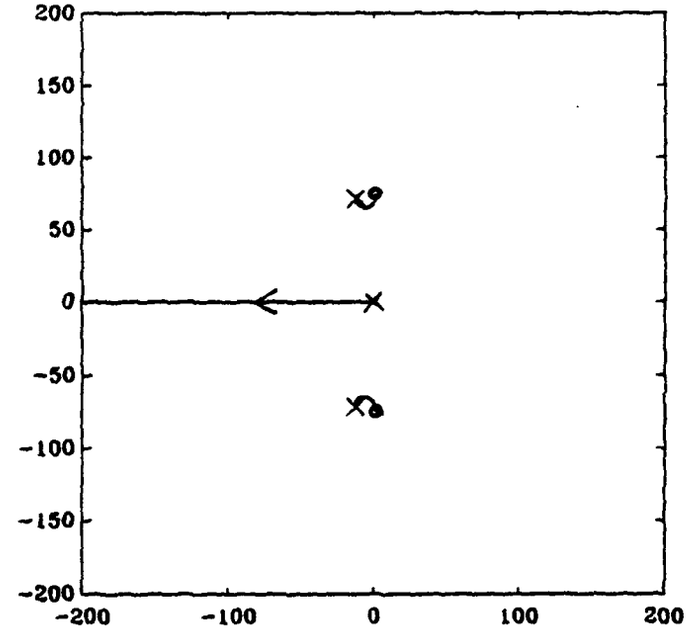

(b) The dominant roots.

Figure 4.5. Root locus of $1+KD_x(s)G_x(s)$.

axis model do not change. In fact, the dominant pole locations cannot be changed regardless of the values of the filter parameters. This type of filter, a lead filter, is not capable of moving the dominant poles to the left and "speeding up" the system using feedback from the servomotor. Therefore, a different type of controller must be used to improve the performance of the X axis when a mechanical flexibility is present.

Y Axis Analysis

The analysis of the Y axis model, shown in Figure 4.6, is similar to that of the X axis model. However, the Y axis has two flexible mechanical elements outside of the servo loop. The root locus in Figure 4.7 shows two pairs of complex poles near the imaginary axis that are not significantly affected by proportional feedback from the servomotor.

The controller was included, as shown in Figure 4.8, to determine its effect on the dynamics of the Y axis. The root locus of the characteristic equation of the closed loop system, $1+KD_y(s)G_y(s)$, was determined for several values of the controller parameters, as with the X axis. An example of these root loci, in Figure 4.9, shows that the dominant roots do not move significantly for these values of the filter pole and zero. Regardless of the filter parameters, the dominant poles of the Y axis do not move significantly with feedback from the servomotor. Therefore, a different type of controller, rather than a lead filter, must also be used with the Y

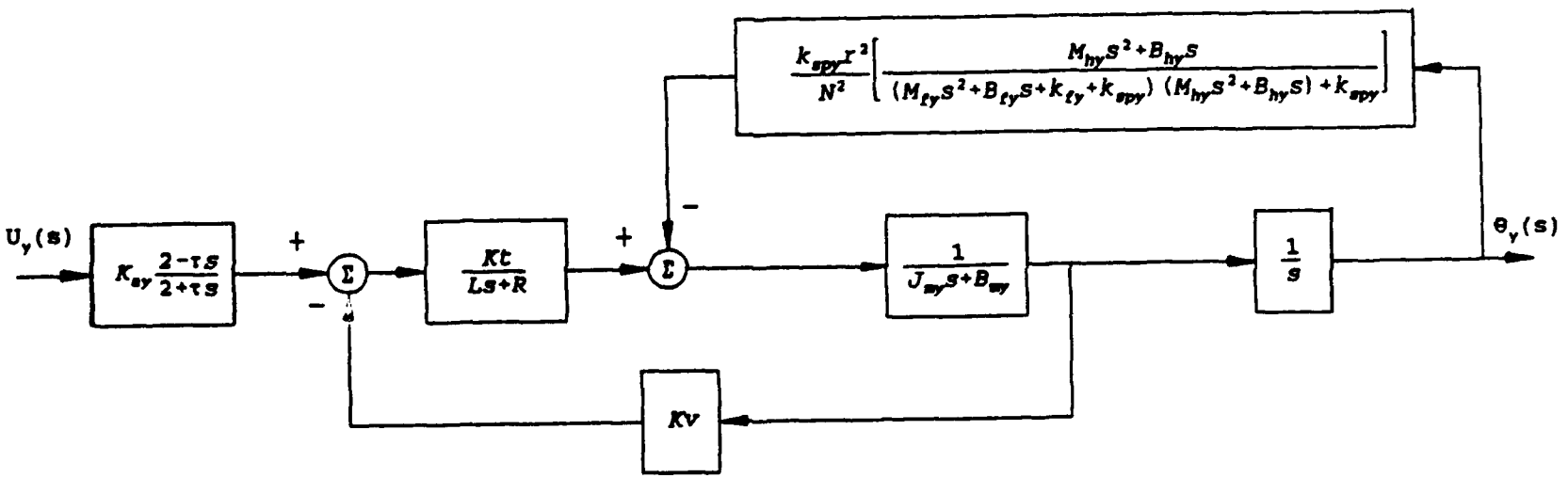

Figure 4.6. The linear continuous model of the Y axis, $G_y(s)$.

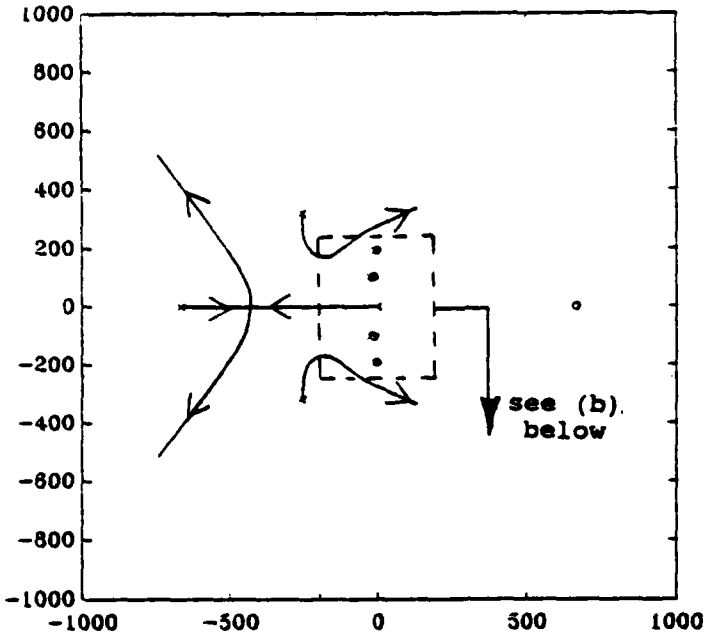

(a) The entire root locus.

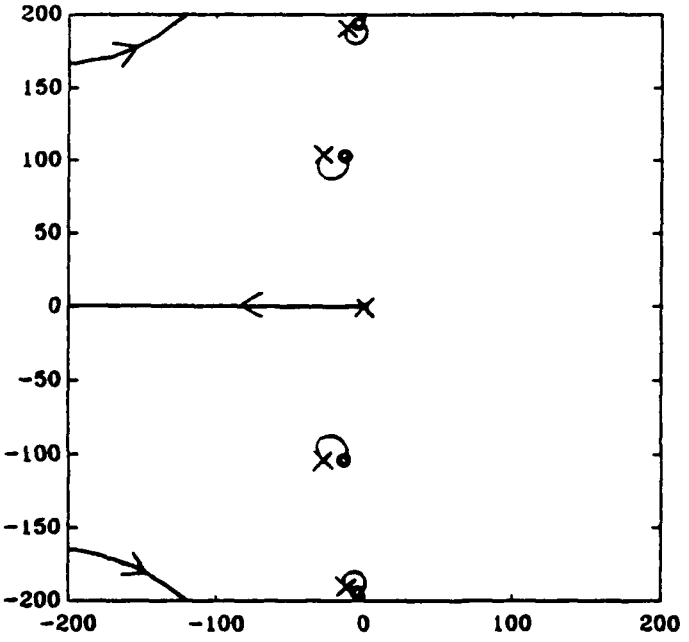

(b) The dominant roots.

Figure 4.7. Root locus of $1+KG_y(s)$.

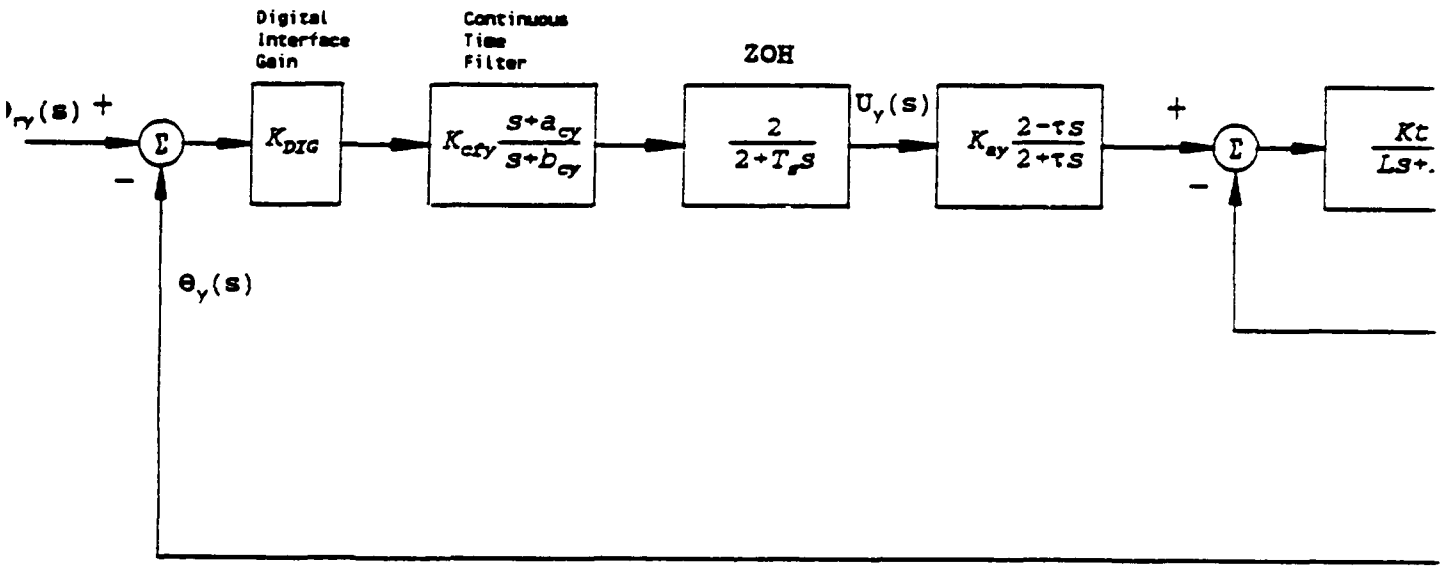

gure 4.8. The linear continuous model of the Y axis and the controller, $D_y(s)G_y(s)$.

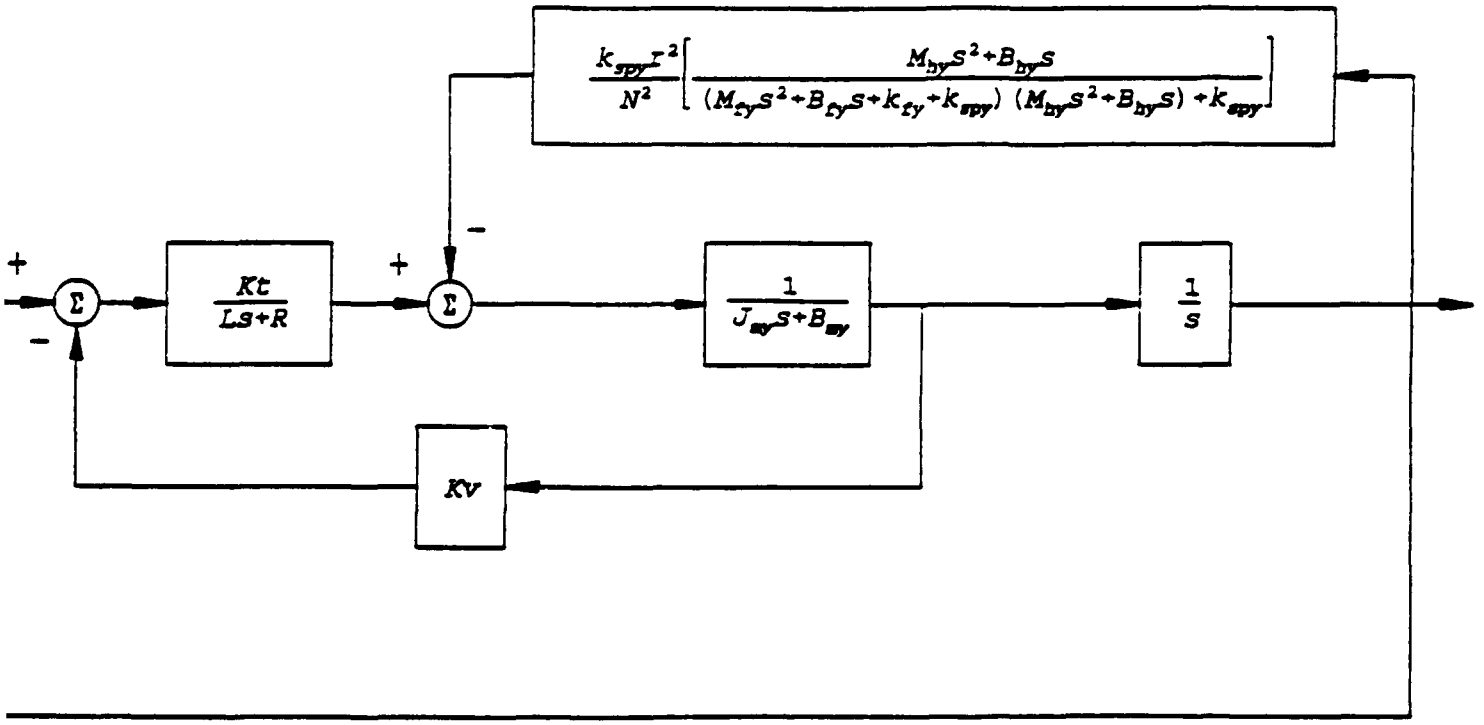

he controller,

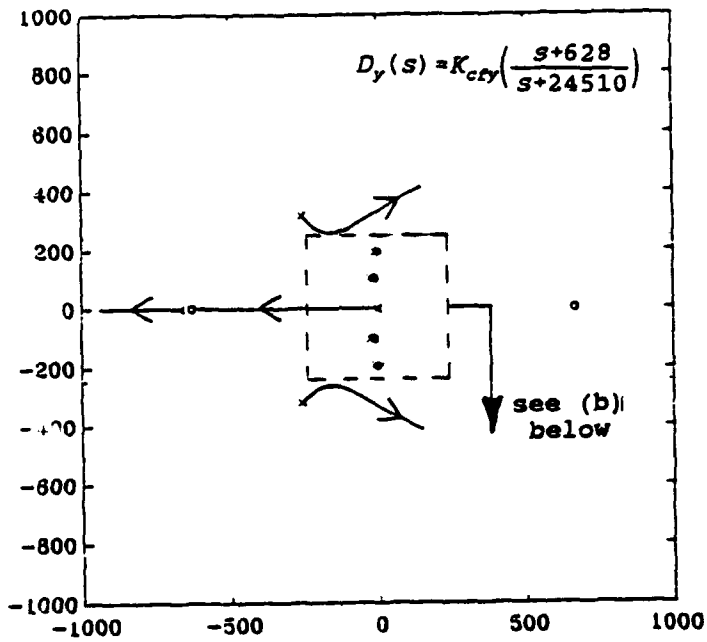

(a) The entire root locus.

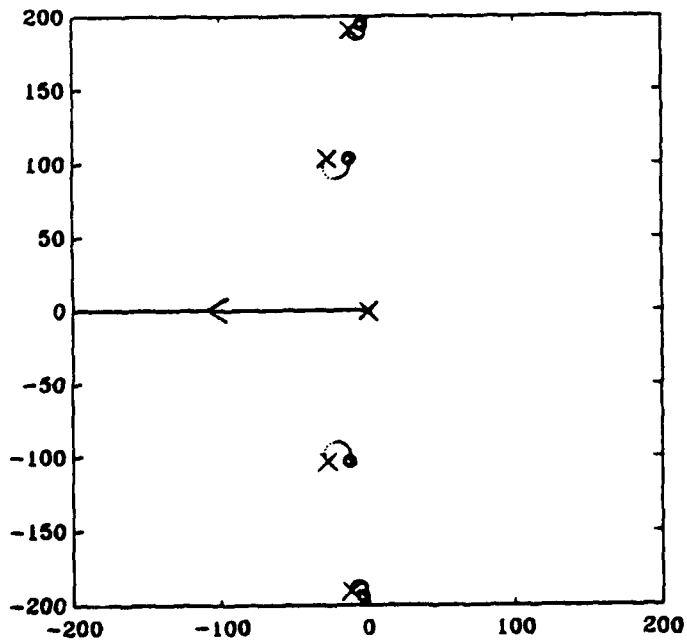

(b) The dominant roots.

Figure 4.9. Root locus of $1+KD_y(s)G_y(s)$.

axis when flexibilities are present outside of the feedback loop.

Tracking Control

Several issues concerning the design of the stitcher must be addressed to improve its tracking performance. These issues include the stiffness of the stitcher frame, the stiffness of the drive trains and the type of controller to be used on each axis. Several design modifications were included in the stitcher model and simulated to judge their effectiveness. The implementation of the design changes was then addressed.

The frequency of vibration of the stitcher frame in the Y axis is not high enough to be considered negligible. Therefore, **the frame must be designed to be stiffer.** All further design and analysis will be based on the assumption that the frame is rigid in the Y direction, reducing the order of the model by two. The model of the Y axis used in the design process is shown in Figure 4.10; it is in the same form as the X axis model.

Two approaches may be used to improve the performance of the CNC stitcher. In one approach, a control system can be designed to be used with the drive train flexibility in the stitcher. In the other approach, the drive train stiffness can be increased and used with a less complex controller.

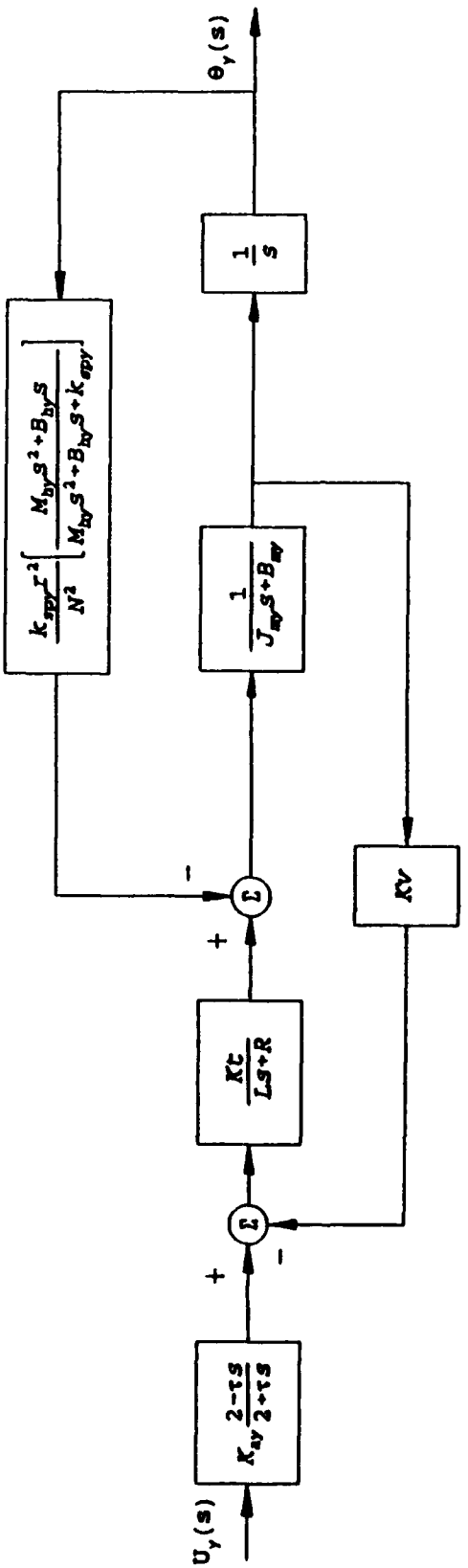

Figure 4.10. The linear continuous model of the Y axis with a rigid frame.

Control with a Flexible Drive Train

Proportion plus derivative (PD) control frequently is not sufficient in the control of systems with flexible mechanical elements such as the stitcher. Other types of control, designed using modern control techniques such as pole placement or optimal control formulations, may be used. However, these design methods utilize full state feedback. The use of full state feedback requires the addition of a sewing head position and velocity sensor on each axis since two of the states of the stitcher are the sewing head position and velocity. These sensors must be sufficiently accurate to control the position of the sewing head within ±0.5 mm of the commanded position and maintain a constant velocity within ±5% of the commanded velocity. These tolerances must be maintained for a stroke length of approximately 12 inches in the Y axis and for any stroke length in the X axis. More complex control hardware, capable of using more than one feedback signal, also must be used with full state feedback. This control option was not used for the stitcher due to the demands placed on the sewing head sensors and the need for a more complex controller.

An observer can also be used to control a system with flexibilities. Rather than using full state feedback, an observer estimates unmeasured states based on those that are measured. The observer simulates a model of the system in real time parallel to the operation of the actual system and uses the simulated and measured states to form the control

law. An observer typically incorporates high gains that can cause saturation in the system elements or amplify high frequency noise. It also requires an accurate, robust model; nonlinearities or parameter variations can significantly degrade the performance of a system that incorporates an observer. Therefore, this option was also not used in the stitcher compensation.

Control with a Rigid Drive Train

Another approach to solving the control problem involves redesigning the drive train of the stitcher. The drive train can be assumed rigid if it is designed sufficiently stiff, making the sewing head position proportional to the motor shaft angular position. This eliminates the sewing head position and velocity as states in the stitcher model, making full state feedback more practical. This approach was used to improve the performance of the stitcher.

The effect of redesigning the drive train can be seen by considering the root loci of $G_x(s)$ (see Figure 4.3, page 86) and $G_y(s)$, shown in Figure 4.11 without the frame dynamics included. The dominant poles move away from the real axis as the drive train is made stiffer. The dynamics of these poles can be considered negligible, and the drive train rigid, if the frequency of the poles is approximately ten times greater than the system bandwidth.

The model of each axis was revised with a rigid drive train for control system design. The load in each axis was reflected onto the motors through the drive ratio currently

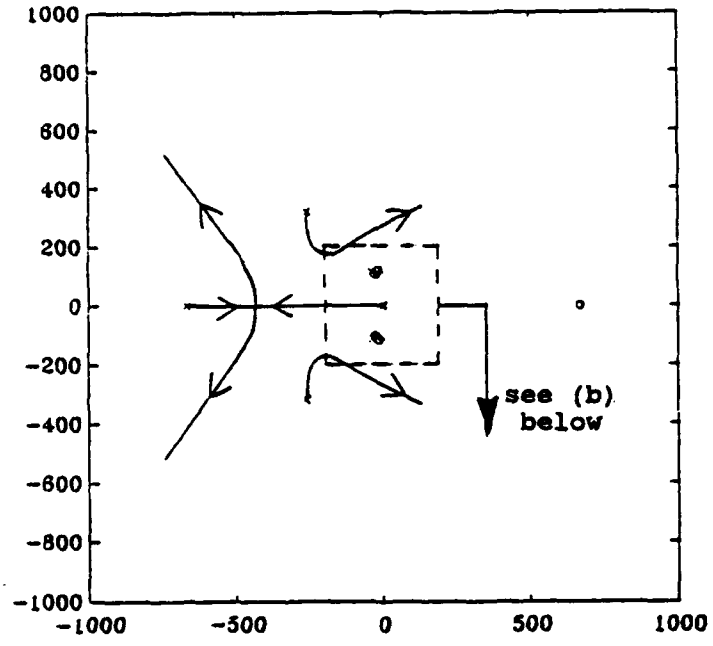

(a) The entire root locus.

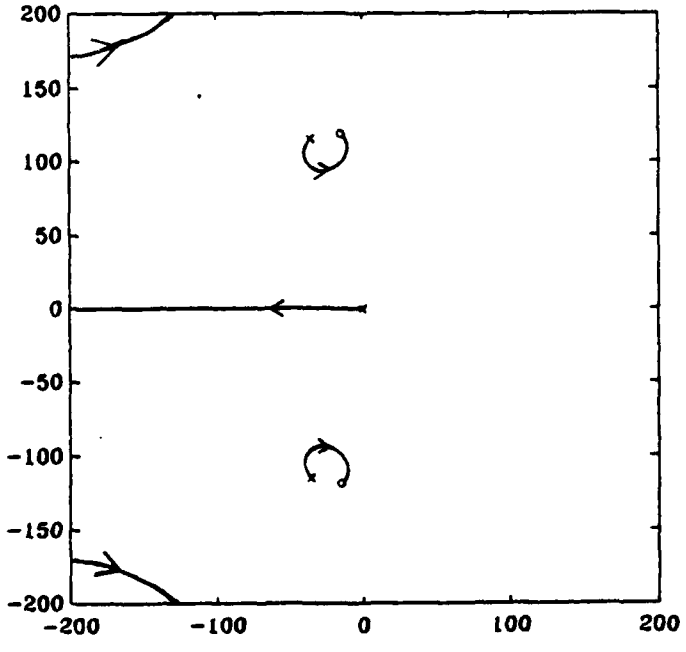

(b) The dominant roots.

Figure 4.11. Root locus of $1+KG_y(s)$ with a rigid frame.

on the stitcher, r/N. The resulting reduced order models, $G_{xro}(s)$ and $G_{yro}(s)$, are shown in Figure 4.12.

Proportional Control

Proportional control was the first type of control considered. The proportional gains, K_{px} and K_{py}, can be determined directly from the root loci in Figure 4.13 based on the desired step response of the system. However, the performance requirements of the stitcher were determined based on its response to the reference signal rather than a step input. Therefore, the linear stitcher model was simulated with various values of K_{px} and K_{py} to determine the acceptable values of the gains. The root loci were used to predict the changes in the response resulting from changes in the proportional gains. The poles in the root loci remain close to the origin of the s-plane when the gains are set to low values. This results in the "cut" corners in the tracking simulation shown in Figure 4.14. When the gains are set to high values, the complex poles move toward the imaginary axis in the root loci, resulting in excessive overshoot in the corners of the simulation in Figure 4.15. The positioning requirements were satisfied in the simulation in Figure 4.16 with $K_{px} = 2$ and $K_{py} = 2$.

The velocity response of each axis to a commanded slew velocity of 7.8 (in/sec) and an acceleration of 546 (in/sec^2) is shown in Figure 4.17. The performance specifications state that each axis must accelerate to 95% of this slew velocity within 2 stitches (approximately 0.027 seconds) and

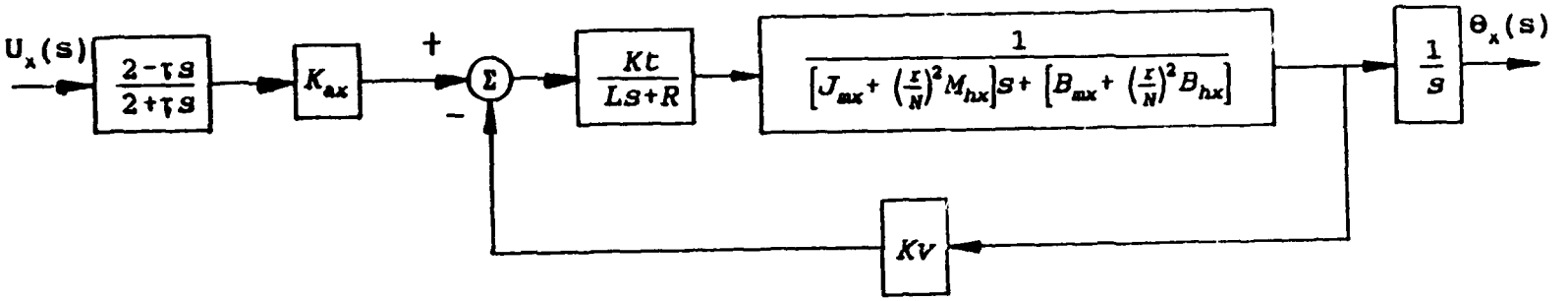

(a) $G_{xro}(s)$.

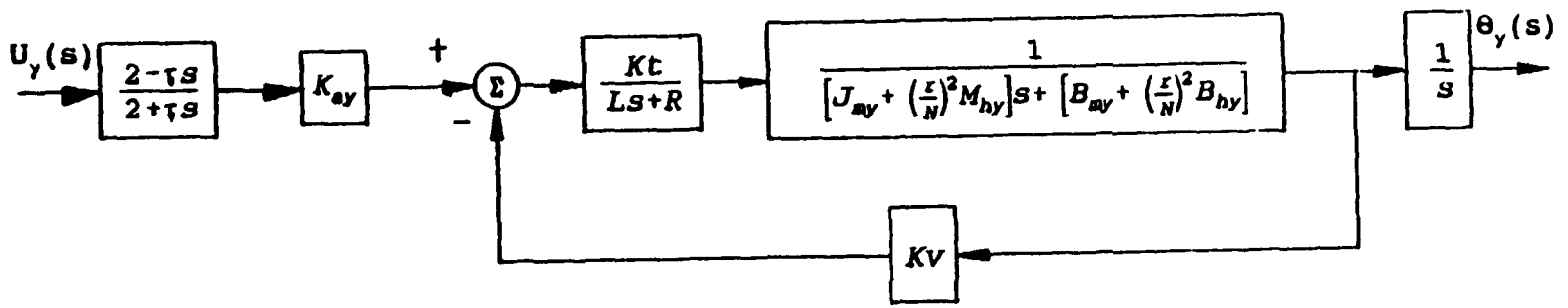

(b) $G_{yro}(s)$.

Figure 4.12. The X and Y axis models with rigid drive trains.

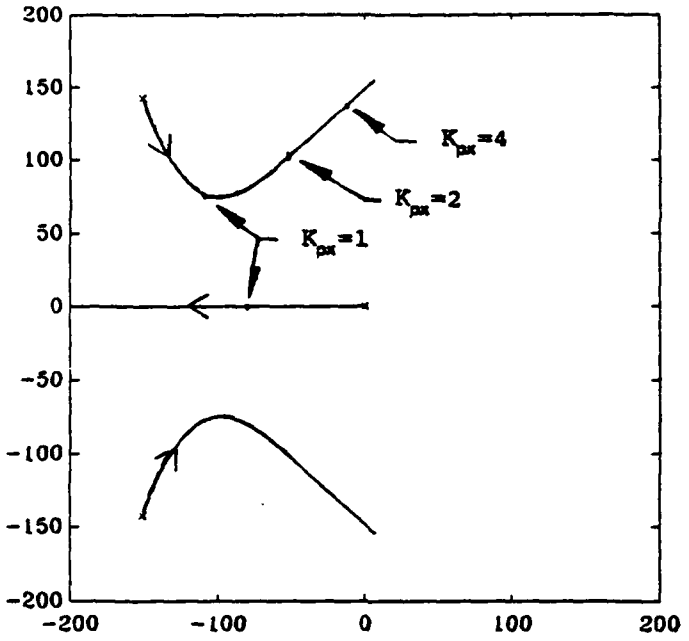

(a) The root locus of $1+K_{px}G_{xro}(s)$.

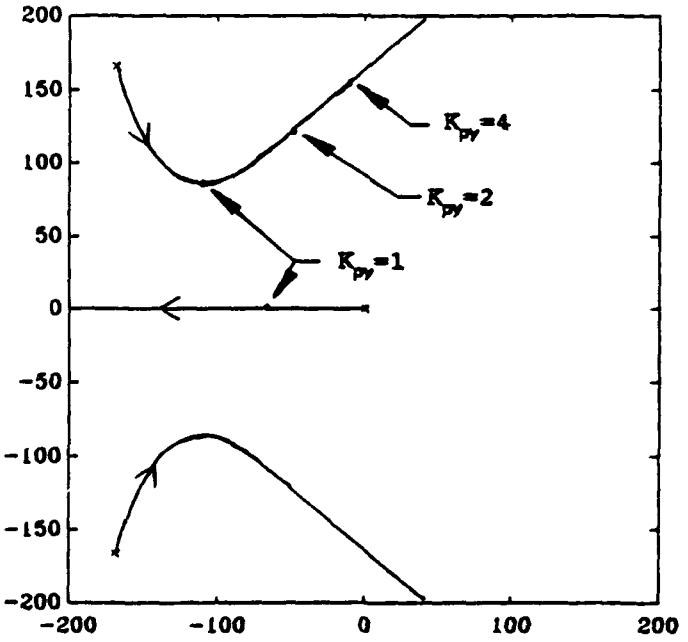

(b) The root locus of $1+K_{py}G_{yro}(s)$.

Figure 4.13. Root loci of the reduced order models.

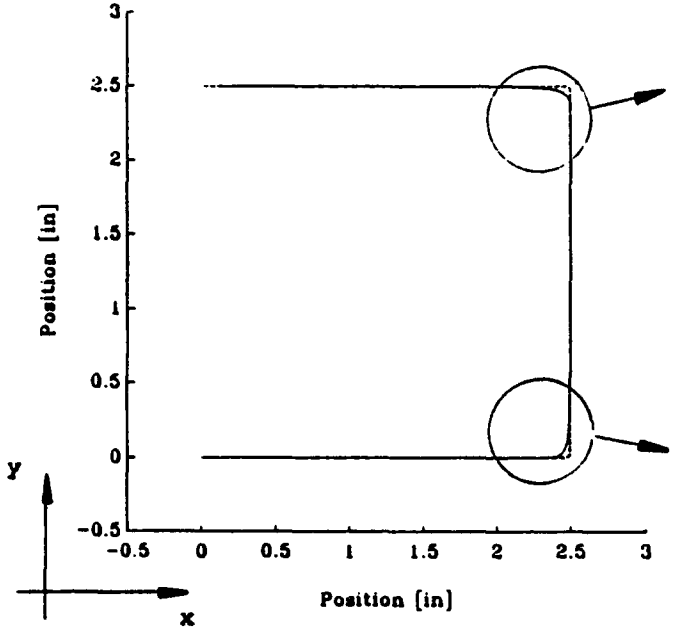

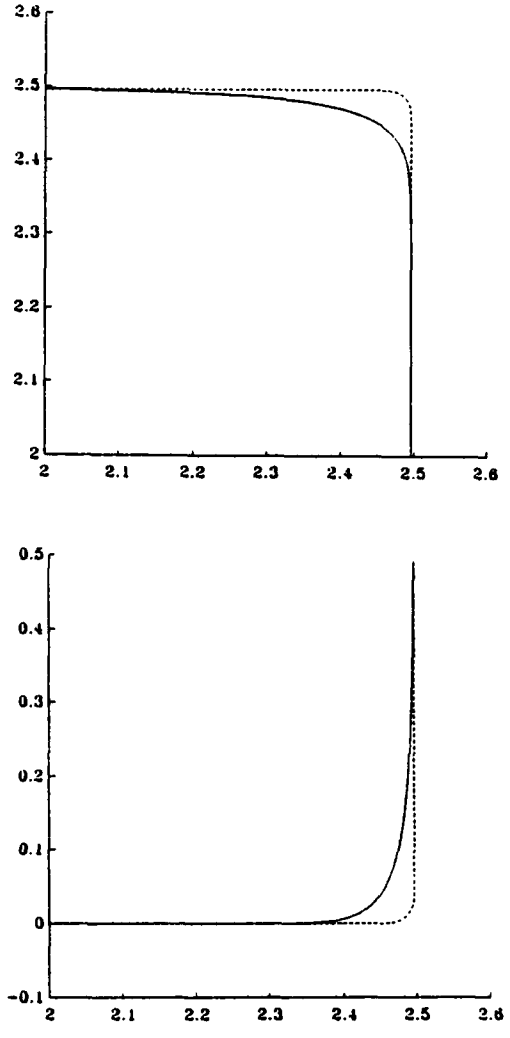

Figure 4.14. The linear model tracking simulation with K_{px} = 1.0 and K_{py} = 1.0.

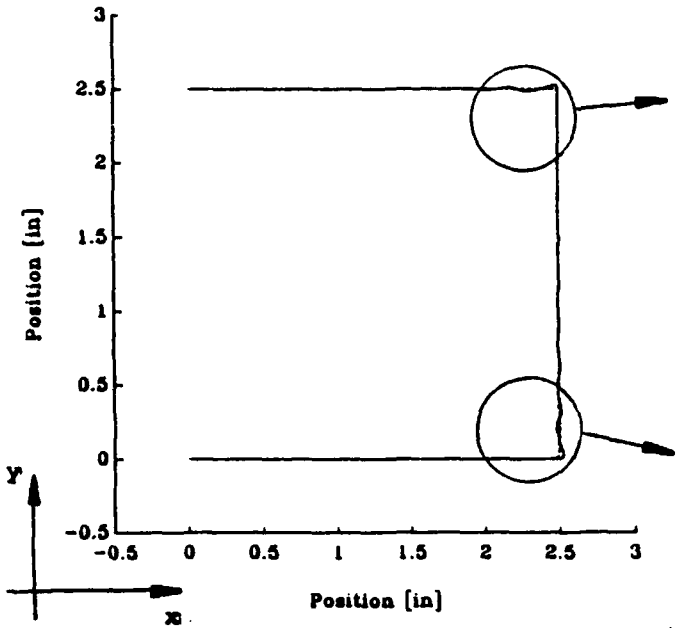

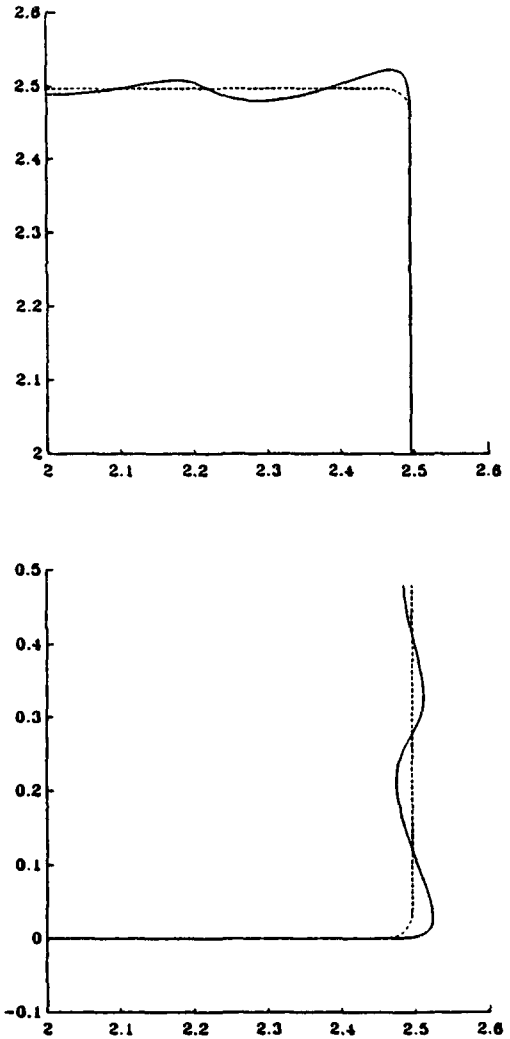

Figure 4.15. The linear model tracking simulation with K_{px} = 4.0 and K_{py} = 4.0.

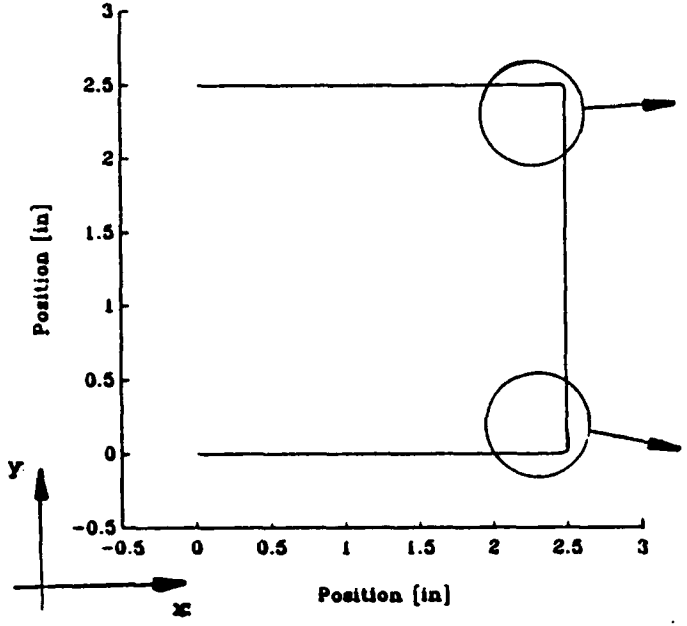

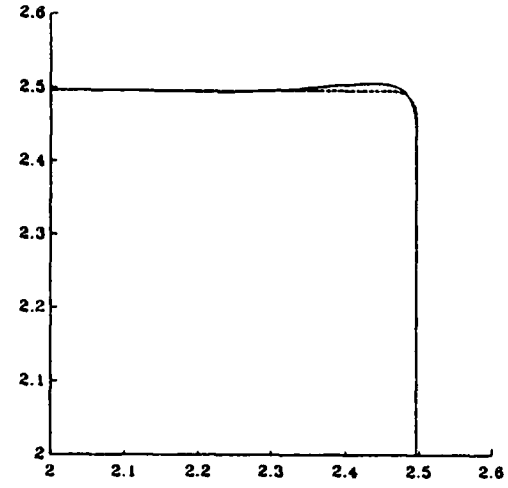

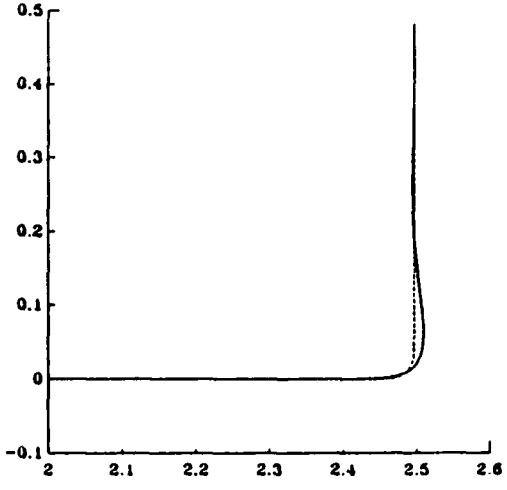

Figure 4.16. The linear model tracking simulation with K_{px} = 2.0 and K_{py} = 2.0.

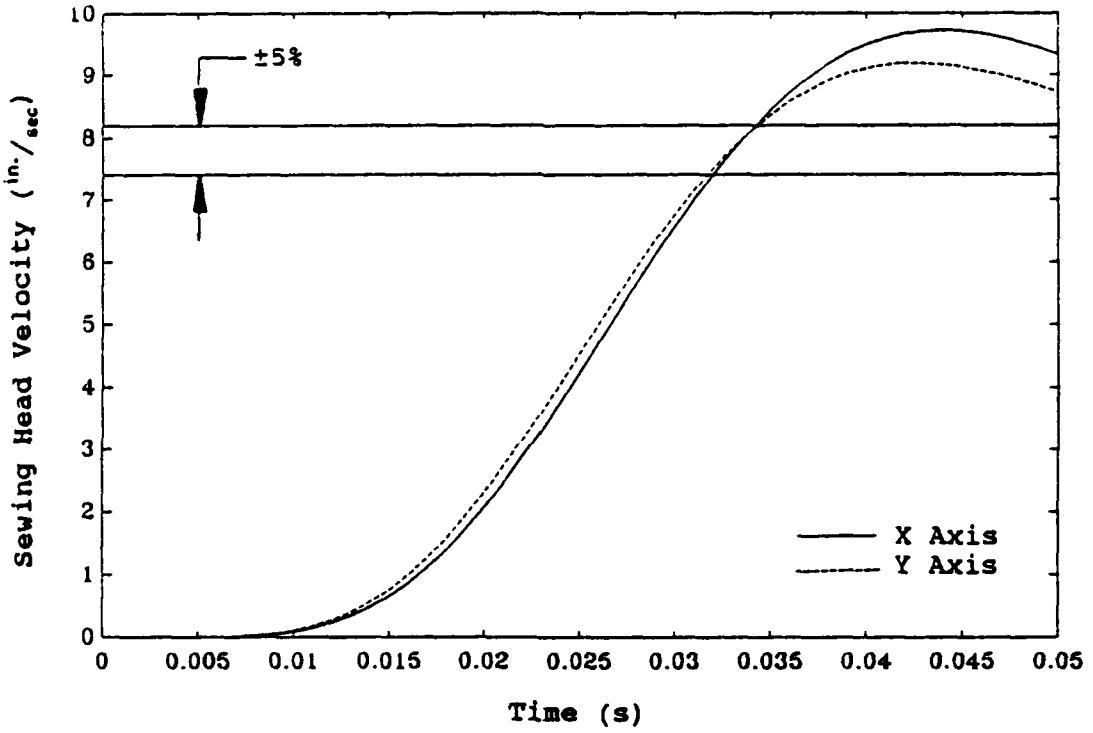

Figure 4.17. Simulated velocity response with K_{px} = 2.0 and K_{py} = 2.0.

maintain the sewing head velocity within ±5% of the commanded velocity. Neither axis meets this specification with proportional control, as shown in the figure. Therefore, derivative control was added to maintain an acceptable position overshoot while improving the velocity response of each axis.

Proportional Plus Derivative Control

The general form of a PD controller is $D(s) = K_p(1+T_D s)$ where K_p is the proportional gain and T_D is the derivative time. The PD controller was implemented with a high frequency pole in the form

$$D(s) = K_{cf}\frac{s+\frac{1}{T}}{s+\frac{1}{\alpha T}}, \qquad (4.1)$$

where $\alpha<1$, to avoid high frequency noise amplification. The frequency response design method was used to determine the values of K_{cf}, T and α.

The response of the stitcher to the reference signal was related to its frequency response by considering the frequency response of two second order axis models. The bandwidth, ω_{BW}, and the phase margin, PM, of each second order axis model were adjusted until the model met the performance specifications of the stitcher. The parameters of the acceptable second order "target" model of each axis, ω_{BW} = 25 Hz and PM = 65°, were used as the initial estimates of the values of the actual axis models in the design process.

The Bode plot of the open loop X axis model, $G_{xro}(s)$, is shown in Figure 4.18. The figure shows that the gain must be

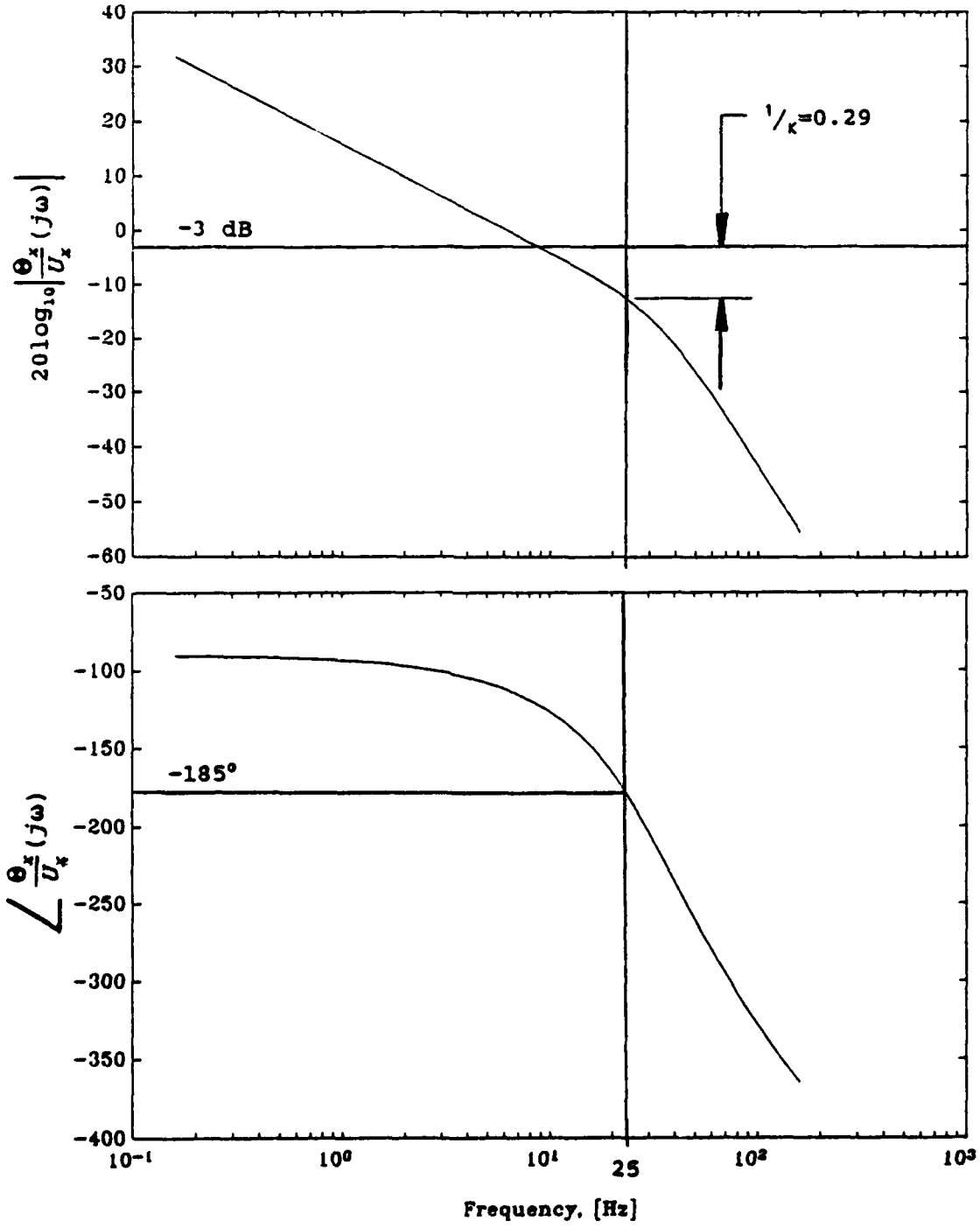

Figure 4.18. The Bode plot of the open loop model $G_{xro}(s)$.

increased by a factor of 3.4 and the phase must be increased by 70° to match the gain and phase margin of the "target" model. The Bode plot of the open loop Y axis model in Figure 4.19 shows that the gain of $G_{yro}(s)$ must be increased by a factor of 3.4 and the phase must be increased by 61°.

The positioning specifications could not be met by the linear stitcher model with the acceleration set point set to 546 (in/sec^2). However, the linear model did meet the position specifications with the acceleration doubled to 1092 (in/sec^2) and the following X and Y axis filters

$$D_x(s) = 178\left(\frac{s+175}{s+14821}\right) \tag{4.2a}$$

and

$$D_y(s) = 170\left(\frac{s+200}{s+14821}\right). \tag{4.2b}$$

The Bode plots in Figure 4.20 of the closed loop models

$$H_x(s) = \frac{D_x(s)\,G_x(s)}{1+D_x(s)\,G_x(s)} \tag{4.3a}$$

and

$$H_y(s) = \frac{D_y(s)\,G_y(s)}{1+D_y(s)\,G_y(s)} \tag{4.3b}$$

show that ω_{BWx} = 33 Hz and ω_{BWy} = 36 Hz. The differences between these values and those of the second order models are due to the phase lag of the time delay and the fact that $G_{xro}(s)$ and $G_{yro}(s)$ are fourth order. The nonlinear model of

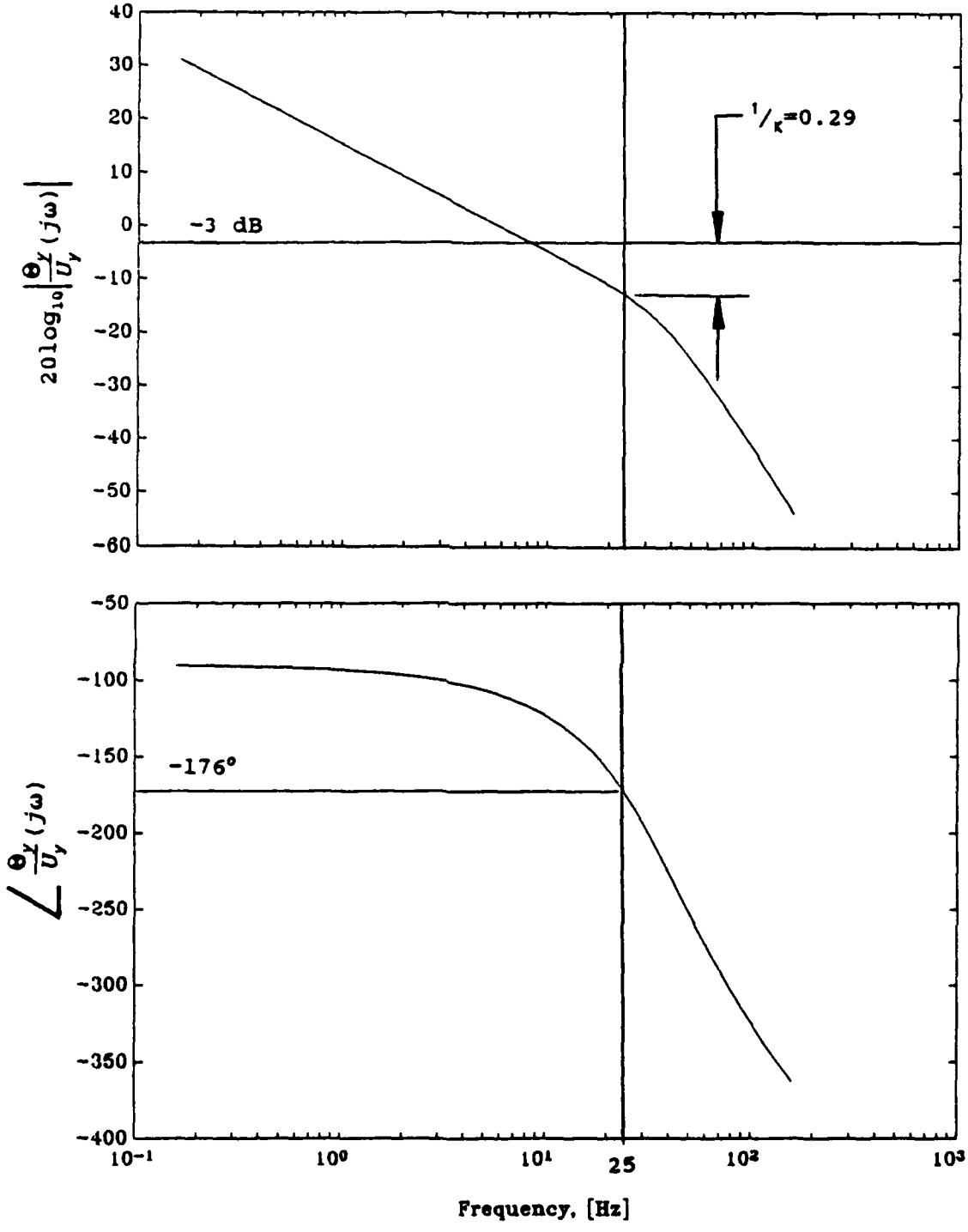

Figure 4.19. The Bode plot of the open loop model $G_{yro}(s)$.

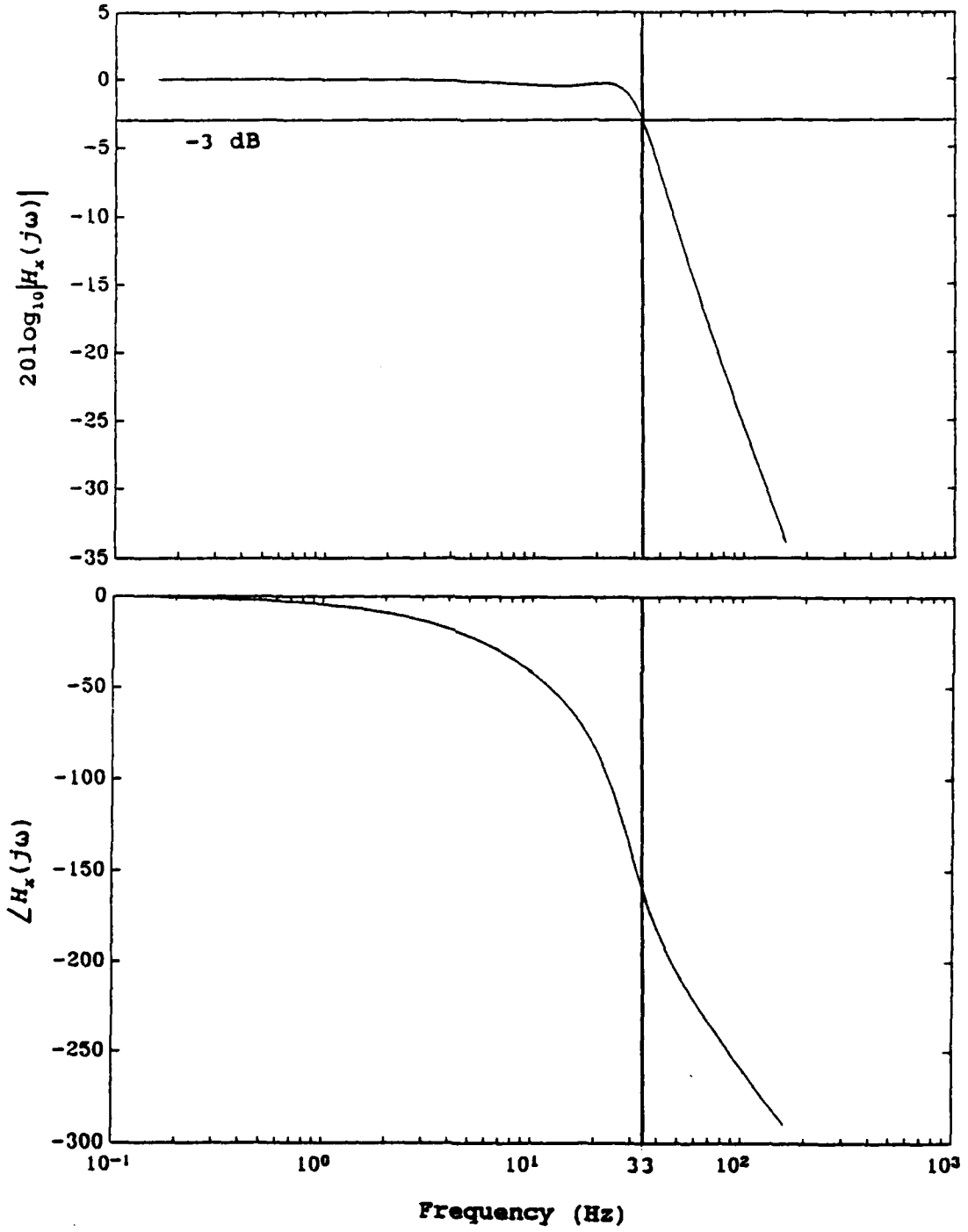

(a) The Bode plot of $H_x(s)$.

Figure 4.20. The Bode plot of the closed loop stitcher model.

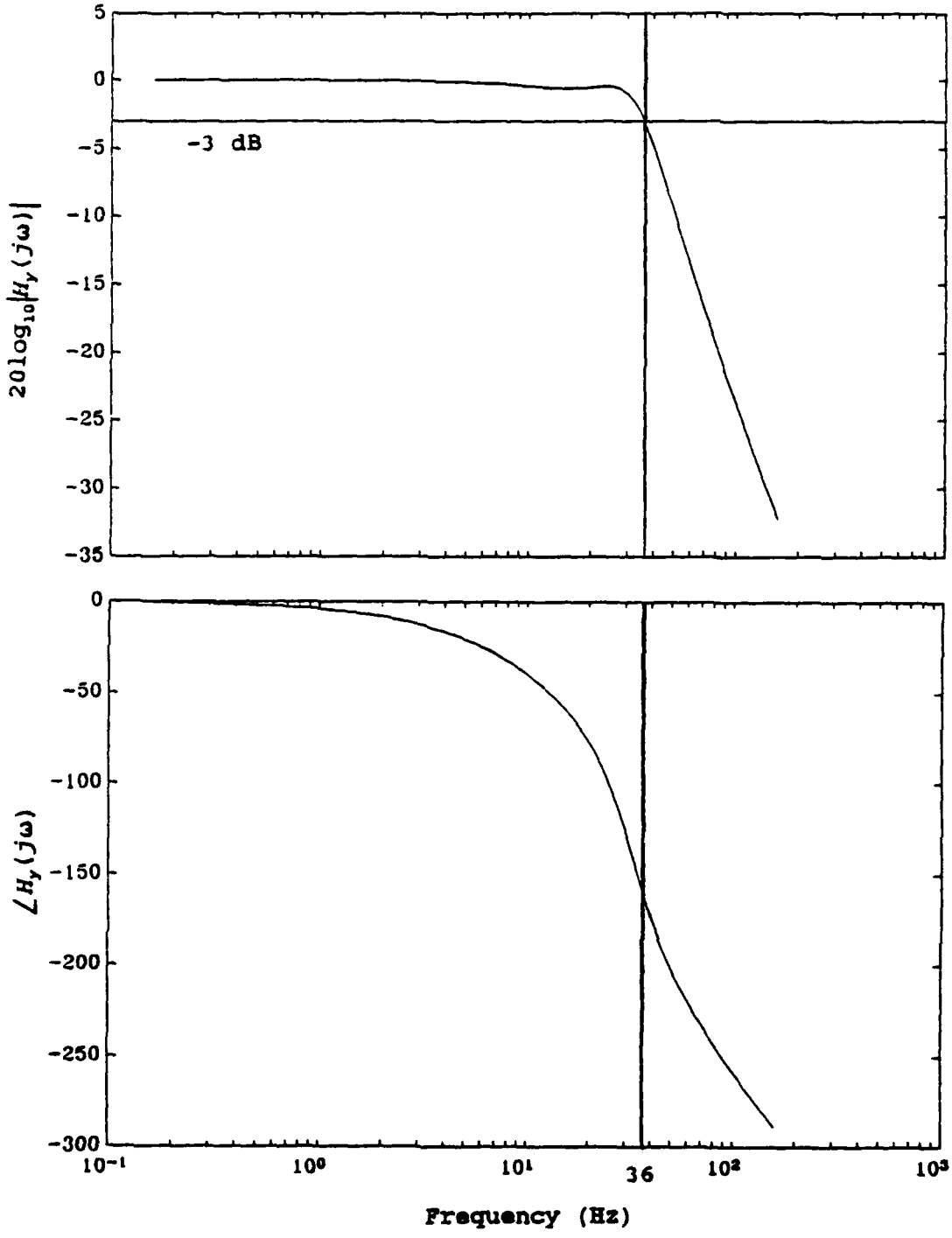

(b) The Bode plot of $H_y(s)$.

Figure 4.20. (Continued).

the stitcher was simulated with the digital form of the filters

$$D_x(z) = 0.89\left(\frac{z-0.976}{z+0.004}\right) \tag{4.4a}$$

and

$$D_y(z) = 0.85\left(\frac{z-0.973}{z+0.004}\right). \tag{4.4b}$$

The simulation results in Figure 4.21 show that the nonlinear system does not meet the velocity response specifications of the stitcher. The current saturation in each amplifier model, which limits the torque developed by the motor, limits the velocity and acceleration in the axes. The presence of current saturation in the amplifier limits the motor torque, indicating that the amplifier is operating near its capacity in the simulation. Therefore, the mass of the loads in the axis models $G_{xro}(s)$ and $G_{yro}(s)$ were reduced by 50%, forming the reduced mass models $G_{x2ro}(s)$ and $G_{y2ro}(s)$. The filter design process was repeated for $G_{x2ro}(s)$ and $G_{y2ro}(s)$ with the reference acceleration set to 1092 (in/sec^2). The simulation in Figure 4.22 of the closed loop, compensated nonlinear model shows that the performance specifications are met when the mass is reduced and the digital filter in the axes are

$$D_x(z) = 0.72\left(\frac{z-0.966}{z+0.047}\right) \tag{4.5a}$$

and

$$D_y(z) = 0.77\left(\frac{z-0.961}{z+0.188}\right). \tag{4.5b}$$

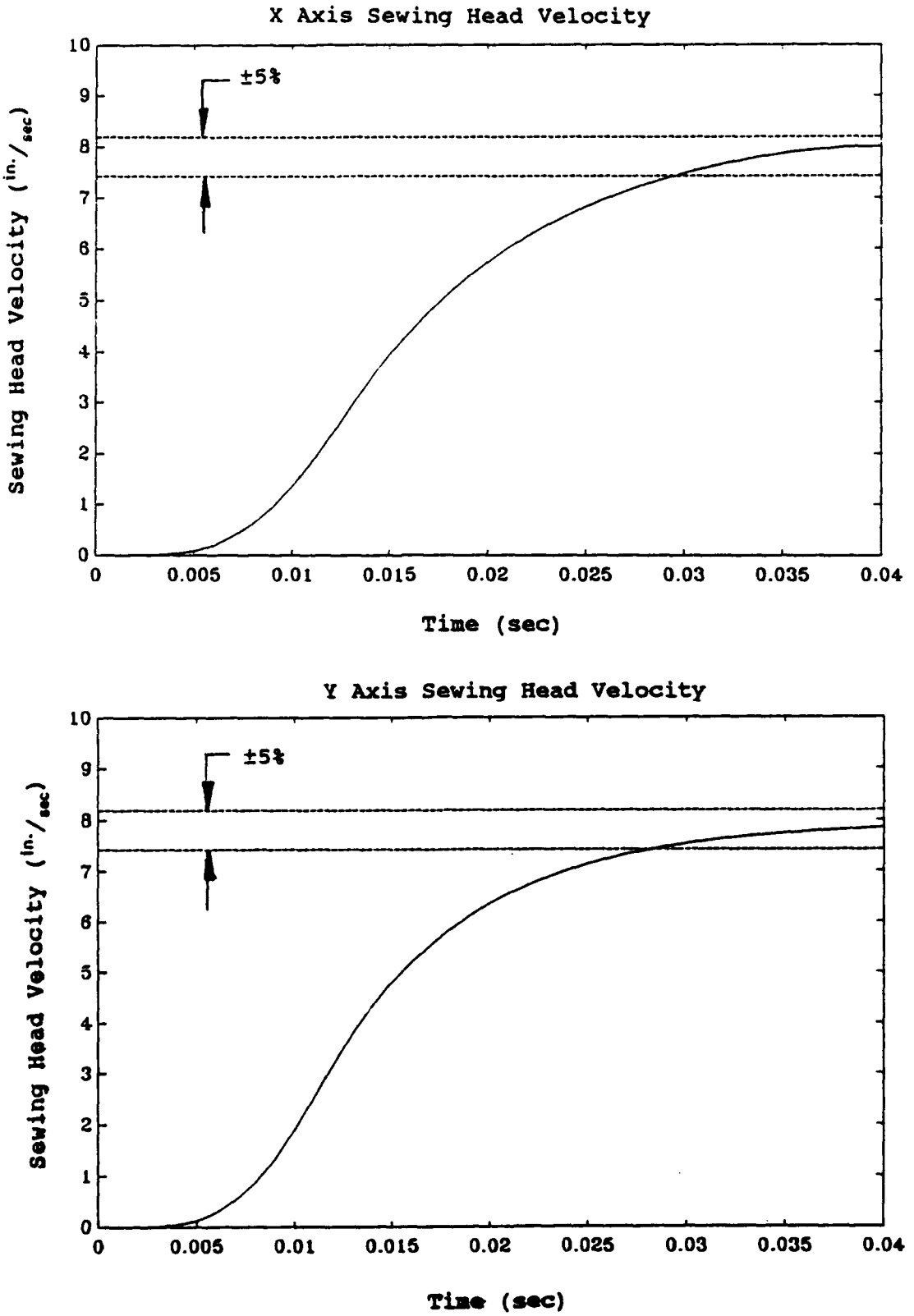

Figure 4.21. The nonlinear model velocity response simulation.

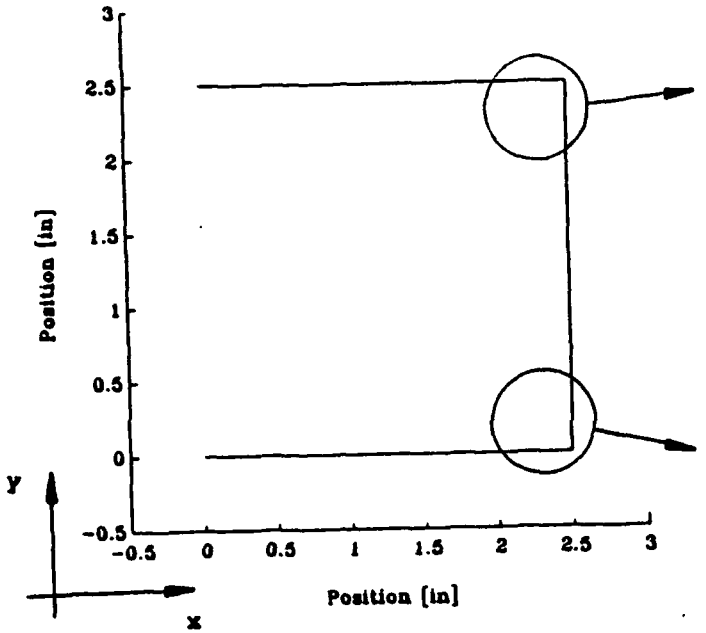

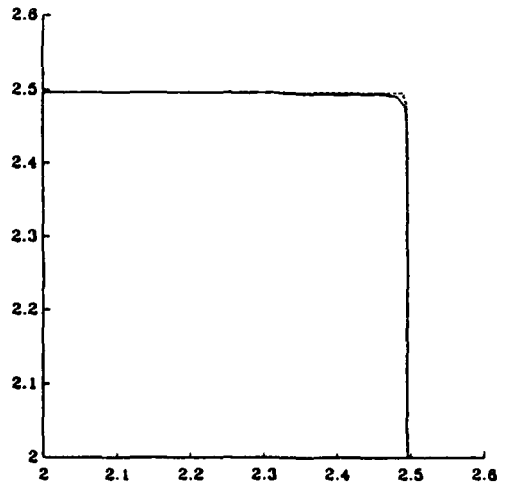

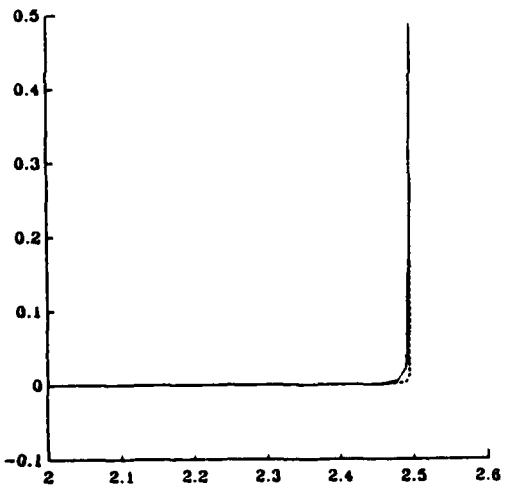

(a) The simulated tracking response.

Figure 4.22. The nonlinear model simulation with the mass reduced by 50% in each axis.

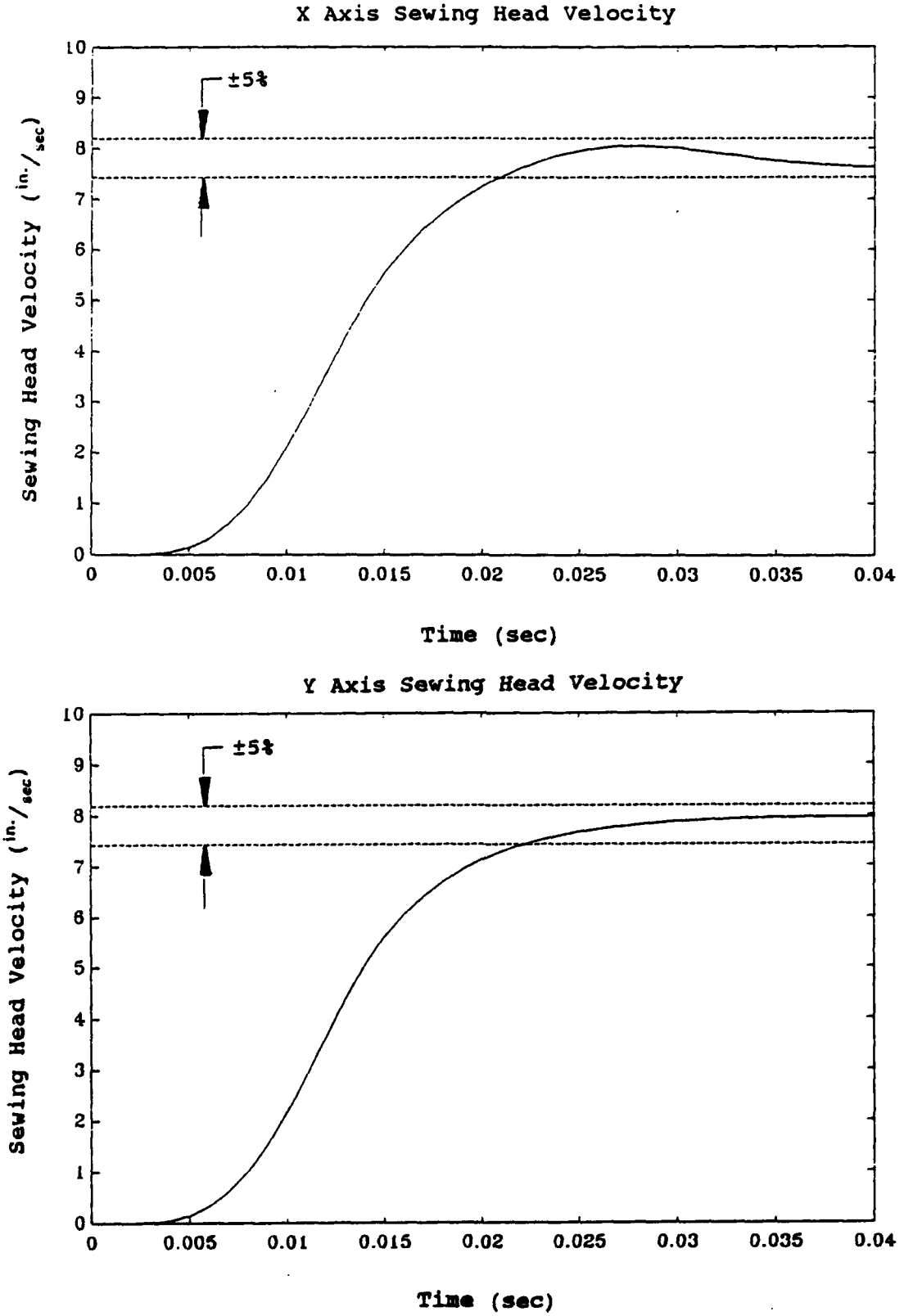

(b) The simulated velocity response.

Figure 4.22. (Continued).

Stitcher Design Modifications

The dynamic analysis of the stitcher indicates that three principal design modifications must be made: (1) the frame must be made stiffer, (2) the mass of the load must be reduced and (3) the drive train must be stiffer. These design modifications were addressed, although the detailed designs are beyond the scope of this study.

Stitcher Frame Design

The stitcher frame consists of two subframes, constructed from square cross sectional steel tubular members, stacked vertically and bolted together. It is expected to become more flexible in the X direction, as it is in the Y direction, because the geometry and construction of the frame is similar in both directions. Therefore, the frame should be redesigned to increase its stiffness with the addition of stiffening cross members, the use of structural members with larger cross sectional areas and/or using a single unit frame rather than two subframes.

Stitcher Design Configuration

The mass of the load in each axis can be significantly reduced if the stitcher is designed such that the fabric workpiece moves in the X and Y axes and the sewing head remains fixed. The complexity of the material handling system associated with this design should be considered. The material handling system associated with the current stitcher design must be capable of loading the fabric workpiece into a

rigid sewing fixture which holds the workpiece fixed during the sewing operation. The material handling system used with the alternate design must load the fabric workpiece into a sewing fixture and transfer the fixture and workpiece to the CNC machine so it can be translated along the stitch path. The additional material handling operation associated with the alternate design involves the manipulation of the sewing fixture, which is typically a small, rigid device. The complexity of this operation is negligible compared to the task of manipulating the limp fabric workpiece, which is common to both stitcher designs.

Drive Train Design

The frequency of the poles of each axis model near the imaginary axis in the s-plane must be approximately ten times greater than the bandwidth of the closed loop compensated system to consider the drive train rigid. Since these poles do not move appreciably when motor shaft position feedback is used, the open loop pole locations were considered when determining the necessary value of k_{spx} and k_{spy}. The bandwidths of the linear models with the reduced mass are ω_{BWx} = 39 Hz and ω_{BWy} = 38 Hz; the spring constant in each axis was found to be k_{spx} = 6e7 (N/m) and k_{spy} = 1e8 (N/m) for the drive train to be considered rigid. This is approximately 100 times greater than the stiffness of the timing belt in each axis. Therefore, some type of transmission device other than the timing belts, such as a ball screw drive or steel belts, must be used in each axis.

Summary

An analysis of each model showed that motor shaft position feedback is not sufficient to control the tracking of the stitcher in its present design due to the flexibility of the timing belts driving the sewing head. Therefore, the stitcher model was modified to include a rigid drive train rather than the flexible timing belts. This design was capable of more accurate sewing head positioning; however, it did not meet the acceleration requirements of the stitcher. The model met the all of the performance requirements of the stitcher when the mass of the load in each axis was reduced by 50%, the acceleration set point in the reference signal was doubled and PD control was used.

The performance improvement in the stitcher model can be realized in the actual stitcher with three principal design modifications. The stitcher frame must be redesigned to be stiffer than the current stitcher frame, eliminating an extra mode of vibration in the Y axis. The mass of the load in each axis must also be reduced. This can be accomplished by altering the configuration of the stitcher such that the fabric workpiece translates along the stitch path and the sewing head remains stationary. The third design modification involves the drive train. A resonant mode can be eliminated in each axis if a stiff transmission device such as a ball screw or steel belt is used rather than the timing belts.

CHAPTER V

CONCLUSIONS AND RECOMMENDATIONS

Conclusions

A two axis CNC stitcher has been developed for use in an apparel assembly workstation. The stitcher is configured so that its geometry facilitates the expansion of the stroke length in the X direction, which is perpendicular to the sewing head throat, so that it can be used in a variety of garment sizes. Most CNC stitchers currently used in the apparel industry do not have this advantage; they can be used on a limited range of garment part sizes. Each axis of the CNC stitcher developed in this research consists of a brushless DC servomotor driving the sewing head through a timing belt. The performance of the stitcher was evaluated, the dynamics of the stitcher were analyzed and a method of improving the performance of the stitcher was presented.

The quality standards in the apparel industry require each stitch in the sewn garment to be placed within ±0.5 mm of the commanded stitch path. The stitch length must be maintained within 5% of the commanded length; however, the two stitches sewn immediately prior to the direction change and the two stitches sewn immediately after the direction change at a corner in the stitch path may have nonuniform lengths accommodating the acceleration and deceleration of the sewing head. With a constant stitch speed of 75

(stitches/sec) and an operating velocity of 7.8 (in/sec), the stitcher must be capable of accelerating at a rate of 281 (in/sec^2) to accelerate to the operating speed within two stitches. The positioning capabilities of the stitcher were evaluated by following a reference stitch path consisting of two right angle corners. The maximum dynamic overshoot was found to be approximately 2.0 mm in the X axis and 1.5 mm in the Y axis.

The models of the stitcher axes were developed by conceptually dividing each axis into three subsystems: the controller, the actuating system and the load. An exact algorithm for the controller is known since it is implemented digitally; the models of the other subsystems were developed based on the experimental behavior of the stitcher.

The actuating systems, consisting of the servomotors, the amplifiers and the speed reduction gears, were disconnected from the other subsystems and evaluated. The Bode plot of the actuating system of each axis was generated by driving the amplifier with a swept sine wave and monitoring the resulting speed of the motor shaft using a FFT analyzer. The frequency response showed that the bandwidth of the X axis actuating system is 80 Hz (500 rad/sec) and the bandwidth of the Y axis actuating system is 64 Hz (400 rad/sec). Furthermore, each actuating system was found to behave like a second order system with a time delay. A linear model of each actuating system was developed to approximate the frequency response data of the actual systems. The frequency

response of the models compared favorably to that of the actual systems at frequencies within the bandwidth of the system. However, the accuracy of the phase of the models deteriorates at frequencies above 100 Hz due to the first order linear approximation of the time delay.

The experimentally determined position step response of the X axis actuating system indicates that the amplifier saturates at a commanded step size of approximately $\pi/2$ radians without the load attached. This behavior was assumed to be present in the Y axis since the amplifiers and motors are the same in each axis.

The frequency response experiment performed on the actuating systems was repeated with the load connected to identify the dynamic characteristics of the load in each axis. The load in the X axis was found to have a resonant frequency at 12 Hz (75 rad/sec) due to the sewing head and the elastic timing belt. The Y axis load was found to have resonant frequencies at 30 Hz (188 rad/sec), due to the sewing head and elastic timing belt, and at 15 Hz (94 rad/sec), due to the vibration of the stitcher frame. Therefore, the X axis load was model as a second order system, and the Y axis load was modeled as a fourth order system.

The nonlinearities of the system were included with the models of the actuating system, load and controller of each axis to form a nonlinear model of the stitcher. The stitcher and the model were tested and simulated with a reference signal containing two right angle corners to determine the

accuracy of the model. The overshoot of actual system is 0.08 inches (2.0 mm) in the X axis and 0.06 inches (1.5 mm) in the Y axis at the corners while the overshoot of the model is 0.067 inches (1.78 mm) in the X axis and 0.05 inches (1.3 mm) in the Y axis. The dynamic differences between the model and the actual system are assumed to be due to the unmodeled higher order dynamics and nonlinearities.

The design changes necessary to improve the performance of the stitcher were determined based on an analysis of the linear model. The most practical design changes that result in the model meeting the performance specifications involve reducing the mass of the load in each axis and reducing the flexibility in the drive train. When the spring constant in each axis drive train is increased by a factor of approximately 100, the dynamics associated with the drive train are negligible. The mass of each load was also reduced by 50% due to the motor torque saturation in the stitcher. The parameters of the lead filter implemented in the digital controller were determined simultaneously with the hardware design changes in the stitcher such that the model met the performance specifications. The redesigned stitcher model accelerates to 95% of the operating velocity in 0.021 seconds and has a position error of 0.016 inches (0.4 mm) in the corner of the simulated stitch path in the X axis. In the Y axis, the positioning error is 0.012 inches (0.31 mm) in the corner of the simulated stitch path, and the stitcher accelerates to 95% of the operating velocity in 0.023 seconds.

The bandwidth of the X axis model is 39 Hz (245 rad/sec), while the bandwidth of the Y axis model is 38 Hz (239 rad/sec).

Recommendations

Mechanical Design Modifications

Three primary design changes must be made in the stitcher to meet the performance requirements. First, the frame must be designed to be made stiffer by using larger structural members, adding stiffening cross members or designing a single unit frame. The timing belts in the drive trains also must be replaced by ball screws, steel reinforced belts or some other stiffer transmission. Finally, the mass of the load must be reduced. This may be accomplished by redesigning the stitcher such that the sewing head remains stationary while the fabric assembly moves in the X and Y axes.

Another issue concerning the stitcher design that must be addressed is the speed reducing gear set in each axis. The large polymer gear in each axis is mounted on its shaft with set screws and a key and keyway. The set screws are not spaced equally around the circumference of the shaft, causing the center of the gear to be offset from the center of the shaft when the screws are tightened. Therefore, the gear rotates eccentrically, resulting in deadband in one position of rotation and excessive friction in another position of rotation. This phenomena will cause a significant degradation in the performance of the stitcher regardless of

the type of drive train used. It was most apparent in the Y axis, possibly causing inaccuracy in the Y axis model. Therefore, either the set screws must be spaced equally around the shaft circumference or a different method of assembly, such as using an interference fit, must be employed.

Suggested Research

Future work should be directed toward the control of the stitcher in its present form, with a flexible drive train. The controller currently used with the stitcher provides closed loop compensation with only a lead filter and one feedback signal. The controller algorithm is implemented in hardware and cannot be altered, limiting the filter compensation.

System nonlinearities can be compensated with a controller that can be used to implement adaptive control. The DC2-PC100 two axis motion controller made by Precision Micro Control implements a linear closed loop PID controller with parameters that can be changed on the fly, allowing a form of adaptive control. The effectiveness of independently controlled acceleration and deceleration, which would significantly improve the cornering dynamics of the stitcher (see Middleditch and Paul [16]), can also be studied with this board.

A control scheme that is implemented in software rather than hardware allows much more flexibility in the type of control and number of feedback variables used. The Spectrum

Signal Processing Corp. TMS320C30, based on a Texas Instruments digital signal processing (DSP) chip, provides the compensation in software, allowing the user to program any type of control scheme, without limitation to traditional PID control. The sewing head position and velocity as well as the motor shaft position and velocity can be used for full state feedback with this type of control board. More elaborate control schemes using adaptive control, preview control or a state estimator may also be implemented and tested with this control board.

APPENDICES

Appendix A

Equipment List and Specifications

Stitcher Equipment

Motion Control Board

Manufacturer: Motion Engineering, Inc.
520 East Monticeito Street
Santa Barbara, CA 93103
(805) 962-5409
Fax (805) 962-8001

Part Number: MCS-200

Description: Two axis servo control board and associated software

Servo Drive System

Manufacturer: Robbins and Meyers/Electro-Craft
6950 Washington Ave. South
Eden Prairie, MN 55344

Part Number: BRU-200 Servo System

Description: DM-30 servo drive and S-4050 brushless servomotor

Motor Specifications	
Rotor Inertia:	4.6E-4 kg-m^2
Max. Operating Speed:	4000 rpm
Torque Constant:	0.5 Nm/A
Voltage Constant:	60 V/krpm
Winding Resistance:	0.8 Ω
Winding Inductance:	4.0 mH
Cont. Stall Torque:	6.78 Nm

Timing Belt

Manufacturer: Browning Manufacturing Division
Emerson Electric Co.
Maysville, KY 41056

Part Number: 800H150

Description: 0.5" pitch, 1.5" wide gear belt

Experimental Equipment

FFT Analyzer

Manufacturer:	Ono Sokki Co., LTD. Shinjuku NS Bldg. P.O. Box 6068 4-1 Nishishinjuku 2-Chome, Shinjuku-Ku, Tokyo 163, Japan
Part Number:	CF-350
Description:	Dual channel FFT analyzer

Linear Potentiometers

Manufacturer:	Maurey Instrument Company Chicago, IL 60629
Part Number:	MI326-4-502
Description:	5 KΩ ±5% linear potentiometer

Power Supply

Manufacturer:	Power Products Division of Computer Products, Inc.
Part Number:	098-013-5
Description:	±15VDC 200 mA output 60 Hz 120VAC 120 mA input power supply

Appendix B

Experimental Procedures and Results

The experimental procedures described below were performed on each axis. The equipment used in the experiments is listed in Appendix A.

Actuating System

The actuating system was isolated from the load by removing the timing belts. Three experiments were then performed to determine the dynamic behavior of the actuating system on each axis. The frequency response, system gain and the step response were determined from the experiments.

Open Loop Actuating System Frequency Response

The controller and load were disconnected from the actuating system and a two channel FFT analyzer was connected as shown in Figure B.1 to determined the frequency response of the system. A swept sine signal, with a frequency varying from 1 Hz to 200 Hz, was generated by the FFT analyzer and used to drive the amplifier. One channel of the FFT analyzer was connected to the driving signal while the other was connected to the programmable amplifier port set to monitor the motor shaft speed. The FFT analyzer determined the frequency response of the actuating system of each axis and generated the Bode plots. The frequency response magnitudes shown in the Bode plots in Figure B.2 were normalized by dividing each by the steady state gains, K_{xss} and K_{yss}.

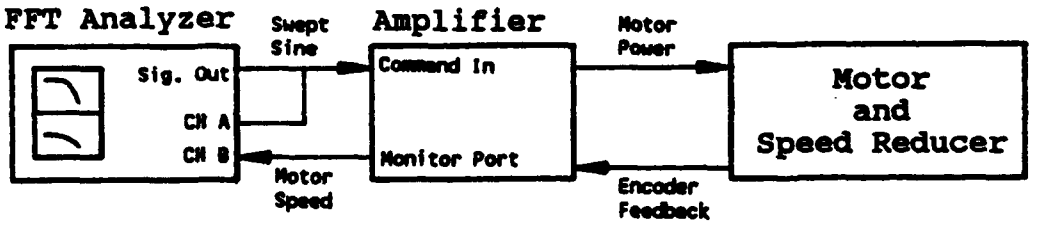

Figure B.1. Actuating system frequency response experimental arrangement.

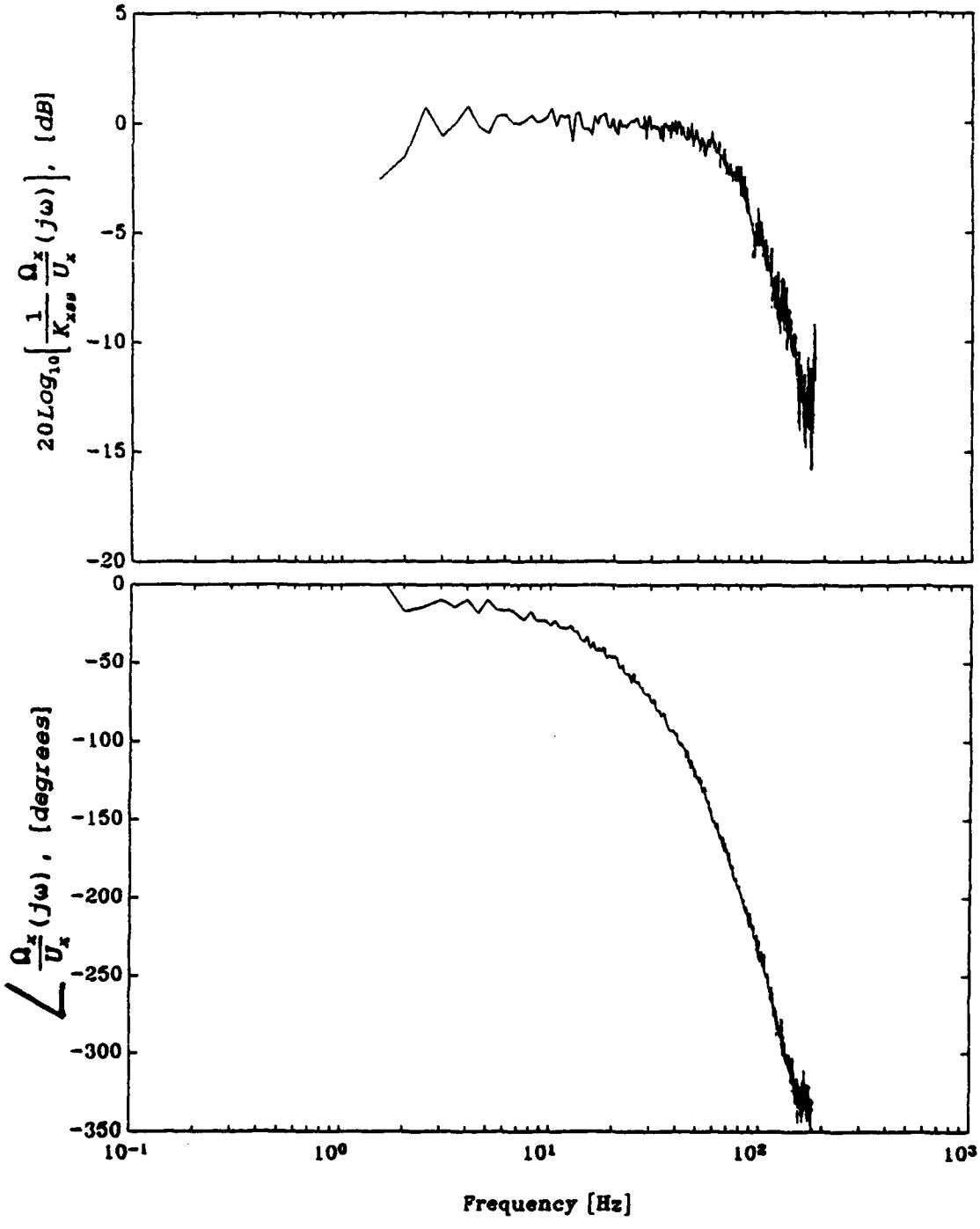

(a) X axis actuating system.

Figure B.2. Open loop actuating system bode plots.

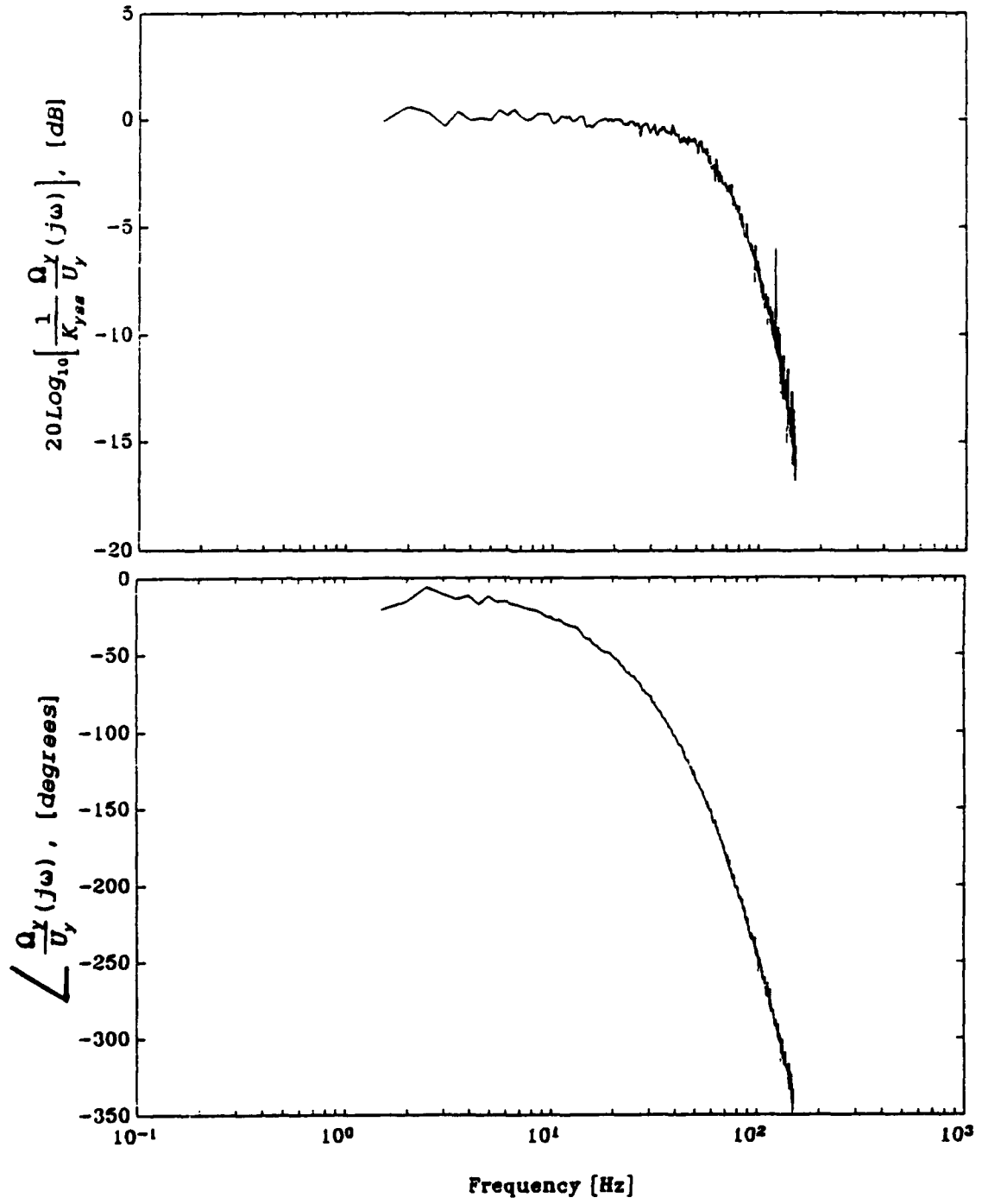

(b) Y axis actuating system.

Figure B.2. (Continued)

Therefore, the Bode plots illustrate the transient dynamics of the system with a zero frequency gain of 0 dB.

System Gain

The servocontroller was connected to the actuating system as shown in Figure B.3 and operated in the open loop mode to determine the actuating system gain. An eight bit motor command word was written to the motor command register of the motion control chip using the MC tuning software. The resulting speed of the driven gear, ω_g, was measured using a optical tachometer. The curves relating the command signal, u, and the motor shaft speed, ω, in Figure B.4 were generated noting that $\omega=6\omega_g$, and $u=K_{DAC}u_{DIG}$, where the DAC gain, K_{DAC}, is 0.078125 (volts/count) and u_{DIG} is the eight bit motor command word.

Step Response

The closed loop position step response of the actuating system was used to identify the presence of system non-linearities. The controller was connected to the actuating system as shown in the experimental arrangement in Figure B.5a and used to drive the system with motor shaft step commands of $\pi/8$, $\pi/4$, $3\pi/8$, $\pi/2$, π, 2π, 4π and 8π radians. The MC tuning program was used to display the response of the system on the PC monitor. The step response plots, shown in Figure B.5b, were normalized to the steady state values. This experiment was not repeated on the Y axis due to the similarities in the actuating systems of the two axes.

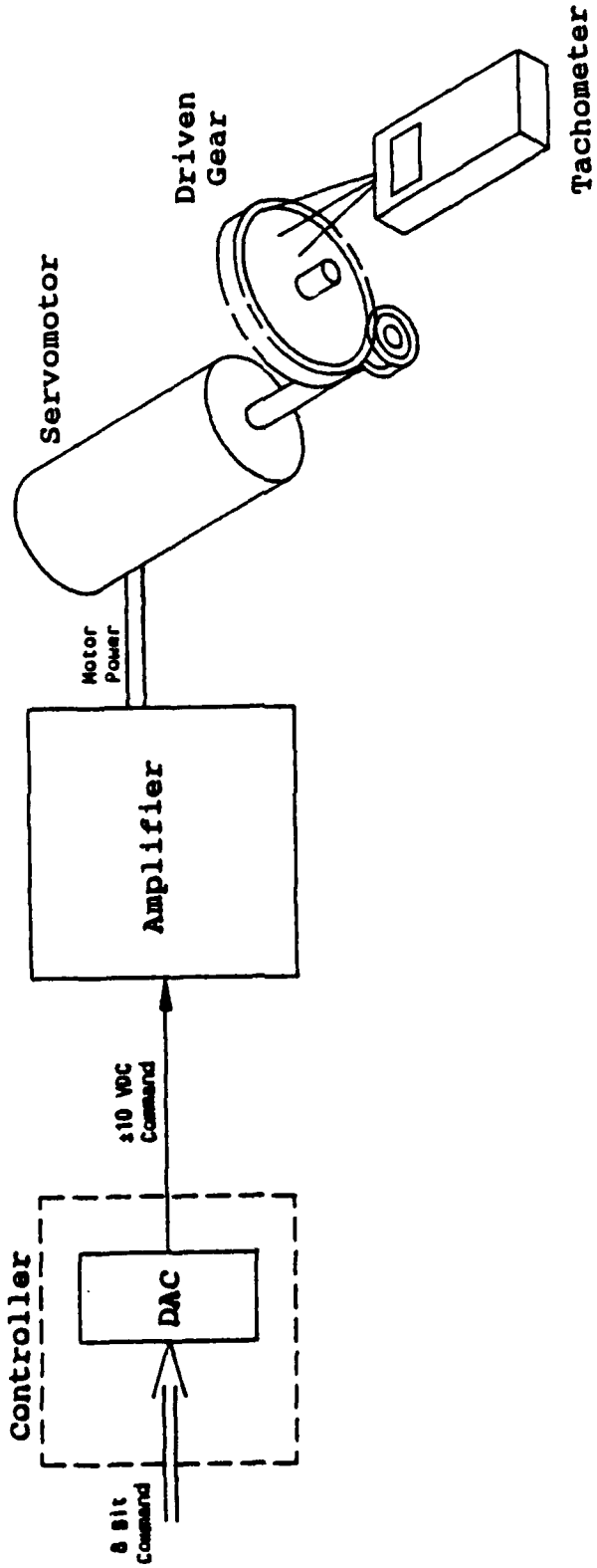

Figure B.3. Actuating system gain experimental arrangement.

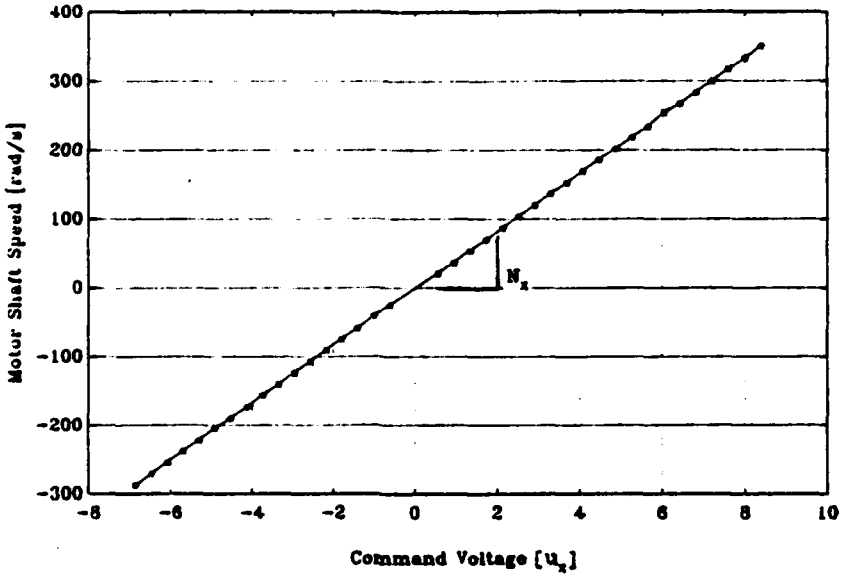

(a) X axis motor speed, ω_x versus command signal, u_x.

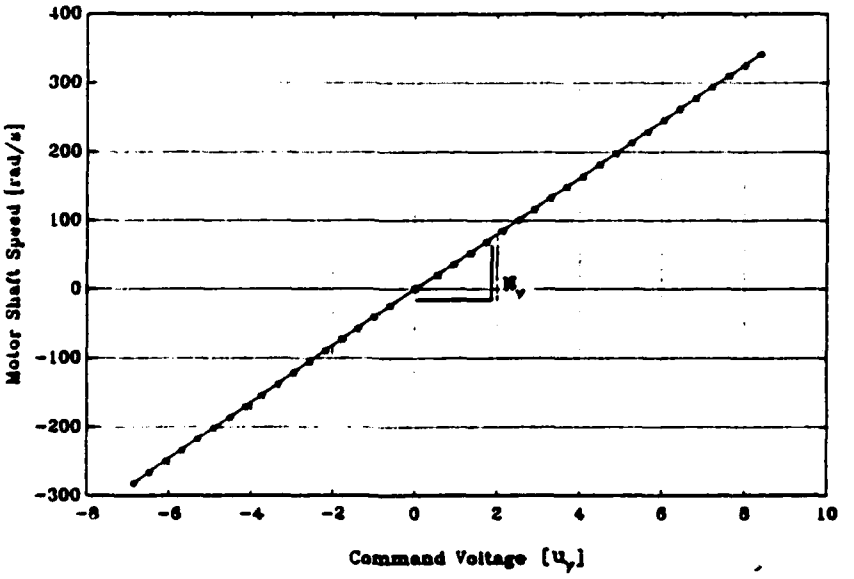

(b) Y axis motor speed, ω_y versus command signal, u_y

Figure B.4. Experimentally determined functions relating motor shaft speed and command signal.

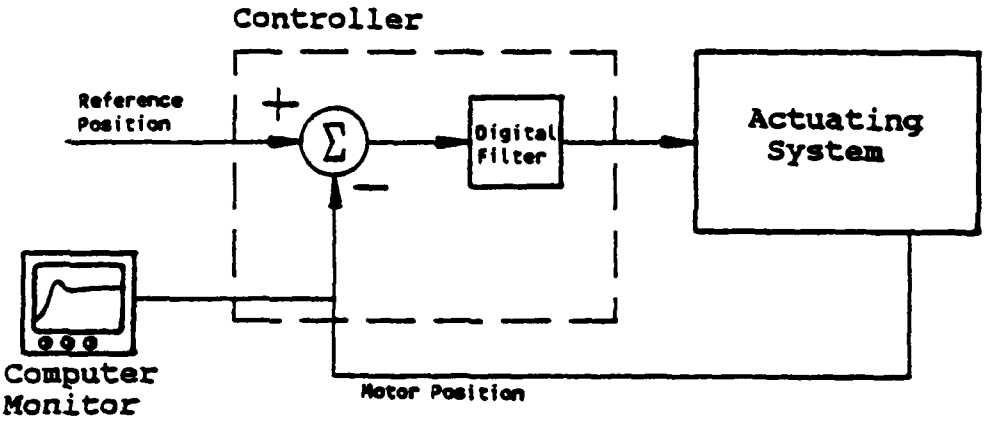

(a) Experimental arrangement.

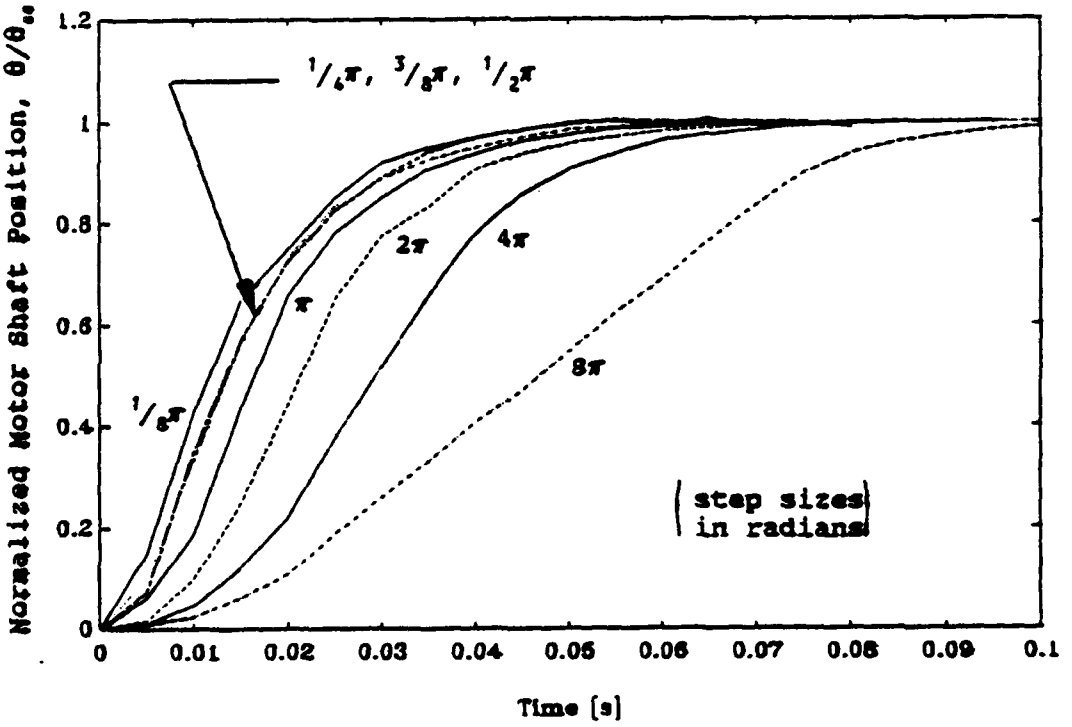

(b) Normalized position step response.

Figure B.5. Actuating system position step response experimental arrangement and results.

System Load

Two experiments were performed on each axis to determine the dynamic characteristics of the system load. The frequency response and the step response of each axis, with the load connected, was determined from the experiments.

Open Loop Actuating System/Load Frequency Response

The experiment used to determine the frequency response of the system load is similar to that used in the case of the actuating system; the experimental arrangement is shown in Figure B.6. A swept sine signal, with frequency varying between 1 and 200 Hz, was generated and monitored by the FFT analyzer and used to drive the system with the load connected. The motor shaft speed was monitored by the FFT analyzer and displayed in the form of the Bode plots, normalized to the steady state gains, in Figure B.7.

Step Response

The controller was connected to the actuating system and load as shown in Figure B.8 to experimentally determined the closed loop position step response of the motor shaft and the sewing head. Motor shaft step commands of $3\pi/8$, $\pi/2$, $5\pi/8$, and $3\pi/4$ radians, corresponding to sewing head displacements of 0.23, 0.30, 0.38 and 0.45 inches, were written to the command register of the motion control chip using the MC tuning software. One channel of the FFT analyzer was used to monitor the motor shaft position through the programmable monitor port on the servo amplifier. The other channel of

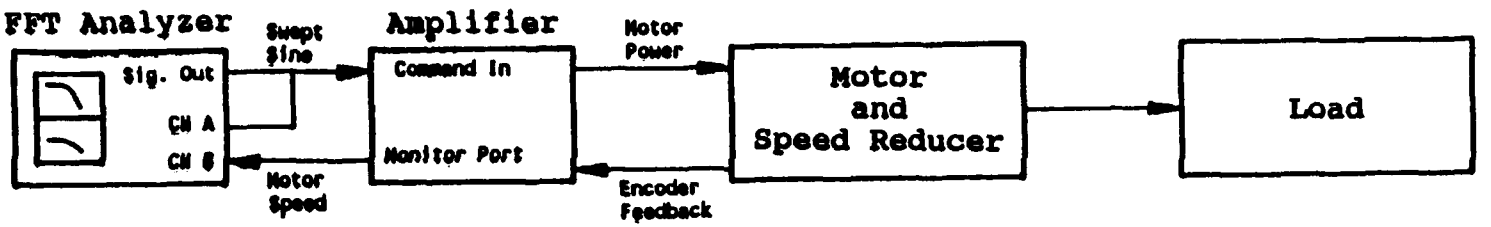

Figure B.6. Actuating system/load frequency response experimental arrangement.

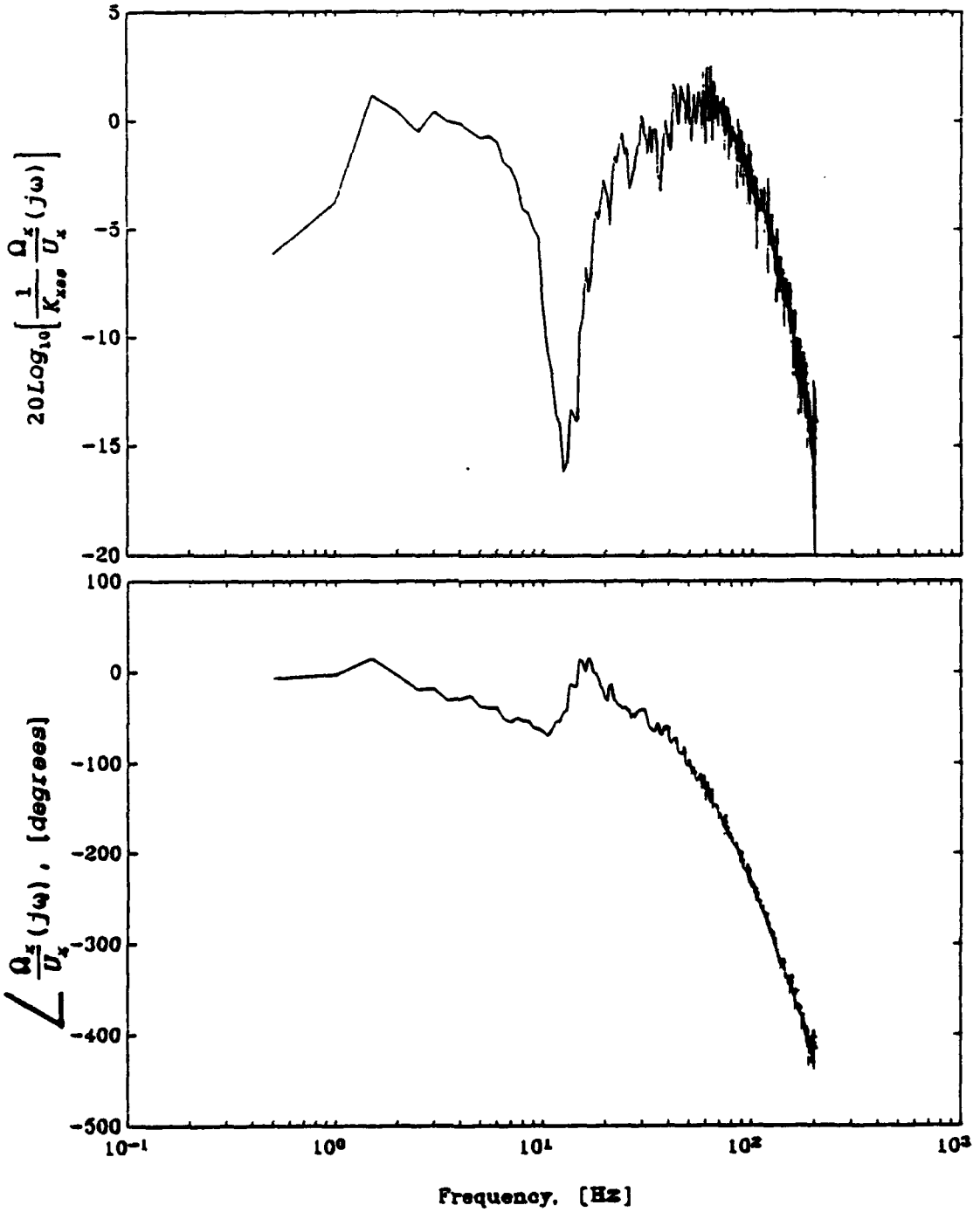

(a) X axis actuating system/load Bode plot.

Figure B.7. Actuating system/load Bode plots.

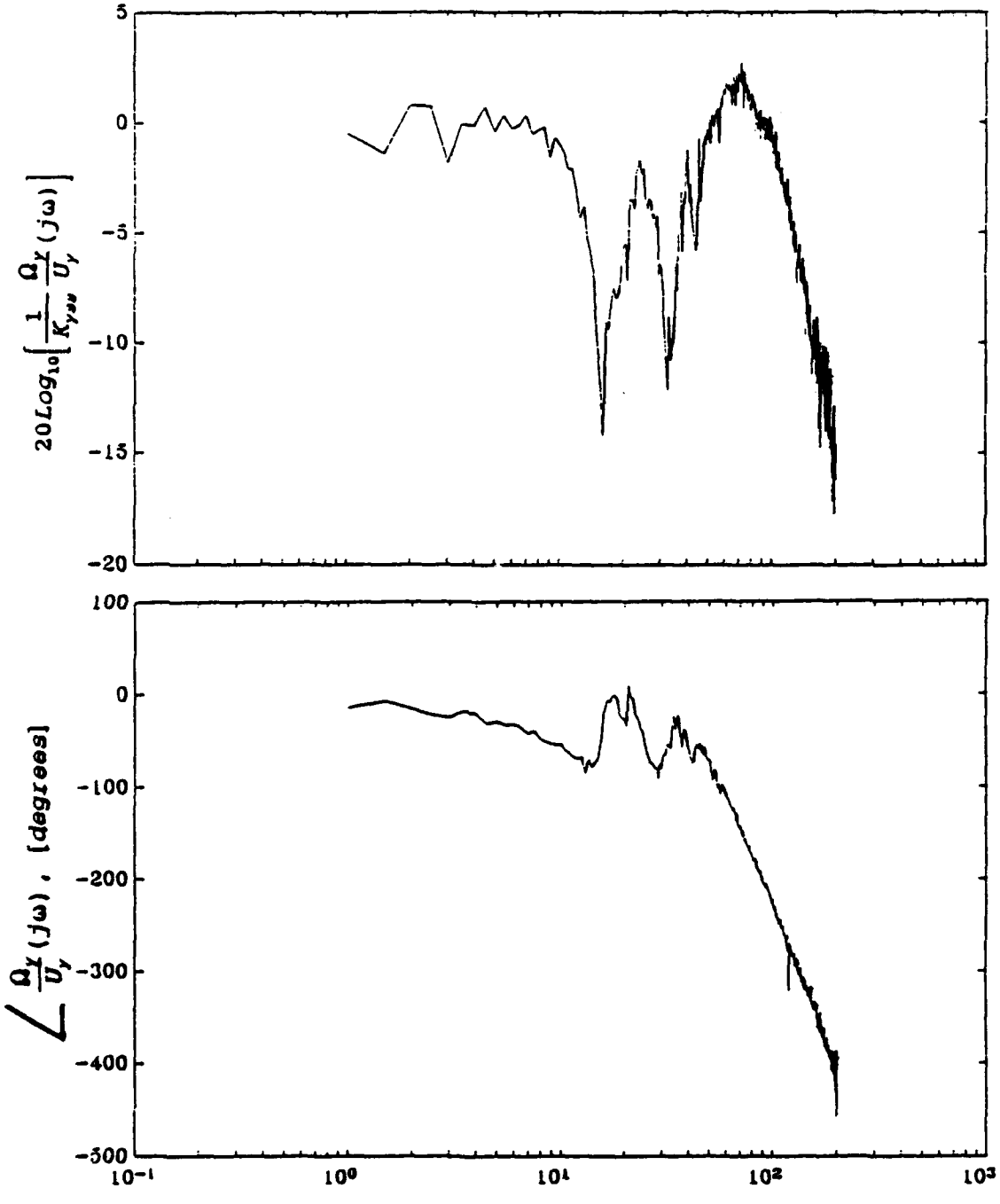

(b) Y axis actuating system/load Bode plot.

Figure B.7. (Continued)

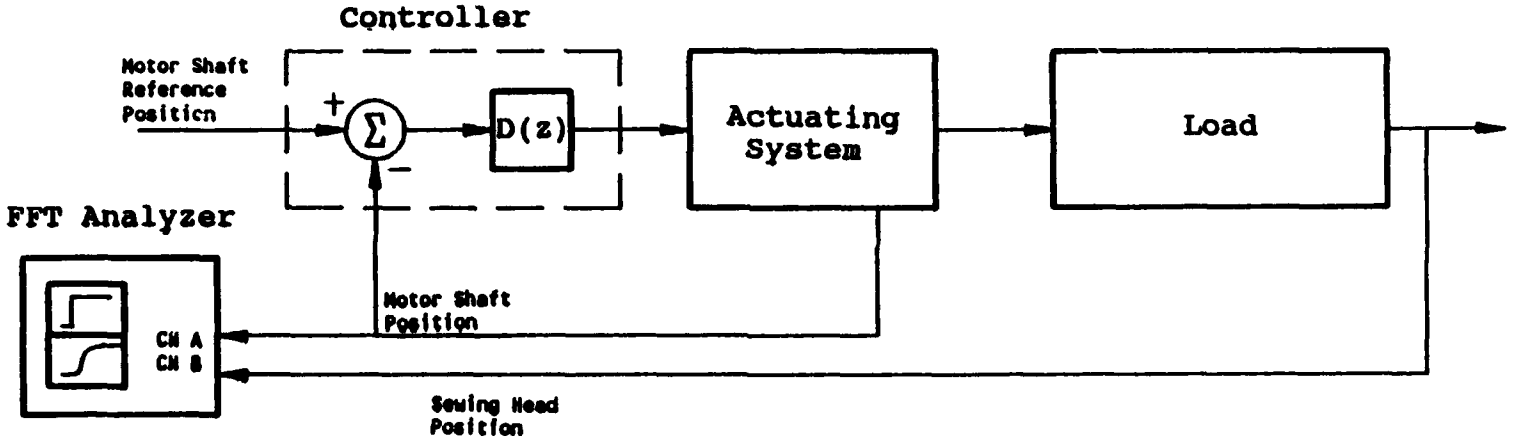

Figure B.8. Axis step response experimental arrangement.

the FFT analyzer was used to monitor the signal generated by the linear potentiometers shown in Figure B.9.

The potentiometers are mounted between the X carriage and the stitcher frame in the X axis and between the Y carriage and the X carriage, which does not move relative to the frame in the Y direction, in the Y axis. Thus, the absolute sewing head position, x_h, was monitored in the X axis since the stitcher frame is stationary in this axis. However, the sewing head position relative to the stitcher frame position, y_h-y_f, was measured in the Y axis because the frame is flexible in the Y direction.

The stroke length of the potentiometers is 4.1875 inches. Approximately 5% of this was used in the experiment with the smallest step size, resulting in a signal step size of approximately 5% of the terminal voltage. Therefore, a 30 volt DC power source was used with the potentiometers, as shown in Figure B.10, to minimize the effect of low voltage noise in the circuit. The closed loop position step response curves of the axes for the four step commands are shown in Figures B.11 and B.12.

This experiment was repeated for the step response of the sewing head using a step size of $3\pi/8$ and $-3\pi/8$ radians of the motor shaft position (0.23 and -0.23 inches displacement of the sewing head) to determine effect of the bilinear spring characteristics of the timing belt. The sewing head was stepped 0.23 inches from its initial position in each axis shown in Figure B.13 and back again. The negative

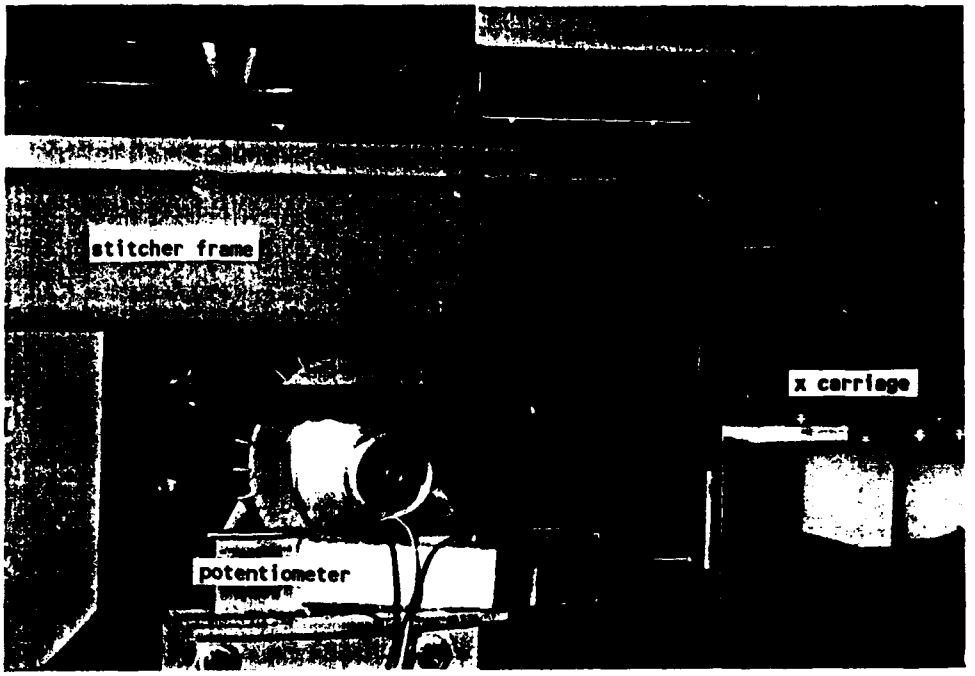

(a) X axis potentiometer.

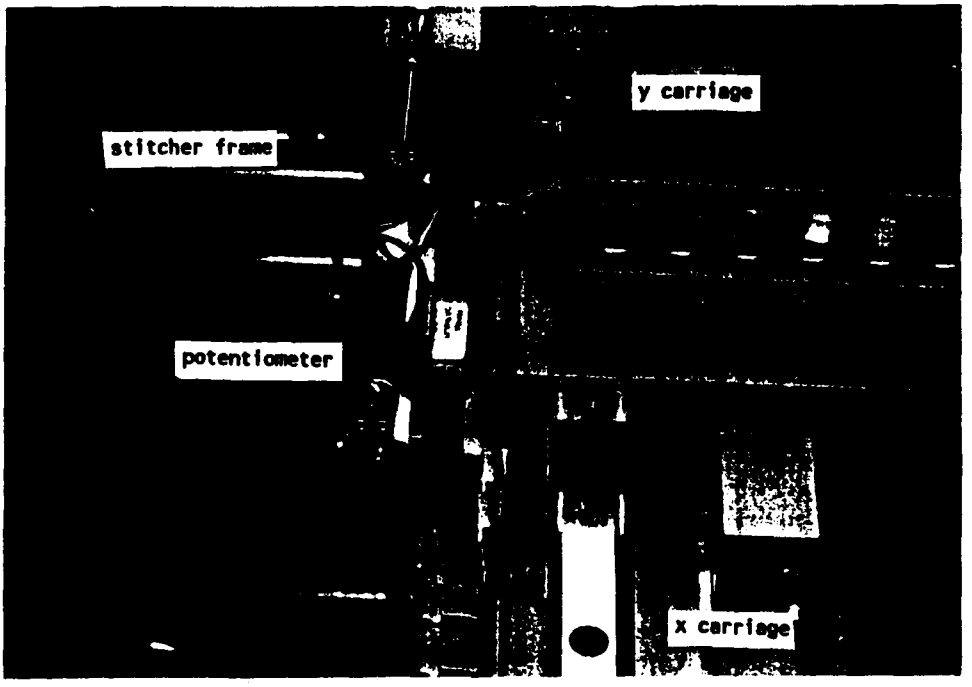

(b) Y axis potentiometer.

Figure B.9. Potentiometer location in each axis.

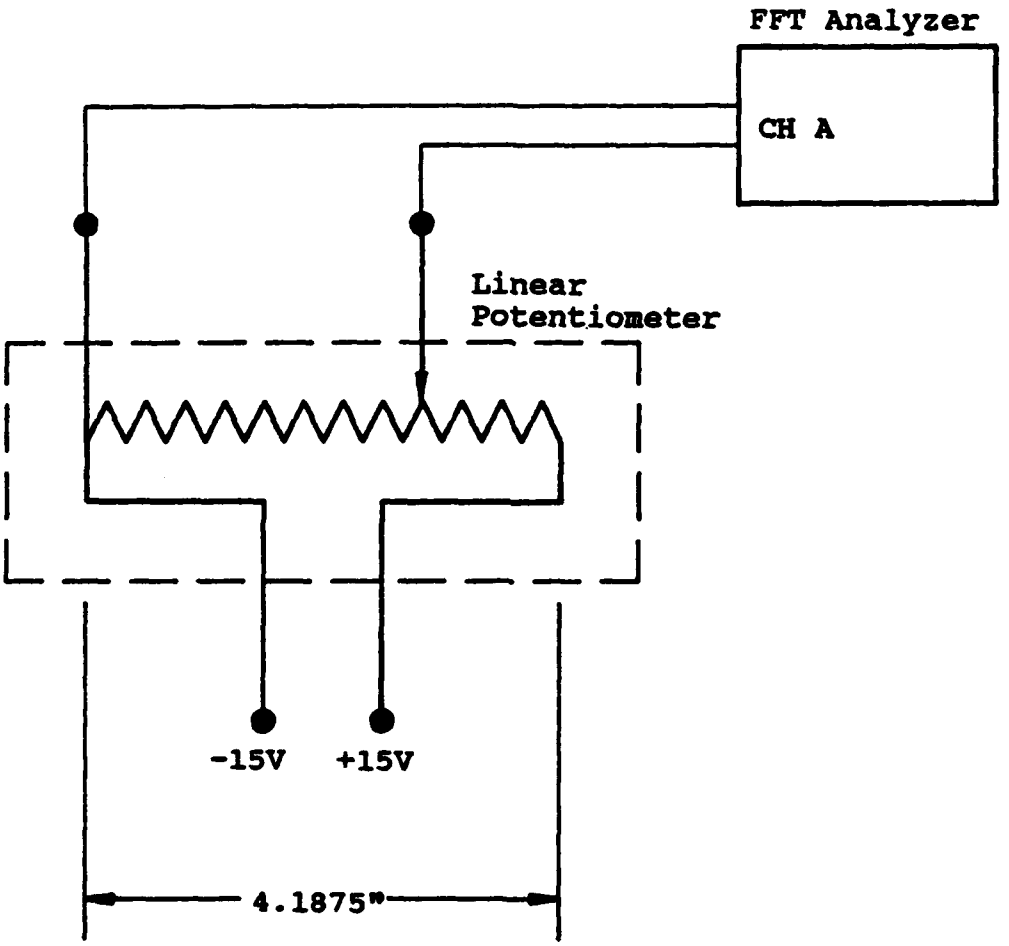

Figure B.10. Potentiometer circuit on each axis.

$$D(z) = 0.25\left(\frac{z-0.918}{z+0.25}\right)$$

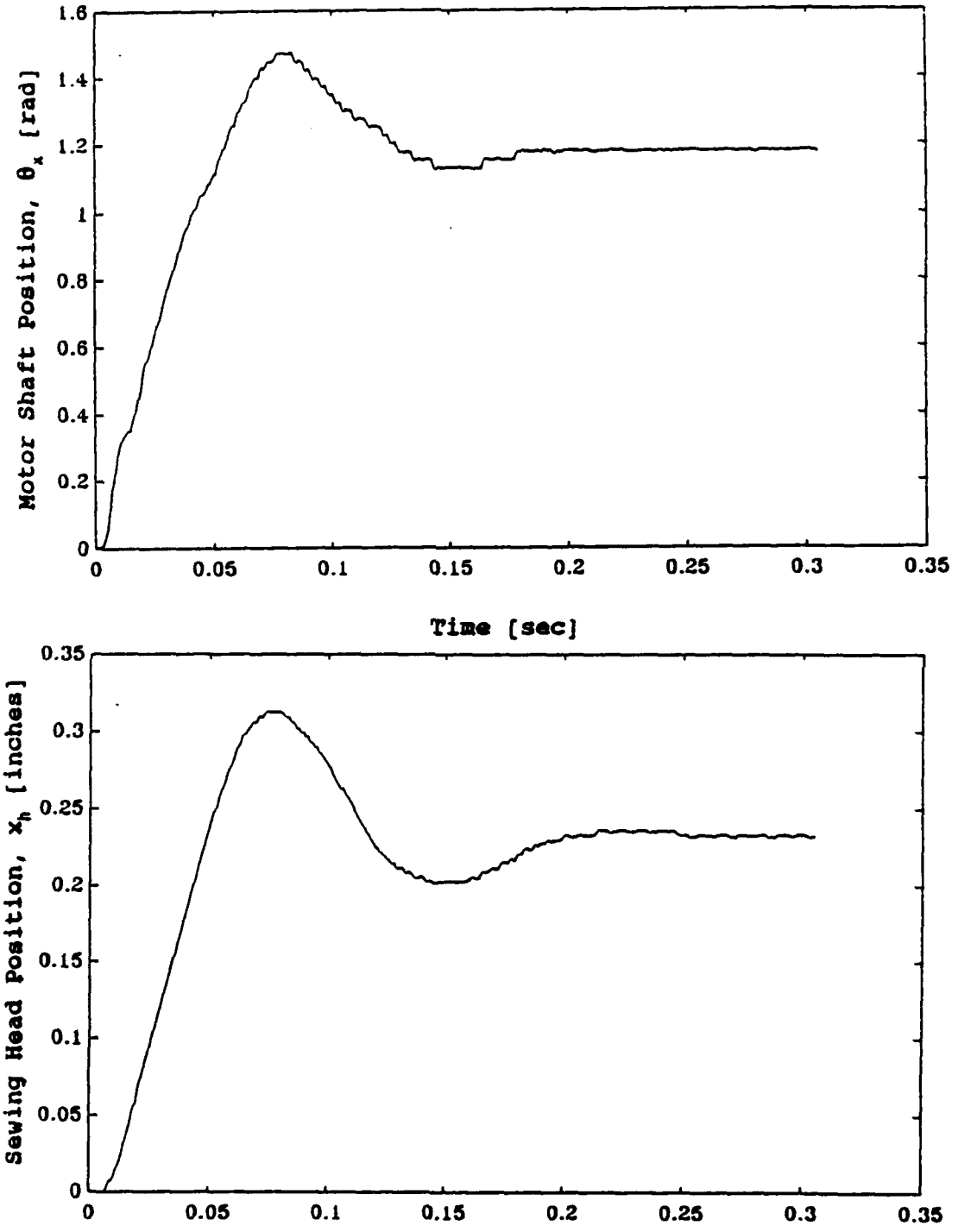

(a) Response to a $^{3\pi}/_{8}$ radian step command.

Figure B.11. X axis sewing head and motor shaft position step response.

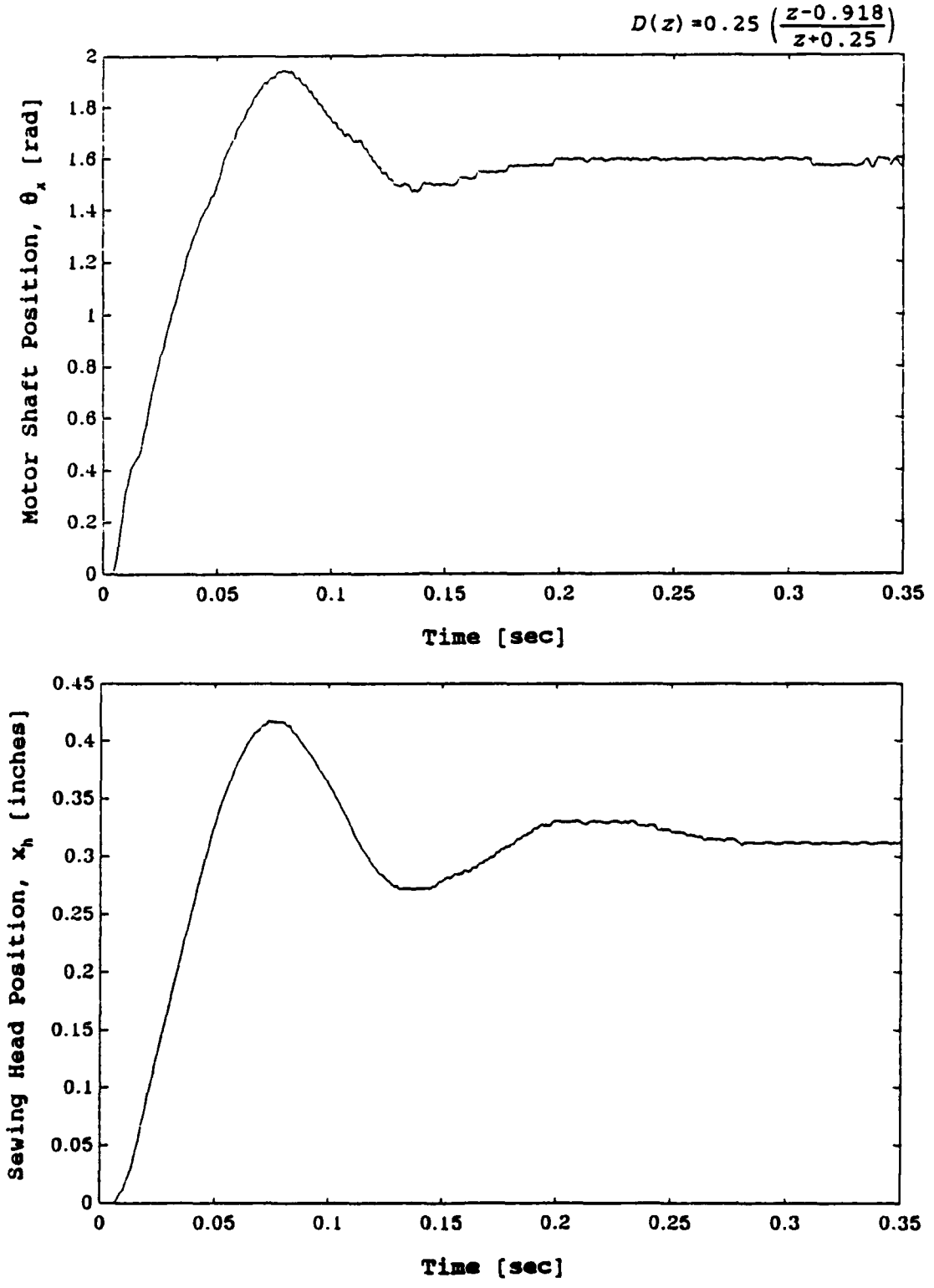

(b) response to a $\pi/2$ radian step command.

Figure B.11. (Continued)

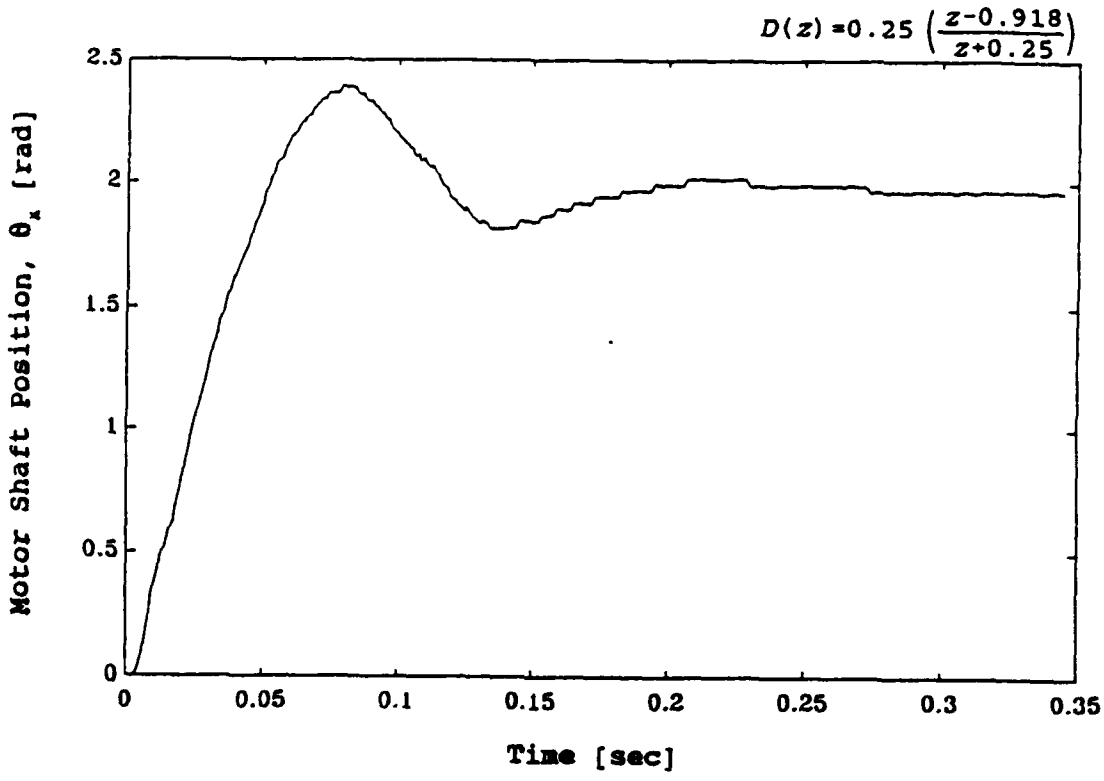

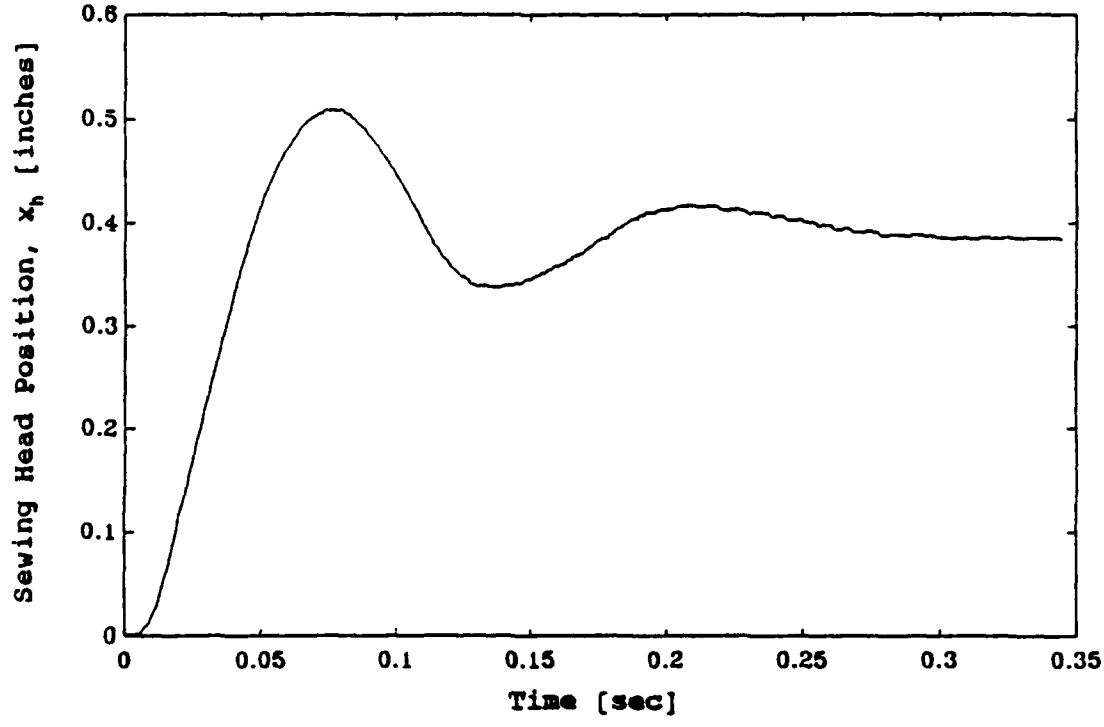

(c) Response to a 5π/8 radian step command.

Figure B.11. (Continued)

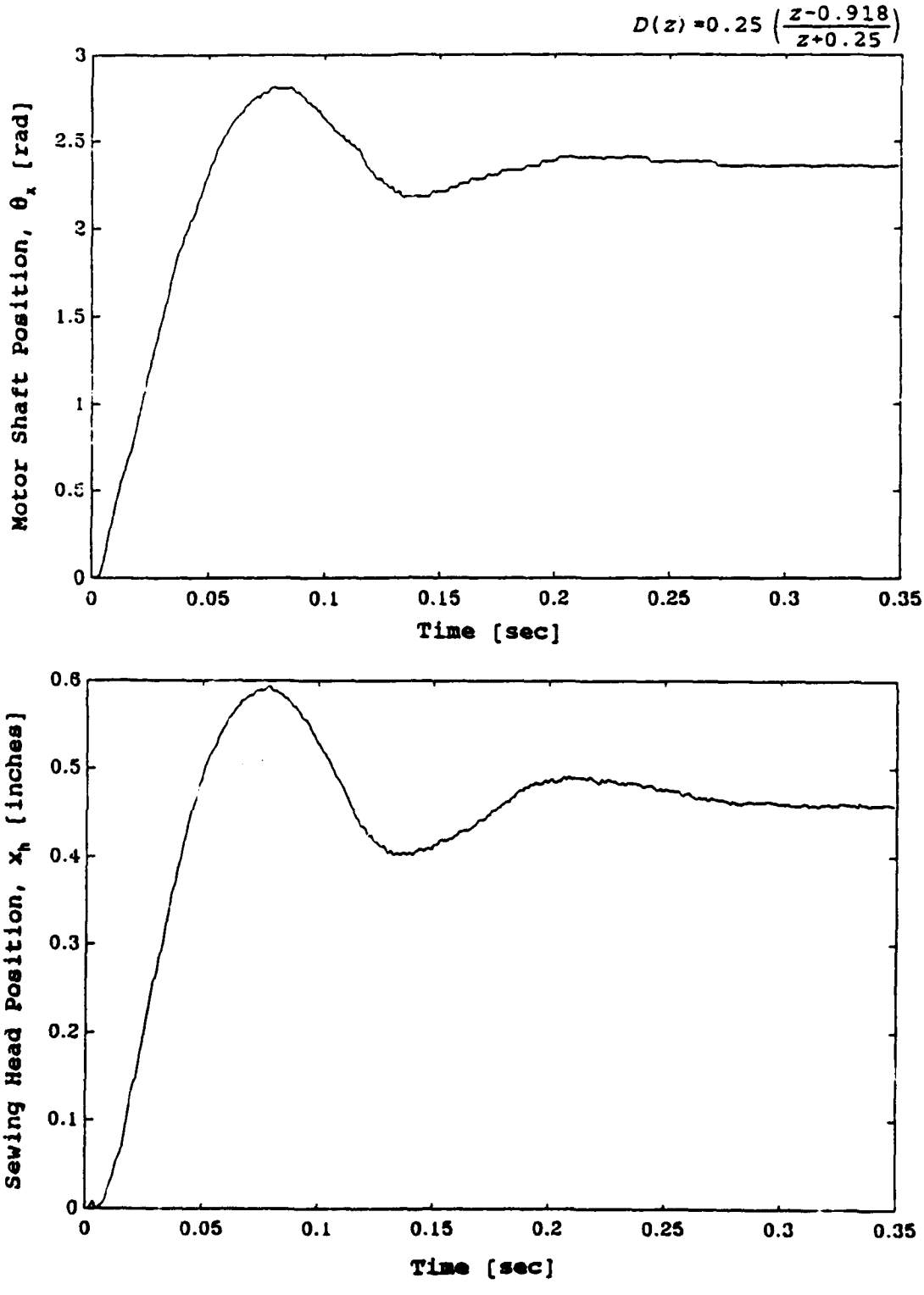

(d) response to a $3\pi/4$ radian step command.

Figure B.11. (Continued)

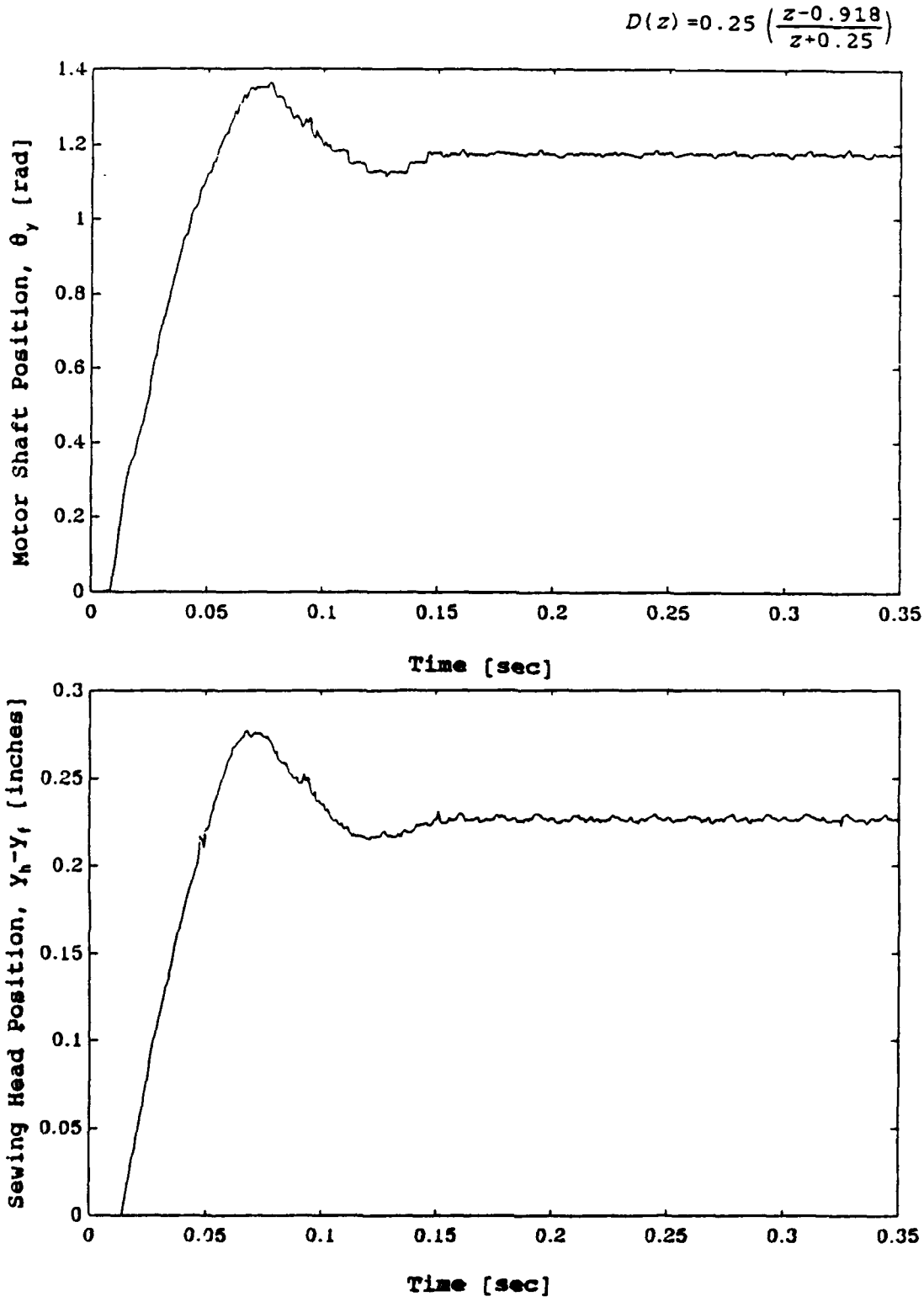

(a) Response to a $^{3\pi}/_{8}$ radian step command.

Figure B.12. Y axis sewing head and motor shaft position step response.

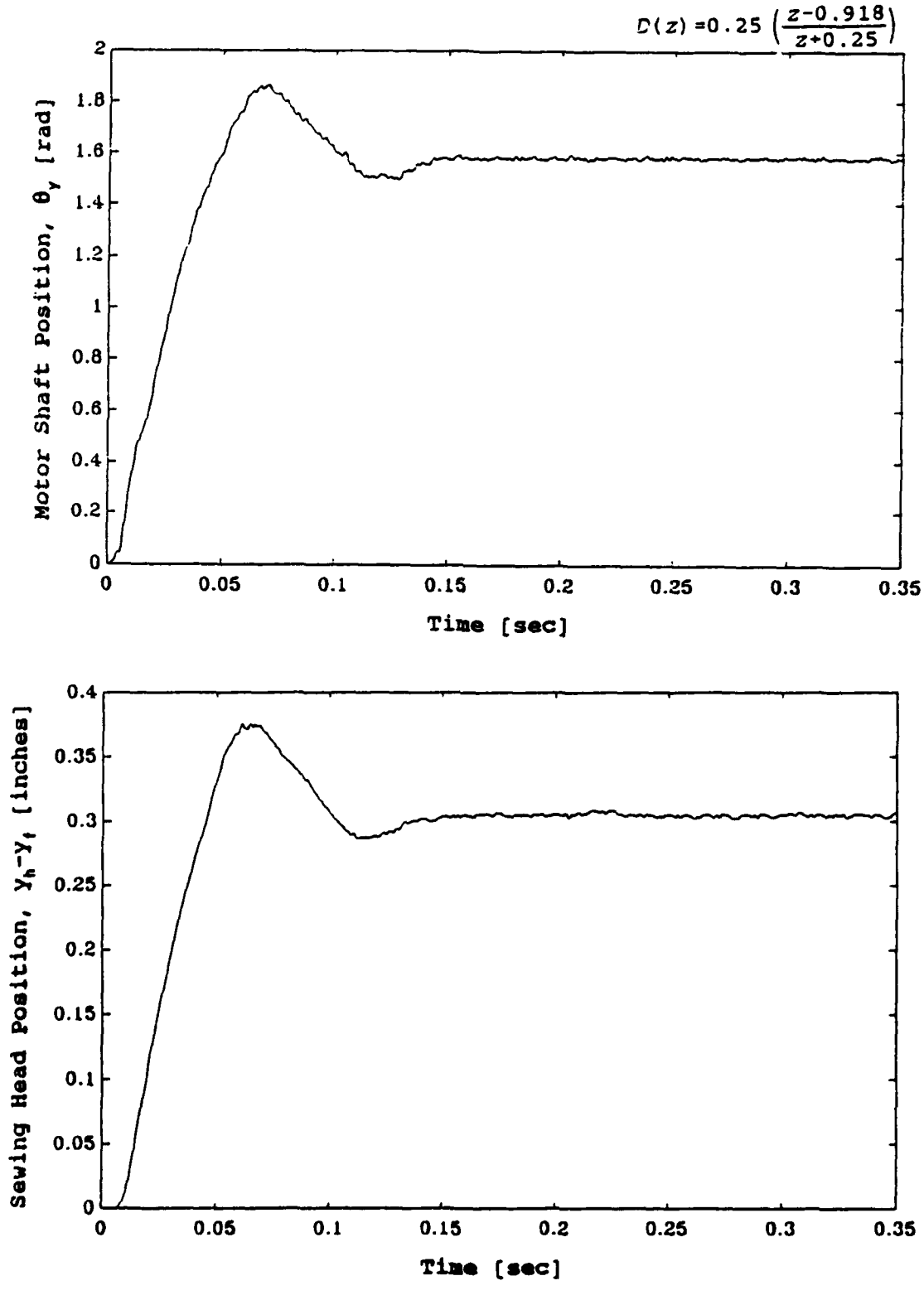

(b) response to a $\pi/2$ radian step command.

Figure B.12. (Continued)

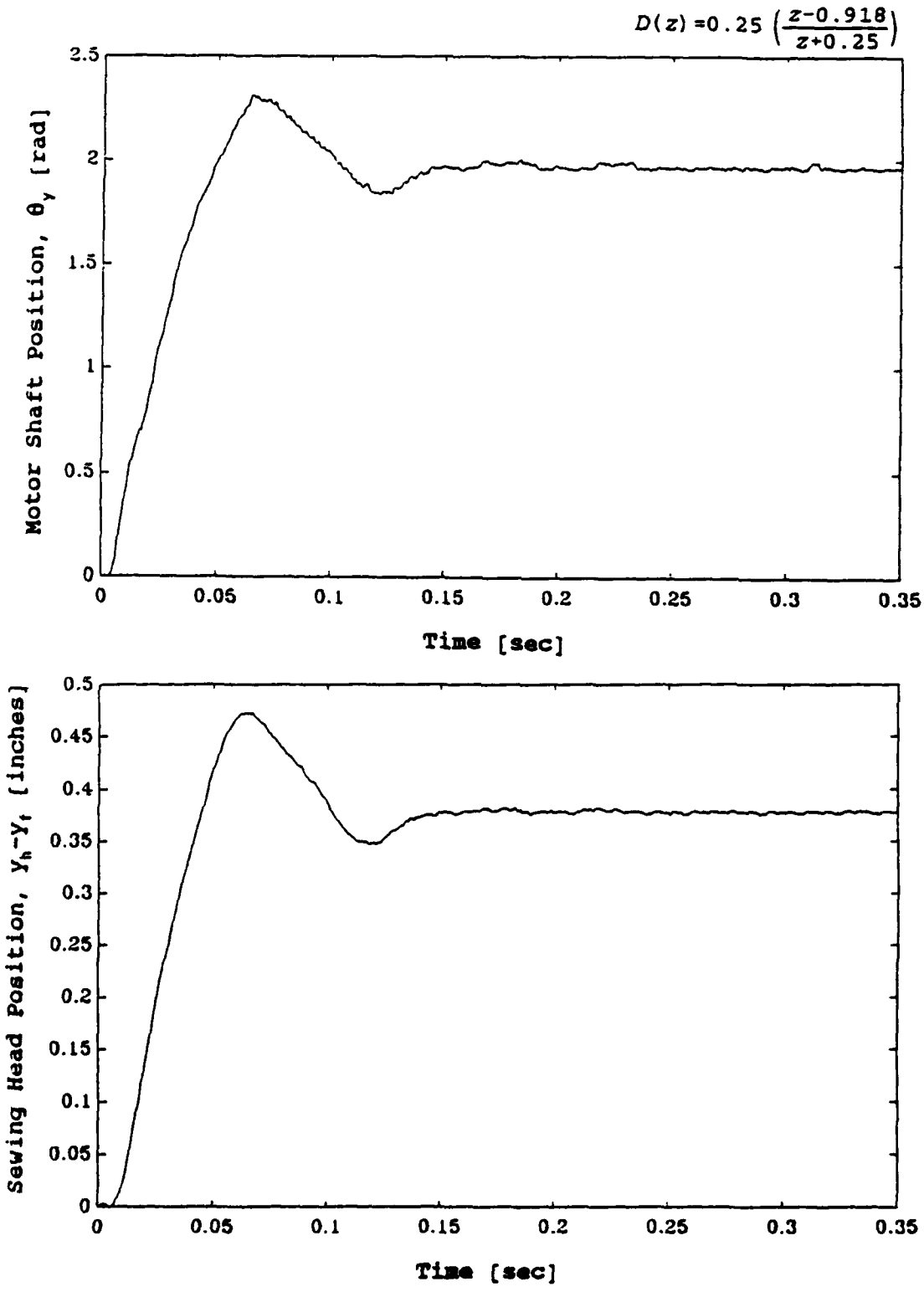

(c) Response to a $5\pi/8$ radian step command.

Figure B.12. (Continued)

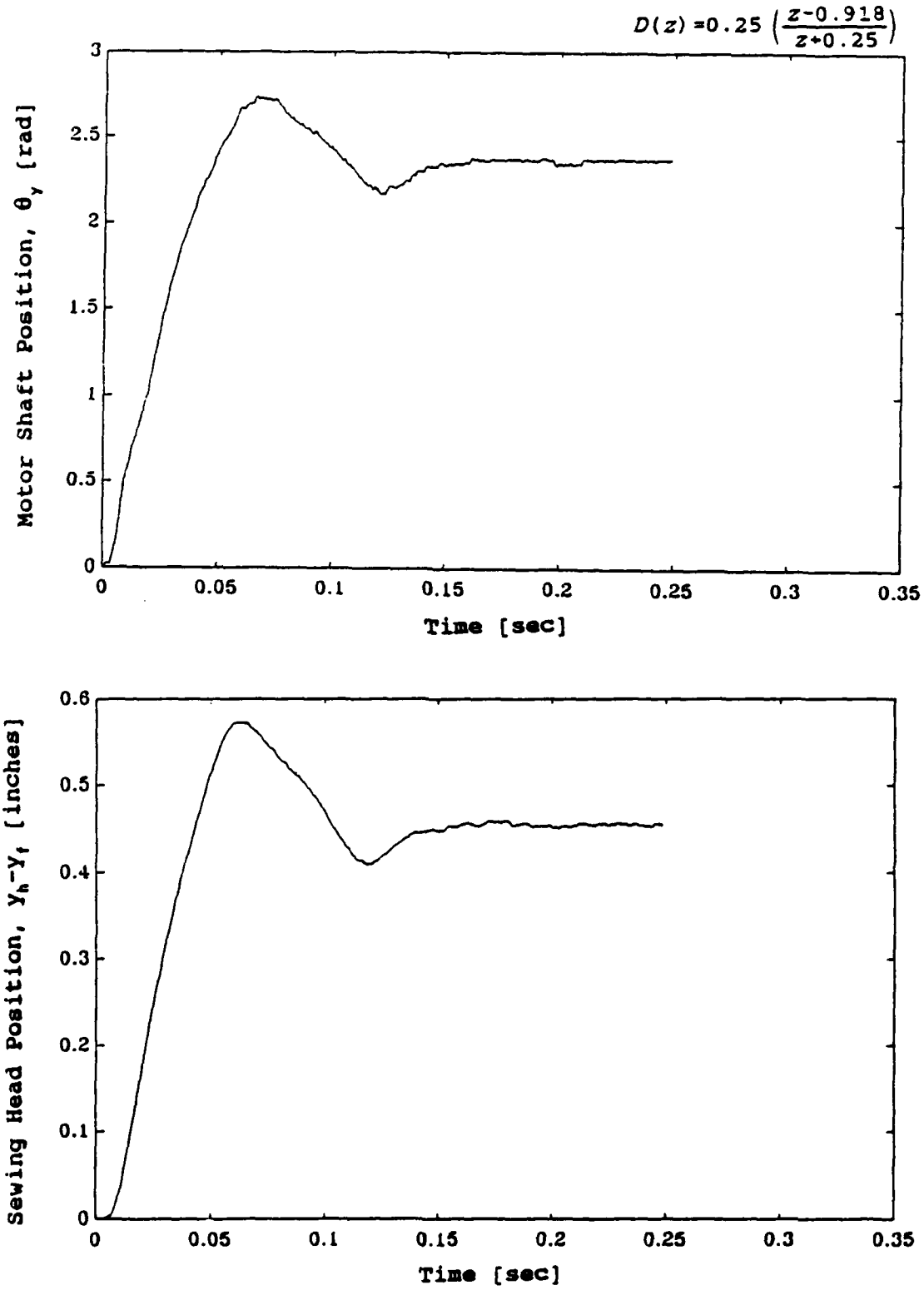

(d) response to a $3\pi/4$ radian step command.

Figure B.12. (Continued)

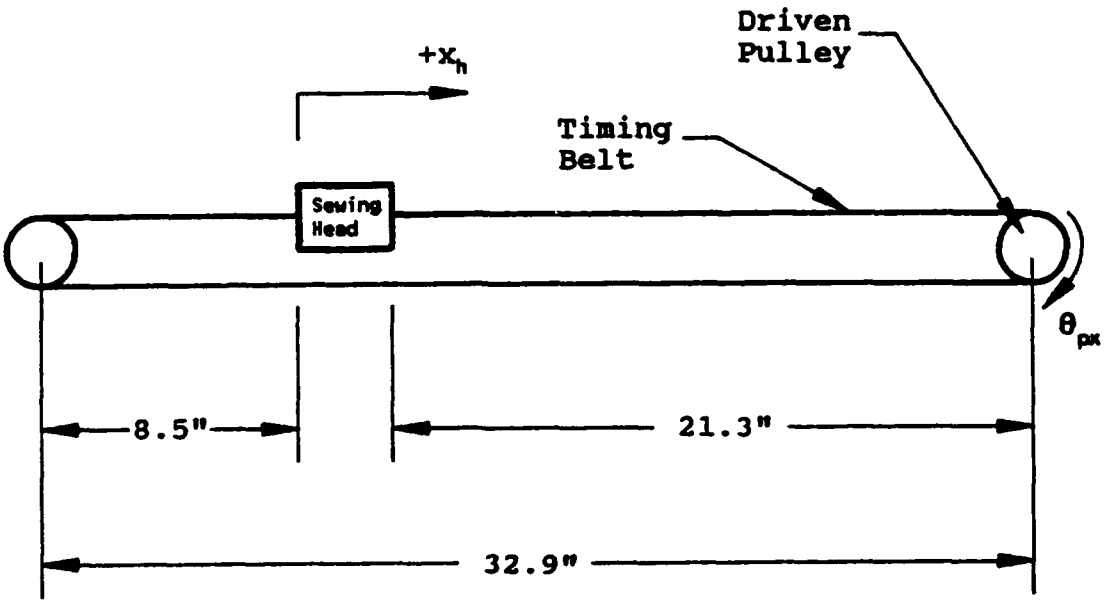

(a) X axis.

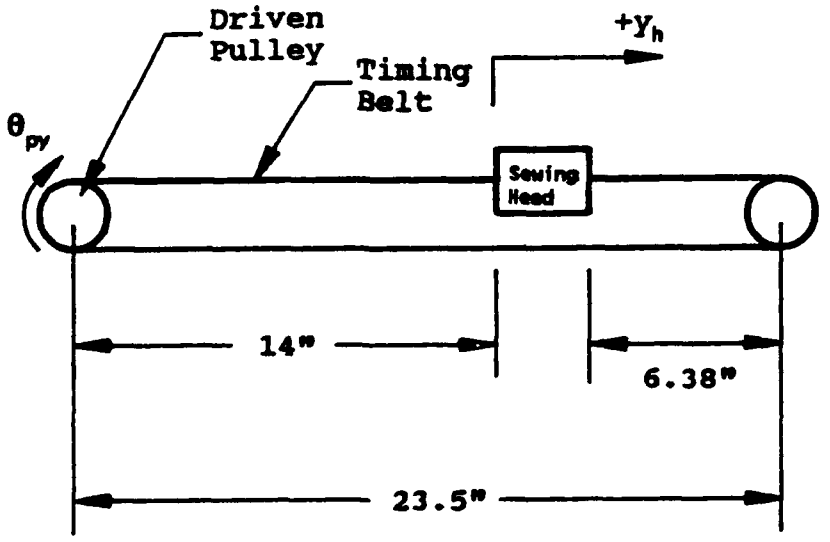

(b) Y axis.

Figure B.13. Sewing head position during step response experiments.

direction step response of the sewing head was subtracted from the positive step command, 0.23 inches, so it could be compared to the positive step response as shown in Figure B.14.

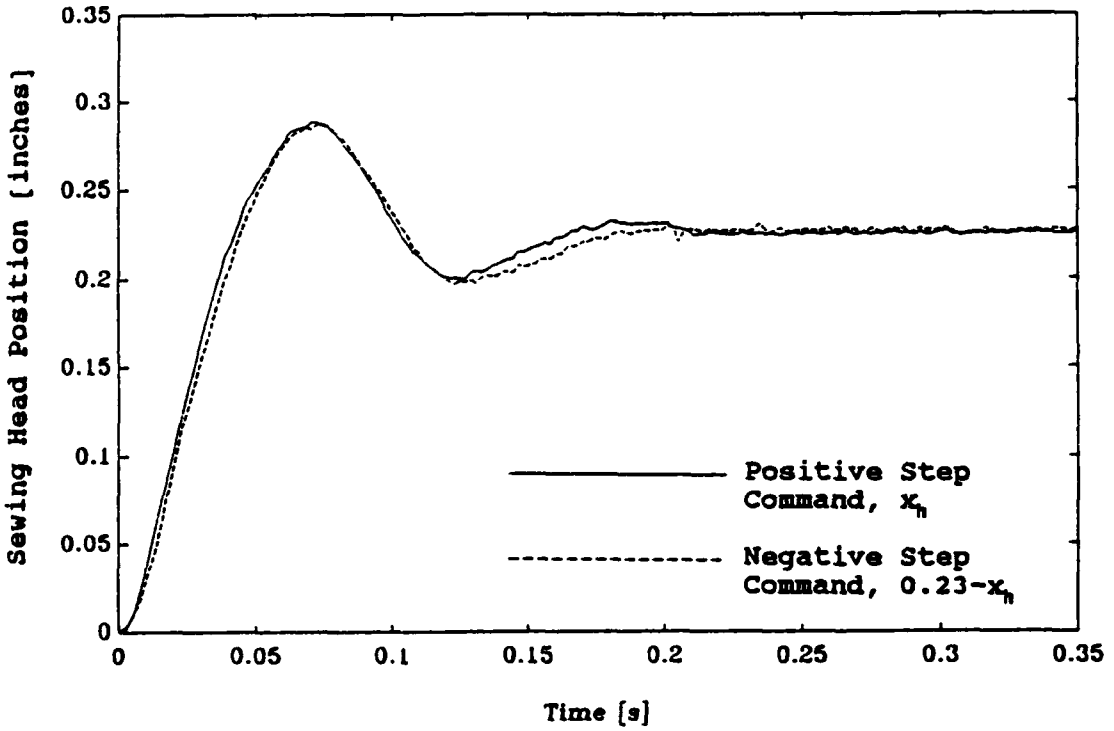

(a) Step response in the X axis, x_h.

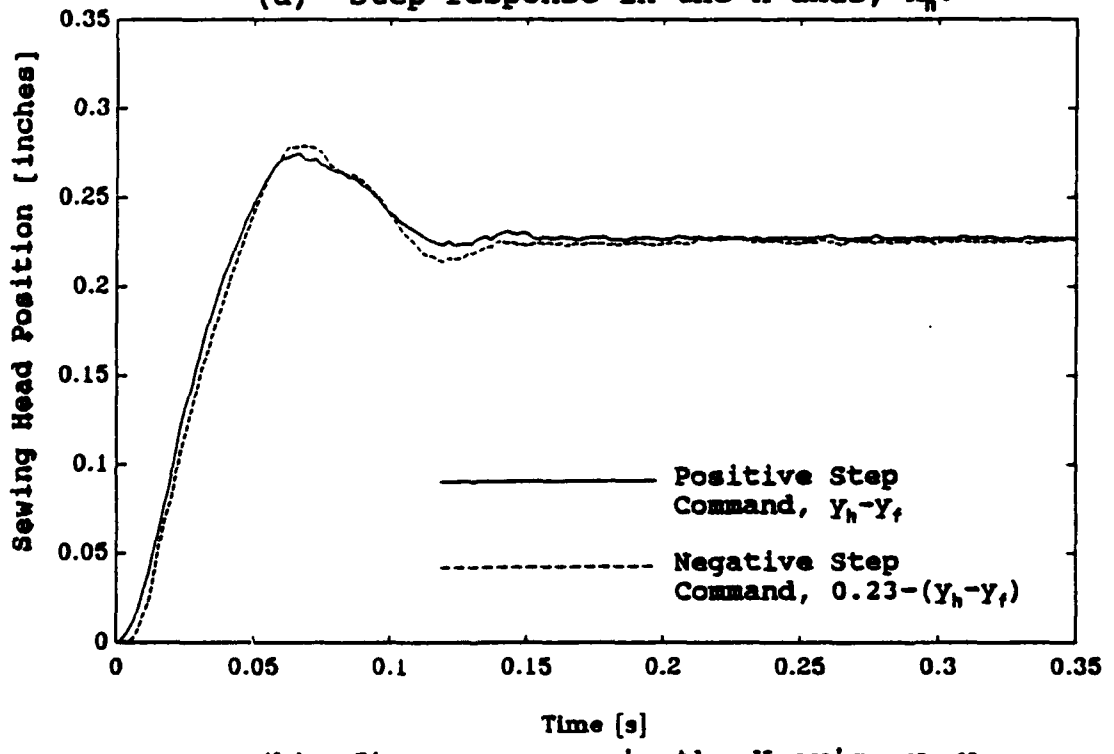

(b) Step response in the Y axis, y_h-y_f.

Figure B.14. Sewing head position step response for a positive and negative step command.

Appendix C

Model Development

Actuating System Model

The actuating system model for each axis, shown in Figure C.1, is a combination of a second order system and a time delay. The development of the model was divided into three phases: (1) developing the second order model, (2) determining the delay time in the system, and (3) determining the amplifier gain in each axis.

Second Order Model Development

The second order systems of the actuating system models,

$$\frac{\Omega_x}{U_x'}(s) = \frac{K_{mx}}{s^2+2\zeta_x\omega_{nx}s+\omega_{nx}^2} \qquad \text{(C.1a)}$$

and

$$\frac{\Omega_y}{U_y'}(s) = \frac{K_{my}}{s^2+2\zeta_y\omega_{ny}s+\omega_{ny}^2} \qquad \text{(C.1b)}$$

were adjusted so the magnitude of the frequency response of the models fit that of the actual system. The magnitude plots of the above models with ω_{nx}=500 (rad/sec), ζ_x=0.7, ω_{ny}=400 (rad/sec) and ζ_y=0.7 are shown with those of the actual system in Figure C.2. These plots indicate that the second order models are an accurate representation of the second order dynamics of the actuating systems.

Each second order model was written in terms of the physical actuating system parameters as

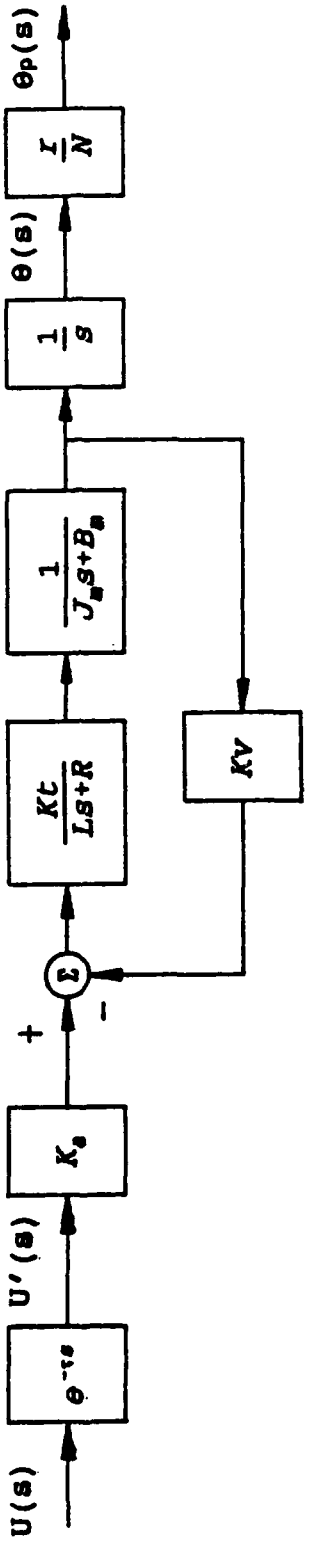

Figure C.1. General block diagram of each actuating system.

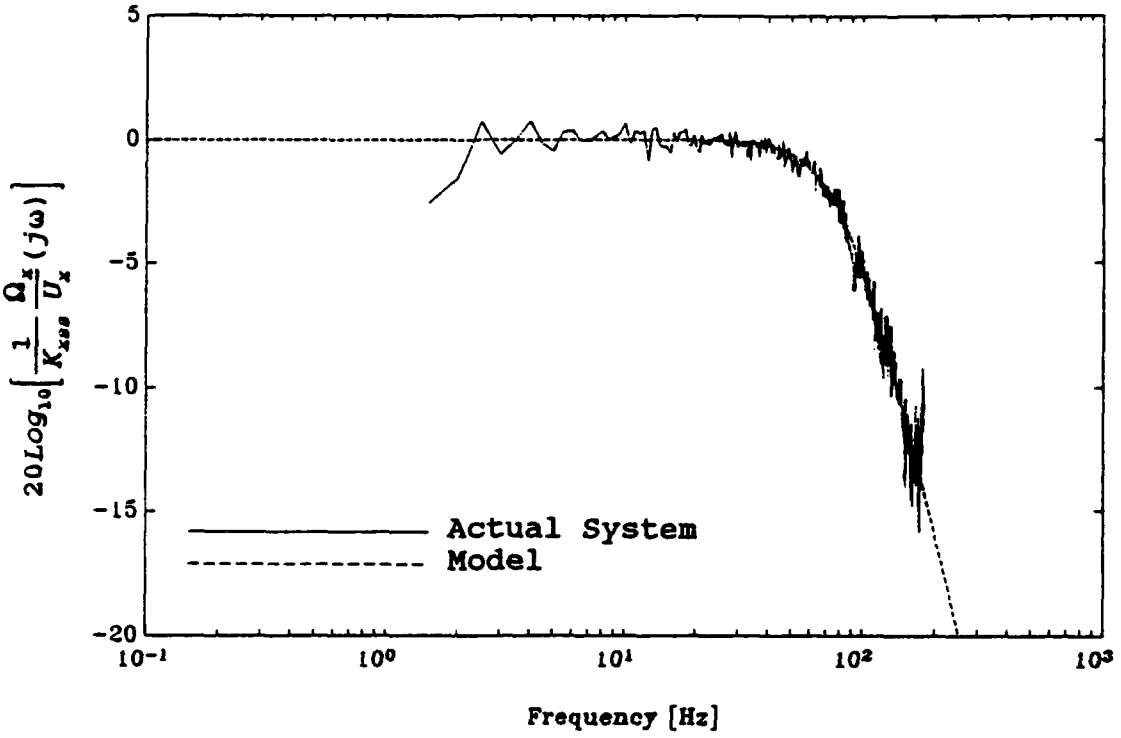

(a) X axis actuating system frequency response magnitude.

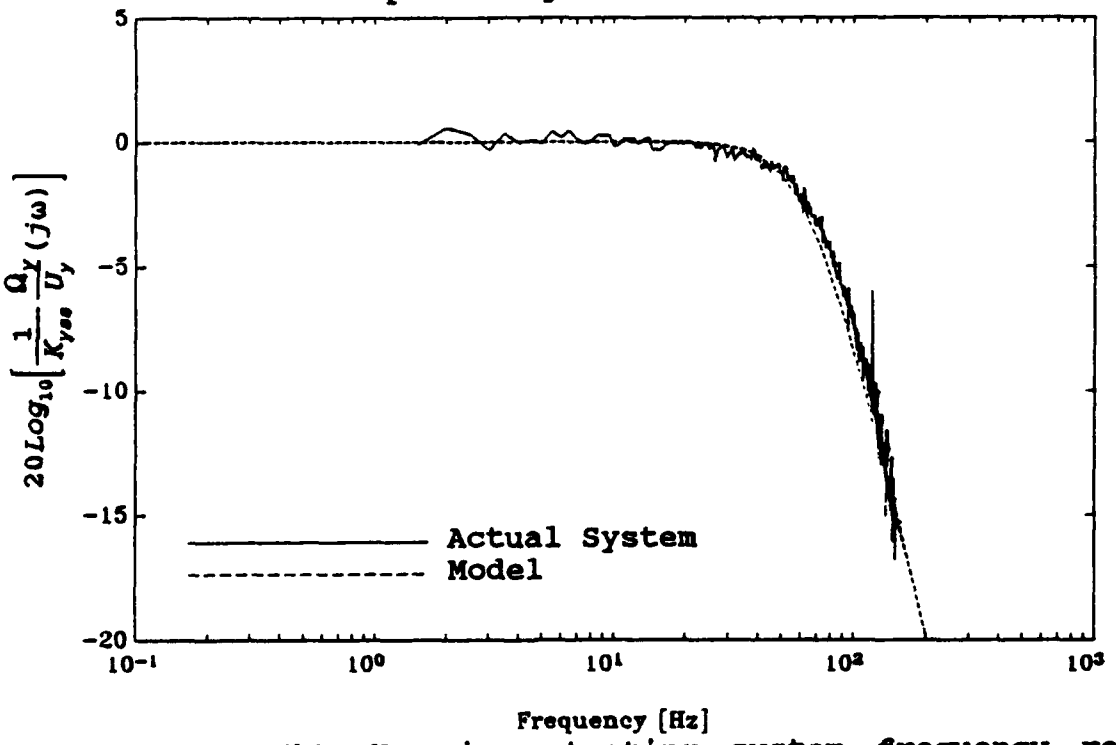

(b) Y axis actuating system frequency response magnitude.

Figure C.2. Actuating system frequency response magnitude, actual system and second order model.

$$\frac{\Omega_x}{U_x'}(s) = \frac{\frac{KtK_{ax}}{LJ_{mx}}}{s^2 + \left(\frac{RJ_{mx}+LB_{mx}}{LJ_{mx}}\right)s + \left(\frac{RB_{mx}+KtKv}{LJ_{mx}}\right)} \qquad \text{(C.2a)}$$

and

$$\frac{\Omega_y}{U_y'}(s) = \frac{\frac{KtK_{ay}}{LJ_{my}}}{s^2 + \left(\frac{RJ_{my}+LB_{my}}{LJ_{my}}\right)s + \left(\frac{RB_{my}+KtKv}{LJ_{my}}\right)}, \qquad \text{(C.2b)}$$

where J_{mx} and J_{my} are the system inertias, B_{mx} and B_{my} are the viscous damping coefficients, K_{ax} and K_{ay} are the amplifier gains and Kt, Kv, R and L are the electrical parameters listed in Appendix A. The coefficients of the characteristic equations of the transfer functions in Equations (C.1) and (C.2) were equated to determine the following values of the unknown parameters:

J_{mx}=4.75e-4 kg-m^2

B_{mx}=0.24 kg-m^2/sec

J_{my}=8.1e-4 kg-m^2

B_{my}=0.29 kg-m^2/sec.

Delay Time Determination

The frequency response of the time delay is expressed as

$$\left|e^{-\tau(j\omega)}\right| = 0\,dB \qquad \text{(C.3a)}$$

and

$$\angle e^{-\tau(j\omega)} = -\tau\omega. \qquad \text{(C.3b)}$$

The time delay function does not affect the magnitude of the frequency response of the actuating systems; however, it does

affect the phase. Therefore, the phase of the frequency response of the actual systems was used to determine the delay time.

The difference between the phase of the previously developed second order model and that of the actual system, shown in Figure C.3 for each axis, represents the phase lag defined Equation (C.3b) that is contributed by the time delay. At ω=200 Hz, $\angle e^{-\tau(j\omega)}$=-230°+110° in the X axis and $\angle e^{-\tau(j\omega)}$=-245°+125° in the Y axis; therefore, from Equation (C.3b), the delay time is 3 msec in each axis. The time delay function was linearized using a first order Padé approximation given by

$$e^{-\tau s} \approx \frac{2-\tau s}{2+\tau s} \quad . \qquad \text{(C.4)}$$

The Bode plot of each model, which includes the linear second order model and the linearized time delay function, is shown in Figure C.4 with the Bode plots of the actual systems. The model of each axis compares favorably to the actual system. However, the accuracy of the model deteriorates at frequencies above 100 Hz because the Padé approximation of the time delay function is used rather than the exact function.

Actuating System Gain

At steady state, the transfer functions in Equations (C.2) reduce to the steady state gains, given by

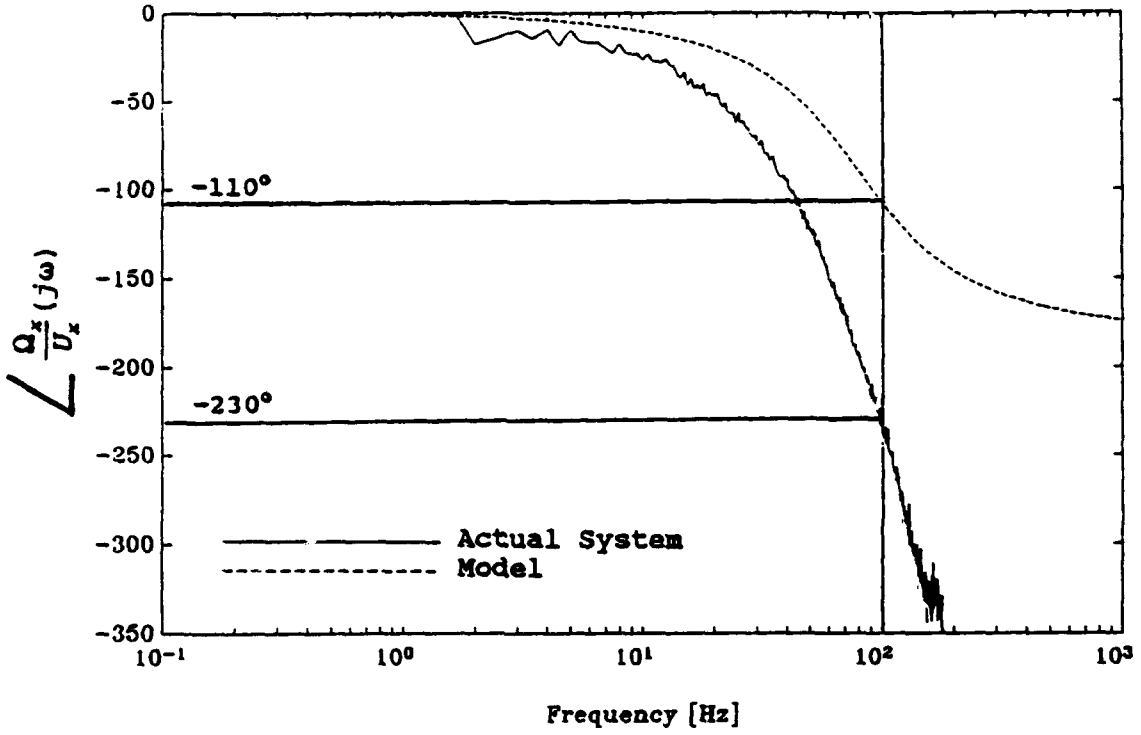

(a) X axis actuating system frequency response phase.

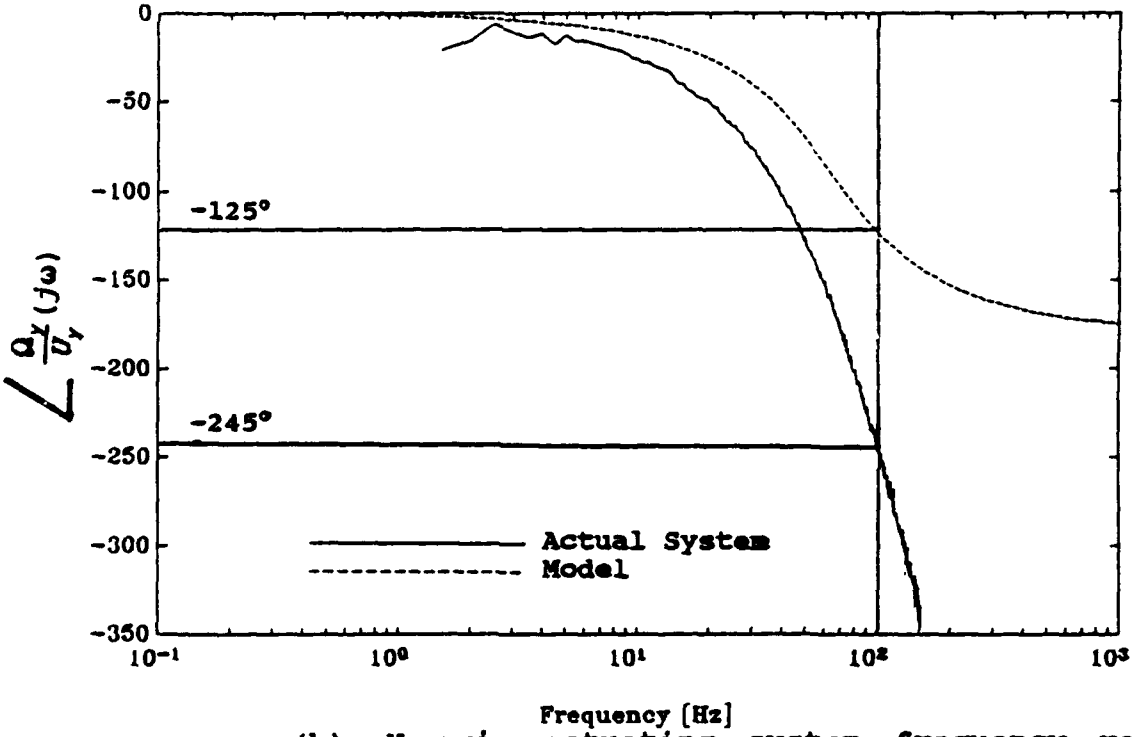

(b) Y axis actuating system frequency response phase.

Figure C.3. Actuating system frequency response phase, actual system and second order model.

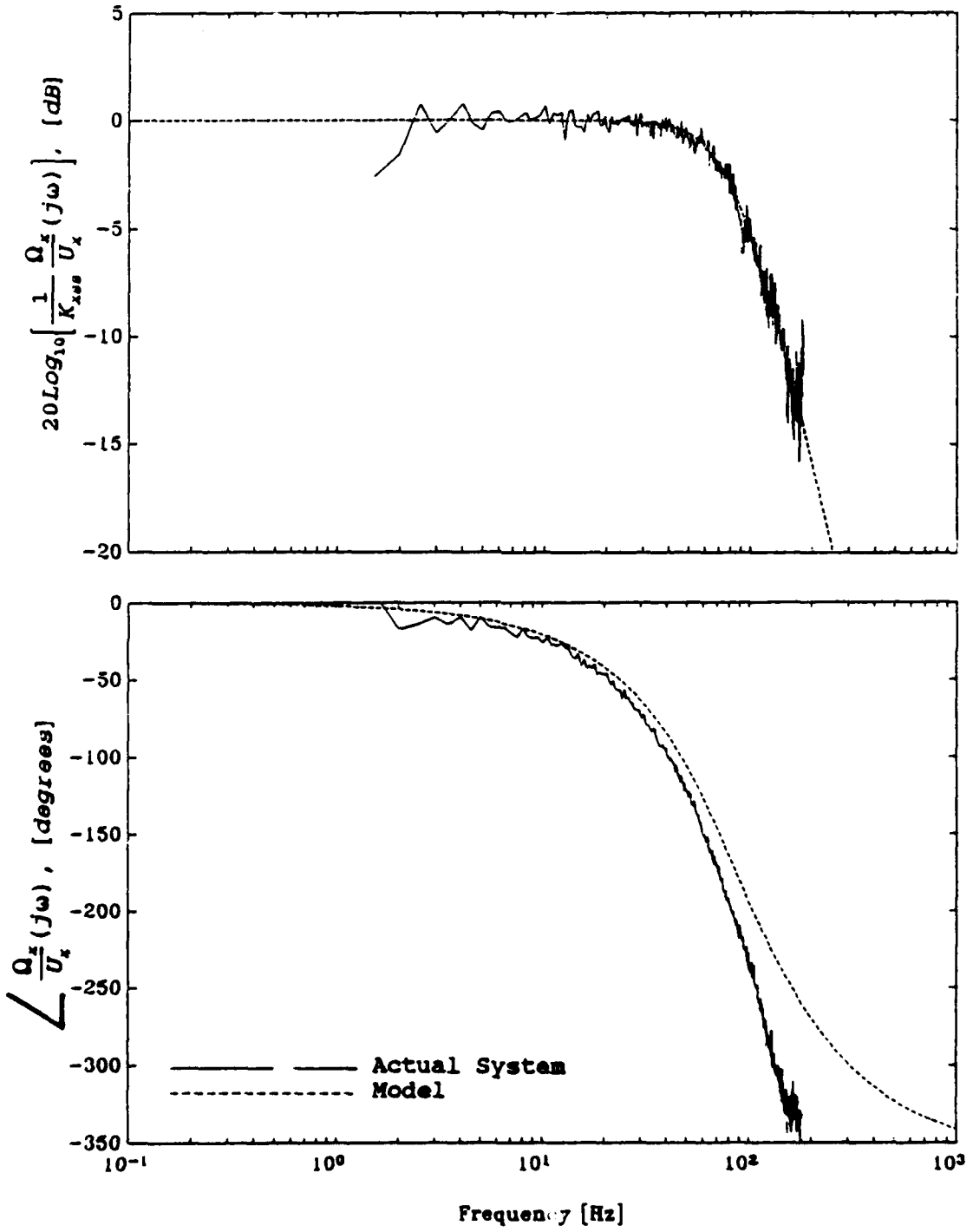

(a) X axis actuating system.

Figure C.4. Actuating system frequency response, actual system and model.

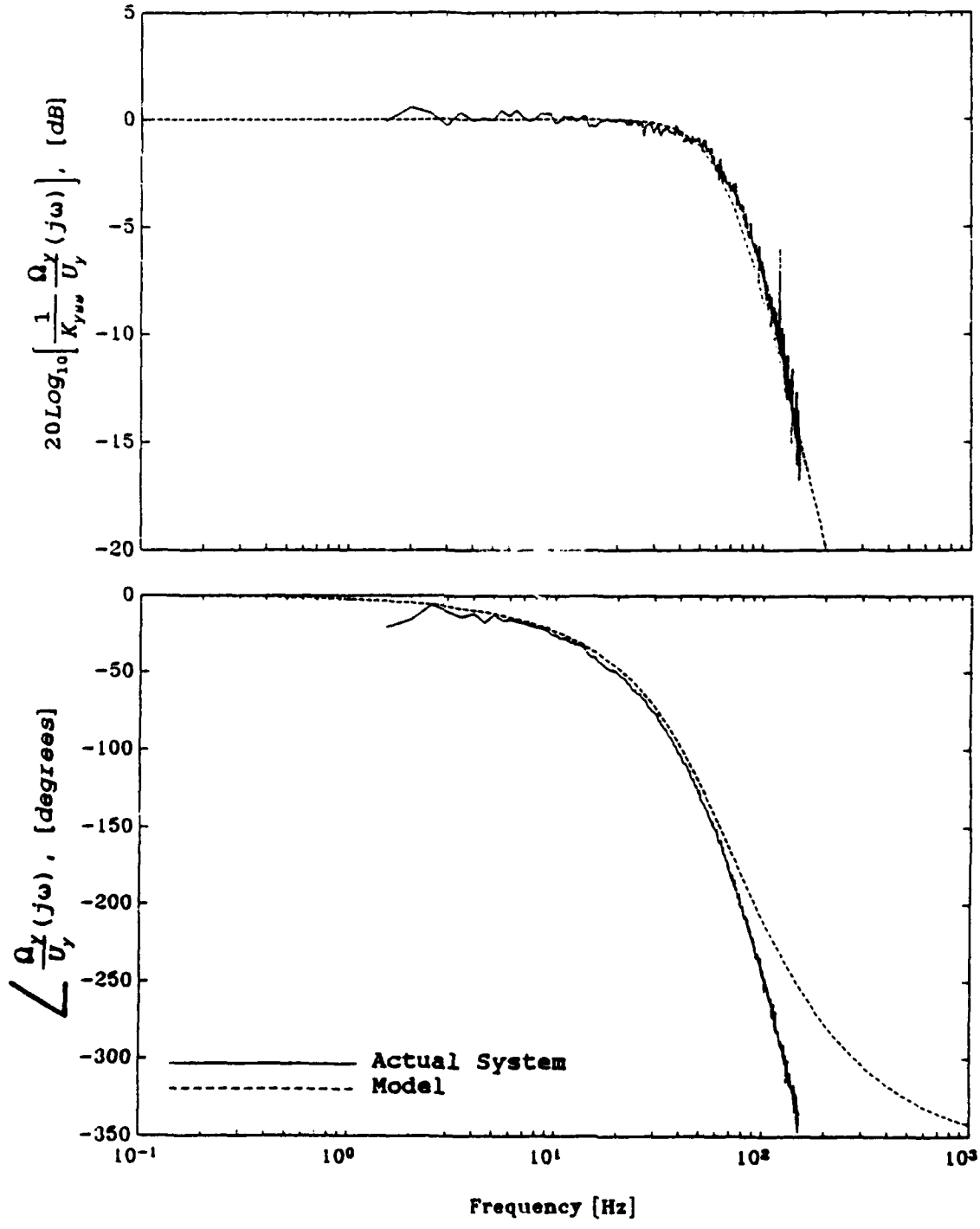

(b) Y axis actuating system.

Figure C.4. (Continued).

$$\frac{\Omega_x}{U_x}(s) = \frac{KtK_{ax}}{RB_{mx}+KtKv} \qquad \text{(C.5a)}$$

and

$$\frac{\Omega_y}{U_y}(s) = \frac{KtK_{ay}}{RB_{my}+KtKv}. \qquad \text{(C.5b)}$$

The curves relating the motor shaft speed and the command signal at steady state, obtained as described in Appendix B, are shown in Figure C.5. The slopes of these curves, N_x=42 (rad/s/V) and N_y=42 (rad/s/V), are the steady state gains in Equations (C.5). Equating these expressions with the slopes yields K_{ax}=40 and K_{ay}=42.

Load Model

The linear models of the load dynamics in each the axes were developed based on the Bode plots in Figure C.6. The Bode plots in the figure show the relation between the forcing function and a signal proportional to the motor shaft speed that is generated by the monitor port on the servo amplifiers. Therefore, the zero frequency gain shown in the figure contains the gain of the measuring system as well as the servo system gain. Rather than determine the gain used to generated the motor speed signal, the Bode plots of the models were shifted to match the zero frequency gain of the experimentally determined Bode plots. A nonlinear model of the stitcher was also developed based on the step response of each axis.

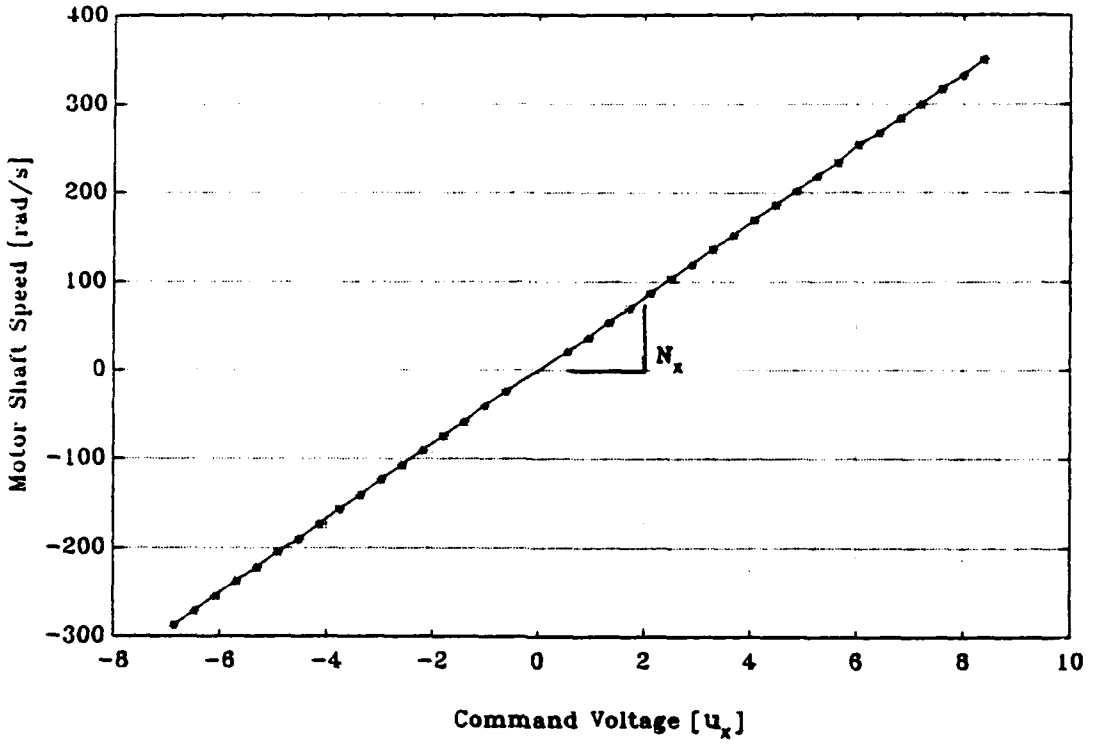

(a) X axis motor speed versus command signal.

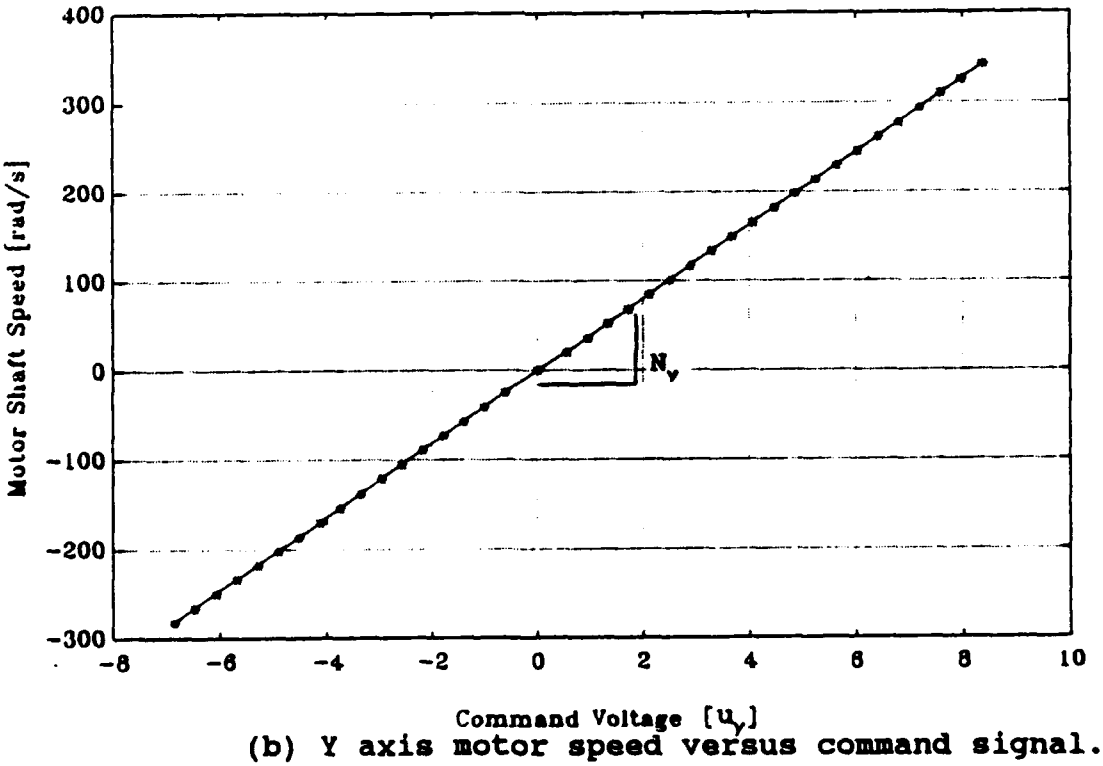

(b) Y axis motor speed versus command signal.

Figure C.5. Function relating the motor shaft speed and the command signal for each axis.

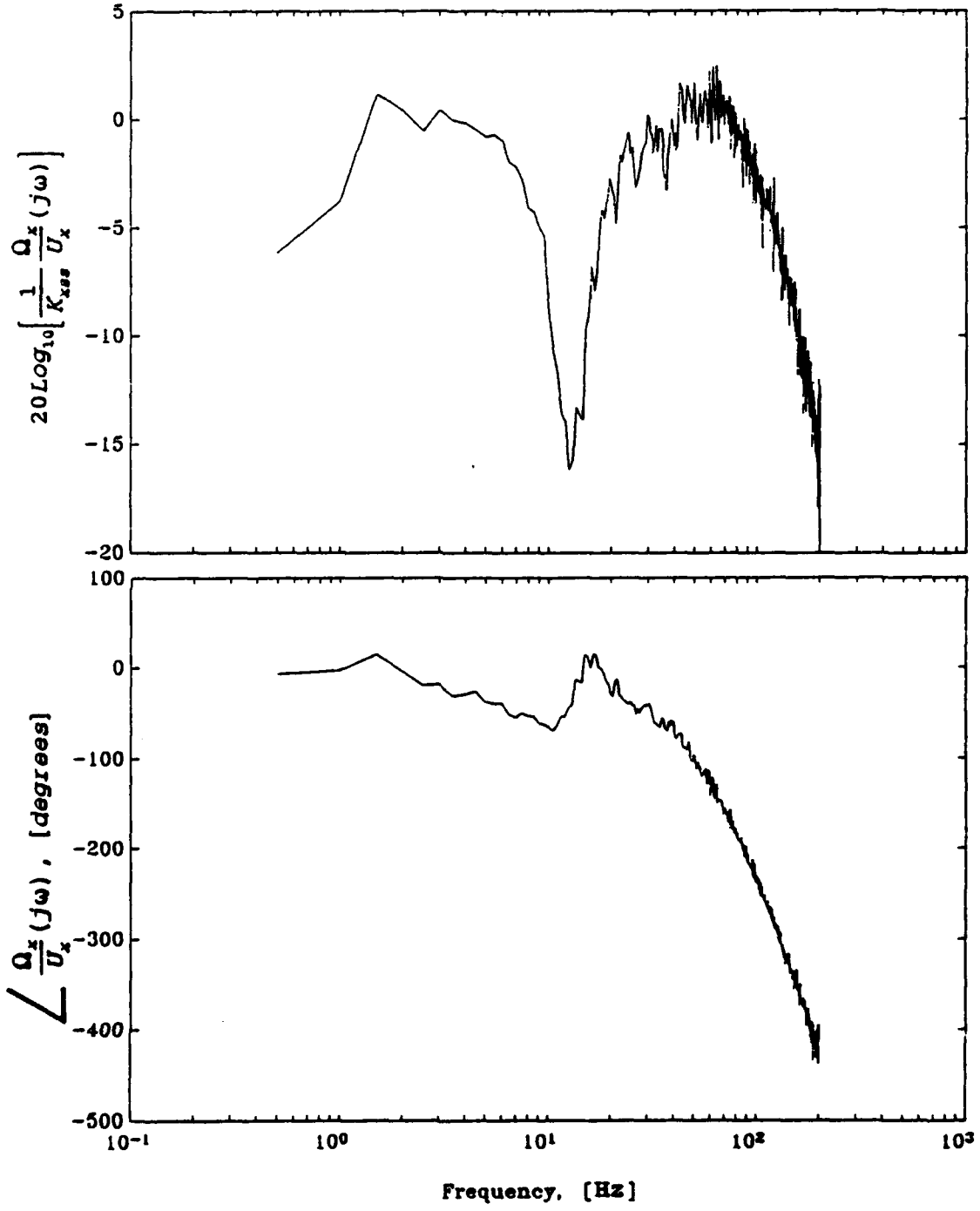

(a) X axis actuating system/load combination.

Figure C.6. Experimentally determined Bode plot of each axis.

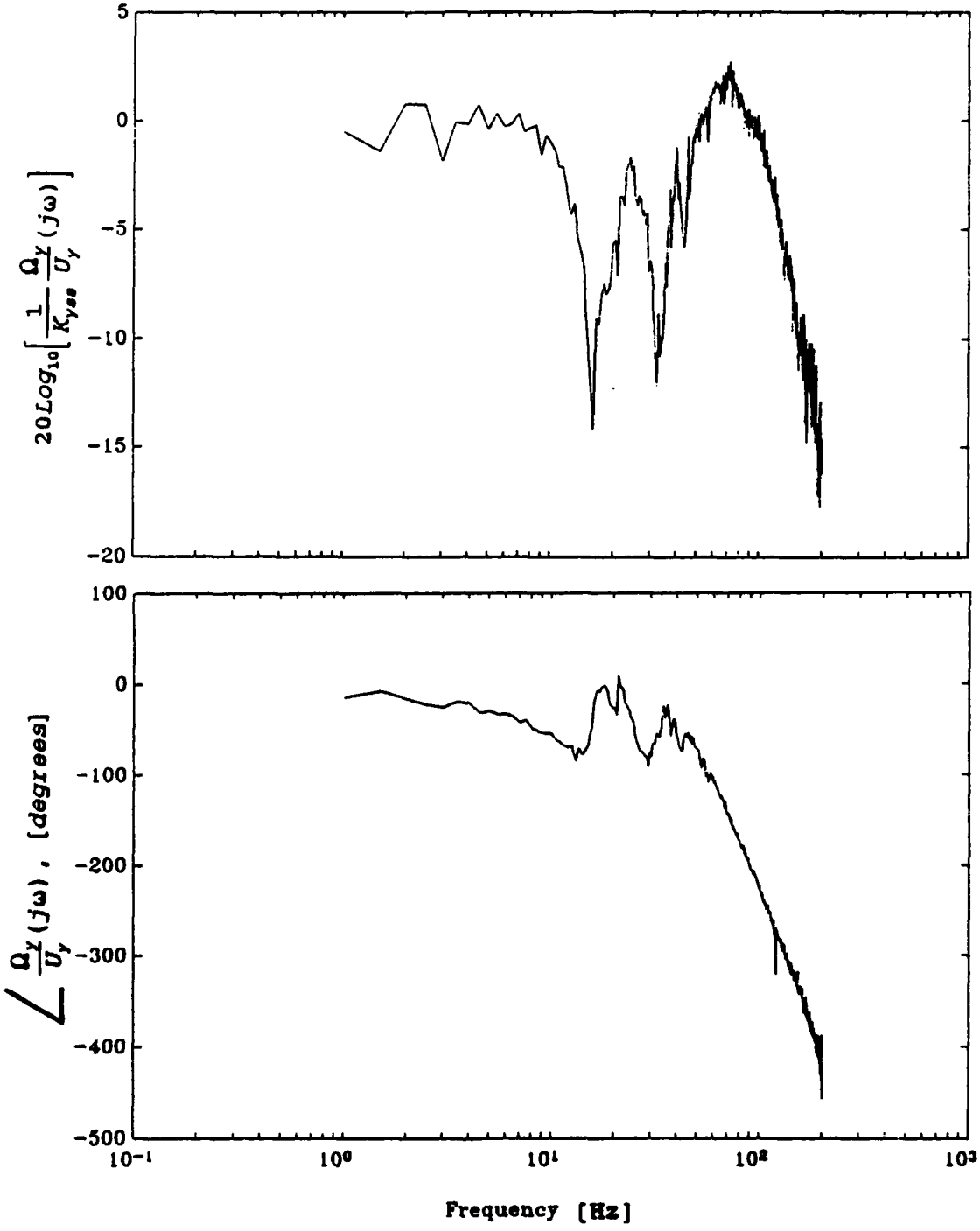

(b) X axis actuating system/load combination.

Figure C.6. (Continued).

Linear Model Development

X axis linear model. The Bode plot of the X axis actuating system/load combination in Figure C.6a shows that the resonant frequency of the load is at 12 Hz (75 rad/sec). This is the natural frequency of the linear model of the load, ω_{nxl}, which can be expressed in terms of the physical parameters of the load as

$$\omega_{nxl}=\sqrt{\frac{k_{spx}}{M_{hx}}}. \qquad (C.6)$$

The mass, M_{hx}, was calculated to be 111 kg based on the weight of the sewing head and the dimensions of the aluminum X carriage. Therefore, the spring constant, k_{spx}, was calculated to be 6.24e5 (N/m) from Equation (C.6). The Bode plot of the model of the actuating system/load combination approximates that of the actual system as shown in Figure C.7 with the viscous damping coefficient, B_{hx}, adjusted to 3330 (kg/sec).

Y axis linear model. The actuating system/load combination of the Y axis has antiresonant frequencies at 15 Hz (94 rad/sec) and 30 Hz (188 rad/sec) as shown in the Bode plot in Figure C.6b. The axis was driven by a sinusoidal signal at each of these frequencies to determine the source of the modes of vibration. The sewing head vibrated excessively at 30 Hz while the frame vibrated excessively at 15 Hz, indicating that one mass/spring/damper combination in the model is the stitcher frame and the other consists of the sewing head and its supporting structure.

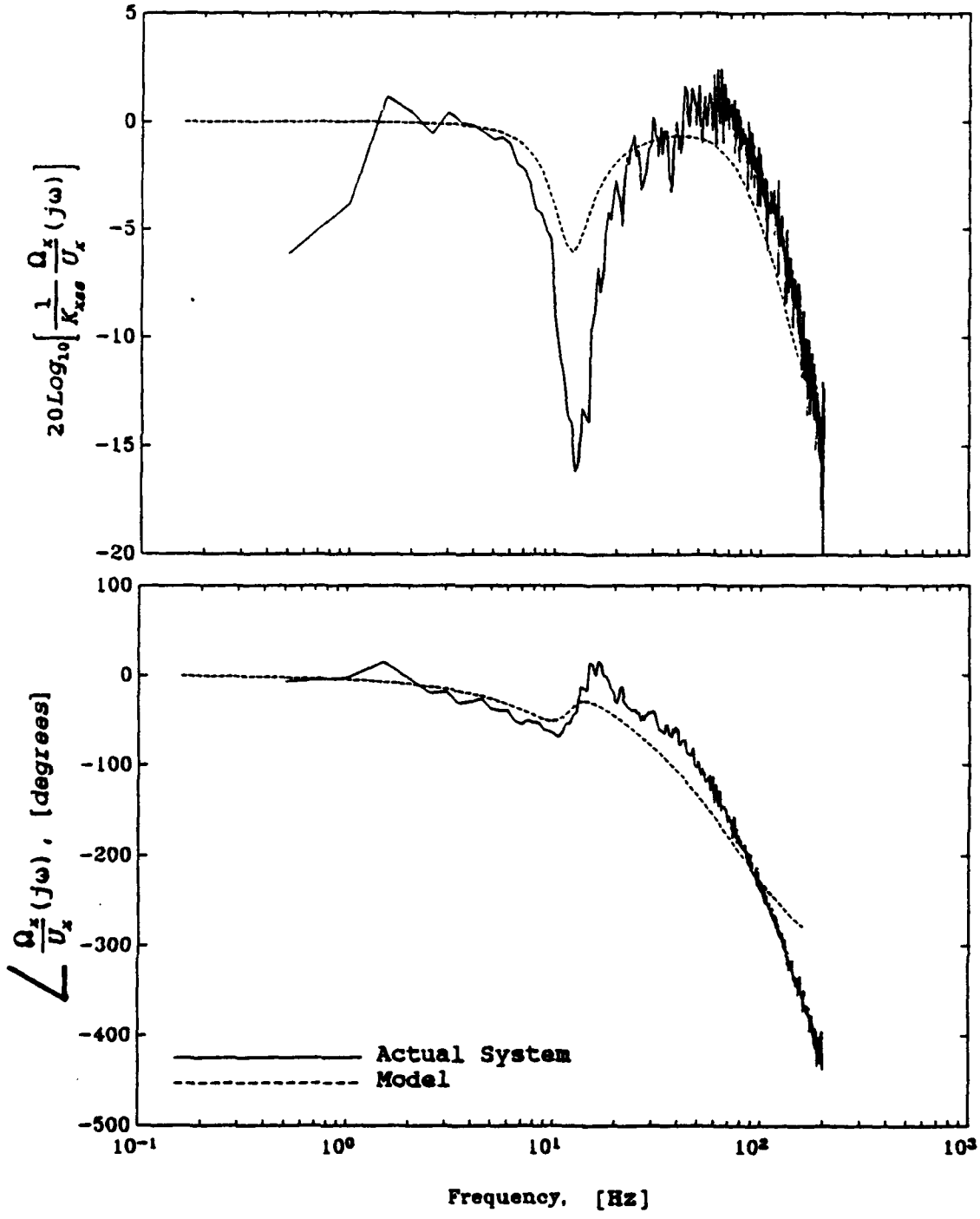

Figure C.7. X axis actuating system/load Bode plot, actual system and model.

The spring constants in the Y axis load model could not be analytically determined as in the case of the X axis because the equations governing the motion of the two masses,

$$M_{hy}\ddot{y}_h = k_{spy}\left(\frac{r}{N}\theta_y - y_h - y_f\right) - B_{hy}\dot{y}_h \qquad \text{(C.7a)}$$

and

$$M_{fy}\ddot{y}_f = k_{spy}\left(\frac{r}{N}\theta_y - y_h - y_f\right) - B_{fy}\dot{y}_f - k_{fy}y_f \qquad \text{(C.7b)}$$

are dynamically coupled. However, the mass, M_{hy}, of the load was measured to be 70 kg. The total mass of the stitcher, M_t, consists of the mass of the X axis load, M_{hx}, (which includes the mass of the Y axis load, M_{hy}) and the mass of the frame, M_{fy}, or $M_t = M_{hx} + M_{fy}$. The shipping weight of the stitcher is approximately 630 lbs., which corresponds to M_t=286 kg; therefore, the mass of the stitcher frame used in the model is 175 kg. The spring constants k_{spy} and k_{fy} were adjusted on a trial and error basis, with the initial approximation of $k_{spy} = k_{spx}$, until the antiresonant frequencies of the model were approximately the same as those of the actual system. The viscous damping coefficients were then adjusted to approximate the damping in the actual system. The parameters of the model of the Y axis load are

M_{hy}=70 kg,

B_{hy}=2080 kg/sec,

k_{spy}=1e6 N/m,

M_{fy}=175 kg,

B_{fy}=1000 kg/sec, and

k_{fy}=5e6 N/m

for the Bode plot shown in Figure C.8.

Linear spring model. The actual configuration of the timing belt and sewing head in each axis is shown in Figure C.9. This figure shows that the stiffness of the spring transmitting force to the mass depends on the relative position of the driven pulley and the sewing head. If $r\theta_p > x$, the length of the spring in tension is l_1 and the effective spring constant is

$$k_1 = k_{sp1}. \tag{C.8a}$$

If $r\theta_p < x$, the length of the portion of the timing belt that is in tension is l_2+l_3 and the effective spring constant of the spring model is

$$k_2 = \frac{k_{sp2}k_{sp3}}{k_{sp2}+k_{sp3}} \tag{C.8b}$$

assuming the idling pulley has zero inertia and friction. Therefore, the actual spring constant is bilinear, based on the quantity $r\theta_p - x$.

The bilinear characteristic of the spring can be neglected if the preload in the timing belt is sufficiently high. This is explained by considering the free body diagram of the mass of Figure C.9. One of two different springs may act on the mass, depending on its position; therefore, the two free body diagrams in Figure C.10, which include the preload force, F_{pl}, are needed to describe the motion of the

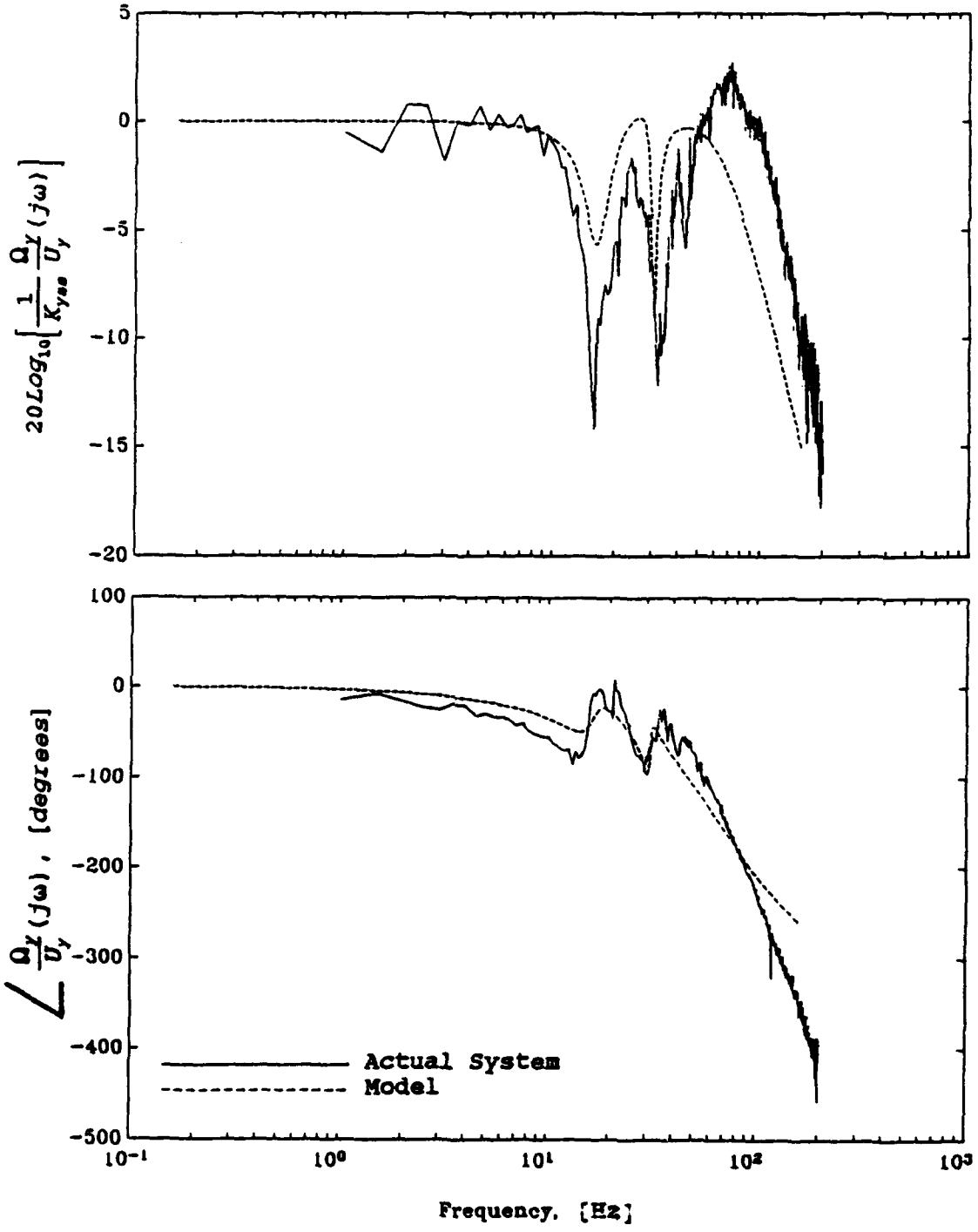

Figure C.8. Y axis actuating system/load Bode plot, actual system and model.

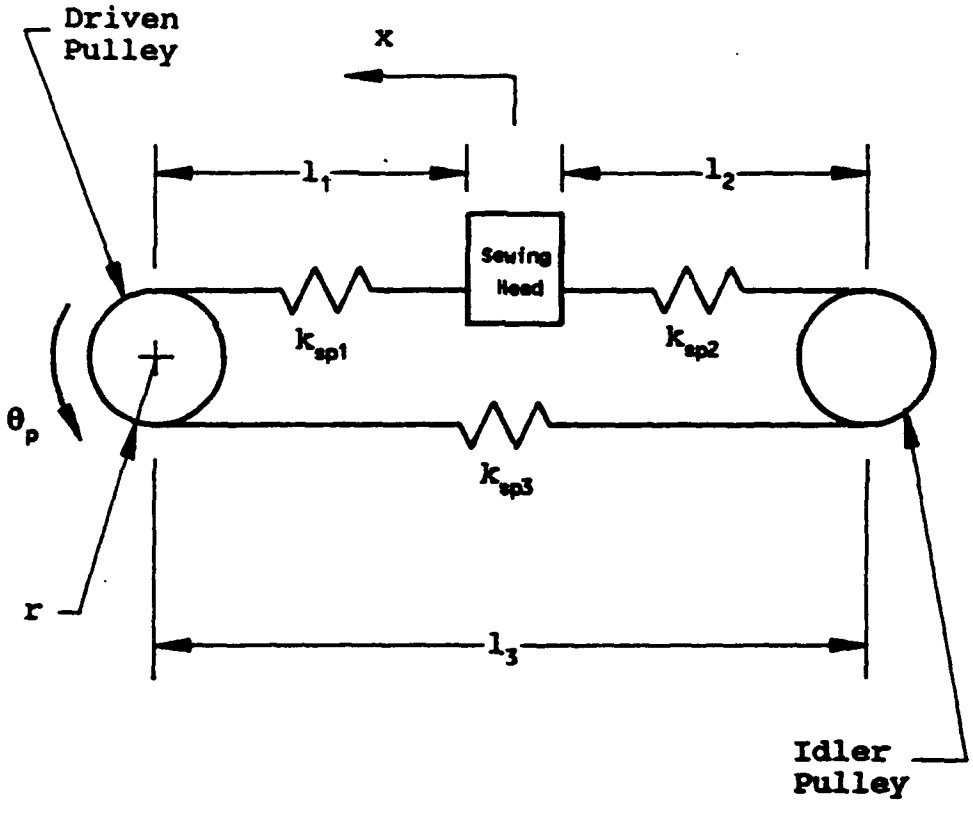

Figure C.9. Configuration of the sewing head and timing belt in each axis.

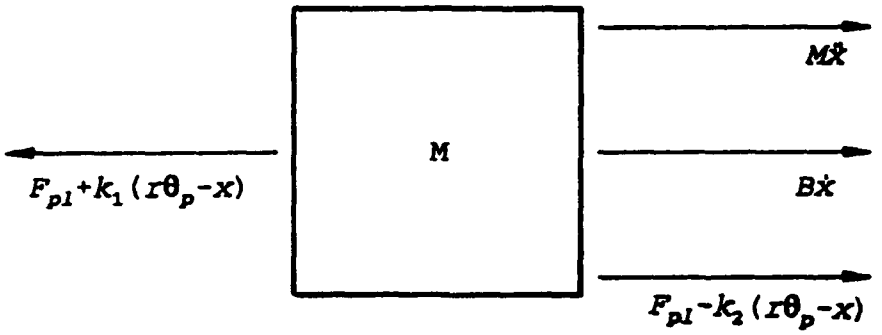

(a) Free body diagram for $r\theta_p > x$.

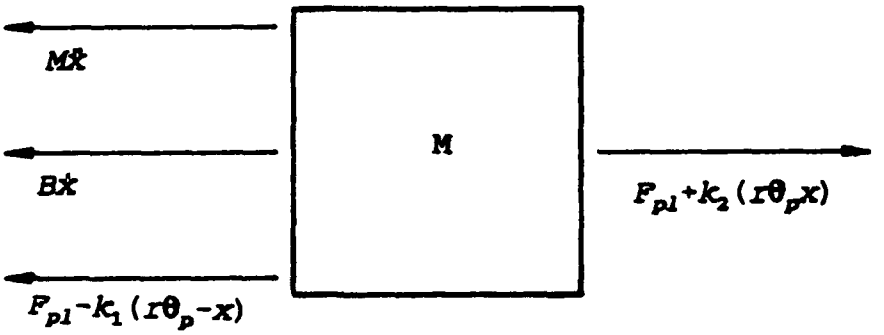

(b) Free body diagram for $r\theta_p < x$.

Figure C.10. Free body diagrams of the sewing head mass in each axis.

mass. The equations derived from the free body diagrams governing the motion of the mass are

$$F_{pl}+k_1(r\theta_p-x)=M\ddot{x}+B\dot{x}+F_{pl}-k_2(r\theta_p-x), \text{ when } r\theta_p>x \qquad \text{(C.9a)}$$

and

$$F_{pl}+k_2(r\theta_p-x)=M\ddot{x}+B\dot{x}+F_{pl}-k_1(r\theta_p-x), \text{ when } r\theta_p<x. \qquad \text{(C.9b)}$$

The timing belts cannot transmit force in compression; therefore, a negative force, as defined in the free body diagram, cannot act on the mass. Thus, when $r\theta_p>x$ and $F_{pl}<k_2(r\theta-x)$, no force is transmitted through the section l_2+l_3 of the timing belt and Equation (C.9a) reduces to

$$F_{pl}+k_1(r\theta_p-x)=M\ddot{x}+B\dot{x}. \qquad \text{(C.10a)}$$

Similarly, the term $F_{pl}-k_1(r\theta_p-x)$ is not present in Equation (C.9b) when $F_{pl}<k_1(r\theta_p-x)$, and the equation reduces to

$$F_{pl}+k_2(r\theta_p-x)=M\ddot{x}+B\dot{x}. \qquad \text{(C.10b)}$$

However, when F_{pl} is greater than $k_2(r\theta_p-x)$ and $k_1(r\theta_p-x)$, both equations of motion reduce to

$$(k_1+k_2)(r\theta_p-x)=M\ddot{x}+B\dot{x}. \qquad \text{(C.11)}$$

Therefore, the spring is bilinear only when $F_{pl}<k_2(r\theta_p-x)$ or $F_{pl}<k_1(r\theta_p-x)$.

This spring characteristic of the timing belt was verified experimentally by determining the response of each axis to a positive and negative position step command, as described in Appendix B. The resulting step response curves in Figure C.11 show that the bilinear effect is negligible; the response curves of each axis are similar for each direction

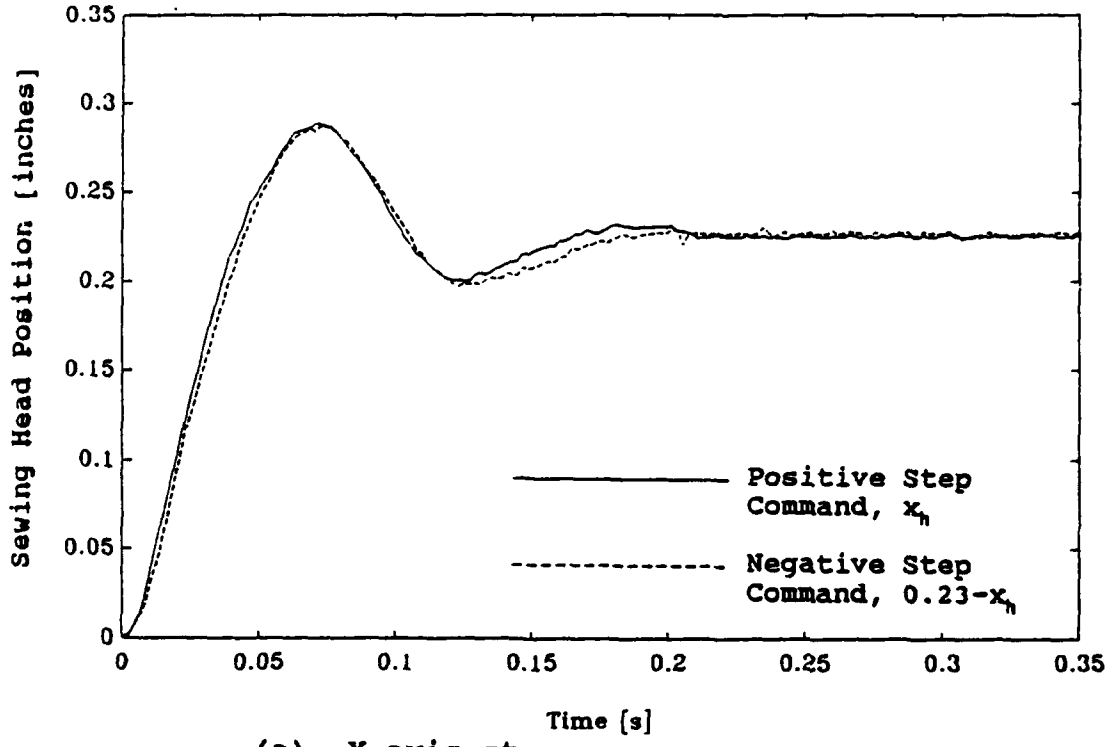

(a) X axis step response.

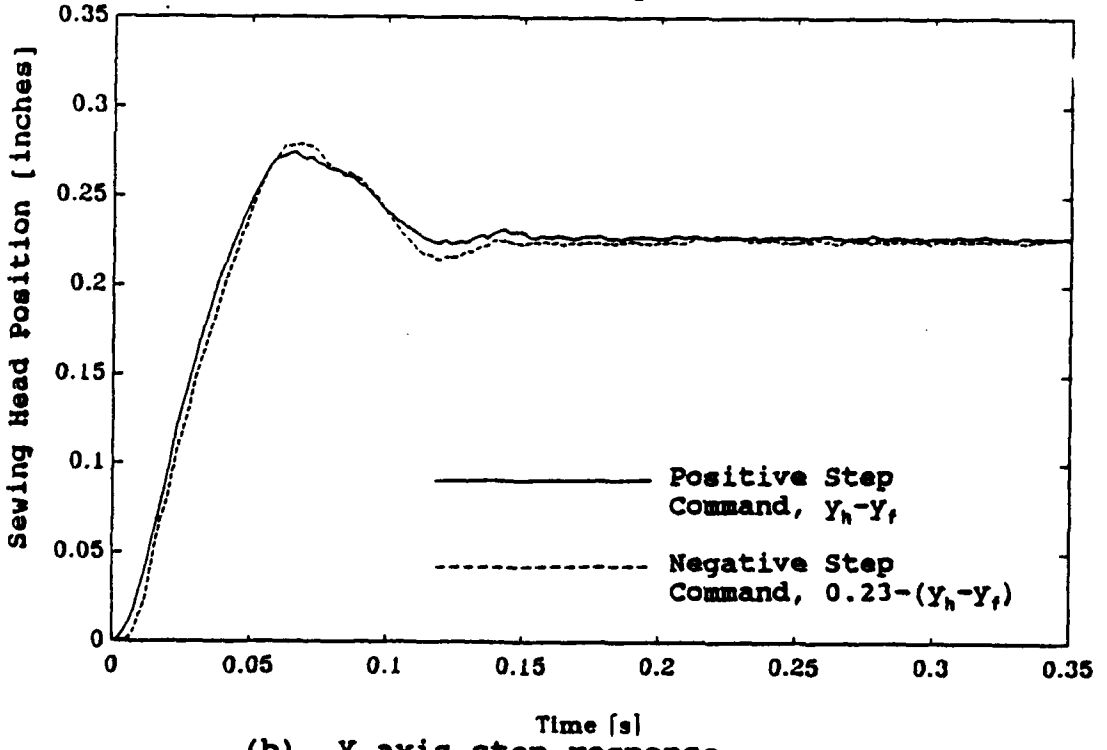

(b) Y axis step response.

Figure C.11. Positive and negative step response of each axis.

of the step command. Although the preload force was not measured directly, it was sufficiently high to neglect the bilinear effect of the timing belt spring model.

Nonlinear Model Development

The closed loop position step response curves of the X axis actuating system in Figure C.12 show that the system begins to saturate when driven by a step size of $\pi/2$ radians. Therefore, the nonlinear model of the stitcher was developed with a current saturation element, which acts as a torque limit, in the amplifiers. The stitcher is not subjected to large step sizes during normal operation; therefore, the current limit was adjusted such that the closed loop position step response of the axes fit that of the actual system for the smallest step size tested, $3\pi/8$ radians. With the current limit set to 27 amperes, corresponding to a torque limit of 13.5 Nm, the step response of the model of each axis compares to that of the actual system as shown in Figures C.13 and C.14 for the four step sizes tested. The deterioration of the model accuracy at higher step sizes is assumed to be due to unmodeled system nonlinearities. These step sizes were not considered when modeling the nonlinear elements since they occur outside of the typical operating range of the stitcher.

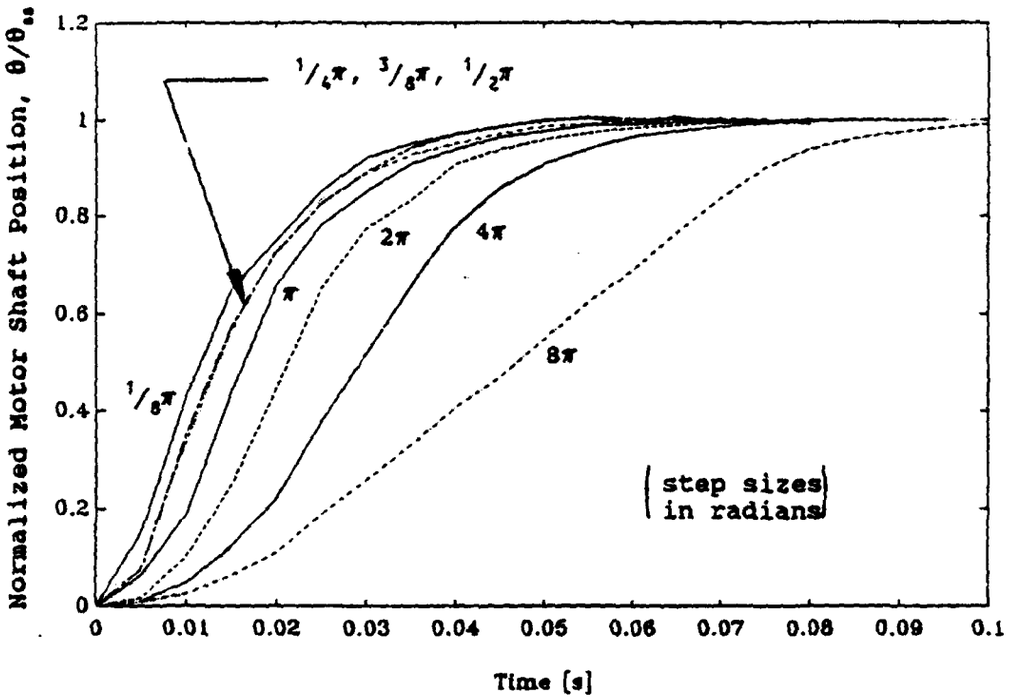

Figure C.12. Closed loop position response of the X axis actuating system.

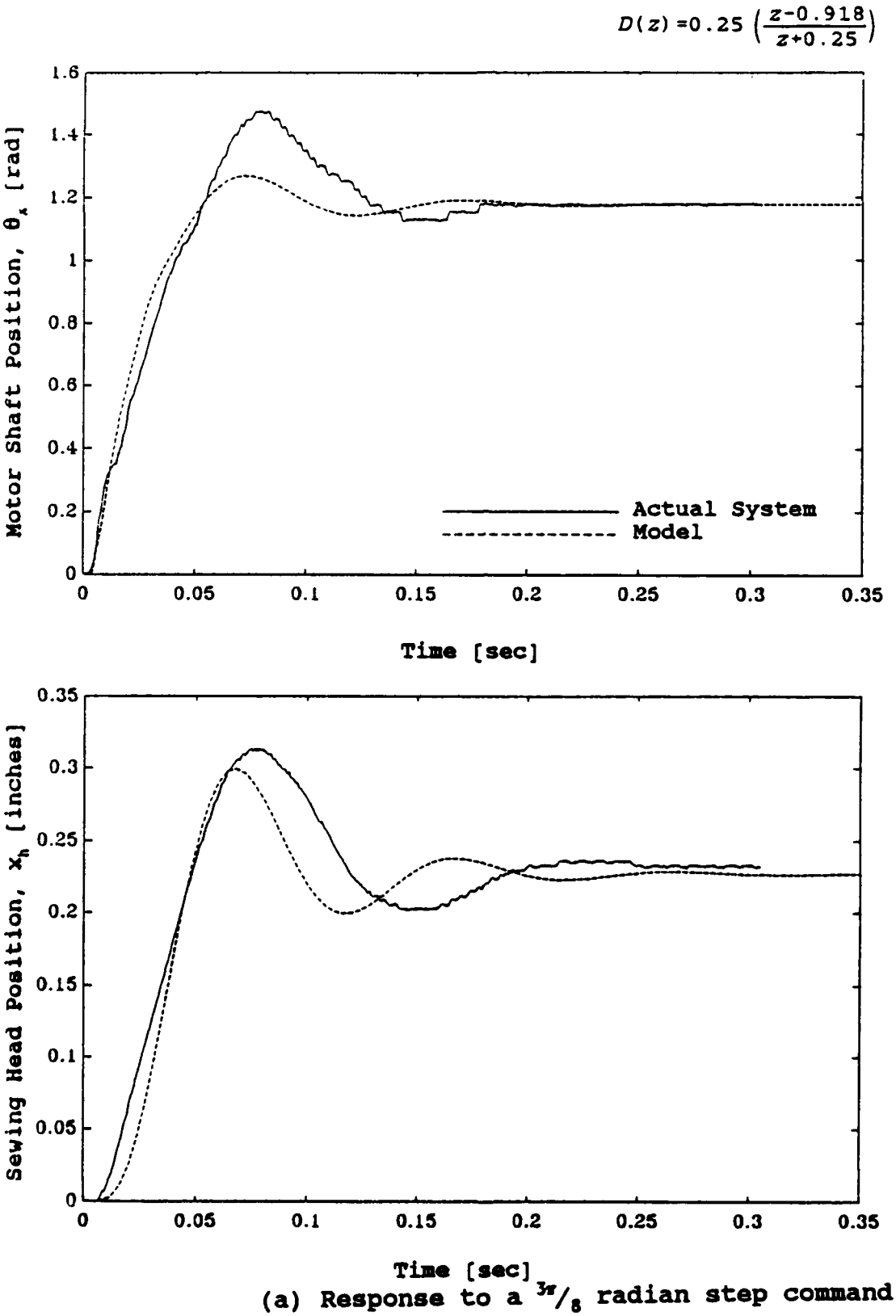

(a) Response to a $^{3\pi}/_{8}$ radian step command.

Figure C.13. X axis sewing head and motor shaft position step response, actual system and model.

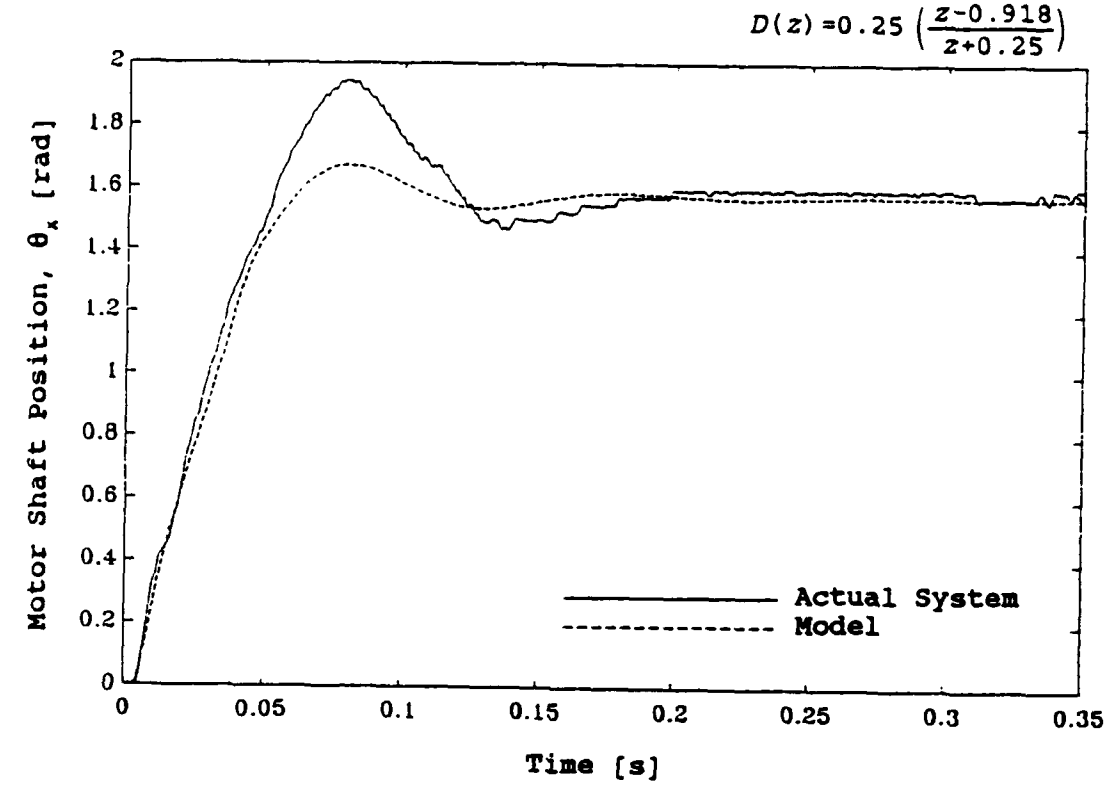

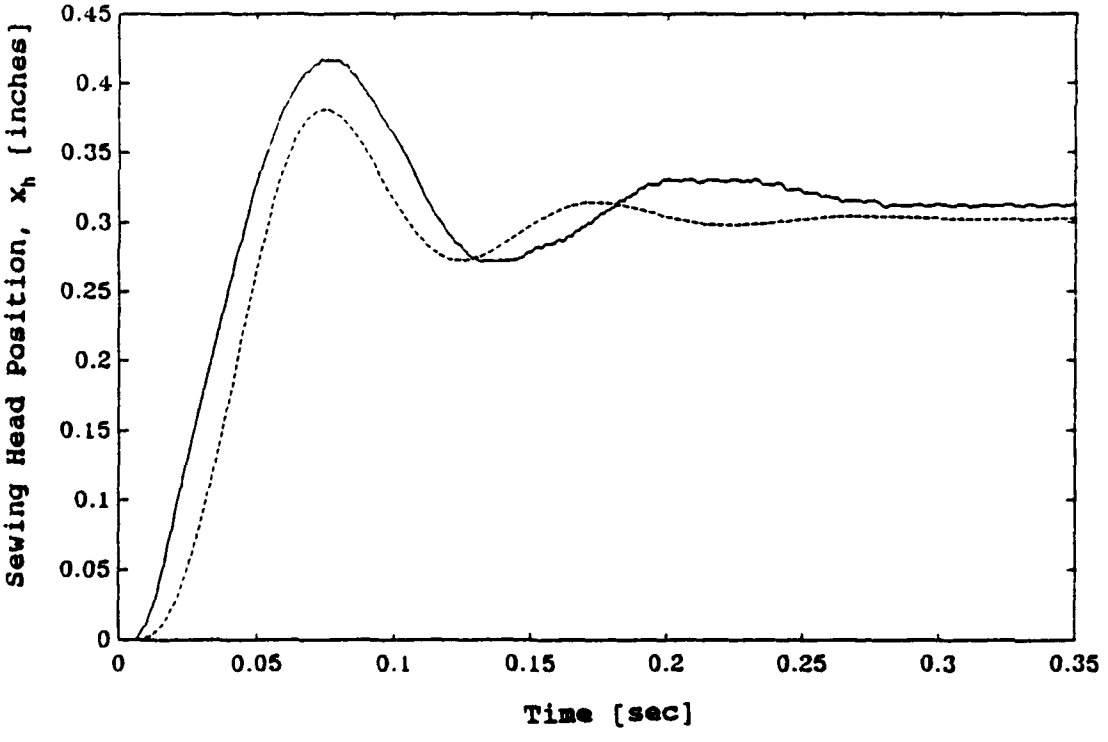

(b) Response to a $\pi/2$ radian step command.

Figure C.13. (Continued).

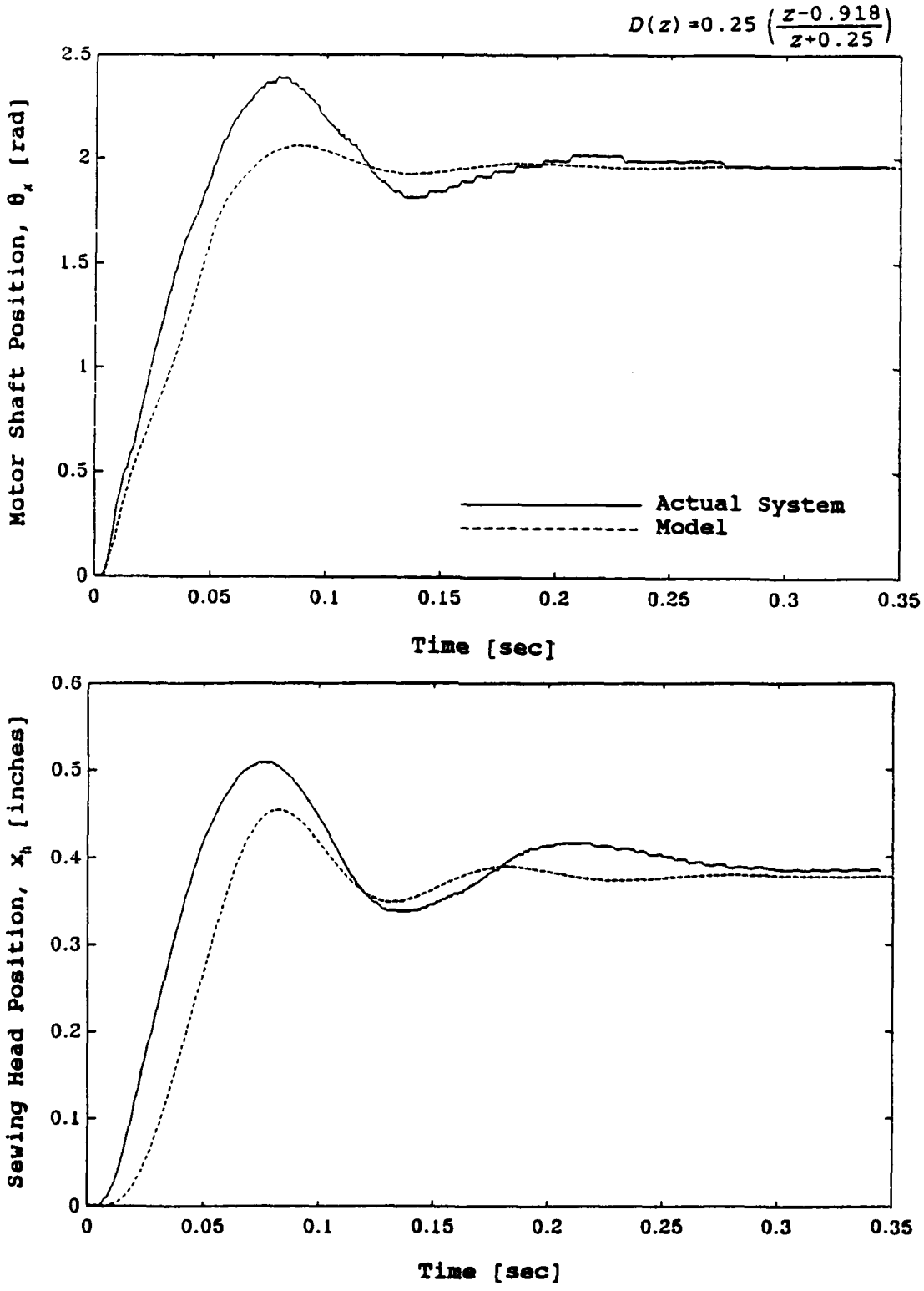

(c) Response to a $5\pi/8$ radian step command.

Figure C.13. (Continued).

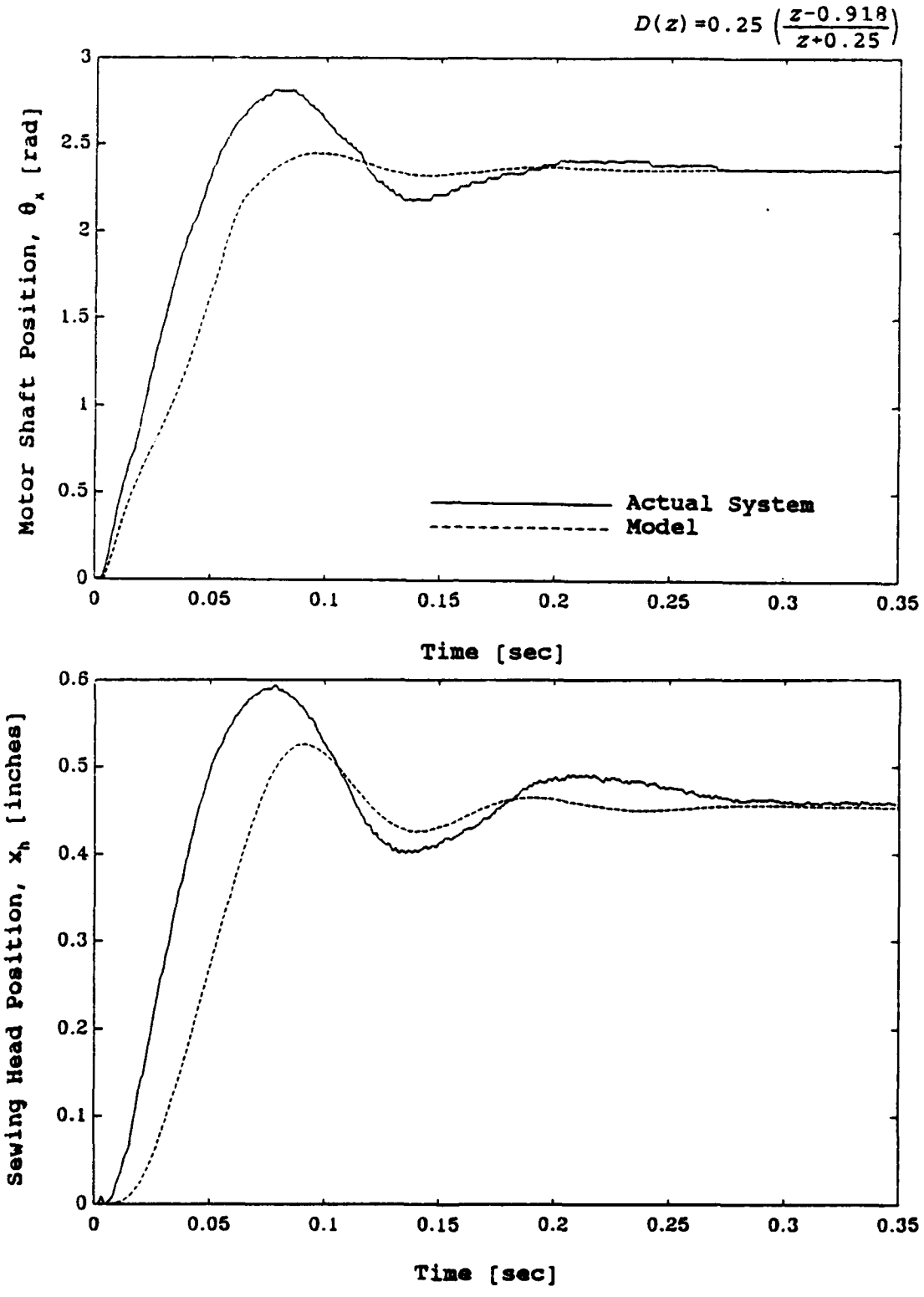

(d) Response to a $3\pi/4$ radian step command.

Figure C.13. (Continued).

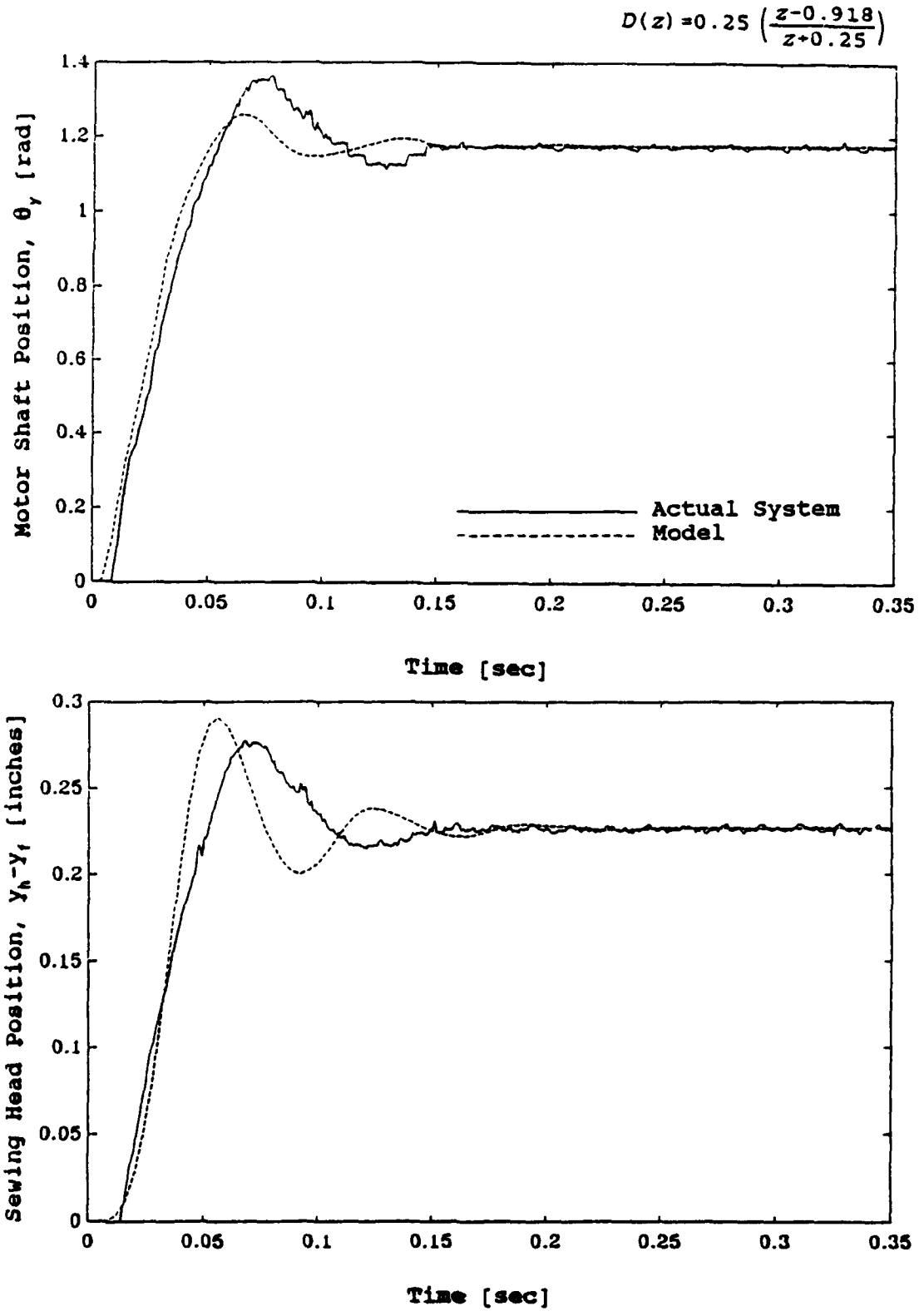

(a) Response to a $^{3\pi}/_{8}$ radian step command.

Figure C.14. Y axis sewing head and motor shaft position step response, actual system and model.

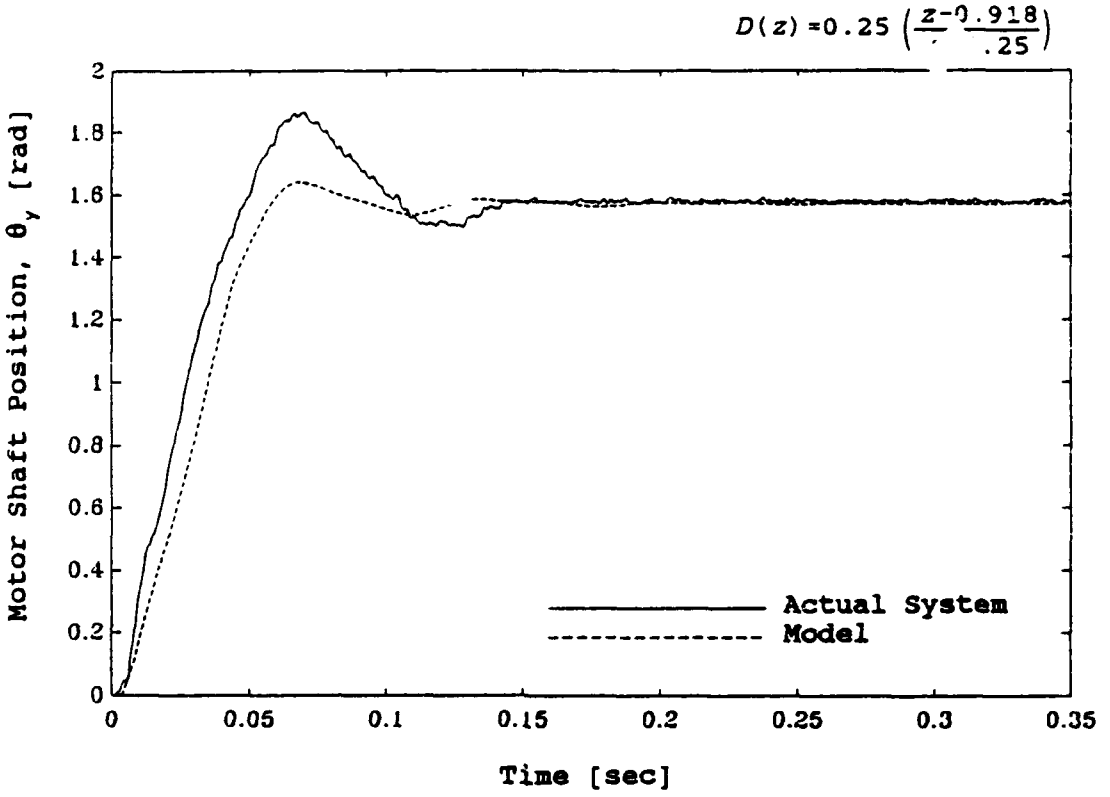

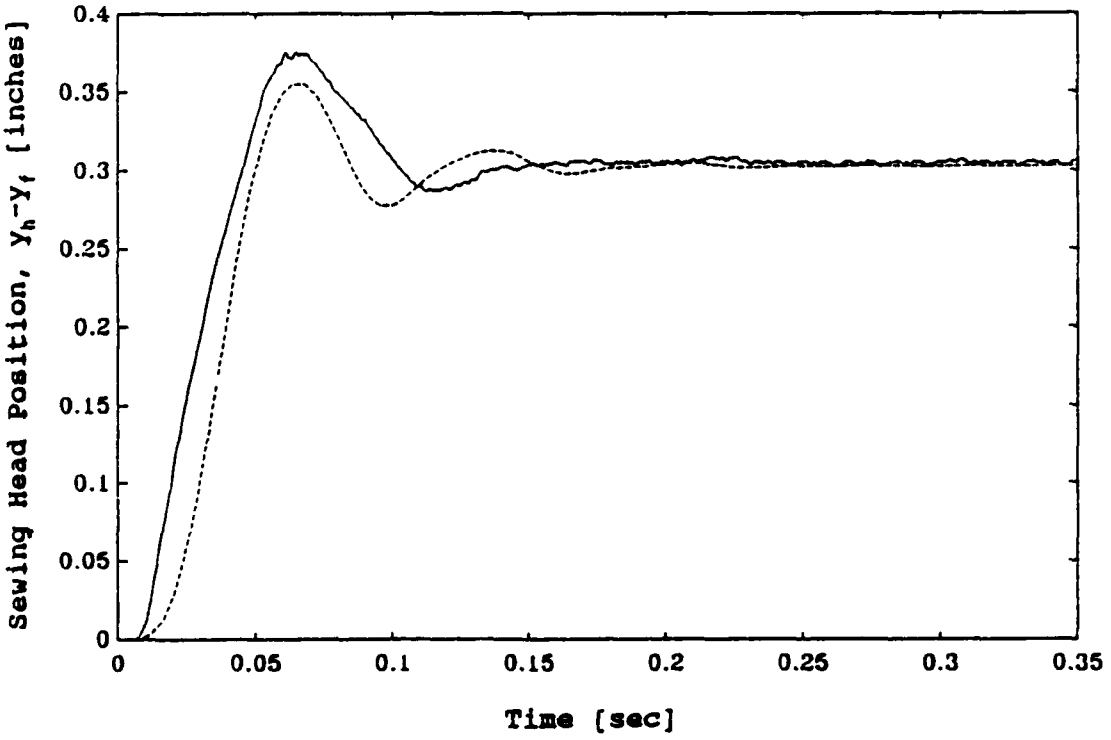

(b) Response to a $\pi/2$ radian step command.

Figure C.14. (Continued).

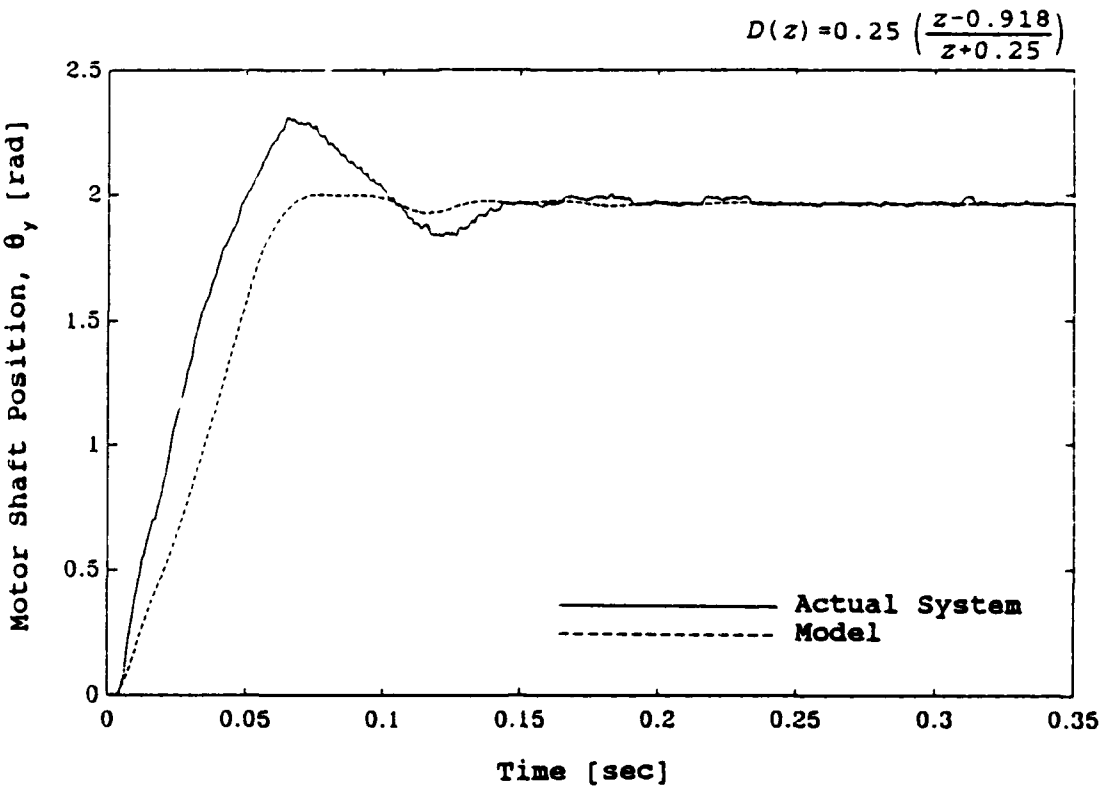

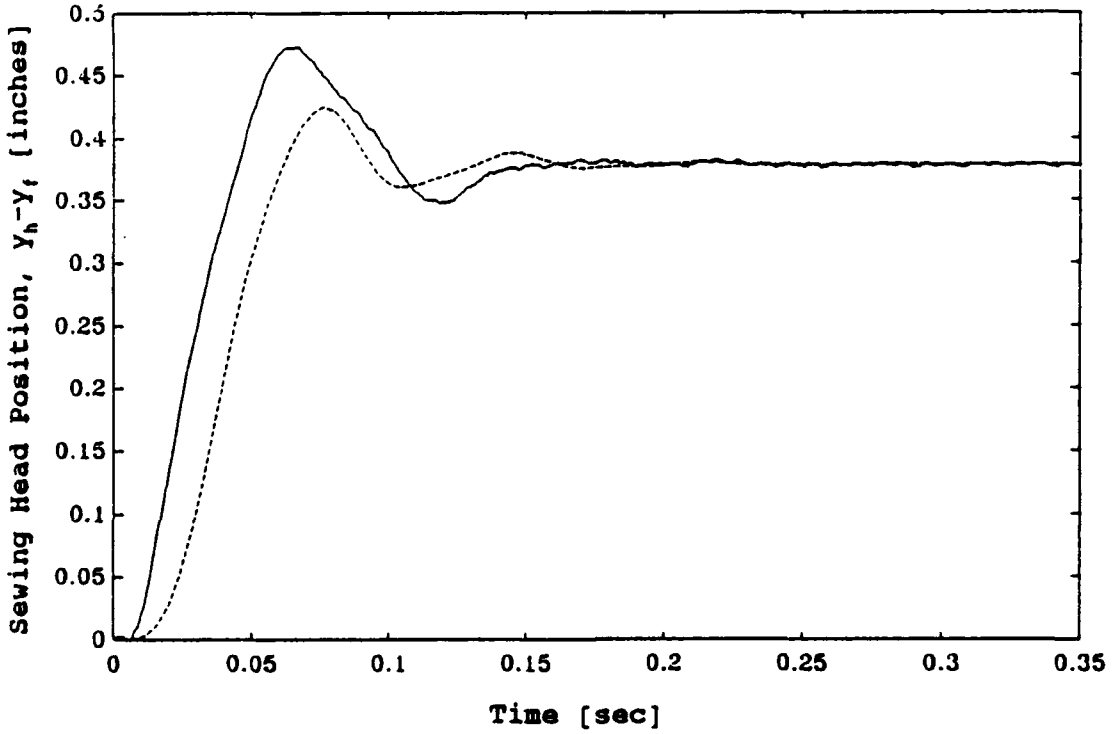

(c) Response to a $5\pi/8$ radian step command.

Figure C.14. (Continued).

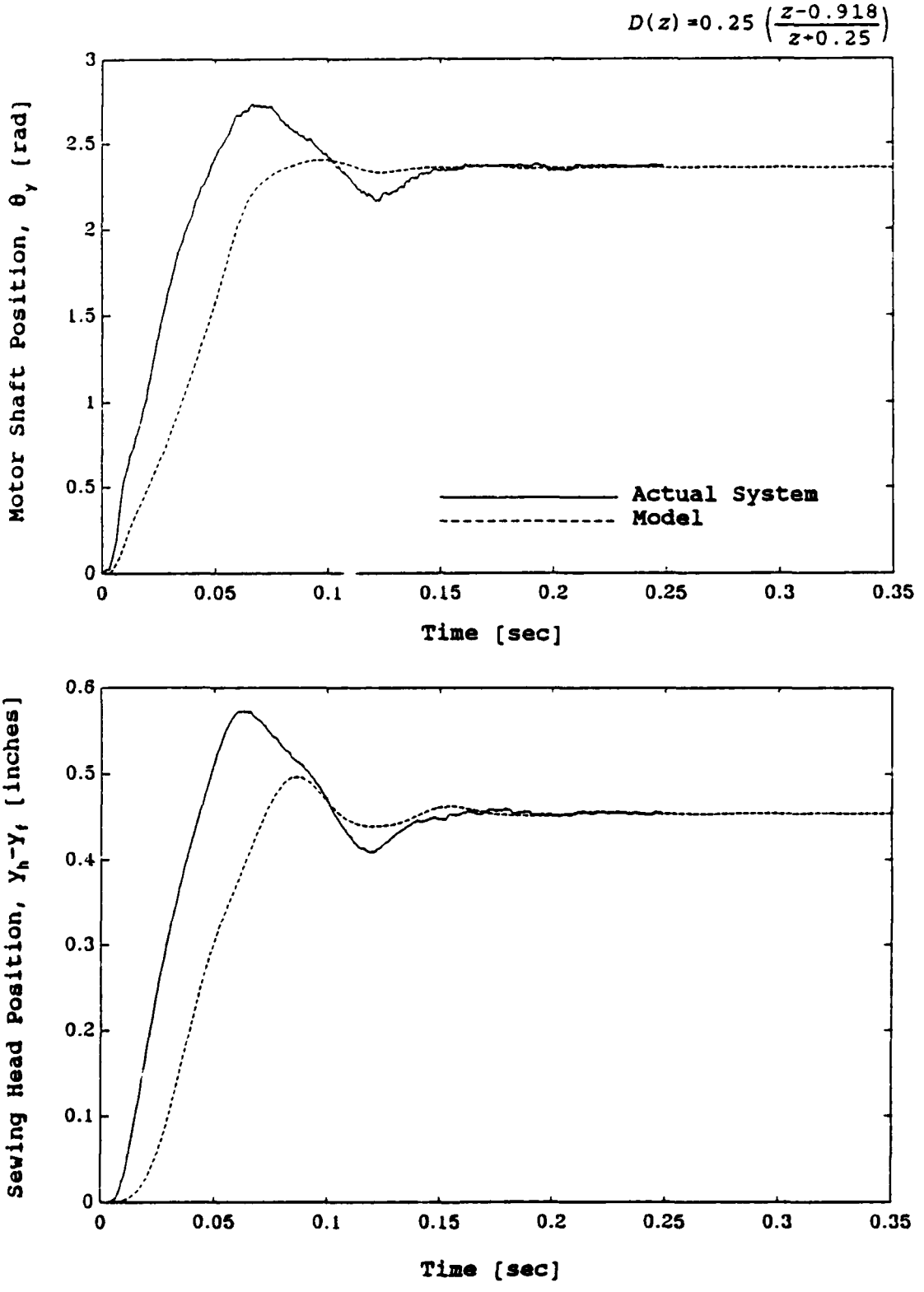

(d) Response to a $3\pi/4$ radian step command.

Figure C.14. (Continued).

REFERENCES

1. Gershon, D. and I. Porat, "Vision Servo Control of a Robotic Sewing System," Proceedings of the IEEE International Conference on Robotics and Automation, Philadelphia, April 1988, pp. 1830-1835.

2. Berkstresser, Gordon A. and David R. Buchanan, ed., Automation and Robotics in the Textile and Apparel Industries, Noyes Publications, Park Ridge, NJ, 1986.

3. Solinger, Jacob, Apparel Manufacturing Handbook: Analysis, Principles and Practice, Van Nostrand Reinhold Company, New York, 1980.

4. Taylor, P.M., A.J. Wilkinson, G.E. Taylor, M.B. Gunner, G.S. Palmer, "Automated Fabric Handling Problems and Techniques," IEEE International Conference on Systems Engineering, Pittsburgh, 1990, pp. 367-370.

5. Torgerson, Eric and F. W. Paul, "Vision Guided Robotic Fabric Manipulation for Apparel Manufacturing", IEEE Control Systems Magazine, Vol. 8, No. 1, February 1988, pp. 14-20.

6. Parker, J. K., R. Dubey, F. W. Paul, R. J. Becker, "Robotic Fabric Handling for Automated Garment Manufacturing", Transactions of the ASME, Journal of Engineering for Industry, October 1982, pp.1-6.

7. Paul, F.W., E. Torgerson, S. Avigdor, D.R. Cultice, A. Gopalswamy, and K. Subba-Rao, "A Hierarchical System for Robot-Assisted Shirt Collar Processing," IEEE International Conference on Systems Engineering, Pittsburgh, 1990, pp. 378-382.

8. Kameya, Toshiro, "Progress Seen in Automated Sewing System," Business JAPAN, December, 1989, pp.63-67.

9. Ishadawa, S., "On the Large-Scale Project: "Automated Sewing System"," JIAM, Japan 1990.

10. Poo, Aun-Neow, John S. Bollinger and George W. Younkin, "Dynamic Errors in Type 1 Contouring Systems", IEEE Transactions on Industry Applications, Vol. IA-8, No. 4, July/August 1972, pp. 477-484.

11. Doraiswami, R. and A. Gulliver, "A Control Strategy for Computer Numerical Control Machine Exhibiting Precision and Rapidity", Transactions of the ASME: Journal of Dynamic Systems, Measurement, and Control, Vol. 106, March 1984, pp. 56-62

12. Tomizuka, M., D. Dornfeld, and M. Purcell, "Application of Microcomputers to Automatic Weld Quality Control," Transactions of the ASME: Journal of Dynamic Systems, Measurement, and Control, Vol. 102, June 1980, pp. 62-68.

13. Kulkarni, P. K., and K. Srinivasan, "Optimal Contouring Control of Multi-Axial Feed Drive Mechanisms," Transactions of the ASME: Journal of Dynamic Systems, Measurement, and Control, Vol. 111, May 1989, pp. 140-148.

14. Houpis, Constantine H., and Gary B. Lamont, Digital Control Systems: Theory, Hardware, Software, 2nd ed., McGraw-Hill, Inc., New York, 1992, Chap. 6.

15. D'Azzo, John J., and Constantine H. Houpis, Linear Control System Analysis and Design: Conventional and Modern, 3rd ed., McGraw-Hill, Inc., New York, 1988, Chap. 7.

16. Middleditch, A. E., and F. W. Paul, "Dynamic Performance of a Computer Numerical Control System for Multi-Axis Contouring Machine Tools," Presented at the ASME Winter Annual Meeting, Detroit, Michigan, November 11-15, 1973.

SUPPLEMENTARY

INFORMATION

AUTOMATED SHIRT COLLAR MANUFACTURING

DLA 900-87-0017 Task 0014

FINAL REPORT

VOLUME III:

Sewing Head Control for High Speed Stitch Contour Tracking

LARRY - PAULSON
703 756 2330

Frank W. Paul
Principal Investigator

and

Alan W. Bennett
Research Assistant

Center for Advanced Manufacturing
and
Clemson Apparel Research

Clemson University
Clemson, SC

June 1992

P00011 to DLA900-87-D-0017

SECURITY CLASSIFICATION OF THIS PAGE

REPORT DOCUMENTATION PAGE

1a. REPORT SECURITY CLASSIFICATION Unclassified	1b. RESTRICTIVE MARKINGS
2a. SECURITY CLASSIFICATION AUTHORITY	3. DISTRIBUTION / AVAILABILITY OF REPORT Unclassified Distribution Unlimited
2b. DECLASSIFICATION / DOWNGRADING SCHEDULE	
4. PERFORMING ORGANIZATION REPORT NUMBER(S)	5. MONITORING ORGANIZATION REPORT NUMBER(S)
6a. NAME OF PERFORMING ORGANIZATION Clemson University Clemson Apparel Research 6b. OFFICE SYMBOL (If applicable)	7a. NAME OF MONITORING ORGANIZATION Defense Personnel Support Center
6c. ADDRESS (City, State, and ZIP Code) 500 Lebanon Road Pendleton, SC 29670	7b. ADDRESS (City, State, and ZIP Code) 2800 South 20th Street P.O. Box 8419 Philadelphia, PA 19101-8419
8a. NAME OF FUNDING / SPONSORING ORGANIZATION Defense Logistics Agency 8b. OFFICE SYMBOL (If applicable)	9. PROCUREMENT INSTRUMENT IDENTIFICATION NUMBER DLA 900-87-D-0017 Delivery Order 0014
8c. ADDRESS (City, State, and ZIP Code) Room 4B195 Cameron Station Alexandria, VA 22304-6100	10. SOURCE OF FUNDING NUMBERS PROGRAM ELEMENT NO. 78011S; PROJECT NO.; TASK NO.; WORK UNIT ACCESSION NO.
11. TITLE (Include Security Classification) Automated Shirt Collar Manufacturing Vol. III: Sewing Head Control for High Speed Stitch Contour Tracking - unclassified	
12. PERSONAL AUTHOR(S) F. W. Paul, Principal Investigator; Alan W. Bennett, Research Assistant	
13a. TYPE OF REPORT Final 13b. TIME COVERED FROM n/a TO _____ 14. DATE OF REPORT (Year, Month, Day) 1992 June 23 15. PAGE COUNT	
16. SUPPLEMENTARY NOTATION	

17 COSATI CODES		
FIELD	GROUP	SUB-GROUP

18. SUBJECT TERMS (Continue on reverse if necessary and identify by block number)

19. ABSTRACT (Continue on reverse if necessary and identify by block number)

A prototype of a two axis belt driven CNC stitching machine has been designed and built for use in the apparel industry. The objectives of this research are: (1) determine the performance requirements of the stitcher; (2) develop a mathematical model of the stitcher; and (3) recommend the design changes necessary for the stitcher to meet the specifications based on the simulation of the stitcher model.

Call back 10/20/93

20. DISTRIBUTION / AVAILABILITY OF ABSTRACT ☒ UNCLASSIFIED/UNLIMITED ☐ SAME AS RPT. ☐ DTIC USERS	21. ABSTRACT SECURITY CLASSIFICATION Unclassified
22a. NAME OF RESPONSIBLE INDIVIDUAL Frank W. Paul	22b. TELEPHONE (Include Area Code) 803-656-3291 22c. OFFICE SYMBOL

DD FORM 1473, 84 MAR 83 APR edition may be used until exhausted. All other editions are obsolete.

SECURITY CLASSIFICATION OF THIS PAGE

H968057

8-27-93
92-22

page 25 missing

Mary M.